ATP-CITRATE LYASE AS A THERAPEUTIC TARGET IN NON-ALCOHOLIC STEATOHEPATITIS

ATP-CITRATE LYASE AS A THERAPEUTIC TARGET IN NON-ALCOHOLIC STEATOHEPATITIS

By

MARISA MORROW, Hon. B.Sc.

A Thesis Submitted to the School of Graduate Studies in Partial Fulfillment of the Requirements for the Degree Doctor of Philosophy

McMaster University

DOCTOR OF PHILOSOPHY (2022) McMaster University
Department of Medical Sciences Hamilton, Ontario, Canada

TITLE: ATP-citrate lyase as a therapeutic target in non-alcoholic steatohepatitis

AUTHOR: Marisa Morrow, Hon. B.Sc.
========== (University of Guelph)

SUPERVISOR: Dr. Gregory Steinberg

PAGES: xxiv, 198

LAY ABSTRACT

A common link between obesity, type 2 diabetes, and heart disease is non-alcoholic fatty liver disease (NAFLD). NAFLD is characterized by an excessive build-up of fat in the liver. In some people, this leads to liver inflammation and scarring, a disease called non-alcoholic steatohepatitis (NASH). This can subsequently lead to liver cancer or liver failure. Due to the epidemics of obesity and type 2 diabetes, NAFLD is becoming the most common cause of liver disease in the world, with 1 in 4 people being affected. One way to potentially reduce the amount of fat in the liver is to simultaneously reduce the production, and increase the burning (oxidation), of fat. ATP-citrate lyase (ACLY) is a protein in the liver that becomes more abundant in those with NAFLD. It has been shown to be important for controlling fat metabolism, however, whether inhibiting its activity may be effective for reducing NAFLD and NASH is not yet known. This dissertation discusses the development of a new mouse model which mimics NAFLD in humans. It also evaluates whether inhibiting ACLY using genetics, or a drug called bempedoic acid reduces NAFLD and NASH in this mouse model. The studies described in this dissertation demonstrate that inhibiting ACLY reduces fat synthesis and increases fat burning and this lowers liver fat accumulation, inflammation, and fibrosis, suggesting that ACLY blockage may be a potential new way of treating NAFLD and NASH.

ABSTRACT

Non-alcoholic fatty liver disease (NAFLD) prevalence is increasing concurrently with obesity, type 2 diabetes (T2D), and cardiovascular diseases (CVDs), with 1 in 4 people being affected. NAFLD is the leading cause of chronic liver disease globally and yet there are still no approved therapeutics for its treatment. NAFLD is characterized by excessive accumulation of hepatic lipids and represents a continuum of pathologies, including fatty liver, non-alcoholic steatohepatitis (NASH) and hepatic fibrosis. The presence of NASH and hepatic fibrosis predict the risk of developing liver cirrhosis, hepatocellular carcinoma (HCC), and liver failure. In addition to these liver-related pathologies, NASH is also closely linked to the pathogenesis of obesity, T2D, and CVDs, the latter being the leading cause of death in NAFLD patients. It has thus become critical to develop new therapies for NASH. A known contributor to NASH is elevated liver *de novo* lipogenesis (DNL), which can be inhibited by targeting acetyl-CoA carboxylase (ACC). However, hypertriglyceridemia limits the use of pharmacological ACC inhibitors as a monotherapy. ATP-citrate lyase (ACLY) sits upstream of ACC and generates acetyl-CoA and oxaloacetate from citrate. Whether inhibition of ACLY is effective for treating NASH is unknown.

The studies in this dissertation describe the characterization of a new mouse model that replicates many of the pathological and molecular drivers of NASH in humans. In this model, genetically inhibiting ACLY in hepatocytes reduces liver malonyl-CoA, oxaloacetate, steatosis and ballooning as well as blood glucose, triglycerides, and cholesterol. Pharmacological inhibition of ACLY mirrors genetic inhibition but has additional positive effects on hepatic stellate cells, liver inflammation and fibrosis.

Mendelian randomization analysis demonstrates that human variants that mimic reductions in ACLY, associate with lower circulating triglycerides and biomarkers of NASH. These data indicate that inhibiting liver ACLY may be an effective approach for the treatment of NASH and dyslipidemia.

THESIS PUBLICATIONS

1. **Morrow MR,** Batchuluun B, Wu J, Ahmadi E, Leroux JM, Mohammadi-Shemirani P, Desjardins EM, Wang Z, Tsakiridis EE, Lavoie DCT, Reihani A, Smith BK, Kwiecien JM, Lally JSV, Nero TL, Parker MW, Ask K, Scott JW, Jiang L, Paré G, Pinkosky SL, and Steinberg GR. Inhibition of ATP-citrate lyase improves NASH, liver fibrosis, and dyslipidemia. *Cell Metabolism*. 34(6):919-936 (2022).
2. **Morrow MR,** Kwiecien JM, Ahmadi E, Tsakiridis EE, Lally JSV, Pinkosky SL, and Steinberg GR (2022). Developing and characterizing a human-relevant mouse model of non-alcoholic steatohepatitis and hepatic fibrosis for genetic and pharmacological intervention testing. *Prepared for submission in Cell STAR Protocols*.

OTHER PUBLICATIONS

1. Day EA, Ford RJ, Smith BK, Mohammadi-Shemirani P, **Morrow MR,** Gutgesell RM, Lu R, Raphenya AR, Kabiri M, McArthur AG, McInnes N, Hess S, Paré G, Gerstein HC, and Steinberg GR. Metformin-induced increases in GDF15 are important for suppressing appetite and promoting weight loss. *Nature Metabolism*. 1:1202-1208 (2019).

ACKNOWLEDGMENTS

To the several brilliant, hardworking, and supportive individuals and scientists I have had the privilege of working with – thank you. I will be forever grateful for the kindness and guidance I have experienced, and the knowledge, expertise, and skills I have gained during my time in the Steinberg lab. To my supervisor, Dr. Gregory Steinberg, thank you for placing your confidence and trust in me and my work. Thank you for the opportunities, and academic and scientific expertise you have given me, and the understanding and compassion you have shown me. I also owe much appreciation to my first mentor in the lab, Dr. Emily Day, who taught me confidence, hard work, and how to always keep passion and excitement at the forefront of our day-to-day work.

Thank you to my best friend in the lab, Evelyn Tskiaridis, your selflessness, and kindness continue to impress me. I do not know what I would have done without you by my side and without all the technical and emotional support you provided. You are truly one of the most genuine people I have ever met, and I feel lucky to have had you as a lab mate and friend. Thank you to Jianhan Wu for always keeping my interest in science and research, even when I was burnt out. I have learned so much from you and your incredible mind! Thank you to Dr. Tseegii Batchuluun, you have been a mother-like figure to me in the lab, and your constant support, expertise, and help with critical components of my research did not go unappreciated. Thank you to Eric Desjardins for the countless hours of training and help with work in the lab. Thank you to Dr. James Lally for guiding me through my projects and for the ongoing academic support and thought-provoking conversations. I would also like to thank Julie Leroux for your immense assistance on the project, it was a

joy to be able to train you and work by your side. To all the other past and present members of the Steinberg lab, thank you for all the amazing memories, for making me feel welcome, and for teaching me so much about science and life.

I would like to also thank Dr. Stephen Pinkosky for the tremendous amount of guidance with this project, the time you took out of your schedule to meet with me, and the expertise you provided for the project. Thank you to my committee members, Hertzel Gerstein and Guillaume Paré and the many collaborators and coauthors that contributed to this work.

I would lastly and most importantly like to thank my incredibly supportive family, whom I offload all my stresses on and who can always make me feel better. Thank you to my siblings and friends, for keeping me sane on the weekends and giving me an outlet during periods in which long lab days consumed my life. My focus and productivity during these times would have been significantly hampered had I not had those memories with you all. To end, I am beyond grateful to have had the opportunity to pursue higher education, I know that this is an immense privilege and I do not take that for granted.

List of Abbreviations

AAV	Adenoassociated virus
AAV8-Ttr-eYFP	Adenoassociated virus 8-transthyretin-enhanced yellow fluorescent protein
AAV8-Ttr-Cre	Adenoassociated virus 8- transthyretin-Cre recombinase
ACC	Acetyl-CoA carboxylase
ACLY	ATP-citrate lyase
ACLY hKO	ATP-citrate lyase hepatocyte knockout
ACSS2	Acyl-CoA synthetase short chain family member 2
ACSVL1	Very long-chain acyl-CoA synthetase
Acta2	Actin alpha 2
ADP	Adenosine diphosphate
Adgre1	Adhesion G protein-coupled receptor E1
AKT	Protein kinase B
ALT	Alanine transaminase
AMP	Adenosine monophosphate
ANOVA	Analysis of variance
AST	Aspartate aminotransferase
ATP	Adenosine 5'triphosphate
AUC	Area under the curve
BCA	Bichroninic acid
BemA	Bempedoic acid
BMDM	Bone marrow derived macrophage
Ccl2	C-C motif chemokine ligand 2
CCL_4	Carbon tetrachloride

CD4+ T cells	Cluster of differentiation 4 positive cells (T helper cells)
CD	Choline-deficient
ChREBP	Carbohydrate-responsive element binding protein
CoA	Coenzyme A
CO_2	Carbon dioxide
CCL_4	Carbon tetrachloride
CIC	Citrate/isocitrate carrier
CKD	Chronic kidney disease
Col1a1	Collagen, type I, alpha 1 chain
Col1a2	Collagen, type I, alpha 2 chain
Col3a1	Collagen, type III, alpha 1 chain
Col4a1	Collagen, type IV, alpha 1 chain
Col4a2	Collagen, type IV, alpha 2 chain
Col5a1	Collagen, type V, alpha 1 chain
Col5a3	Collagen, type V, alpha 3 chain
Col6a3	Collagen, type VI, alpha 3 chain
CPT1	Carnitine palmitoyltransferase 1
CPT2	Carnitine palmitoyltransferase 2
CTGF	Connective tissue growth factor
CVD	Cardiovascular disease
C57BL/6J	C57 black 6J
DAGs	Diacylglycerides
DAMPs	Damage-associated molecular patterns
dL	Decalitre
Dll1	Delta like canonical Notch ligand 1

Dll4	Delta like canonical Notch ligand 4
DMEM	Dulbecco's modified eagle medium
DNL	*De novo* lipogenesis
DPM	Disintegrations per minute
EA	Effect allele
EAF	Effect allele frequency
EDTA	Ethylenediaminetetraacetic acid
EGTA	Ethylene-bis(oxyethylenenitrilo)tetraacetic acid (Egtazic acid)
ER	Endoplasmic reticulum
F0	Fibrosis stage 0
F1	Fibrosis stage 1
F2	Fibrosis stage 2
F3	Fibrosis stage 3
F4	Fibrosis stage 4
FAS	Fatty acid synthase
FDA	Food and drug administration
FDR	False Discovery Rate
FFA	Free fatty acids
Foxo1	Forkhead box protein O1
GCK	Glucokinase
GCKR	Glucokinase regulator
GGT	Gamma-glutamyl transferase
GLP1R	Glucagon-like peptide 1 receptor
GLUT2	Glucose transporter 2

GLUT4	Glucose transporter 4
gm	Gram
GPAT1	Glycerol-3-phosphate acyltransferase 1
GSEI	Gene Set Enrichment Index
GSK1	Glycogen synthase kinase 1
GSK3	Glycogen synthase kinase 3
GTPase	GTP-binding proteins
GTT	Glucose tolerance test
HCC	Hepatocellular carcinoma
Hh	Hedgehog
HMG-CoA	3-hydroxy-3-methylglutaryl coenzyme A
HMGCR	3-hydroxy-3-methylglutaryl coenzyme A reductase
HSC	Hepatic stellate cell
HSD17B13	17β-Hydroxysteroid dehydrogenase type 13
HbA_{1c}	Hemoglobin A1C
HCl	Hydrochloric acid
HFD	High-fat diet (45% fat)
Hprt1	Hypoxanthine-guanine phosphoribosyltransferase 1
hsCRP	High sensitivity C-reactive protein
H & E	Hematoxylin and eosin
ICD	International Classification of Diseases
Ihh	Indian hedgehog protein
IL6	Interleukin 6
IL17	Interleukin 17
IL22	Interleukin 22

IRS2	Insulin receptor substrate 1
ITT	Insulin tolerance test
Jag1	Jagged1
kg	Kilogram
KHK	Ketohexokinase
KOH	Potassium hydroxide
LDL	Low-density lipoprotein
LDL-c	Low-density lipoprotein cholesterol
LFD	Low-fat diet (10% fat)
LOLXL2	Lysyl oxidase like 2
LPS	Lipopolysaccharides
LRAT	Lecithin retinol acyltransferase
LSEC	Liver sinusoidal endothelial cells
MCD	Methionine-choline deficient diet
MBOAT7	Membrane bound O-acyltransferase domain containing 7
mg	Milligram
Mki67	Marker of proliferation Ki-67
mL	Milliliter
mM	Millimolar
MR	Mendelian randomization
MRI-PDFF	Magnetic resonance imaging protein density fat fraction
mRNA	Messenger ribonucleic acid
MTC	Masson's trichrome
mTOR	Mammalian target of rapamycin
NAFL	Non-alcoholic fatty liver

NAFLD	Non-alcoholic fatty liver disease
NASH	Non-alcoholic steatohepatitis
ND	Non-alcoholic steatohepatitis diet (40% fat, 20% fructose, 2% cholesterol)
Ng	Nanograms
OA	Other allele
OAA	Oxaloacetate
OCA	Obeticholic acid
OGTT	Oral glucose tolerance test
T2D	Type 2 Diabetes
TAA	Thioacetamide
TCA	Tricarboxylic acid
TG	Triglyceride
Thr446	Threonine 446
TLR4	Toll-like receptor 4
TLR	Toll-like receptor
TM6SF2	Transmembrane 6 superfamily member 2
TMA	Trimethylamine
TN-ND	Thermoneutral NASH diet
TN	Thermoneutral
TNFα	Tumor necrosis factor alpha
Ttr	Transthyretin
p38 MAPK	p38 mitogen-activated protein kinase
pACLY	Phospho-ATP-citrate lyase
PCA	Principal component analysis

PI3K	Phosphoinositide 3-kinases
PKCε	protein kinase Cε
PNPLA3	Patatin-like phospholipase domain-containing protein 3
PPAR	Peroxisome proliferator-activated receptor alpha
PRS	Polygenic score
pSMAD2	Phospho-SMAD family member 2
pSMAD3	Phospho-SMAD family member 3
PSR	Picrosirius red
PTT	Pyruvate tolerance test
RER	Respiratory exchange ratio
RFI	Relative fluorescence units
Rho	Ras homologous
RNA-seq	Ribonucleic acid sequencing
RT	Room temperature
RT-PCR	Reverse transcription polymerase chain reaction
SCD1	Stearoyl-coenzyme A desaturase 1
ScRNA-seq	Single cell ribonucleic acid sequencing
SEM	Standard Error of the Mean
Ser450	Serine 450
Ser454	Serine 454
shRNA	Short hairpin RNA
siRNA	Short interfering ribonucleic acid
Slc27a2	Solute carrier family 27 member 2
Smad2	SMAD family member 2
Smad3	SMAD family member 3

Smad7	SMAD family member 7
SNP	Single nucleotide polymorphism
SPF	Specific pathogen free
SREBP1c	Sterol response element binding protein 1c
ssGSEA	Single-sample Gene Set Enrichment Analysis
STZ	Streptozotocin
TAZ	Tafazzin
TN	Thermoneutrality
Tnf	Tumor necrosis factor
TGF-β	Transforming growth factor-beta
UPLC-MRM MS	Ultra-performance liquid chromatography (UPLC) mass spectrometry (MS) in multiple-reaction-monitoring (MRM)
VEGF	Vascular endothelial growth factor
Veh	Vehicle
VLDL	Very-long density lipoprotein
WT	Wildtype
YAP	Yes-associated protein
α-SMA	Alpha smooth muscle actin
μM	Micromolar

Statement of contributions

Chapters 2 & 3:

These chapters are an extraction from a manuscript published in *Cell Metabolism*. 2022. 34(6): pp. 919-936.e8 and includes all research projects completed during the Ph.D. These projects were completed between January 2019 and April 2022. Together, they summarize the development and characterization of a novel mouse model of NASH and hepatic fibrosis, and utilizing this model, they investigate the role of genetic and pharmacological ACLY targeting in NASH.

Authors: **Morrow MR**, Batchuluun B, Wu J, Ahmadi E, Leroux JM, Mohammadi-Shemirani P, Desjardins EM, Wang Z, Tsakiridis EE, Lavoie DCT, Reihani A, Smith BK, Kwiecien JM, Lally JSV, Ask K, Jiang L, Paré G, Pinkosky SL, and Steinberg GR.

Contributions:

MRM, SLP, JSVL, and GRS were responsible for the conception and design of the studies. MRM managed mouse cohorts used in Figures 3.1-3.9, 3.11-3.12 and Appendix B. BB performed primary hepatic stellate cell isolations and experiments, and flow cytometry experiments (Figure 2.1, 3.13, 3.15). JW performed all transcriptomics analyses included in Figures 3.1, 3.2, 3.4, 3.11, 3.12. JMK and EA assigned liver histology scorings (Figures 3.2B, 3.3B, 3.6E, 3.7C, 3.8E). JML weighed mice, measured mouse adiposity (Figures 3.1A-B, 3.6D-E, 3.7B), and assisted with metabolic testing (Figure 3.9A-C). EMD helped manage mouse cohorts used in Figure 3.8-3.9. ZW and LJ performed GC/MS analysis on serum and liver tissue (Figure 3.5G-I, 3.6B, 3.7D, 3.8F). EET assisted in managing mouse cohorts used in Appendix B. DCTL and AR performed %picrosirius red positive quantifications (Figure 3.2E, 3.3C, 3.6I, 3.7H, 3.8K). BKS performed BMDM experiments (Figure 3.14A-B). PMS and GP performed Mendelian randomization analysis (Tables 2.1, 3.1-3.2). All experiments in Figure 3.10 were performed by SMC laboratories Inc. MRM completed all other experiments included in the figures of this dissertation, including performing all *in vivo* measurements (GTT, ITT, PTT, metabolic cages, weighing mice, measuring adiposity), mouse tail-vein injections of AAV8, changing mouse diets, tissue extraction, tissue processing, taking microscope images, mRNA extraction and qRT-PCR, western blots, primary hepatocyte and hepatic stellate cell experiments, analysis on serum, liver, and primary cell media (cholesterol, triglycerides, ALT, AST, glucose, insulin, ketone bodies), primary hepatocyte and stellate cell experiments, and analysis and visualization of data. MRM and GRS wrote the *Cell Metabolism* manuscript. SLP and GRS supervised the project and edited the *Cell Metabolism* manuscript.

Table of Contents

Chapter three

Chapter four

LIST OF TABLES

LIST OF FIGURES

CHAPTER 1: INTRODUCTION

1. Introduction

1.1 NAFLD

1.1.1 Background

Non-alcoholic fatty liver disease (NAFLD) is a collection of liver pathologies that stem from an excessive accumulation of fat in the liver. NAFLD is often considered the hepatic manifestation of metabolic disease as its prevalence is concurrent with non-communicable diseases such as obesity, type 2 diabetes (T2D), and cardiovascular diseases (CVDs) (Glass *et al.*, 2019). It has become the most common cause of chronic liver disease in the developed world, making it a significant burden on the healthcare system and the general population (Younossi *et al.*, 2016). While historically, NAFLD presents in middle to late adulthood, paralleling the rising rates of childhood obesity, its appearance in children has also increased (Peng *et al.*, 2021).

NAFLD encompasses a continuum of liver pathologies ranging from simple steatosis (non-alcoholic fatty liver) to non-alcoholic steatohepatitis (NASH) and hepatic fibrosis (Chalasani *et al.*, 2018). NAFLD is defined as hepatic fat accumulation (>5% of liver weight) in the absence of excessive alcohol and is estimated to have a global prevalence of 25% (Younossi *et al.*, 2016). Through mechanisms not entirely understood, the build-up of fat in the liver can cause lipotoxicity, which in turn triggers hepatic inflammation and hepatocellular injury (hepatocyte ballooning), the defining features of NASH (Chalasani *et al.*, 2018). This lipotoxicity and inflammation is what ultimately contributes to hepatic fibrogenesis. Given the invasiveness of current diagnostic techniques

for NASH, the exact prevalence is likely underrepresented but is estimated to be between 1.5% and 6.45% (Younossi *et al.*, 2016).

The presence of NASH and fibrosis greatly increases the risk of additional hepatic complications including hepatocellular carcinoma (HCC), hepatic cirrhosis, and liver failure. Patients with NASH have increased mortality, and NASH is on a trajectory to pass hepatitis C virus (HCV) as the leading cause of liver transplantation (Wong *et al.*, 2015). The clinical burden of NAFLD however is not confined to liver-related complications, as there is growing evidence that NAFLD increases the risk of T2D, CVDs, and chronic kidney disease (CKD) (Musso *et al.*, 2011, 2014; Cao *et al.*, 2021).

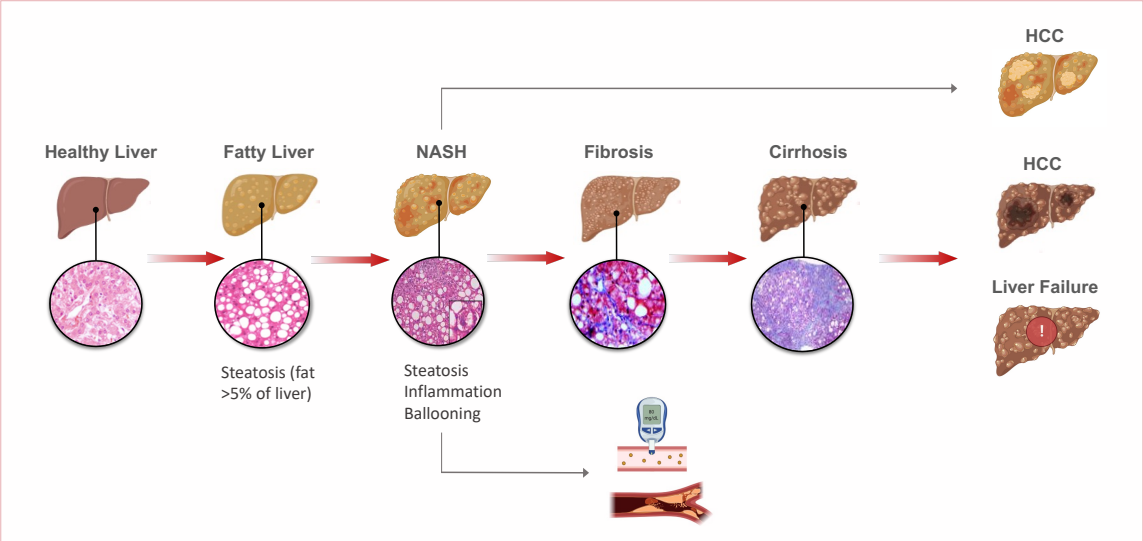

Figure 1.1 NAFLD is a continuum of liver pathologies

NAFLD pathologies range from simple steatosis to cirrhosis, HCC, or liver failure. A combination of genetic and environmental factors, and comorbidities, contributes to the development of fatty liver (steatosis), which is defined by liver fat accumulation exceeding 5% of the liver. In some individuals, fatty liver will progress to NASH, which is characterized by the presence of hepatic inflammation and cell death (ballooning) in addition to steatosis. NASH greatly increases the risk for the development of liver fibrosis, HCC (without cirrhosis), insulin resistance, and CVDs. If hepatic fibrosis persists, hepatic cirrhosis and the replacement of healthy tissue with scar tissue may develop. This further increases the risk for the development of HCC or the loss of the liver parenchyma and subsequent liver failure. Histology images used in this figure are adapted from (Friedman, 2013; Rinella, 2015; Glen *et al.*, 2016). NASH: non-alcoholic steatohepatitis; HCC: hepatocellular carcinoma. CVDs: cardiovascular diseases.

1.1.2 Fibrosis development in NAFLD

Although increases in steatosis may be the initiator of disease development, habitual, excessive, and untreated accumulation of collagen and extracellular matrix components are the underlying contributors to fibrosis development (Tsuchida and Friedman, 2017; Khomich, Ivanov and Bartosch, 2019). In normal tissue injury, fibrogenesis is a beneficial wound-healing process, which acts to preserve and regenerate tissue structure and integrity. However, in a chronically inflamed environment with sustained and progressive signals, fibrogenesis remains elevated and scar tissue accumulates.

Human hepatic fibrosis stages range from F0 - F4 (Table 1.1) (Heyens *et al.*, 2021). In attempts to capture the high heterogeneity of human fibrosis progression and presentation, stage F1 is subclassified into A, B, and C, which include a distinction between fibrosis development in different hepatic areas. 1A and 1B reflect mild (delicate collagen fibers) and moderate (dense collagen fibers) perisinusoidal fibrosis respectively, and 1C reflects portal-only fibrosis, without perisinusoidal. Stage 1C is typically observed in pediatric patients but has been reported in severely obese adults (Takahasi and Fukusato, 2014). Stage F2 to F4 are considered clinically significant, while stages F3 to F4 are classified as advanced fibrosis (Alkhouri and McCullough, 2012). Fibrosis progression can develop over years and often remains asymptomatic until a late stage (F3 or F4).

Table 1.1. Human fibrosis stages

Fibrosis Stage	Description
F0	None
F1	Mild to moderate fibrosis 1A Mild zone 3 perisinusoidal fibrosis 1B Moderate zone 3 perisinusoidal fibrosis 1C Only portal/periportal fibrosis
F2	Moderate zone 3 perisinusoidal/pericellular and portal/periportal fibrosis
F3	Bridging fibrosis
F4	Cirrhosis

1.1.3 Methods used to assess NAFLD

Currently, a liver biopsy is the only way to definitively prove a NASH and fibrosis diagnosis (see Table 1.2 for NAFLD scoring criteria). However, there are several non-invasive biomarkers and tools, which are being developed and/or are in use, to estimate the presence of NAFLD. For example, indices and scores are used to estimate disease severity based on measurements of risk factors (BMI, blood triglycerides, insulin resistance, HbA_{1c}, hypertension, blood glucose), and levels of circulating liver disease biomarkers (alanine transaminase (ALT), aspartate transaminase (AST), platelet count, and gamma-glutamyl transferase (GGT)) (Wong *et al.*, 2018). Diagnostic scores such as the fibrosis-4 score (Fib-4), the fatty liver index, and the NAFLD fibrosis score, have been developed based on cut-off values for these risk factors and biomarkers (Wong *et al.*, 2018). Liver imaging is also

employed to detect liver fat (abdominal ultrasonography or MRI-PDFF) and liver fibrosis (measured as liver stiffness by transient elastography (Fibroscan) or magnetic resonance elastography (MRE)) (Wong *et al.*, 2018).

There have been great advancements in the development of non-invasive biomarkers for NASH, however many of these still have their drawbacks and do not represent a gold standard for detecting all components of NAFLD (steatosis, NASH, and fibrosis). Current NAFLD guidelines suggest using screening tools to determine whether individuals present a high risk for NASH and advanced fibrosis, (e.g., the presence of metabolic syndrome, a high Fib-4 or NAFLD liver score). If patients are at high risk, liver biopsies are warranted to confirm the degree of disease (Alkhouri and McCullough, 2012). There is therefore still a great need for better predictive non-invasive diagnostic tools.

Table 1.2. Human NASH scoring criteria

Item	Definition	Score
NAFLD Activity Score (NAS)		
Steatosis score (0-3)	<5%	0
	5%-33%	1
	>33-66%	2
	>66%	3
Hepatocellular Ballooning (0-2)	None	0
	Few balloon cells	1
	Many cells/prominent ballooning	2
Lobular inflammation (0-3)	No foci	0
	<2 foci per 200X field	1
	2-4 foci per 200X field	2
	>4 foci per 200X field	3

1.1.4 Therapeutic importance of targeting NASH

As mentioned, NASH greatly increases the risk for progression to fibrosis, cirrhosis, and HCC. Fibrosis occurs in approximately 30-40% of individuals with NASH (Ekstedt *et al.*, 2006), and once developed, fibrosis stage becomes the strongest predictor of mortality in NASH patients (Angulo *et al.*, 2015; Ekstedt *et al.*, 2015; Taylor *et al.*, 2020). If the initiation and progression of fibrosis are left untreated, this may lead to cirrhosis and subsequent liver failure, or HCC, conditions, which collectively, are more challenging to treat. Most patients with NASH remain asymptomatic without clinical outcomes for decades, while others progress rapidly. Therefore, when most patients present clinically, they have likely progressed to NASH and advanced fibrosis (F3-F4), or possibly to end-stage liver disease (e.g., liver cirrhosis or HCC) (Heyens *et al.*, 2021). It is, therefore, of great clinical importance to target the reversal of NASH and fibrosis. To study this, it is important to first understand the underlying disease mechanisms causing the progression of NAFLD, to NASH and fibrosis; this will be the focus of the following sections.

1.2 Liver cell types

The liver performs an array of biological functions that support digestion, metabolism, detoxification, and vitamin storage, among others. Its dual blood supply results in the exposure to a multitude of compounds from the environment, diet, and peripheral organs. These functions are executed by the harmonized activity of four main liver cell types – hepatocytes, liver sinusoidal endothelial cells (LSECs), Kupffer cells, and hepatic stellate cells (Ding *et al.*, 2016). Hepatocytes, the parenchymal cells of the liver, constitute

approximately 70% of the total liver cell population and perform the basic functions of the liver, including lipid and drug metabolism (Ding *et al.*, 2016). LSECs are highly specialized endothelial cells that form the lining of the hepatic sinusoids. They have high endocytic activity and play important roles in substance exchange (including bidirectional lipid exchange), blood flow regulation, and immune regulation (Hammoutene and Rautou, 2019; Wang and Peng, 2021). Fenestrations that exist between adjacent LSECs are essential in enabling efficient substrate exchange between the sinusoid and hepatocytes. Kupffer cells, the liver's resident macrophages, contribute to innate immunity and protect against inflammation and infection. Hepatic stellate cells in their quiescent state function to store vitamin A and lipids and upon NASH-induced activation become a key cell type in the development of fibrosis.

Apart from these 4 main cell types, there are indeed several others that play essential roles in the hepatic microenvironment but make up a smaller percentage of the hepatic cell population; these include cholangiocytes (biliary epithelial cells) and various immune cells (neutrophils, B lymphocytes, T lymphocytes, and natural killer (NK) cells). Under pathologic conditions, including those in NAFLD, drastic changes in cell type composition and cell function are observed.

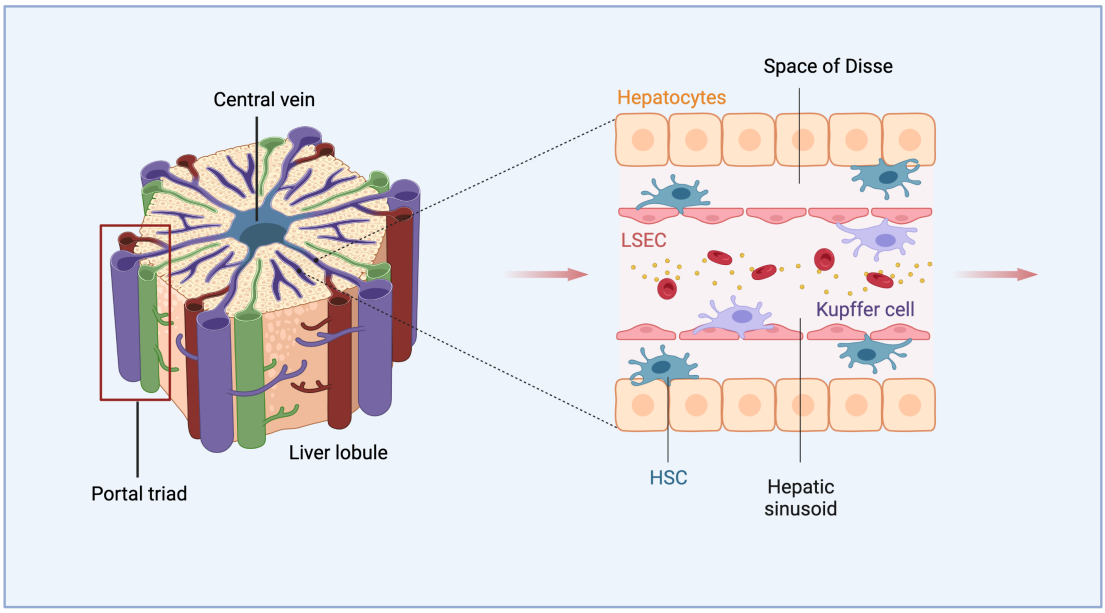

Figure 1.2. Anatomy of the liver sinusoid

The liver is made up of several repeating hexagonal structures called liver lobules. Liver lobules contain six portal triads (each triad is made up of a portal vein, hepatic artery, and bile duct) that drain their contents into the central vein. Blood and bile flow from the portal triads through the hepatic sinusoid and eventually into the central vein. The hepatic sinusoid is a type of small blood vessel that is lined with LSECs, which control material exchange from the sinusoid into hepatocytes. Specialized resident macrophages, named Kupffer cells, also exist in the sinusoid and play an important role in hepatic immune function. The space of Disse sits between the sinusoid and hepatocytes and is home to hepatic stellate cells. Hepatic stellate cells store Vitamin A and are thought to play a role in immune function and maintenance of the sinusoid's basement membrane. LSECs: liver sinusoidal endothelial cells.

1.2.1 NASH-driven changes to liver cells

In NAFLD, fat accumulation and subsequent lipotoxicity contribute to cell type-specific changes. In hepatocytes, fat accumulation leads to lipotoxicity, cell stress, and cell death. Accumulation of fat in Kupffer cells results in the adoption of an inflammatory phenotype, and in hepatic stellate cells leads to cell activation and the production of pro-fibrotic factors (Heyens *et al.*, 2021). Kupffer cells increase the secretion of inflammatory cytokines, such as interleukin-6 (IL-6) and tumour necrosis factor (TNF), which are associated with NASH progression (Tomita *et al.*, 2006; Herck *et al.*, 2019). In NAFLD, LSECs are subject to capillarization, loss of *fenestrae*, and reduced vasodilator production. LSECs also release inflammatory mediators, which increase inflammatory cell recruitment and further promote liver injury and inflammation (Hammoutene and Rautou, 2019).

In addition to changes in cell functions, single-cell RNA sequencing (scRNA-seq) of healthy and NASH adult livers, reveals significant changes in cell type composition (Pantano *et al.*, 2021). As disease progresses, a loss of hepatocytes and gain of hepatic stellate cells and macrophages is observed (Pantano *et al.*, 2021). Immune cell infiltration is also observed in NASH, where monocyte-derived macrophages and CD4+ T cells are recruited to the inflammatory microenvironment (Jiang *et al.*, 2021; Nati, Chung and Chavakis, 2022). These changes in the various cell types are communicated to one another through inflammatory and metabolic signals, in most cases causing, or further perpetuating, the pathologic phenotype.

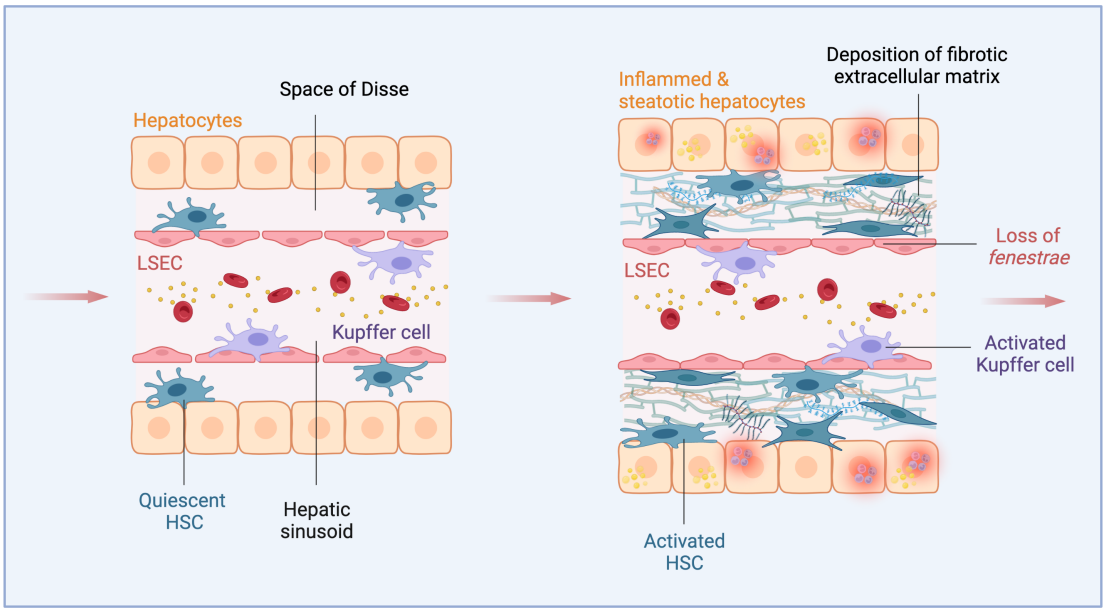

Figure 1.3. NASH-driven changes to the liver sinusoid

In NASH, hepatocytes become steatotic, inflamed, and injured. Kupffer cells become "activated" and develop a pro-inflammatory, immune cell recruiting phenotype. LSECs lose their fenestrations – pores between cells that facilitate efficient material exchange between the sinusoid lumen and hepatocytes. Hepatic stellate cells transdifferentiate from their quiescent state to an activated state characterized by increased proliferation and increased production and secretion of extracellular matrix. This accumulation of extracellular matrix leads to hepatic fibrosis. LSEC: liver sinusoidal endothelial cells.

1.2.2 Hepatic stellate cells

Hepatic stellate cells are liver-specific mesenchymal cells that play an essential role in liver physiology and fibrogenesis. Cell lineage analysis supports that hepatic stellate cells, along with other liver fibrogenic cells, originate from the mesoderm-derived mesothelium (Asahina, 2012). Hepatic stellate cells are nestled between LSECs and hepatocytes, in the space of Disse (Tsuchida and Friedman, 2017). In normal physiological conditions, quiescent hepatic stellate cells exude dendritic-like extensions in the space of Disse where they form a basement membrane-like matrix (LeCluyse, Norona and Presnell, 2018). They maintain and regulate the sinusoidal structure by synthesizing extracellular matrix proteins. They are also thought to play a role in the immune response to injury (LeCluyse, Norona and Presnell, 2018). For example, hepatic stellate cells express toll-like receptor 3s (TLR3), which function to induce interferon, cytokine, and chemokine expression and secretion (Wilson *et al.*, 2014).

In chronic states of inflammation and injury, such as that caused by NASH lipotoxicity, hepatic stellate cells drastically change their phenotype and transdifferentiate into an active state. Activated cells lose their ability to store vitamin A and begin synthesizing extracellular matrix proteins and proinflammatory cytokines. These activated cells obtain a myofibroblast-like phenotype with proliferative, contractile, inflammatory, and chemotactic capabilities (Tsuchida and Friedman, 2017; Khomich, Ivanov and Bartosch, 2019). Cell fate tracing establishes that hepatic stellate cells contribute to 82-96%

of liver myofibroblasts in models of toxic, biliary, and fatty liver disease, and thus are the key contributors to fibrosis development (Mederacke *et al.*, 2013).

1.2.3 Mechanisms involved in hepatic stellate cell activation

As discussed, NASH is characterized by a microenvironment of stressed and damaged hepatocytes, increased immune cell filtration, and pro-inflammatory LSECs and Kupffer cells. These cell types communicate with each other and with hepatic stellate cells to induce activation through a panoply of signals. These signals are communicated via the following mediators: inflammatory cytokines (e.g., IL-17, IL-22), Hedgehog (Hh) ligand, damage-associated molecular patterns (DAMPs), vascular endothelial growth factor (VEGF), transforming growth factor-β (TGF-β), platelet-derived growth factor (PDGF), Notch receptor ligands (e.g., Delta-like-ligand 1 (DII1), Delta-like-ligand 4 (DII4), and Jagged 1 (Jag-1)), G protein-coupled receptor (GPCR) agonists, Wnt-protein ligand, innate immune signals via TLRs, and reactive oxygen species (Tsuchida and Friedman, 2017). Most of these factors extracellularly bind to hepatic stellate cells and trigger signalling cascades that contribute to some component of hepatic stellate cell activation. Some of these factors, as well as others, are expressed and released from activated hepatic stellate cells, and act in an autocrine or paracrine manner to exacerbate the pro-fibrotic environment.

Key fibrogenic and proliferative signalling events in hepatic stellate cells that are initiated by external stimuli include TGF-β/SMAD, Notch, Wnt/-catenin, Hedgehog, and Hippo-YAP/TAZ signalling (Mannaerts *et al*., 2015; Tsuchida and Friedman, 2017). TGF-

β is a crucial cytokine in fibrosis progression. TGF-β binds to TGF-β receptors on hepatic stellate cells and induces α-smooth muscle actin (α-SMA) and type I collagen expression, major components of the fibrotic extracellular matrix. TGF-β induces these transcriptional changes through SMAD signalling or non-SMAD-dependent signalling (e.g., Rho/GTPase, PI3K/Akt, mTOR, P38 MAPK) (Dewidar *et al.*, 2019). In addition to extracellular signals, intracellular mediators of hepatic stellate cell activation have been identified and include ER stress, autophagy, and free cholesterol accumulation (Tsuchida and Friedman, 2017). These mechanistic discoveries of the causes of hepatic stellate cell activation have led to great prospects for developing novel therapeutics in NASH-driven hepatic fibrosis. In summary, stellate cell activation is a key feature of NASH, and it is therefore important to understand the mechanisms that lead to a microenvironment that favours this activation.

1.3 The metabolic basis of NASH

The cause of NAFLD and its progression to NASH and fibrosis is complex and multifactorial. This is reflected in its high heterogeneity, progressing at different rates, and showing different clinical manifestations in those affected. While historically, most liver diseases were associated with toxicity caused by viruses and drugs, this represents only a small portion of the people with NAFLD. And although fibrosis and inflammation are the clinical defining triggers of a NASH diagnosis, it is becoming increasingly recognized that NASH is a metabolically driven disease. Therefore, to understand its etiology, it is important to first define the role of the liver in regulating whole-body energy metabolism and the molecular pathways, that when altered, drive disease development.

1.3.1 Hepatic regulation of energy metabolism

1.3.1.1 Hepatic energy metabolism in the postprandial state

Under normal physiological conditions, the liver elegantly integrates nutrient signals with the energetic demands of the entire body. In the postprandial state, elevated blood glucose stimulates the release of insulin from pancreatic β-cells, which signals cells to enter an energy-storing and molecule-building, fed state. In peripheral tissues (adipose and skeletal muscle) insulin increases glucose uptake and oxidation. Dietary fat and cholesterol (from gut-derived chylomicrons) are taken up by the adipose tissue and stored as triglycerides in lipid droplets.

Following a meal, the liver will be exposed to high levels of glucose from the portal vein, and therefore will take up large amounts of glucose to help maintain normoglycemia. Although this hepatic glucose uptake is insulin-independent, insulin regulates several processes in the liver to assist with glucose utilization and storage, including suppression of gluconeogenesis, glycogenolysis and fatty acid oxidation, while increasing glycogenesis and *de novo* lipogenesis (DNL). The resulting free fatty acids from DNL, chylomicron remnants (from the gut), and other systemic sources (namely adipose tissue) are then esterified to synthesize triglycerides, phospholipids, or cholesterol esters. These lipid species are successively stored in hepatic lipid droplets and membrane structures or secreted into circulation as part of very-low-density lipoprotein (VLDL) particles (Rui, 2014). In the postprandial state, however, increases in parasympathetic activity favour lipid storage by inhibiting VLDL secretion (Enjoji, Kohjima and Nakamuta, 2016). Fatty acid

and cholesterol synthesis are bioenergetic processes. ATP generated from high rates of glycolysis and oxidative phosphorylation will provide energy to support these pathways. This high ATP therefore also acts as a cellular signal to shift into an anabolic state.

1.3.1.2 Hepatic energy metabolism in the fasted state

In the fasted state, the primary role of the liver is to synthesize and secrete glucose. A reduction in blood glucose stimulates glucagon release and decreases insulin secretion. High blood glucagon signals tissues to transition into a fasted state of metabolism, characterized by restoring blood glucose and activating ketogenesis. Glucagon signals to the liver to inhibit glycolysis, increase glycogenolysis, and increase gluconeogenesis, resulting in increased cellular glucose production from glycogen breakdown and endogenous biosynthesis respectively. With glycolysis inhibited, the liver also shifts to utilizing fatty acid oxidation as a primary source of ATP to sustain gluconeogenesis. Amino acids are delivered from the skeletal muscle to be used as gluconeogenic substrates and further sustain hepatic glucose production.

A reduction in circulating insulin also relieves the inhibition of adipose tissue lipolysis. This leads to increased plasma free fatty acids, which are then delivered to the liver and represent a major source of free fatty acids in the liver. A smaller portion of free fatty acids can also be derived from liver lipolysis. These fatty acids are then oxidized to create ATP through fatty acid oxidation, which simultaneously produces several acetyl-CoA molecules (Enjoji, Kohjima and Nakamuta, 2016). This abundance of mitochondrial acetyl-CoA will flux through the TCA cycle and fully oxidize to CO_2 to produce energy.

However, in the fasted state, oxaloacetate, is used as a key carbon source in gluconeogenesis and is therefore limited. Acetyl-CoA levels will exceed the oxidative capacity of the TCA cycle. This limits the flux of acetyl-CoA through the TCA cycle and shunts acetyl-CoA to ketogenesis for the formation of ketone bodies. Ketogenesis is also induced directly by low insulin and high glucagon (Jones, 2016). Ketone bodies enter the circulation to be used by peripheral tissues as an alternative source of energy (through conversion back to acetyl-CoA). Gluconeogenesis is a liver-specific process and thus in peripheral organs oxaloacetate is abundant and TCA cycle flux is high, allowing for energy production from ketone-body derived acetyl-CoA.

In summary, in the fasted state, hepatic fatty acid oxidation and glucose production are elevated, while DNL activity is inhibited. The catabolic inflow of carbons (i.e., in acetyl-CoA) from fatty acid oxidation into the TCA cycle, sustains the gluconeogenic outflow of carbons (i.e., oxaloacetate). This TCA cycle flux in the fasted state has been confirmed with metabolic tracing in humans and rodents (Magnussons *et al.*, 1991; Large *et al.*, 1997; Jones *et al.*, 1998, 2001; Burgess *et al.*, 2005; Jin *et al.*, 2005; Sunny *et al.*, 2011).

1.3.2 The role of ACLY in regulating hepatic metabolism

As both a product of oxidative phosphorylation and the primary building block for fatty acid and cholesterol biosynthesis, acetyl-CoA is used by cells to integrate nutrient status with energy levels. Acetyl-CoA concentrations control the flow of substrates toward storage or energy production in the fed or fasted states respectively. High levels of acetyl-

CoA act as a signal for growth or fed states and promote its use in DNL (Shi and Tu, 2015). In contrast, under fasted conditions, acetyl-CoA is concentrated in the mitochondria for ATP and ketone body synthesis (Shi and Tu, 2015).

A key enzyme that synthesizes acetyl-CoA and sits at this intersection of nutrient catabolism and biosynthesis in the liver is ACLY. ACLY is a cytosolic enzyme that is most abundantly expressed in the liver and the adipose tissue (Chypre, Zaidi and Smans, 2012). The crystal structure of human ACLY has recently been resolved (Verschueren *et al.*, 2019; Wei *et al.*, 2019). ACLY is comprised of an N-terminal acyl-CoA synthase homology (ASH) domain (residues 1-806) connected by a flexible linker (residues 807-858) to a C-terminal citrate synthase homology (CSH) domain (residues 859-1101) (Verschueren *et al.*, 2019; Wei *et al.*, 2019). It is a homotetramer of four identical subunits and contains six domains, with domain 1 containing the CoA-binding site, domain 2 containing the catalytically phosphorylated His760 residue, domains 3 and 4 forming the ATP binding site, and domain 5 containing the citrate-binding site (Wei *et al.*, 2019).

As indicated, when nutrient signals are high, TCA cycle intermediates accumulate, and citrate is transported back into the cytosol by the citrate/isocitrate carrier (CIC). In the presence of ATP and CoA, ACLY catalyzes the cleavage of cytosolic citrate to oxaloacetate and acetyl-CoA (Softic, Cohen and Kahn, 2016). The reaction is initiated when the enzyme is phosphorylated on its histidine 760 residue by ATP, which initiates phosphorylation of bound citrate, forming an enzyme-bound citryl-phosphate. Citryl-CoA is formed by the addition of a CoA group, and then cleaved to release acetyl-CoA and oxaloacetate

(Pinkosky *et al.*, 2017). As described, oxaloacetate is a substrate for gluconeogenesis while acetyl-CoA is a precursor for both DNL and cholesterol synthesis. In DNL, acetyl-CoA is catalyzed by acetyl-CoA carboxylase (ACC) to malonyl-CoA, which is a substrate for fatty acid synthase (FAS) and an allosteric inhibitor of fatty acid oxidation. In cholesterol synthesis, three molecules of acetyl-CoA are used to form mevalonate. The conversion of 3-hydroxy-3-methylglutaryl-coenzyme A (HMG-CoA) to mevalonate is the rate-limiting step in cholesterol synthesis and is catalyzed by the enzyme HMG-CoA reductase (HMGCR). Thus, alterations in ACLY activity have the potential to impact fatty acid and cholesterol synthesis, and gluconeogenesis.

Hepatic ACLY activity is regulated by gene expression and post-translational modifications. ACLY expression is regulated by 3 main transcription factors that regulate the entire lipogenic enzyme set: sterol regulatory element-binding protein 1c (SREBP1c), carbohydrate-response element binding protein (ChREBP) (Ishii *et al.*, 2004; Ma, Robinson and Towle, 2006), and liver X receptors (LXRs) (Cha and Repa, 2007). ACLY expression, however, is largely regulated by elevated levels of SREBP1c in response to elevated glucose and insulin (in the postprandial state). In addition to transcriptional regulation, ACLY activity is enhanced by insulin through phosphorylation at Ser454 by phosphoinositide 3-kinase (PI3K)/protein kinase B (Akt) signalling (Ramakrishna, D'Angelo and Benjamin, 1990; Hughes *et al.*, 1992). Insulin, therefore, increases both the expression and activity of ACLY. With its critical positioning in hepatic metabolism, ACLY has become an attractive target for several diseases, including NAFLD. To

emphasize the therapeutic potential of this, it is important to first discuss some of the underlying mechanisms of NAFLD.

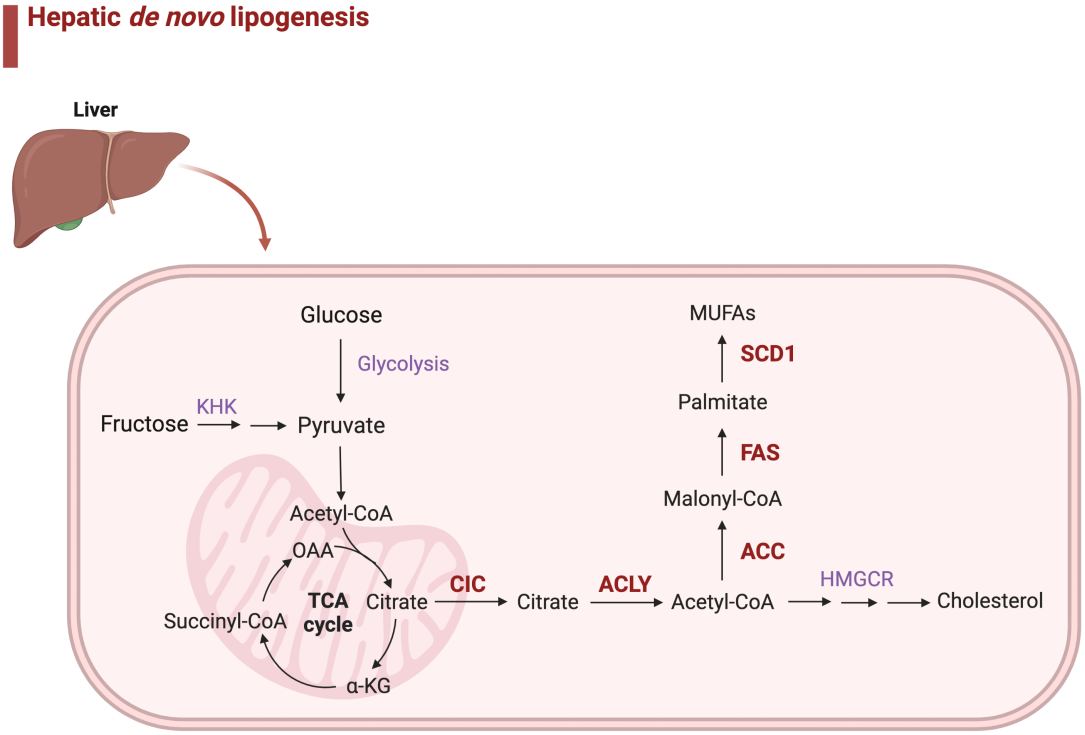

Figure 1.4. Hepatic DNL

Under normal conditions, DNL converts excess glucose and fructose into fatty acids. Mitochondrial acetyl-CoA derived from glucose or fructose will enter the TCA cycle and be converted to citrate. If nutrient availability is high, rather than being fully oxidized to CO_2, citrate will exit the mitochondria via CIC. Cytosolic citrate is converted to acetyl-CoA by ACLY. Cytosolic acetyl-CoA is then used as a substrate for fatty acid synthesis by DNL enzymes ACC, FAS, and SCD1, and cholesterol synthesis by the rate-limiting enzyme HMGCR. DNL: *de novo* lipogenesis; KHK: ketohexokinase; oxaloacetate: oxaloacetate; α-KG: α-ketoglutarate; CIC: citrate/isocitrate transporter; ACLY: ATP-citrate lyase; ACC: acetyl-CoA carboxylase; FAS: fatty acid synthase; SCD1: stearoyl-CoA desaturase 1; HMGCR: HMG-CoA reductase.

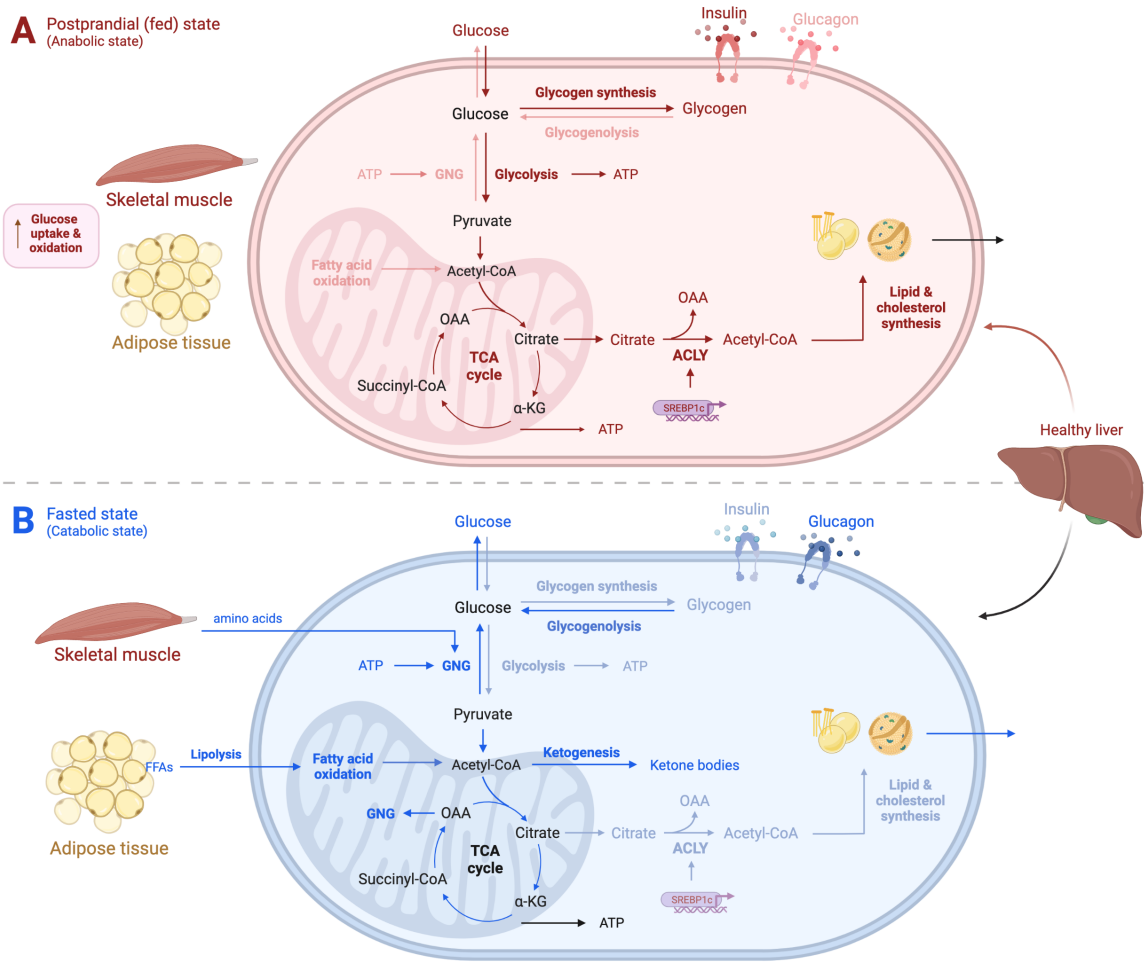

Figure 1.5. Hepatic metabolism in postprandial and fasted states

A) In the postprandial state, insulin signals are high. Insulin-dependent pathways include increased glucose uptake and oxidation in the skeletal muscle and adipose tissue. At the liver, insulin-dependent pathways include increased glycogen synthesis and glycolysis and decreased glycogenolysis and gluconeogenesis, which together promote glucose oxidation to acetyl-CoA. Insulin also signals the liver to decrease lipolysis and fatty acid oxidation, increase SREBP1c and lipogenic genes, such as ACLY, and increase DNL and cholesterol synthesis. TCA cycle flux and ATP production via oxidative phosphorylation are high. Pathways, arrows, enzymes, receptors, or metabolites in dark red are upregulated or highly active, and light pink arrows, receptors, enzymes, or metabolites are downregulated or lowly active in the fed state.
B) In the fasted state, insulin signals are low and glucagon signals are high. Glucagon-dependent pathways in the liver include suppression of glycolysis and increased

glycogenolysis and gluconeogenesis, resulting in increased glucose to sustain stable blood glucose concentrations. Gluconeogenic substrates (amino acids) are delivered to the liver from the skeletal muscle to further support this hepatic glucose production. Glucagon also signals to the liver to increase fatty acid oxidation and ketogenesis and decrease DNL and cholesterol synthesis. Reduced circulating insulin relieves the suppression of adipose tissue lipolysis, increasing circulating free fatty acids, which are taken up by the liver. Hepatic free fatty acids are oxidized in the mitochondria to create ATP. Excess acetyl-CoA from fatty acid oxidation will be used in ketogenesis to generate ketone bodies, which will be transported to peripheral tissues and used as alternative energy sources. Pathways, arrows, enzymes, receptors, or metabolites in dark blue are upregulated or highly active, and light blue arrows, receptors, enzymes, or metabolites are downregulated or lowly active in the fasted state. GNG: gluconeogenesis; ATP: adenosine triphosphate; TCA: tricarboxylic acid; OAA: oxaloacetate; α-KG: α-ketoglutarate; ACLY: ATP-citrate lyase; SREBP1c: sterol response element binding protein 1c; FFAs: free fatty acids.

1.4 Etiology of NAFLD

The main cause of NAFLD is thought to be excess energy intake and reduced energy expenditure through overnutrition and sedentarism respectively (Stefan, Häring and Cusi, 2019). These behavioural patterns along with the overconsumption of fructose, have been strongly linked to gut microbiome dysbiosis, obesity, insulin resistance, and dyslipidemia, all of which are primary contributors to NAFLD (Stefan, Häring and Cusi, 2019). Other factors, including genetic variants, and exposure to liver-damaging drugs, have been linked to NAFLD, but are thought to play a smaller role in most cases (Friedman *et al.*, 2018; Stefan, Häring and Cusi, 2019; Satapathy *et al*., 2015).

1.4.1 Lipotoxicity in NAFLD

Despite the complexities in the etiology of NAFLD, hepatic lipid accumulation is indisputably the defining feature of this disease. Before discussing the main causes of this lipid accumulation, it is first important to understand the key role these lipids play in the progression of NAFLD. Through mechanisms that are not fully understood, safely stored lipids (i.e., triglycerides) can be converted into lipotoxic species. An increase in lipid species substrate may be a key contributor to this process. When the liver's capacity to use, store, and export fatty acids as triglycerides becomes overwhelmed, lipid substrates may enter alternative pathways including those synthesizing more harmful lipid species (Rada *et al*., 2020). It also, however, seems that comorbidities that cause dysregulated lipid metabolism, inflammation, and insulin resistance (e.g., obesity, T2D, and microbiome dysbiosis), also play a key role in the production of lipotoxic metabolites.

In NAFLD, hepatic free fatty acid accumulation begins to overwhelm the mitochondria. In healthy individuals, these free fatty acids are easily catabolized via fatty acid oxidation. However, in NAFLD, where mitochondrial dysfunction is present, mitochondrial uncoupling leads to the inability to effectively oxidize fats (Koliaki *et al*., 2015). This contributes to the blunting of fatty acids to pathways that synthesize toxic lipid species, such as diacylglycerides, free cholesterol, cholesterol esters, ceramides, and phospholipids. These lipid species are thought to cause several of the downstream disturbances observed in NASH. These include reactive oxygen species production, endoplasmic reticulum (ER) stress, cellular inflammation, oxidative stress, cell death, immune cell infiltration, cytokine production, and the potentiation of mitochondrial dysfunction and impaired insulin signalling that present simultaneously with hepatic lipid accumulation (Pierantonelli and Svegliati-Baroni, 2019; Geng *et al*., 2021). It is, of course, hard to delineate which of these mechanisms come first, as often several of them present concurrently. These mechanisms, however, that contribute to, or present with, increased lipotoxic lipids, will be reviewed in the following sections.

1.4.2 Genetic predisposition

Genome-wide association studies have revealed several genetic variants that are associated with NAFLD. These include variants in PNPLA3, TM6SF2, MBOAT7, GCKR, and HSD17B13 genes (Romeo *et al*., 2008; Kozlitina *et al*., 2014; Mancina *et al*., 2016; Lin *et al*., 2014; Zhang *et al*., 2022). Specifically, the best genetic predictors of NAFLD, PNPLA3 and HSD17B13, are localized to the lipid droplet while TM6SF2 is involved in

hepatic VLDL secretion (BasuRay *et al*., 2017; Zhang *et al*., 2022; Luo *et al*., 2021). These studies are important for defining defects in lipid metabolism as an important causal driver of NAFLD and NASH, but these genetic mutations can only explain why a small number of people develop the disease. The rising rates of NAFLD over the past few decades suggest that genetics only reflect a predisposition to disease development; in most cases, this genetic predisposition needs to be coupled with environmental factors to trigger NAFLD development.

1.4.3 Dietary constituents and NAFLD

General weight gain and increased adiposity are indeed contributors to NAFLD development; however, studies have suggested that dietary constituents, including saturated fats and fructose, may also promote disease development, even when consumed isocalorically. Saturated fat has been linked to hepatic lipid synthesis, hepatic and adipose inflammation, and insulin resistance (Parks, Yki-Järvinen, and Hawkins, 2017). In an overeating study in obese adults, saturated fat was shown to significantly increase liver fat content, liver enzymes, and blood lipids, relative to calorically matched polyunsaturated fat (Rosqvist *et al*., 2019). Other studies suggest that this is insufficient if energy intake does not exceed energy expenditures (Chalasani *et al.*, 2018).

The monosaccharide fructose, a major component of commonly used sweeteners, is thought to be a robust driver of NAFLD (Federico *et al.*, 2021). Fructose consumption over the decades has increased concurrently with rates of NAFLD. When consumed in small quantities, fructose is largely processed in the gastrointestinal tract by the gut

bacteria, which are highly adept at metabolizing fructose (metabolizing ~90% of dietary fructose) (Marinho *et al*., 2019; C. Jang *et al*., 2018; Febbraio and Karin, 2021). However, when habitually consumed in large quantities, fructose is thought to cause gut epithelial barrier dysfunction and will spill over into portal circulation. Fructose in the portal vein is then very efficiently taken up by the liver, where it causes mitochondrial dysfunction and enhances the expression of genes critical for driving DNL (Marinho *et al*., 2019; C. Jang *et al*., 2018; Febbraio and Karin, 2021).

Fructose stimulates DNL in the liver by providing substrate and by inducing the expression of transcription factors SREBP1c and ChREBP, which subsequently increase lipogenic gene expression (Jegatheesan and De Bandt, 2017). Fructose also induces the expression of its own metabolizing enzyme ketohexokinase (KHK), which synthesizes fructose-1 phosphate. This phosphorylation event is ten times faster than glucose phosphorylation by glucokinase (GCK), suggesting that fructose is more lipogenic than glucose (Asipu *et al.*, 2003). In support of this, KHK inhibitors improve steatosis and NASH in mice (Futatsugi *et al.*, 2020; Gutierrez *et al.*, 2021; Shepherd *et al.*, 2021), and lower liver fat and inflammatory markers in adults with NAFLD (Kazierad *et al.*, 2021). Animal studies have also revealed that this rapid fructose phosphorylation, uses up ATP, and creates high levels of cellular AMP. AMP, a substrate in purine metabolism, is eventually converted to uric acid. High levels of uric acid are known to cause mitochondrial oxidative stress and TCA cycle dysfunction. This results in the partitioning of citrate out of the mitochondria, where it gets converted to acetyl-CoA, further increasing DNL and lipotoxicity, and reducing fatty acid oxidation (Jegatheesan and De Bandt, 2017).

It has more recently been proposed that fructose overconsumption modulates the microbiome, induces gut permeability, and increases gastrointestinal inflammation. Inflammatory mediators or metabolites will easily travel to the liver and have direct effects on hepatic DNL and inflammation (Cheng *et al.*, 2021; Choi *et al.,* 2017; Do *et al*., 2018; Herman and Birnbaum, 2021; Febbraio and Karin, 2021). For example, in mice, high fructose feeding increases gut-derived acetate, which travels to the liver through the portal vein and contributes to elevated hepatic DNL in the absence of ACLY (Zhao *et al.*, 2020). It is thought that these gut-mediated effects might be larger contributors to fructose-induced liver damage, than direct fructose actions in the liver.

In general, there seem to be direct and indirect mechanisms linking fructose overconsumption to NASH pathogenesis, and both are likely contributing to fructose-induced liver injury. However, whether these mechanistic observations implicating fructose in NASH translate to humans is still under question. Many mouse studies use doses of fructose that are six times that of a typical Western diet (50-60 kcal% fat diets) (Marinho *et al*., 2019; Zhao *et al*., 2020; Choi *et al*., 2017; Tan *et al*., 2021; Do *et al*., 2018; Marriot *et al*., 2009). In the US, the average consumption of fructose accounts for ~9% of energy intake, and at the high end of consumption, fructose accounts for ~15%. Therefore, studies looking at more human-relevant levels of fructose are necessary to further explore its impacts on NAFLD.

1.4.4 Gut microbiome dysbiosis

As highlighted by fructose's effects on the gut-liver axis, gut microbiome dysbiosis is a key component of NAFLD. Damage to the gut epithelial barrier, caused mostly by dietary factors, results in increased gut permeability. This allows for the translocation of bacterial components and metabolites from the gut to the liver, triggering metabolic changes and inflammation in the liver (Safari and Gérard, 2019). Key messengers of gut dysbiosis and NAFLD include short chain fatty acids (acetate, propionate, butyrate), bacterial lipopolysaccharides (LPS), cytokines, bacterially derived ethanol, impaired choline metabolism, and increased trimethylamine (TMA). These mediators are implicated in one way or another in modulating hepatic inflammation and/or metabolism, including DNL (Leung *et al*., 2016; Zhao *et al*., 2020).

1.4.5 The relationship between NAFLD, insulin resistance, and T2D

NAFLD, insulin resistance, and T2D are closely related metabolic pathologies, that often present together (Leite *et al.*, 2009). With the close relationship between glucose and lipid metabolism, it is not surprising that perturbations in one will affect the other. The relationship between T2D and NAFLD is complex and whether T2D is a consequence or cause of NAFLD is highly debated. Younossi et al. report that 45-75% of T2D patients have NAFLD and 37.3% have NASH, 23% of NAFLD patients have T2D, and 47% of NASH patients have T2D (Younossi *et al.*, 2016; Younossi, Golabi, *et al.*, 2019). This supports that the etiology of T2D and NAFLD are closely intertwined, and it is unlikely that one always precedes the other. Regardless, the presence of one of these diseases

introduces a high risk for the development or exacerbation of the other (Lonardo *et al.*, 2006).

Insulin resistance is the key link between lipid accumulation in NAFLD and the development of T2D (Friedman *et al.*, 2018). Insulin resistance occurs when cells are unable to respond to insulin, leading to impaired blood glucose control and eventually, hyperglycemia. Pancreatic β-cells will try to overcome the reduced insulin sensitivity by increasing the production and secretion of insulin, over time leading to hyperinsulinemia (Fonseca, 2009). The pancreas eventually becomes overworked and insulin production and secretion become impaired. This inability to provide enough insulin to control blood glucose may result in the requirement for exogenous insulin administration. T2D is, therefore, characterized by this insulin resistance, hyperglycemia, hyperinsulinemia, and subsequent decline in pancreatic β-cells function leading to the inability to produce sufficient insulin (Fonseca, 2009).

The mechanisms connecting insulin resistance to NAFLD progression are complex and are mediated by interorgan crosstalk. In insulin resistance, the ability of insulin to suppress adipose tissue lipolysis is impaired. This leads to elevated lipolysis and free fatty acid release into circulation and results in an influx of free fatty acids to the liver (Perry *et al.*, 2014). At the skeletal muscle, insulin-mediated glucose uptake is impaired, resulting in the diversion of glucose to DNL in the liver (Perry *et al.*, 2014). At the liver, insulin resistance leads to ineffective suppression of gluconeogenesis but continues to drive the upregulation of lipogenic enzymes including ACLY through both transcriptional and

posttranslational regulation (Perry *et al.*, 2014). These altered metabolic fluxes have been confirmed in tracing studies in NAFLD patients and in HFD mouse studies (Sunny *et al.,* 2011; Satapati *et al.,* 2012). The combination of high cytosolic glucose (from skeletal muscle and liver gluconeogenesis) and an influx of free fatty acids from the adipose tissue, results in high DNL activity, low fatty acid oxidation, and hepatic lipid accumulation. In addition to insulin resistance, hyperglycemia alone seems to play a role in dyslipidemia and NAFLD. This is evidenced by streptozotocin (STZ) treated animals, which lose the ability to produce insulin and therefore develop hyperglycemia, which results in dyslipidemia and severe liver damage in the absence of insulin resistance (Jensen *et al.,* 2021; Saito *et al.,* 2015).

As alluded to, the relationship between insulin resistance and steatosis progression is bidirectional. The overaccumulation of hepatic free fatty acids can worsen insulin resistance through direct and indirect mechanisms. Lipotoxic metabolites can both, directly and indirectly, impair hepatic insulin signalling, through mitochondrial dysfunction, oxidative stress, and cellular inflammation (Wong *et al.*, 2015). Key lipid metabolites that have been directly associated with impairing insulin signalling, include ceramides, acylcarnitines, and diacylglycerides. For example, free fatty acids in NAFLD may be esterified to diacylglycerides, which activate protein kinase Cε (PKCε). PKCε inhibits insulin receptor substrate 2 (IRS2), thus inhibiting insulin signalling and sensitivity, and increasing gluconeogenesis and hepatic glucose output. This also further exacerbates hepatic steatosis by shunting glucose to DNL (Perry *et al.*, 2014). Ceramides, also derived from free fatty acids, inhibit insulin induced Akt activation. This relieves the inhibition of

lipolysis and gluconeogenesis and suppresses glycogen synthesis and GLUT4 glucose uptake. This results in increased fat synthesis and accumulation, and hyperglycemia respectively (Perry *et al.*, 2014). Compounds in clinical development that reduce hepatic steatosis in humans have also shown improvements in glycemic control, further supporting this bidirectional relationship (Calle *et al*., 2021; Masson *et al*., 2020). In summary, several mechanisms demonstrate the strong interconnectivity between insulin resistance, NAFLD, and T2D, and support the importance of targeting both conditions.

1.4.6 Elevated DNL is a key contributor to NAFLD

The three main sources of free fatty acids that contribute to the hepatic triglyceride pool are dietary fat, circulating free fatty acids (mostly derived from adipose tissue lipolysis), and hepatic DNL. Tracing studies, using VLDL-TAG as a proxy marker for hepatic triglycerides (Donnelly *et al.*, 2005), have provided insight into the proportional contributions of these sources to intrahepatic triglycerides. Many of these reports vary but show that in lean and healthy individuals dietary fat contributes 12-39%, systemic free fatty acids contribute 75-84%, and fatty acids synthesized in DNL contribute 10-22% (Diraison, Pachiaudi and Beylot, 1996, 1997; Barrows and Parks, 2006; Parks and Hellerstein, 2006; Vedala *et al.*, 2006; Hodson *et al.*, 2007; Lambert *et al.*, 2014). It is important to note however that most of these studies are performed in the fasted state where DNL is low, do not allow for long enough isotope administration to detect newly synthesized lipids, and/or do not consider the proportion of systemic fatty acids that may have been derived from hepatic DNL. These values may, therefore, be grossly underestimating the contribution of

DNL (Smith *et al.*, 2020). Nonetheless, in lean and healthy individuals, adipose-derived free fatty acids seem to be the largest contributors to intrahepatic triglycerides.

More recent studies have revealed that in obese patients stratified by high and low liver fat content, the contribution of DNL to hepatic fat was 3.5-fold greater in those with NAFLD, compared to those with low liver fat content (Lambert *et al.*, 2014). The contribution of dietary fat and adipose-derived free fatty acids was unchanged between the two groups, implicating DNL as a central mediator in NAFLD (Lambert *et al.*, 2014). Similar findings were replicated by Smith and colleagues, who found that the contribution of hepatic DNL to intrahepatic triglycerides was 11%, 19%, and 38% in lean, obese, and obese individuals with NAFLD, respectively, (Smith *et al.*, 2020). Further, studies in lean and obese men reveal that elevated DNL is associated with insulin resistance and hepatic steatosis (Diraison *et al.*, 2002; Eissing *et al.*, 2013). Rodent studies also support the notion that elevated hepatic DNL is a key contributor to NAFLD (Knebel *et al.*, 2012; Cordoba-Chacon *et al.*, 2015; Sanders *et al.*, 2018). These findings strongly linking DNL to NAFLD have led to the development of several DNL inhibitors, many of which have reached the clinical stage for the treatment of NAFLD (Batchuluun, Pinkosky and Steinberg, 2022).

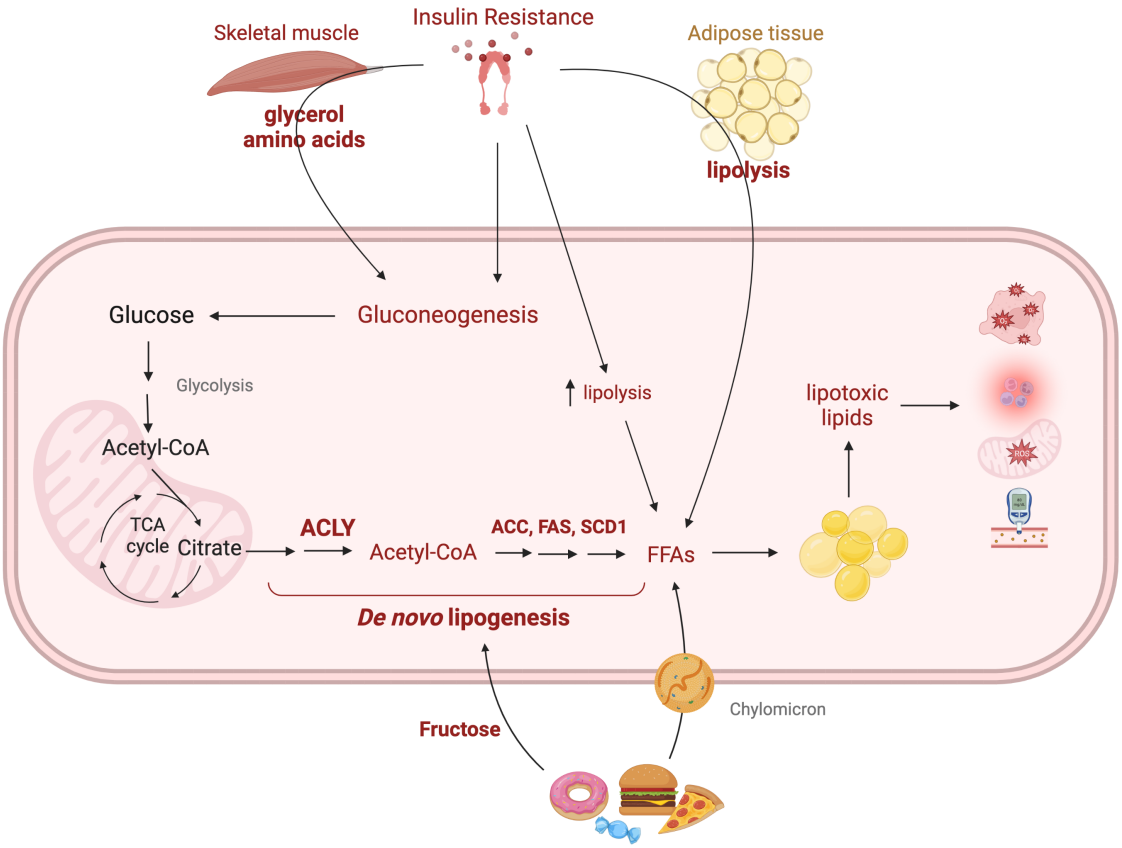

Figure 1.6. Insulin resistance and elevated DNL in NAFLD

Elevated free fatty acids in the liver can be attributed to a combination of hepatic insulin resistance, high dietary fat intake, and elevated adipose tissue lipolysis. Insulin resistance at the liver ineffectively suppresses gluconeogenesis, increasing substrate for *de novo* lipogenesis. Insulin resistance at the skeletal muscle leads to increased secretion of amino acids, which get taken up in the liver and support hepatic glucose production via gluconeogenesis. A Western diet, high in fructose and fat stimulates *de novo* lipogenesis and free fatty acid uptake via chylomicrons respectively. Insulin resistance at the liver also relieves inhibition of lipolysis, resulting in further free fatty acid accumulation. Insulin resistance at the adipose tissue leads to increased lipolysis and circulating free fatty acids, which then get taken up in the liver. The resulting elevated DNL and free fatty acids in the liver lead to the accumulation of lipids, which over time can be converted into lipotoxic lipid species. These lipids contribute to hepatic oxidative stress, inflammation, mitochondrial dysfunction and further impairments in insulin signalling, processes that together, underly the progression of fatty liver to NASH. TCA: tricarboxylic acid; ACLY: ATP-citrate lyase; ACC: acetyl-CoA carboxylase; FAS: fatty acid synthase; SCD1: stearoyl-CoA desaturase 1; FFAs: free fatty acids.

1.5 ACLY as a therapeutic target in NAFLD

1.5.1 Current evidence for ACLY inhibition in NAFLD

One way to achieve DNL inhibition is by inhibiting ACLY. Consistent with elevations in DNL, upregulation of ACLY expression has been reported in several pathologies, including cancers (liver, lung, prostate, bladder, breast, stomach, and colon) (Turyn *et al.*, 2003; Yancy *et al.*, 2007; Migita *et al.*, 2008; Staaf *et al.*, 2010; Pinkosky *et al.*, 2017), and metabolic disorders, most notably NAFLD. Several human and mouse gene expression studies have demonstrated that ACLY is significantly upregulated in NAFLD (Ahrens *et al.*, 2013; Muir *et al.*, 2013; Ryaboshapkina and Hammar, 2017; Ma *et al.*, 2018). A meta-analysis of gene expression studies also demonstrated ACLY upregulation in the transition from simple steatosis to NASH (Ryaboshapkina and Hammar, 2017).

Genetic deletion studies in rodents show that ACLY is required for embryonic development and therefore tissue-targeted deletion is required (Beigneux *et al.*, 2004). In mice, the genetic suppression of liver ACLY has yielded mixed results in the context of hepatic steatosis. Liver-directed ACLY siRNA in *db*/*db* mice reduces liver steatosis and improves glucose homeostasis (Wang *et al.*, 2009). However, when liver ACLY is reduced from birth using Albumin-Cre, liver fat remains unchanged when mice are exposed to a high-fructose diet (Zhao *et al.*, 2020). This lack of an effect was attributed to gut microbiome-induced increases in acetate and compensatory upregulation of acetyl-CoA synthetase 2 (ACSS2), which provided an alternative source of acetyl-CoA, bypassing ACLY (Zhao *et al.*, 2020). Additionally, while preparing this dissertation, Yenilmez et al.

reported that deletion of hepatocyte ACLY increased liver triglycerides in mice fed a HFD (Yenilmez *et al*., 2022). It is important to note that the models used in these studies do not accurately replicate the obesity, steatosis, inflammation, and fibrosis that exists in human NASH, nor were they performed as interventions (i.e., when the disease had already developed). The high fructose (60 kcal%) or high-fat (60 kcal%) diets used in the studies are supraphysiological and are not accurate to human consumption. The findings by Yenilmez et al. are likely a result of HFDs significantly suppressing ACLY expression, which, as mentioned, is upregulated in human NASH. These studies highlight the importance of using physiological diets with nutrients in similar quantities to that of human diets. It is therefore surprisingly unknown whether genetic or pharmacological inhibition of liver ACLY may exert beneficial effects as an intervention in NASH.

1.5.2 Bempedoic acid

ACLY can be pharmacologically inhibited in hepatocytes following the conversion of the pro-drug bempedoic acid (bemA; ETC-1002) to a coenzyme A (CoA) ester (bempedoyl-CoA) by the long-chain acyl-CoA synthetase (ACSVL1) (Pinkosky *et al.*, 2013). Bempedoyl-CoA inhibits ACLY in a CoA competitive, but citrate and ATP non-competitive manner, suggesting it may interact with the CoA binding site (Pinkosky *et al.*, 2013). Treatment of rodents and humans with bempedoic acid lowers serum low-density lipoprotein-cholesterol (LDL-c), HbA_{1c}, atherosclerosis (in rodents only), and high sensitivity C-reactive protein (hsCRP), without increasing serum triglyceride levels, a risk factor for CVD incidence and mortality (Thompson *et al*., 2015; Ballantyne *et al*., 2016;

Pinkosky *et al*., 2016; Goldberg *et al*., 2019). Rodent and human studies have demonstrated its safety and tolerability (Ballantyne *et al.*, 2013; Pinkosky *et al.*, 2016). Bempedoic acid is approved for patients with hypercholesterolemia as an adjunct to diet and maximally tolerated statins (US, EU, Switzerland, and UK), or alone or in combination with other lipid-lowering therapies in patients who are statin intolerant or for whom a statin is contraindicated (EU, Switzerland, and UK). Phase III clinical trials for the treatment of hypercholesterolemia and CVD to investigate long-term cardiovascular outcomes are ongoing (clinicaltrials.gov identifier: NCT02993406) (Nicholls *et al.*, 2021).

In addition to its cardiovascular-related benefits, bempedoic acid has been shown to reduce hepatic acetyl-CoA, DNL, steatosis, and inflammation, indicating a potential use in treating NASH (Ballantyne *et al.*, 2012, 2016; Thompson *et al.*, 2015, 2016; Samsoondar *et al.*, 2017). However, the current studies demonstrating these outcomes have been performed in obesity-driven atherosclerosis models. These models do not advance to hepatic fibrosis and thus do not mimic the etiology of late-stage disease severity observed in human NASH. Therefore, studies in clinically relevant animal models that accurately reflect the NASH patient population, are required for conclusions to be made regarding ACLY inhibition by bempedoic acid for the treatment of NASH.

1.6 Modelling NASH in mice

1.6.1 Background

As detailed above, NASH is tightly linked to obesity as well as dysregulation of the gastrointestinal tract, microbiome, liver, adipose tissue, skeletal muscle, and immune

system. To accurately represent this interorgan complexity, the use of *in vivo* models is required. Most models only recapitulate certain arms of NASH and therefore do not accurately predict the therapeutic response that would occur in humans.

1.6.2 Characteristics of a human-relevant mouse model of NASH

To accurately study disease response to a therapeutic, the model must mimic human disease as closely as possible. Santhekadur et al. and Brenner et al. have outlined specific criteria for accurate preclinical modelling of human NASH (Brenner, 2018; Santhekadur, Kumar and Sanyal, 2018). Diet-induced obesity is a common risk factor for NASH and therefore animals should be fed diets similar in macronutrients to human obesogenic diets. These diets should not contain high levels of unnatural toxins (e.g., cholesterol or DEN), as humans do not develop NASH through high intakes of these. The model should develop additional metabolic parameters that typically present with human NASH, including obesity, insulin resistance, dyslipidemia, and systemic inflammation. The model should also demonstrate biopsy-proven NASH using a histological examination of steatosis, lobular inflammation, hepatocellular ballooning, and fibrosis. The model should display similar patterns in hepatic signalling pathway modulation as observed in human NASH, including upregulated DNL, oxidative stress, ER stress, and pro-apoptotic, -fibrotic, and -inflammatory pathways). Using transcriptomics to demonstrate a strong similarity between human and mouse gene signatures would further strengthen these changes in signalling pathways. Ideally, once fibrosis has developed in the model, the mice should have a

susceptibility to liver cirrhosis and HCC development, as is seen in humans with end-stage NASH (Santhekadur, Kumar and Sanyal, 2018).

1.6.3 Importance of housing temperatures in animal disease models

Animal vivariums are typically maintained below their thermoneutral zone, at ambient temperatures between 20°C - 26°C (James, Olejniczak and Repasky, 2022). The thermoneutral zone represents a range of temperatures in which the basal metabolic rate is sufficient to maintain core body temperature, without the need for additional thermoregulatory processes, such as thermogenesis. This zone for mice is generally accepted as around 29°C - 31°C (James, Olejniczak and Repasky, 2022). When chronically housed below their thermoneutral zone, activation of thermogenesis occurs to maintain body temperature. The high surface-to-volume ratio of mice causes them to expend twice as much energy and dedicate a much larger portion of their resting metabolic rate to maintain euthermia, compared to humans (Ganeshan and Chawla, 2017). This causes substantial changes in their metabolic and cardiovascular responses, as well as a chronic suppression of regular immune responses (Ganeshan and Chawla, 2017).

Thermoneutral housing of mice accelerates HFD-induced NASH and removes the chronic suppression of the immune response, thus better representing the human immune response to NAFLD (Giles *et al.*, 2017). HFD-fed mice housed at thermoneutrality compared to those housed at room temperature, develop significant NASH, and demonstrate similar inflammatory and immune responses observed in humans with NASH. The C57BL/6 mice used in this study however do not develop hepatic fibrosis, a

histological characteristic of severe NASH development (Giles *et al.*, 2017). It is now evident that most animal disease models should be housed at thermoneutrality, especially those with large metabolic and immune components, such as NAFLD.

1.6.4 Current NAFLD and NASH mouse models

Numerous mouse models of NASH have been developed and are reviewed in Appendix A. In summary, most studies investigating NASH have used one of, or a combination of, the following types of models: dietary-, toxin-, or genetically induced. Dietary models typically use combinations of high fat, high carbohydrate, and high fructose, or methionine and/or choline-deficient diets. High-fat and high-carbohydrate diet combinations induce insulin resistance and hepatic steatosis, however, typically do not induce fibrosis (Farrell *et al.*, 2019). It is also important to note that fat or fructose levels used in mouse diets are often as high as 50-60 kcal%, which are also not relevant to human intake. As discussed, compared to dietary lipids, fructose is a superior driver of DNL. The inclusion of fructose to a high-fat diet (HFD) accelerates NASH development and mice develop moderate fibrosis in 20-30 weeks (Clapper *et al.*, 2013). A recent systemic review of NAFLD animal models found that this high-fat, high-fructose diet most accurately resembles human disease (Im *et al.*, 2021). Methionine and choline-deficient diets (MCD) and choline-deficient (CD) diets develop NASH, however, do not develop obesity and insulin resistance (Rinella *et al.*, 2008; Achiwa *et al.*, 2016). Chemotoxins, such as carbon tetrachloride (CCL_4) (Nakamura *et al.*, 2014), thioacetamide (TAA) (Lefebvre *et al.*, 2016), or diethylnitrosamine (DEN) (Kishida *et al.*, 2016), also cause NASH and fibrosis in the

absence of metabolic syndrome by inducing hepatocellular injury. Various genetic models, such as leptin-deficient (*ob*/*ob*) and leptin-receptor-deficient (*db*/*db*) mice, induce NASH through obesity but do not induce significant fibrosis. A commonly used combination model is the STAM™ mouse model, which uses STZ and a HFD to induce metabolic syndrome and NASH in merely 7 weeks (Saito *et al.*, 2017). However, its acute disease severity has been criticized as not properly translating to the chronic human condition. In summary, few models develop advanced fibrosis while still reflecting the metabolic etiology or pathologies that exist in human NASH. This is problematic because of the importance of the fibrosis stage in predicting mortality in human NASH. Overall, there is no gold standard mouse model in NASH research, which has led to a large inconsistency in the models used. This greatly limits the comparison and interpretation of current preclinical drug studies for the treatment of NASH.

1.7 Current therapeutic development for NASH

There are no FDA-approved drugs for NAFLD or NASH treatment. Weight loss through environmental intervention (exercise and caloric restriction), or bariatric surgery are the only accepted treatments for NAFLD. Therapies prescribed to patients are often targeted at treating underlying risk factors, such as insulin resistance, rather than NASH itself (Wong *et al.*, 2015). The American Association for the Study of Liver Disease (AASLD) guidelines do support the use of a few agents for the treatment of NASH, but only under circumstances where the benefits outweigh the therapy's risk (Mudaliar *et al.*, 2013). For example, pioglitazone (adiponectin upregulator), vitamin E, and liraglutide

(glucagon-like peptide-1 receptor (GLP1R) agonist) use are supported when liver biopsies indicate severe NASH and fibrosis, and all side effects are considered (Mudaliar *et al.*, 2013).

With the large clinical need and attractive commercial opportunity, several companies have developed compounds for the treatment of NASH. Over 20 distinct metabolic, inflammatory, or fibrotic targets have been used to develop potential NASH therapeutics (Romero *et al.*, 2020). Many drugs have advanced to clinical trials; however, none have been successful in receiving FDA approval. Obeticholic Acid (OCA), a Farnesoid X Receptor (FXR) agonist, showed significant promise, however, was rejected by the FDA in 2020 based on interim analysis from their phase III trial in NASH patients with fibrosis (clinicaltrials.gov identifier: NCT02548351). OCA improves insulin sensitivity after six weeks, and histology-proven NASH and liver fibrosis after 72 weeks, compared to placebo (Mudaliar *et al.*, 2013; Neuschwander-Tetri *et al.*, 2015). The rejection of an accelerated approval was based on safety concerns, such as elevated LDL-c, total cholesterol, HOMA-IR, and insulin (Mudaliar *et al.*, 2013; Neuschwander-Tetri *et al.*, 2015; Siddiqui *et al.*, 2020). The FDA requested longer-term safety and efficacy data and phase III trials are still ongoing. Elafibranor, a dual PPARα and PPARδ agonist is currently in phase II clinical trials and in the interim analysis showed reductions in liver enzymes, however, there was no change in liver steatosis observed by MRI-PDFF (Romero *et al.*, 2020). Sodium-glucose co-transporter (SGLT-2) inhibitor, dapagliflozin (clinicaltrial.gov identifier: NCT03723252), GLP1R agonist semaglutide (clinicaltrial.gov

identifier: NCT04822181), SCD1 inhibitor aramchol (clinicaltrial.gov identifier: NCT04104321), and thyroid hormone receptor (THR) β-selective agonist, resmetirom (clinicaltrial.gov identifier: NCT03900429), are also all in advanced phase III clinical trials.

As previously stated, owing to the key role of DNL in NAFLD, several companies have developed compounds targeting lipid metabolism (e.g., inhibitors of FASN, DGAT2, SCD1, ACC and agonists of PPARs, AMPK) (Romero *et al.*, 2020). Many of these show promise in reducing NASH through lowering hepatic lipid content and even liver insulin resistance and blood glucose. Pharmacological inhibition of ACC for example reduces DNL and hepatic steatosis and improves markers of liver fibrosis. ACC inhibition, however, results in increases in circulating triglycerides, limiting its use as a monotherapy in patients with NASH where cardiovascular risk is high (Stiede *et al.*, 2017; Lawitz *et al.*, 2018; Loomba *et al.*, 2018).

Despite the advancements made with NASH therapeutics, there is still no therapy with proven safety and efficacy for patients with NASH and there is a strong need for novel therapeutics to reverse NASH. The immense drug development in targeting lipid metabolism, particularly DNL, demonstrates this as a promising strategy for NASH treatment.

1.8 Main Objective

Identify and characterize novel mechanisms that contribute to NASH and hepatic fibrosis development and investigate their therapeutic potential in preclinical disease models.

1.9 Thesis Aims

To further the study of novel targets and mechanisms for NASH and hepatic fibrosis and to test novel therapies to address this large unmet medical need. Specifically, develop and characterize a novel mouse model of NASH that accurately reflects the progression of human disease. Establish the physiological relevance of lipid metabolism in NASH and determine whether targeting hepatocyte lipid synthesis through ACLY inhibition is an effective treatment. Determine whether inhibiting ACLY with bempedoic acid provides similar benefits that can support its testing in clinical trials with NAFLD and NASH patients.

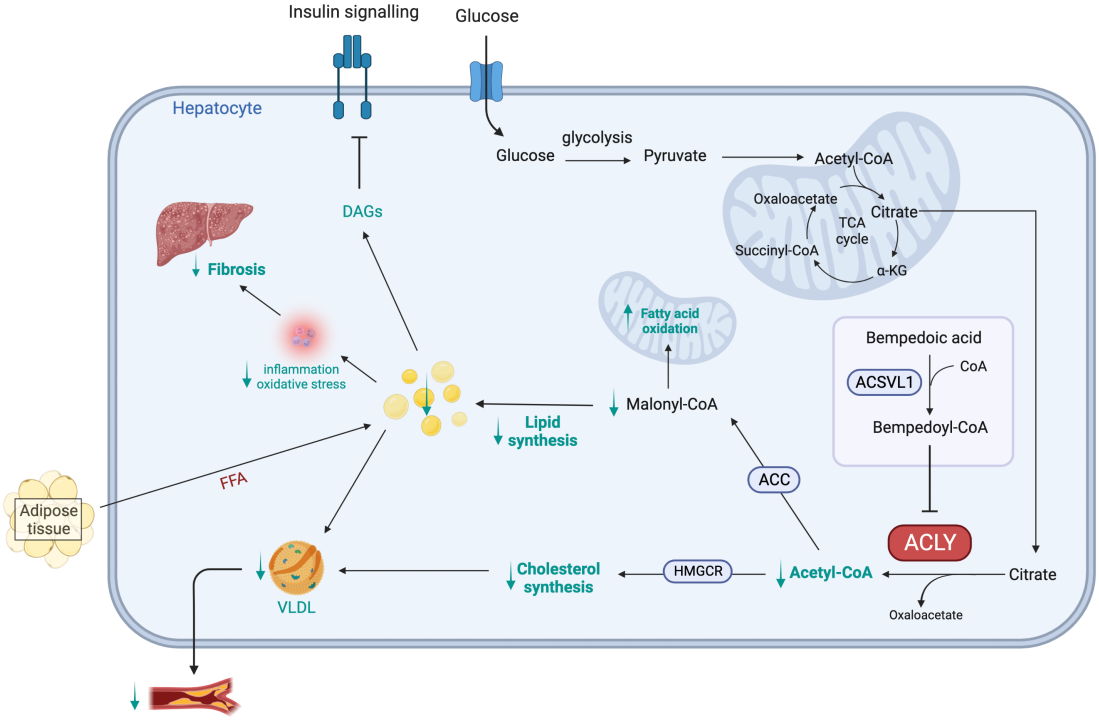

Figure 1.7. Proposed mechanisms and outcomes of ACLY inhibition in NASH

ACLY and DNL are upregulated in NASH, which leads to the accumulation of triglycerides and lipotoxic lipid metabolites in the liver. Bempedoic acid is a pro-drug that requires the liver-specific ACSVL1 enzyme to convert it to its active bempedoyl-CoA form, which inhibits ACLY. It is hypothesized that targeting ACLY by bempedoic acid or genetic deletion will reduce cytosolic acetyl-CoA production, a substrate for both cholesterol and lipid synthesis. Reduced lipid synthesis will also increase reciprocally regulated fat oxidation and reduce the accumulation of lipids. A reduction in lipids may help reduce some of the downstream effects of lipid accumulation, including impaired insulin signalling, and the cellular inflammation and oxidative stress that contribute to liver injury and fibrosis. Reduced acetyl-CoA, should also reduce cholesterol synthesis and downstream VLDL-c secretion into circulation, helping reduce CVD risk, which is high in NASH populations. Inhibiting ACLY could potentially help target several underlying components of NASH and its risk factors. TCA: tricarboxylic acid; OAA: oxaloacetate; α-KG: α-ketoglutarate; CoA: coenzyme A; ACSVL1: very long-chain acyl-CoA synthetase; ACLY: ATP-citrate lyase; ACC: acetyl-CoA carboxylase; HMGCR: HMG-CoA reductase; DAGs: diacylglycerides; FFA: free fatty acids; VLDL: very-low-density lipoprotein; VLDL-c: very-low-density lipoprotein-cholesterol.

CHAPTER 2: MATERIALS AND METHODS

2. Materials and methods

2.1 Experimental model details

2.1.1 Diet-induced NASH model

All animal procedures were approved by the McMaster University Animal Ethics Research Board. All mice were group-housed on a 12-hour light/dark cycle with *ad libitum* access to food and water. All mice used were males on a C57BL/6J background purchased from JAX. All mice were housed in either Solace Zone Heated Cage Units with HEPA filtered ventilation and temperature regulated cages kept at 29°C or in specific-pathogen free (SPF) microisolators in a room kept at 29°C. Mice were fed a chow diet (10% fat) or a high-fat, high-fructose diet (NASH Diet; ND; 40% fat, 20% fructose, 0.02% cholesterol). All mice used in chronic *in vivo* experiments were placed on respective diets and housing conditions at 8 weeks of age. Mice were sacrificed in a fed-state. Bempedoic acid was incorporated into the diet by Research Diets, Inc. at a dose of 10 mg/kg (40% fat, 20% fructose, 0.02% cholesterol + 10 mg/kg bempedoic acid). Mice were anesthetized using ketamine/xylazine.

Glucose and insulin tolerance tests were performed following a 6-hour fast and mice were injected with 1 g/kg of D-glucose and 1.3 U/kg insulin respectively. For pyruvate tolerance tests (PTT), mice were fasted overnight for 15 hours to induce a fasted state and upregulate gluconeogenesis. At 9 am mice were injected with 1.5 g/kg sodium pyruvate. Subsequent blood glucose levels reflect rates of gluconeogenesis (Hughey *et al.*, 2014). For all tests, blood glucose was measured from a drop of tail blood using Accu-Chek Aviva

blood glucometer. The blood glucose values were presented as repeated measures over time. Area under the curve analysis was performed using GraphPad Prism (version 8.4.1). All metabolic parameters (RER, VO_2 and VCO2, energy expenditure) were measured after 22 weeks on diet using the Comprehensive Laboratory Animal Monitoring System (CLAMS). Mice were acclimated to the CLAMS cages for 24 hours prior to a testing period of 48 hours.

2.1.2 Generation of inducible liver ACLY knockout mice

Acly$^{f/f}$ mice were generated with *loxP* sites flanking exon 9 of the *Acly* gene using homologous recombination by Wellen and colleagues (Zhao *et al.*, 2016). Mice were injected in their tail vein with 4.0 x 10^{11} viral genomes of AAV-DJ8-Ttr-eYFP or AAV-DJ8-Ttr-Cre (Vector Biolabs, PA, USA) to generate WT and ACLY hepatocyte knockout (hKO) respectively (Malato *et al.*, 2011).

2.1.3 STAM™ mouse model

C57BL/6 mice were obtained from Japan SLC, Inc. All animals used in the study were housed and cared for in accordance with the Japanese Pharmacological Society Guidelines for Animal Use. The animals were maintained in a SPF facility under controlled conditions of temperature (23 ± 2°C), humidity (45 ± 10%), lighting (12-hour artificial light and dark cycles; light from 8:00 to 20:00) and air exchange. The animals were housed in TPX cages with a maximum of 4 mice per cage. Sterilized solid high-fat diet (HFD; 45 kcal% fat) was provided *ad libitum*. Body weight was recorded before the treatment. Food consumption was measured twice weekly per cage during the treatment period. Mice were

sacrificed 24 ± 2 hours after the last dose at 9 weeks of age by exsanguination through direct cardiac puncture under ether isoflurane anesthesia.

NASH was induced in male mice by a single subcutaneous injection of 200 μg streptozotocin solution 2 days after birth and feeding with HFD after 4 weeks of age. Bempedoic acid was administered orally in a volume of 10 mL/kg at 3 dose levels of 3, 10 and 30 mg/kg once daily. The individual dosage was calculated by body weight each day. The test substances were administered from 9 to 11 am. Mice were randomized and separated into five treatments groups, n =16/group. NASH baseline was determined at the initiation of bempedoic acid treatment in mice fed with HFD *ad libitum* without any treatment and sacrificed at 5 weeks of age. Mice were orally administered vehicle [0.5% CMC (pH 7-8)], or bempedoic acid (3, 10, or 30 mg/kg in a volume of 10 mL/kg once daily from 5 to 9 weeks of age. Satellite groups (n =15/group) were treated in parallel and used for oral glucose tolerance test (OGTT) analyses. OGTT was performed at 8 weeks of age (Day 27). After an overnight fast, mice were given a 20% glucose solution (50 mg glucose/mouse) by oral gavage. Whole blood glucose was measured by Stat Strip glucose meter at 0, 15, 30, 60, 90 and 120 minutes post oral glucose administration. For serum biochemistry, blood was collected in polypropylene tubes with anticoagulant and centrifuged at 1,000 x*g* for 15 minutes at 4°C. The supernatant was collected and stored at -80°C until use.

2.2 Method details

2.2.1 Serum analysis

Following sacrifice, serum was collected and centrifuged at 13,000 rpm for 10 minutes and supernatant was collected and stored at -80°C for further analysis. Serum ketone bodies (acetoacetone + 3-hydroxybutyrate), triglycerides, cholesterol, ALT, and AST were measured following commercially available kit protocols.

2.2.2 Tissue lipids

Lipids were extracted from approximately 5-10 mg of frozen liver by homogenizing in 1.0 mL chloroform/methanol (2:1) (Folch, Lees, and Sloane Stanley, 1957). Samples were dried and re-solubilized in isopropanol and analyzed for triglyceride or cholesterol concentration using kits per the manufacturer's instructions.

2.2.3 *In situ* hybridization and histological analysis

Following fixation with 10% neutral buffered formalin for 46 hours, the median lobe of the liver was dissected and switched to 70% ethanol. Livers were then processed, paraffin embedded, serially sectioned, and stained with haemotoxylin and eosin (H&E), Masson's trichrome (MTC), and picrosirius red (PSR), or stained for automated *in situ* hybridization by the McMaster Immunology Research Centre histology Core Facility. Images were taken using Nikon 90i Eclipse upright microscope at indicated magnifications.

In situ hybridization was performed following the RNAscope® 2.5 HD duplex assay (Advanced Cell Diagnostics) protocol. Liver slides were stained with RNAscope® 2.5 LS Duplex Reagent kit, LS Green Acessory Pack, and *Acly* probe (red) in channel 1 and *Acta2* probe (green) in channel 2 (Advanced Cell Diagnostics) using the Leica Bond RX automated stainer and the ACD Leica Bond program. Positive staining was visualized as red (channel 1 probe) and green (channel 2) dots.

Blinded liver histology scores were assigned to liver sections by a pathologist. Steatosis grade, lobular inflammation, and hepatocellular ballooning scores were assigned from H&E-stained liver sections as described by Kleiner and colleagues (Kleiner *et al.*, 2005). Steatosis grade was determined by % of lipid droplets in the total tissue area, lobular inflammation was determined by the number of inflammatory foci, and hepatocellular ballooning was determined by the number of ballooned hepatocytes. NAFLD Activity Scores (NAS) were obtained from the sum of these three scores. Fibrosis scores were assigned from analysis of both MTC- and PSR-stained liver sections as described by Kleiner and colleagues (Kleiner *et al.*, 2005).

2.2.4 Lysate preparation and Western blotting

Homogenates were prepared using 1X lysis buffer containing, 20 mM Tris-HCl (pH 7.5), 150 mM NaCl, 1 mM Na_2EDTA, 1 mM ethylene glycol tetraacetic acid (EGTA), 1% Triton, 2.5 mM, sodium pyrophosphate,1 mM β glycerophosphate,1 mM Na_3VO_4, 1 μg/mL leupeptin, 1 mM phenylmethylsulfonyl fluoride (PMSF), and 1X phosphatase inhibitor cocktail. Total lysate protein concentrations were determined using the BCA Protein Assay.

Protein concentrations were adjusted and diluted in 4X SDS (sodium dodecyl sulfate gel sample buffer) containing 50 mM DTT. Proteins were separated using sodium dodecyl sulfate polyacrylamide gel electrophoresis (SDS-PAGE) (4%-12%) Bis/Tris, MOPS running buffer. Separated proteins were electrophoretically transferred to polyvinyl difluoride (PVDF) membranes. Nonspecific binding was blocked, and membranes were probed with antibodies against β-actin or β-tubulin.

2.2.5 mRNA analysis

Cells and tissues (10-15 mg of frozen liver tissue per mouse) were lysed in TRIzol reagent to remove lipid, and the aqueous phase was applied to the RNeasy kit column for subsequent purification. Relative gene expression was calculated using the comparative Ct (2-ΔΔCt) method where values were normalized to a housekeeping gene. Taqman® primers were purchased from ThermoFisher Scientific.

2.2.6 Transcriptome analysis

2.2.6.1.1 *Nanostring differential gene expression and pathway analysis*

RNA was extracted from liver tissue using RNeasy kit as per manufacturer's protocol. All RNA samples passed the BioAnalyzer quality control test. The expression of 770 target genes in the nCounter Fibrosis Panel (NanoString Technologies) and an additional 22 orthologous mus musculus genes corresponding to the 25-gene NASH severity signature (Govaere *et al.*, 2020) was determined according to manufacturer's protocol at the McMaster Genomics Facility. Technical and biological normalization

against global geometric mean was performed in nSolver 4.0 software (NanoString Technologies). Briefly, technical normalization was performed in the nSolver software (version 4.0.70) by normalizing sample target raw counts to the geometric mean of positive control spike-ins. Biological normalization was performed by normalizing sample target raw counts to the geometric mean of selected housekeeping genes (*Ppia, Nubp1, Nol7, Armh3, Rplp0, Cnot10, Pgk1, and Acad9*). Pathway scores were calculated as the first principal component of the normalized expression values for all genes in each pathway and samples were compiled according to experimental groups to determine average pathway scores. Statistical significance was calculated between experimental groups using multiple t-tests and p-values were corrected for multiple comparisons using Benjamin-Hochberg false discovery rate.

2.2.6.1.2 RNA-Seq differential gene expression analysis

Sequence quality control, alignment and count were performed (Govaere *et al.*, 2020). Counts were obtained from GEO repository (GSE135251). Normalized and rlog transformed gene expression values of human healthy and NASH/NAFLD biopsies were determined using DESeq2 relative log expression normalization method (Love, Huber and Anders, 2014).

2.2.6.1.3 Gene set analysis

To compare variations in pathway enrichment between human and mice, Gene Set Enrichment Analysis (GSEA) was performed on Nanostring normalized expression values

derived from diseased and treated mice using the Nanostring nCounter Fibrosis v2 Panel pathways as gene sets (Subramanian *et al.*, 2005) and using chow-fed mice as the control phenotype. Similarly, GSEA was performed using matching orthologous genes on DESeq2 normalized count data derived from human NASH/NAFLD patients grouped by fibrosis stage and using healthy liver samples as the control phenotype. Signal to noise GSEA ranking metric and 1,000 gene-set permutations were applied to calculate statistical significance of each pathway modulation. Subsequently, a pathway enrichment index was calculated to enable comparison between human and mice pathway enrichment (Nakagawa *et al.*, 2016). Briefly, gene set enrichment p-value underwent $\log_{10}$ transformation, rank-ordered, and assigned numerical signs corresponding to the normalized enrichment score to denote pathway enrichment or suppression. Additionally, single sample GSEA (ssGSEA) was performed using log transformed human and mice gene expression data independently. Furthermore, gene level comparisons were performed by standardizing the log transformed gene expression data of each disease phenotype against that of the entire dataset for each gene on the z-scale. Similarity between samples were determined based on Euclidean distance, Pearson correlation metrics, and PCA.

2.2.7 Metabolic assays and stable isotope tracing

Mice were administered [U-$^{13}C_6$]-D-glucose by IP injection. Mice were sacrificed either 15 minutes or 2 hours post injection to measure incorporation of [$^{13}C_6$]-D-glucose into glycolytic/TCA cycle intermediates or lipid metabolites respectively. Mice sacrificed with 15-minute tracing were fasted for 6 hours prior to IP injection (7am-1pm) and mice

sacrificed with 2-hour tracing were in the fed-state (7am). Tissues were snap frozen and stored in liquid nitrogen, 15-30 mg of liver tissue was chipped and homogenized in 80% methanol on ice (Z. Wang *et al.*, 2020). Samples were frozen and thawed 3 times and centrifuged, then the supernatant was transferred and dried down for further GC/MS sample preparation (Cheng *et al.*, 2011). Dried samples were derivatized for 2 hours at 42ºC in 50 µL of methoxyamine hydrochloride (10 mg/ml) and 100 µL N-tert-Butyldimethylsilyl-N-methyltrifluoroacetamide for 90 minutes at 72ºC. Metabolites were then analyzed using Agilent 7890B gas chromatograph and Agilent 5977B mass selective detector. Tissue pellets were dissolved with 500 µL 0.1 M NaOH and protein concentrations were determined using a BCA assay. Total metabolite abundances were measured as area of the total ion current peak normalized to protein content. The measured distributions of mass isotopomers was corrected for natural abundance of ^{13}C. Incorporation of [$^{13}C_6$] into each metabolite was represented as abundance of the mass isotopologue relative to mg of protein or L of serum. m+2, m+4, and m+6 represent a metabolite with 2, 4, and 6 ^{13}C's incorporated respectively.

2.2.8 Primary mouse cell isolation and experiments

Primary hepatocytes, hepatic stellate cells, and bone-marrow derived macrophages (BMDM) were isolated from 20–24-week-old male WT or ACLY hKO *Acly*$^{f/f}$ mice. Mice were injected with AAV8-Ttr-eYFP or AAV8-Ttr-Cre one week prior to cell isolation to generate either WT or ACLY hKO mice respectively. Livers were perfused with 500 µM EGTA followed by a collagenase solution (320 U/mL) (Li, Ralphs and Tosh, 2010).

For hepatocyte isolation, following perfusion, livers were dissected and gently teased apart in William's Medium E (WME) supplemented to a final concentration of 10% FBS, 1% antibiotic-antimycotic solution and 1% glutamine ("complete WME"). Cells were then centrifuged, resuspended in complete WME and plated in 12-well collagen coated plates to approximately 85% confluency. Cells were allowed to adhere overnight. All experiments were performed the next morning, where cells were washed with PBS and switched to fresh FBS-free (serum free) WME for 2 hours prior to treatments. For Western blot samples, media was rapidly removed, cells were placed on ice, and 100 µL of cell lysis buffer was added to each well. Cells were scraped, centrifuged, and cell lysate was stored at -80°C for further analysis. Following hepatocyte isolation, the remaining cells were washed and resuspended in 32 ml Gey's Balanced Salt Solution (GBSS) B with 120 µL DNase I for hepatic stellate cell isolation (Mederacke *et al.*, 2015). The cell suspension was then mixed with a Nycodenz solution (4.94 g of Nycodenz dissolved in 15 ml GBSS/A). Gently, the cell-Nycodenz suspension was overlayed with 1.5 ml of GBSS/B using a 3 ml syringe. The suspension was then centrifuged at 1380g for 17 minutes (4°C) without brake. After centrifugation, hepatic stellate cells form a visible thin white layer at the cell-Nycodenz solution and GBSS/B interface. Cells were collected with a 5 ml pipette and transferred to a new tube. Collected cells were washed and centrifuged at 580g for 10 minutes and then cultured in DMEM.

When comparing gene expression in the liver to isolated mouse hepatic stellate cells, it was observed that isolated hepatic stellate cells had very low relative expression of *Alb* (hepatocyte marker) and *vWF for* liver sinusoid endothelial cells, indicating low

contamination with *Alb* or *vWF* expressing cells (Figure 2.1A). In comparison, isolated hepatic stellate cells had a 1500-fold increase in the mRNA expression of *Acta2* and *Col1a1,* markers quite specific to hepatic stellate cells (Figure 2.1B). To assess hepatic stellate cell purity, flow cytometry was performed using endogenous retinoid fluorescence of hepatic stellate cells and gating by retinoid/FITC as previously described (Mederacke *et al.*, 2015). BMDMs were used as a negative control for retinoid and positive control for macrophages following staining with an F4/80-APC antibody (Figure 2.1B). Isolated hepatic stellate cells were cultured in DMEM containing 10% FBS, and 1% antibiotic-antimycotic solution for 3 days prior to experiments.

For hepatic stellate cell isolation following a NASH cohort, a lobe of the liver was digested with enzyme solution buffer containing 0.5 mg/mL pronase E, 0.088 U/mL collagenase D and 1% (vol/vol) DNase I for 30 minutes at 37°C and filtered through a 100 μM cell strainer. hepatic stellate cells were isolated from the cell suspension as described above (Mederacke *et al.*, 2015). Isolated hepatic stellate cells were stored at -80°C until analysis.

For BMDMs, isolation was performed as previously described (Galic *et al.*, 2011), where mice tibias and femurs were isolated, the ends of each bone were cut off and bone marrow cells were collected by centrifuging in DMEM at 2,000 rpm for 4 minutes. Cells were resuspended and plated in 100 mL of DMEM supplemented with 10% FBS and 1% penicillin/streptomycin. After 4 hours, cells were plated into 10 cm tissue culture dishes in the presence of 20% L929 medium (as a source of macrophage colony-stimulating factor)

and differentiated for 7–8 days. One day prior to the experiment, cells were seeded for subsequent experiments. For TNF production experiments, cells were treated with 0.5 mM palmitate in 2% BSA +/- 100 µM bempedoic acid for 24 hours and TNF was measured using ELISA (Galic *et al.*, 2011).

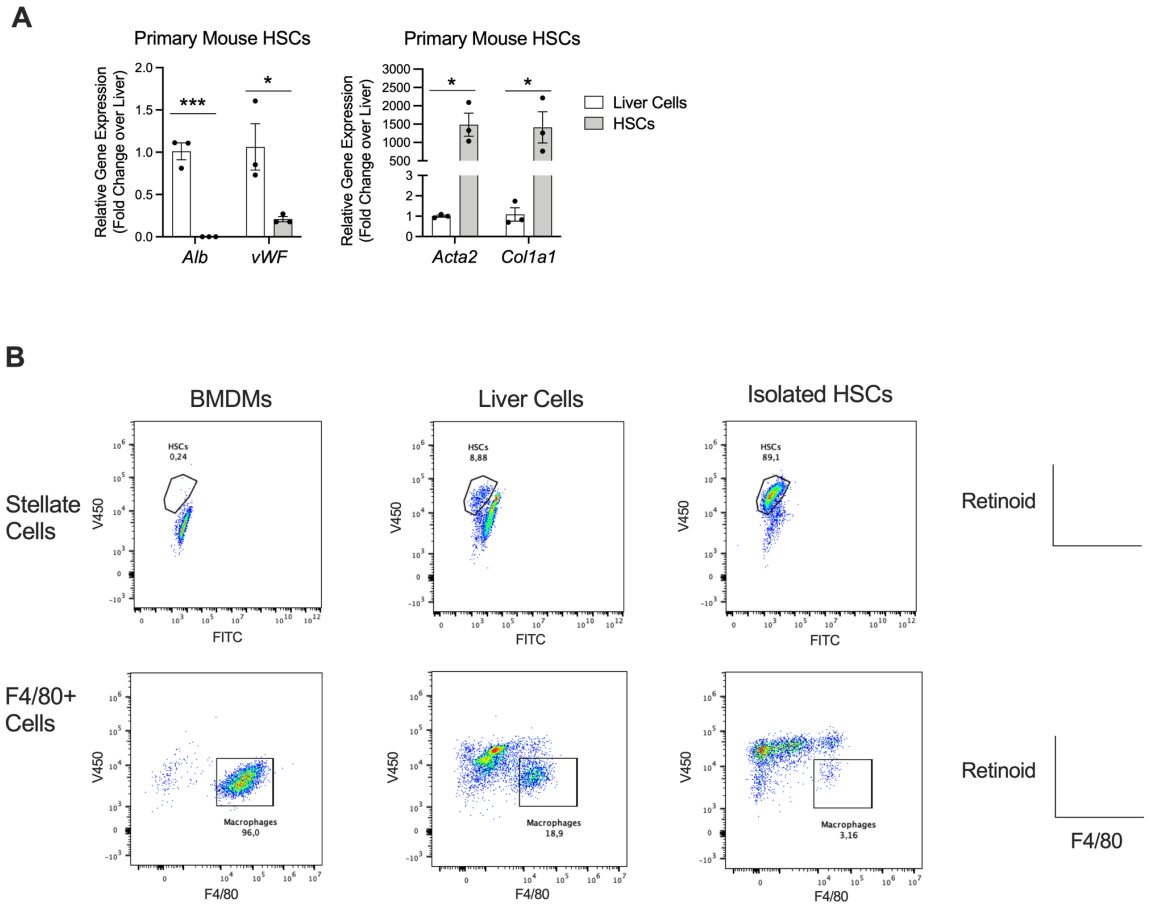

Figure 2.1. Validation of primary mouse hepatic stellate cell isolation

(A) mRNA expression of *Alb* (hepatocyte marker), *vWF* (endothelial cell marker), *Acta2* and *Col1a1* (hepatic stellate cell marker) measured by RT-qPCR in liver and hepatic stellate cell samples (n=3 in triplicate).
(B) Flow cytometry plots of retinoid (V450)+ and F4/80+ cells from BMDM, liver, and hepatic stellate cell samples.

2.2.8.1 Primary human hepatic stellate cell experiments

Primary hepatic stellate cells were obtained from 3 healthy donors (2 donors from Zen-Bio. Inc and 1 donor from Sciencell Research Laboratories). The cells were cultured in hepatic stellate cell growth media and experiments were performed in cells up to 10 passages.

2.2.8.2 Hepatic stellate cell activation assay

Hepatic stellate cells were serum starved for 1-hour, followed by a pre-treatment with vehicle or bempedoic acid (30 μM) for 1-hour. Culture media was then removed, and cells were treated with either vehicle (0.1% DMSO + 4 mM HCL, 1 mg/mL BSA vehicle) or TGF-β (5 ng/mL) with and without bempedoic acid (30 μM) in serum free DMEM for primary mouse hepatic stellate cells or in serum free hepatic stellate cell growth media for human hepatic stellate cells to assess the ability of bempedoic acid to block TGF-β-stimulated hepatic stellate cell activation. Following a 48-hour treatment, media was removed, and RNA was isolated from the cells using the RNeasy kit. mRNA expression of *Acta2*/*ACTA2* and *Col1a1*/*COL1A1* (for hepatic stellate cell activation) were measured using RT-qPCR as markers of hepatic stellate cell activation using Taqman gene expression assay probes. A subset of cells was analyzed by flow cytometry for αSMA protein expression, following a cell viability staining, a fixation (4% PFA), permeabilization (100% ice cold methanol), blocking (MACS buffer containing 0.5% BSA and 2 mM EDTA) and staining with an αSMA-FITC antibody. In addition, procollagen 1a1 secretion

was measured in hepatic stellate cell culture media using a human procollagen 1a1 ELISA. Finally, a subset of cells was analyzed for cell proliferation following staining with a KI67-Briliant Violet 421 antibody using flow cytometry. For this analysis, the cells were fixed with 70% ethanol according to the suggested protocol for this antibody.

2.2.8.3 *De novo* lipid synthesis assay

For hepatocytes and hepatic stellate cells, cells were serum-starved for 2 hours, PBS washed, then treated with media containing 1 μCi/mL [^{14}C]-lactate. Immediately after, cells were untreated (ACLY hKO experiments), or treated with vehicle (0.1% DMSO) or bempedoic acid (30 μM) (Pinkosky *et al.*, 2013) for 4 hours. Following treatment, cells were washed with ice-cold PBS and scraped in 1 M KOH/EtOH for lipid extraction by saponification (Entenman, 1957). Non-saponified lipids (cholesterol) were isolated using 1 part H_2O and 2 parts n-hexane. Saponifiable lipids (fatty acids) were then isolated using 1-part 2 N HCl and 2 parts petroleum ether to the remaining layer. Ultima Gold scintillation fluid was added to the fractions and disintegrations per minute (DPM) were measured by scintillation counting. For BMDMs, cells were serum starved with serum-free DMEM, PBS washed, and serum-free media containing [^{3}H]-acetate was added. Cells were then treated with vehicle (0.1% DMSO), bempedoic acid (30 μM) or salicylate (1 mM) for 16 hours. Lipids were extracted using Folch extraction, Ultima Gold scintillation fluid was added to lipid fractions, and DPMs were measured by scintillation counting.

2.2.8.4 Fatty acid oxidation assay

Following the 2-hour serum starve, media was removed, cells were washed with PBS, and fatty acid oxidation media was added to the cells (2% fatty acid free-BSA, 0.05 mM Na-palmitate, and 0.5 μCi/mL [^{14}C]-palmitate) for 4 hours. Immediately after, cells were treated with vehicle (0.1% DMSO) or bempedoic acid (30 μM) for 4 hours. A small Eppendorf tube filled with 450 μL of benzethonium hydroxide was placed inside a larger Eppendorf tube, and then placed upright in a glass vial. 1 mL of acetic acid was then carefully added to the bottom of the glass vial. Following treatments, media was removed and carefully added to the acetic acid layer in the vial. Plates were placed on ice. The glass vial was immediately sealed following the addition of media. Acetic acid liberates CO_2 produced by fatty acid oxidation through the TCA cycle. Glass vials are placed on an orbital shaker at 75 RPM for 2 hours to allow the benzethonium hydroxide in the inner Eppendorf tube to trap the released CO_2 (Huynh *et al.*, 2014). The inner Eppendorf containing benzethonium hydroxide was carefully placed into a plastic scintillation vial, 5 mL of scintillation fluid was added, and is allowed to quench overnight in the dark. Leftover plates were scraped in 1:2 chloroform:methanol solution into Eppendorf tubes and vortexed to isolate acid-soluble intermediates. One part chloroform was added, followed by H_2O, samples were centrifuged, and the aqueous phase was then transferred to a plastic scintillation vial. 5 mL of scintillation fluid was added to the vial and DPMs were measured by a scintillation counter. Data is represented as the sum of DPMs from the CO_2 and acid soluble intermediates. The amount of radioactivity in the sample is proportional to rates of fatty acid oxidation in the cells (Huynh *et al.*, 2014).

2.2.8.5 Glucose production assay

Before hepatocyte isolation mice were fasted overnight for 15 hours to upregulate gluconeogenesis. Following isolation, cells were plated in complete WME overnight. The next morning, cells were serum starved for 2 hours. The assay was performed in glucose-free DMEM without phenol red supplemented with 20 mM sodium lactate, 2 mM sodium pyruvate, 2 mM L-glutamine and 15 mM HEPES (glucose production media) for 6 hours. Glucose concentration in the media was measured with a colorimetric glucose assay kit (Autokit Glucose).

2.2.9 Mendelian randomization analysis

2.2.9.1 Definitions and outcomes in UK Biobank

The UK Biobank is a large-scale longitudinal cohort study that recruited over 500,000 subjects between the ages of 37-73 across the United Kingdom from 2006-2010 (Sudlow *et al.*, 2015). This study was restricted to the White British subset of the UK Biobank with genetic data (n=343,737). Blood biomarkers were defined using blood biochemistry measurements at recruitment. If necessary, quantitative variables were natural log-transformed to approximate a normal distribution. Detailed definitions are provided in Table 2.1.

Table 2.1. Description of NASH-related and metabolic outcomes assessed in the UK Biobank.

Trait	UK Biobank Field ID	ICD-10 Coding (if applicable)	Transformation (if applicable)
Apolipoprotein B	30640	N/A	N/A
Alanine aminotransferase (ALT)	30620	N/A	Natural log
Aspartate aminotransferase (AST)	30650	N/A	Natural log
Gamma glutamyltransferase (GGT)	30730	N/A	Natural log
LDL	30780	N/A	N/A
Triglycerides	30870	N/A	Natural log

*ICD: International Classification of Diseases; N/A: not applicable.

2.2.9.2 Genetic variants associated with ACLY gene expression

Genetic variants associated with *ACLY* were derived from genome-wide association summary statistics of *ACLY* gene expression in blood from the eQTLGen consortium (n=31,864) (Võsa *et al.*, 2018). Genetic variants were selected for Mendelian randomization analyses if associated with *ACLY* gene expression ($p<0.05$) and within 500 kb of the *ACLY* gene. A set of independent genetic variants were derived by LD pruning at a threshold of $r^2<0.01$ using European from 1000 Genomes phase 3 as the reference panel (Altshuler *et al.*, 2012). These independent genetic variants were carried forward to construct the GRS.

2.2.9.3 Polygenic score for ACLY

A single value representing the weighted GRS for *ACLY* gene expression was calculated by summing the effect size of each ACLY-associated genetic variant multiplied by the number of effect-corresponding alleles for each individual. The GRS represented an individual's genetically determined *ACLY* expression and was tested for association with each outcome using linear regression models. The model was adjusted for age, age^2, sex, chip type, assessment centre, and the first 10 genetic principal components. After correction for multiple hypotheses, a p-value less than 8.33×10^{-3} (0.05/6 outcomes) was considered statistically significant. A less conservative threshold for multiple hypothesis testing was also included using Benjamini-Hochberg correction of p-values to control for the false discovery rate ($p < 0.05$).

2.3 Quantification and statistical analysis

All statistical analyses were performed using GraphPad Prism (version 9.3.1). All values are reported as mean ± S.E.M. unless stated otherwise. Data were analyzed using Student's t tests or one-way with Tukey's post-hoc tests where appropriate. Histological scores were analyzed using non-parametric tests: Mann-Whitney U test when comparing two independent groups and the Kruskal-Wallis test followed by Dunn's multiple comparisons when comparing multiple independent groups. Differences were considered significant (*) when $p < 0.05$. Sample sizes were selected based on experience from previous publications. Data were excluded only in the case where a technical error occurred in sample preparation or analysis. Descriptions of additional software and statistical

analysis used for transcriptomic and mendelian randomization analysis can be found under their respective methods.

2.4 Key resources table

REAGENT or RESOURCE	SOURCE	IDENTIFIER
Antibodies		
ATP-Citrate Lyase Rabbit Antibody	Cell Signaling Technology	Cat#4332; RRID: AB_2223744
Phospho-ATP-Citrate Lyase (Ser455) Rabbit Antibody	Cell Signaling Technology	Cat#4331; RRID: AB_2257987
AceCS1 Rabbit Antibody	Cell Signaling Technology	Cat#3658; RRID: AB_2222710
Anti-Rabbit IgG, HRP-linked Antibody	Cell Signaling Technology	Cat#7074; RRID: AB_2099233
-actin Rabbit mAb (HRP Conjugated)	Cell Signaling Technology	Cat#5125; RRID: AB_1903890
Mouse Anti--tubulin	Fisher Scientific	Cat#322600
AKT (pan) (C67E7) Rabbit mAb	Cell Signaling Technology	Cat#4691; RRID: AB_915783
Phospho-AKT (Ser 473) Antibody	Cell Signaling Technology	Cat#4060; RRID: AB_2315049
Human/Mouse/Rat Smad7 Antibody	R&D Systems	Cat#MAB2029; RRID: AB_2193479
Human phospho-Smad2/3 Antibody	R&D Systems	Cat#MAB8935
Smad2/3	Cell Signaling Technology	Cat#3102; RRID: AB_10698742
TAZ, YAP (D24E4) Rabbit mAb	Cell Signaling Technology	Cat#8418; RRID: AB_10950494
CTGF (D8Z8U) Rabbit mAB	Cell Signaling Technology	Cat#86641; RRID: AB_2800085
Alpha-Smooth Muscle Actin Monoclonal Antibody (1A4), Alexa Fluor 488, eBioscience™	Invitrogen	Cat#53-9760-80
Ki67-Brilliant Violet 421™ anti-mouse Ki-67 Antibody	Biolegend	Cat#652411; RRID: AB_2562663
F4/80 Monoclonal Antibody, APC, eBioscience™	Thermofisher Scientific	Cat#17-4801-82
Bacterial and virus strains		

REAGENT or RESOURCE	SOURCE	IDENTIFIER
AAV/DJ8-Ttr-Cre	Vector Biolabs	Cat#7102
AAV/DJ8-Ttr-eYFP	Vector Biolabs	N/A
Chemicals, enzymes, peptides, and recombinant proteins		
Dulbecco's Modified Eagle Media (DMEM)	Wiscent Inc.	Cat#319005 CL
1X PBS	Wiscent Inc.	Cat#311010 CL
Penicillin-Streptomycin	Wiscent Inc.	Cat#450201 EL
Collagenase, Type I	Fisher Scientific	Cat#17100017
Benzethonium hydroxide	Sigma-Aldrich	Cat#B2156
Sodium palmitate	Millipore Sigma	Cat#P9767
Dextrose	Caledon Laboratory Chemicals	Cat#3260-1-70
Insulin, Human Recombinant	Fisher Scientific	Cat#12585014
L-carnitine Hydrochloride, synthetic	Sigma-Aldrich	Cat#C0283
EGTA MB GRADE	Fisher Scientific	Cat#32462625GM
EDTA	BioShip	Cat#6381-92-6
Ammonium persulfate, Electrophoresis Grade	BioShop® Canada Inc.	Cat#AMP001.100
Acetic acid, glacial, ReagentPlus®, ≥99%	Sigma-Aldrich	Cat#A6283
Hexane, anhydrous, 95%	Sigma-Aldrich	Cat#296090
Petroleum Ether	Fisher Scientific	Cat#E139-1
[U-$^{13}C_6$]-D-glucose	Cambridge Isotope Laboratories, Inc.	Cat#1CCLM1396
Lactic acid, sodium salt L-[14C(U)]	PerkinElmer	Cat#NEC5990
Palmitic acid, [1-14C]	PerkinElmer	Cat#NEC075H0
Isoflurane	Fresenius Kabi	Cat#CP0406V2
William's E Media, no phenol red	ThermoFisher Scientific	Cat#A1217601
DMEM, 1X, with L-glutamine, phenol red without glucose and sodiuim pyruvate	Wiscent Inc.	Cat#319-061-CL
Ultima Gold Scintilation fluid	PerkinElmer	
L-glutamine, 200 mM	Wiscent Inc.	Cat#609-065-EL
1M HEPES Solution	Wiscent Inc.	Cat#330-050-EL
Sodium L-lactate	Sigma-Aldrich	Cat#L7022
Formalin Buffered 10%	ACP Chemicals	Cat#F6000
TRIzol™ Reagent	ThermoFisher Scientific	Cat#15596026
Sodium Pyruvate 100 mM (liquid)	Wisent Inc.	Cat#600110 EL

REAGENT or RESOURCE	SOURCE	IDENTIFIER
Sodium Pyruvate (powder)	Sigma-Aldrich	Cat#P2256
Streptozotocin	Sigma-Aldrich	Cat#18883-66-4
Hepatic/Pancreatic Stellate Growth Medium	Zen-Bio Inc.	Cat#HSGM-500
Human Stellate Grown Medium, WITHOUT serum	Zen-Bio Inc.	Cat#HSGM-500-SF
Stellate Cell Growth Supplement	Sciencell Research Laboratories	Cat#5352
Stellate Cell Medium	Sciencell Research Laboratories	Cat#5301(SC)
Stellate Cell Medium-basal	Sciencell Research Laboratories	Cat#5301-B
Pronase E	Sigma-Aldrich	Cat#P5147
Collagenase D	Roche	Cat#11088888001
Collagenase from Clostridium Histolyticum	Sigma-Aldrich	Cat#C5138
DNase I	Roche	Cat#10104159001
eBioscience™ Fixable Viability Dye eFluor™ 660	Invitrogen	Cat#65086414
PrestoBlue™ Cell Viability Reagent	ThermoFisher Scientific	Cat#A13261
N-*tert*-Butyldimethylsilyl-N-methyltrifluoroacetamide	Sigma-Aldrich	Cat#394882
Methoxyamine Hydrochloride	Sigma-Aldrich	Cat#226904
Nycodenz	Accurate Chemical	Cat#1002424
Gey's Balanced Salt Solution B (GBSS/B)	Sigma-Aldrich	Cat#G9779
DMEM	Gibco	Cat#11965-092
Critical commercial assays		
RNeasy Mini Kit	Qiagen	Cat#74106
Alanine Transsminase Microplate Assay Kit	Cohesion Biosciences	Cat#CAK1002
Aspartate Transaminase Microplate Assay Kit	Cohesion Biosciences	Cat#CAK1004
Wako Autokit Glucose	Fujifilm	Cat#997-03001
Cholesterol E kit	Fujifilm	Cat#999-02601
Triglyceride Kit	Cayman Chemical	Cat#10010303

REAGENT or RESOURCE	SOURCE	IDENTIFIER
Pierce™ BCA Protein Assay Kit	ThermoFisher Scientific	Cat#23225
Clarity™ Western ECL Substrate	Bio-Rad Laboratories	Cat#1705060
Ultra-Sensitive Mouse Insulin ELISA kit	Crystal Chem	Cat#90080
nCounter Fibrosis Panel	NanoString Technologies, Inc.	Cat#115000388
Human Pro-collagen I alpha 1 Duoset ELISA	R&D Systems	Cat#DY6220-05
Wako Autokit Total Ketone Bodies: Autokit Total Ketone Bodies R1 Set Autokit Total Ketone Bodies R2 Set Ketone Body Calibrator 300 Ketone Body Calibrator 40	Fujifilm	 Cat#415-73301 Cat#411-73401 Cat#412-73401 Cat#418-73891
Mouse TNF-alpha DuoSet	R&D Systems Inc.	Cat#DY410
RNAscope® 2.5 LS Duplex Reagent kit	Advanced Cell Diagnostics, Inc	Cat#322440
LS Green Accessory Pack	Advanced Cell Diagnostics, Inc	Cat#322550
Deposited data		
Human NAFLD livers with different fibrosis stages	Govaere *et al*., 2020	NCBI GEO: GSE135251
UK BioBank	Sudlow *et al*., 2015	RRID:SCR_012815
eQTLgen	Võsa *et al*., 2021	N/A
Experimental models: Organisms/strains		
Cryopreserved Human Hepatic Stellate Cells	Zen-Bio Inc.	HP-F-S
Human Hepatic Stellate Cells	Sciencell Research Laboratories	5300(SC)
Mouse: C57BL/6J	The Jackson Laboratory	Cat#000664; RRID: AB_IMSR_JAX:000664
Mouse: *Acly*$^{tm1.1Welk}$/MmJax	The Jackson Laboratory	Cat#:43555; RRID: AB_MMRRC_043555-MU

REAGENT or RESOURCE	SOURCE	IDENTIFIER
Oligonucleotides		
Hprt1 (Human)	ThermoFischer Scientific	Cat#4331182; Assay ID: Hs02800695_m1
Col1a1 (Human)	ThermoFischer Scientific	Cat#4331182; Assay ID: Hs00164004_m1
Acta2 (Human)	ThermoFischer Scientific	Cat#4331182; Assay ID: Hs00426835_g1
Mki67 (Human)	ThermoFischer Scientific	Cat#4331182; Assay ID: Hs04260396_g1
Hprt1 (Mouse)	ThermoFischer Scientific	Cat#4331182; Assay ID: Mm03024075_m1
Col1a1 (Mouse)	ThermoFischer Scientific	Cat#4331182; Assay ID: Mm00801666_g1
Acly (Mouse)	ThermoFischer Scientific	Cat#4331182; Assay ID: Mm01302282_m1
Slc27a2 (Mouse)	ThermoFischer Scientific	Cat#4331182; Assay ID: Mm00449517_m1
Acss2 (Mouse)	ThermoFischer Scientific	Cat#4331182; Assay ID: Mm00480101_m1
Smad2	ThermoFischer Scientific	Cat#4331182; Assay ID: Hs00998187_m1
Smad3	ThermoFischer Scientific	Cat#4331182; Assay ID: Hs00969210_m1
Smad7	ThermoFischer Scientific	Cat#4331182; Assay ID: Hs00998193_m1
RNAscope® LS probe – *Mm-Acta2-C2*	Advanced Cell Diagnostics, Inc	Cat#319538-C2
RNAscope® LS probe – *Mm-Acly-C1*	Advanced Cell Diagnostics, Inc	Cat#460398-C1
Software and algorithms		

REAGENT or RESOURCE	SOURCE	IDENTIFIER
Image J		https://imagej.nih.gov/ij/
nSolver Analysis Software 4.0	NanoString	https://nanostring.com/products/analysis-solutions/nsolver-advanced-analysis-software/
R version 3.6.0 (R Core Team (2022)	R	https://www.r-project.org/
GraphPad Prism version 9.3.1 (350)	GraphPad	https://www.graphpad.com/scientific-software/prism/
MATLAB software	MathWorks®	https://www.mathworks.com/products/matlab.html
Other		
Rodent diet with 40 kcal% fat, 20 kcal% fructose, 0.02% cholesterol	Research Diets, Inc.	Cat#D19101102
Rodent diet with 10 kcal% fat	Research Diets, Inc.	D09100304
Rodent diet with 45 kcal% fat	Research Diets, Inc.	D12451
High Fat Diet 32	CLEA Japan, Inc.	HFD32
Accu-Chek® Inform II system (glucometer)	Roche	N/A
Accu-Chek® Guide (test strips)	Roche	N/A
Solace zone heated cage units	Alternative Design Manufacturing & Supply Inc.	N/A
Comprehensive Laboratory Animal Monitoring System	Columbus Instruments	N/A
Specific-pathogen free (SPF) Microisolators	The Jackson Laboratory	N/A
TPX Cages	CLEA Japan, Inc.	N/A
Polypropylene tubes with anticoagulant	Novo-Heparin, Mochida Pharmaceutical Co. Ltd.	N/A
Nikon 90i Eclipse	Nikon Inc.	N/A

REAGENT or RESOURCE	SOURCE	IDENTIFIER
7890B Gas Chromatograph (GC) System	Agilent	N/A
5977B GC/MSD Instrument	Agilent	N/A

CHAPTER 3: INHIBITION OF ATP-CITRATE LYASE IMPROVES NASH, LIVER FIBROSIS, AND DYSLIPIDEMIA

3. Inhibition of ATP-citrate lyase improves NASH, liver fibrosis, and dyslipidemia

3.1 Results

3.1.1 Developing and characterizing a mouse model of NASH and fibrosis

To study the role of ACLY in NASH, we developed and characterized a novel mouse model of NASH that replicates many of the metabolic, histological, and transcriptional characteristics of advanced NASH patients. Housing mice fed a high-fat diet (HFD) at 28-30°C, a temperature range known as thermoneutrality (TN), for 24 weeks, suppresses energy expenditure and promotes the development of NAFLD compared to room temperature (RT) housing (Giles *et al.*, 2017). However, a HFD suppresses liver DNL (Duarte *et al.*, 2014) and is therefore not optimal to model the development of NASH where this pathway is known to be upregulated (Knebel *et al.*, 2012; Fullerton *et al.*, 2013; Lambert *et al.*, 2014; Cordoba-Chacon *et al.*, 2015; Samuel and Shulman, 2018; Sanders *et al.*, 2018). To accelerate the development of NASH, studies have housed mice at RT and fed them a diet high in fat and fructose (Clapper *et al*., 2013). However, whether this diet also promotes NASH when mice are housed at TN and if so whether disease development is greater than at RT is not known. We therefore examined mice fed a control chow diet or a high fat (40% fat), high fructose (20 kcal%) diet (herein named the NASH diet (ND)) for 24 weeks (32-33 weeks of age) at RT or TN.

3.1.2 Housing mice fed a high-fat, high-fructose diet at thermoneutrality promotes histological and molecular characteristics similar to advanced human NASH

Compared to RT housing, TN housing did not change body mass, fat mass, glucose tolerance, insulin tolerance, serum triglycerides, serum cholesterol or serum aspartate transaminase (AST) in mice fed the ND (Figure 3.1A-G). Despite similar body mass and adiposity, mice housed at TN had increased liver mass (Figure 3.1H) and serum alanine transaminase (ALT) (Figure 3.1G), findings that corresponded with increased histological scoring of liver steatosis, inflammation, and ballooning, resulting in an increase in the NAFLD activity scores (NAS) in TN housed mice (Figure 3.2A-B). Fibrosis was increased in mice fed the ND and housed at TN (Figure 3.2C-E). Importantly, mice fed the ND and housed at TN also had other histological features that parallel markers of steatosis, inflammation, and cell injury in human NASH (Kleiner *et al.*, 2005), including megamitochondria, glycogenated nuclei, Mallory-Denk bodies, acidophilic bodies, atypical mitosis, lymphoid aggregation, microgranulomas, pigmented macrophages, lipogranulomas, and microvesicular and macrovesicular steatosis (Figure 3.2F).

3.1.3 Disease development trajectory between 11 and 25 weeks

To examine the trajectory of disease development in mice housed at TN and fed the ND we assessed histology between 11-25 weeks on the diet and found that maximal steatosis, hepatocellular ballooning, and NAS occur after 11 weeks, with inflammation progressing at 25 weeks (Figure 3.3A-B). Fibrosis was modest at 11 and 16 weeks but increased between weeks 18-25 (Figure 3.3C). There were no differences in liver

triglycerides or cholesterol, serum cholesterol or ALT, and there were modest reductions in serum triglycerides and AST with time (Figure 3.3D-F). There was also no significant change in the expression or phosphorylation of ACLY, however, ACSS2, which produces compensatory acetyl-CoA from acetate, was lower at 25 weeks compared to earlier time points (Figure 3.3G). Compared to chow-fed mice, the ND did not change protein expression of ACLY (Figure 3.3H), however, mRNA expression levels of *Acly and Accs2* were higher compared to mice fed a 45% HFD (no added fructose) (Figure 3.3I). These data indicate that mice fed a ND and housed at TN develop steatosis, followed by inflammation and then fibrosis paralleling many of the histological features of NASH in humans.

3.1.4 Housing mice fed a high-fat, high-fructose diet at thermoneutrality promotes transcriptionally characteristics similar to advanced human NASH

To determine if histological findings correspond with transcriptional changes in human NASH progression, we profiled the expression of a gene signature panel that characterizes the progression of human liver from a healthy state to pre-fibrotic and fibrotic/cirrhotic stages of NASH (Govaere *et al.*, 2020). Hierarchical clustering of human and mouse samples reveal two distinct groups differentially enriched for pre-fibrotic or fibrotic stages of disease (Figure 3.2G and 3.4A). While both RT-ND and TN-ND samples clustered with fibrotic human samples, aggregate Pearson pairwise correlation shows that the expression pattern of the gene panel is more positively correlated between TN-ND mice and fibrotic F2 – F4 NASH samples than RT-ND mice (Figure 3.1I). In contrast, RT- and TN-Chow mice are more positively correlated with pre-fibrotic NAFLD and F0-F1

biopsies. Principal component analysis (PCA) further corroborates this finding (Figure 3.2H and 3.4B). Disease progression from NAFLD to F4 NASH is coordinated by the first principal component (PC1) and progressively increases from NAFLD to F4 NASH in human and from RT-Chow to TN-ND conditions in mice (Figure 3.2H and Figure 3.4B). Additionally, TN-ND samples are in closer proximity to the center of F3 and F4 ellipsoids than RT-ND samples. These data show that mice housed at TN and fed a diet high in fat and fructose exhibit many physiological, histological, and transcriptional similarities with advanced (F3 and F4) NASH in humans, thus representing a clinically relevant experimental model for testing genetic and pharmacological interventions.

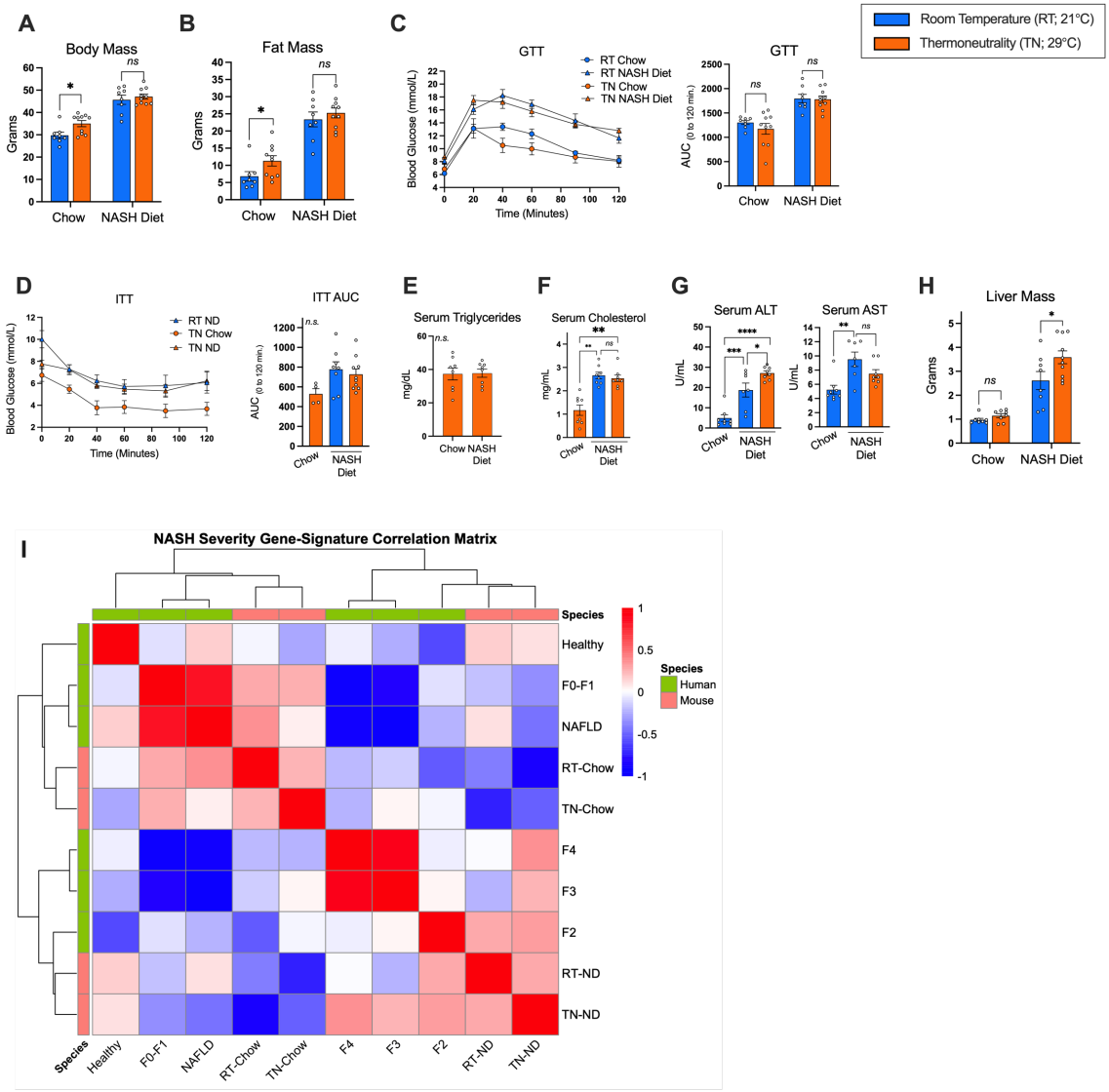

Figure 3.1. A metabolically induced mouse model of NASH and liver fibrosis

(A-B) Body and fat mass in grams at sacrifice.
(C) Glucose tolerance test (GTT) performed via IP injections of 1 g/kg D-glucose at 29 weeks of age and $AUC_{0\text{-}120\ min}$ was calculated.
(D) Insulin tolerance test (ITT) performed via IP injections of 1.3 U/kg insulin at 30 weeks of age, and $AUC_{0\text{-}120\ min}$ was calculated (n=4 for TN-chow, n=8 for RT-ND, n=10 for TN-ND).
(E-F) Serum triglycerides and cholesterol measured at sacrifice (n=8/group).
(G) Serum ALT and AST measured at sacrifice (n=8/group).

(H) Liver mass in grams at sacrifice.
(I) Heatmap depicting pairwise Pearson correlation matrix between human and mouse samples at varying stages of NASH severity (n=6/group, mice; n=10-54, human).
Data are presented as mean ± SEM. Statistical significance * ($p < 0.05$) by unpaired t-test within each dietary condition. (n=8 for RT, n=8-10 for TN unless stated otherwise).

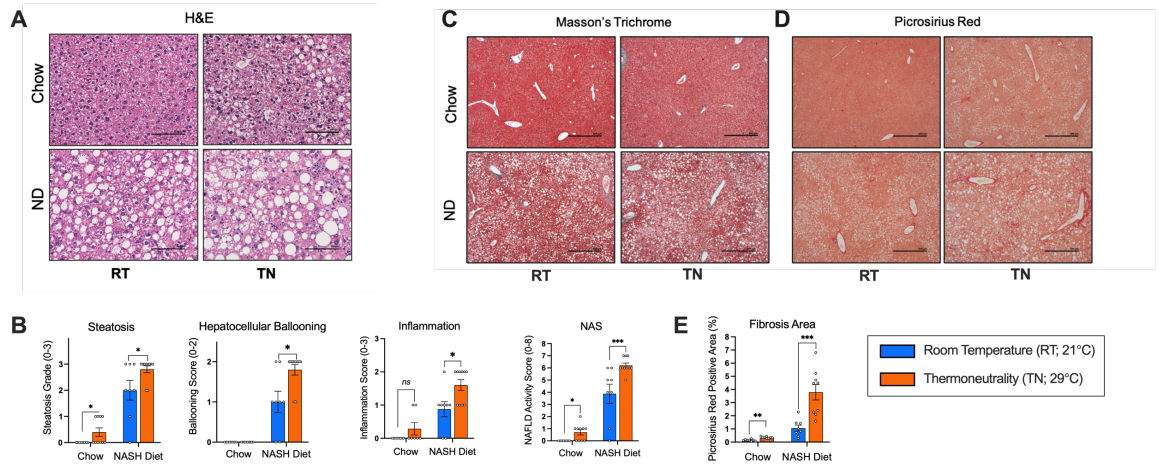
A
H&E
Chow
ND
RT
TN
C
Masson's Trichrome
D
Picrosirius Red
B
Steatosis
Hepatocellular Ballooning
Inflammation
NAS
Steatosis Grade (0-3)
Ballooning Score (0-2)
Inflammation Score (0-3)
NAFLD Activity Score (0-8)
Chow
NASH Diet
E
Fibrosis Area
Picrosirius Red Positive Area (%)
Room Temperature (RT; 21°C)
Thermoneutrality (TN; 29°C)

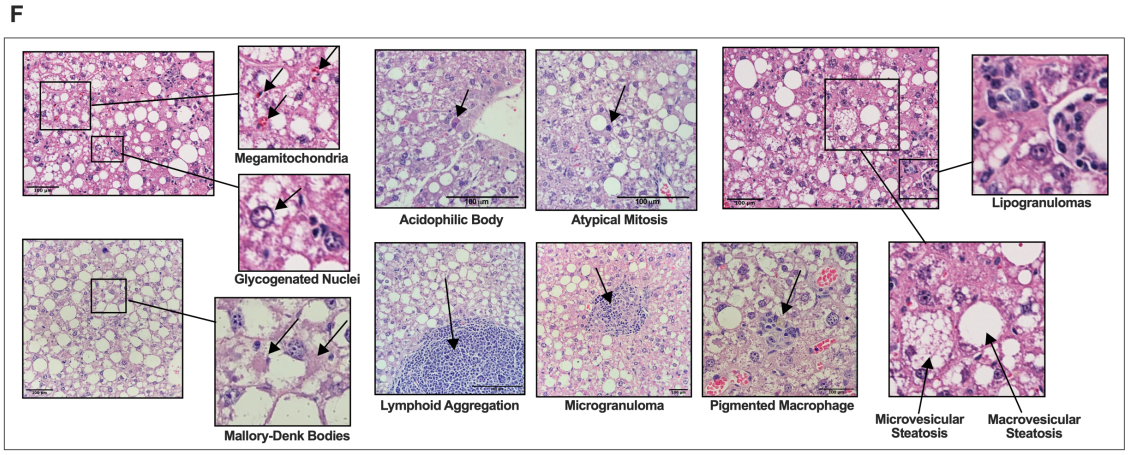
F
Megamitochondria
Glycogenated Nuclei
Mallory-Denk Bodies
Acidophilic Body
Atypical Mitosis
Lipogranulomas
Lymphoid Aggregation
Microgranuloma
Pigmented Macrophage
Microvesicular Steatosis
Macrovesicular Steatosis

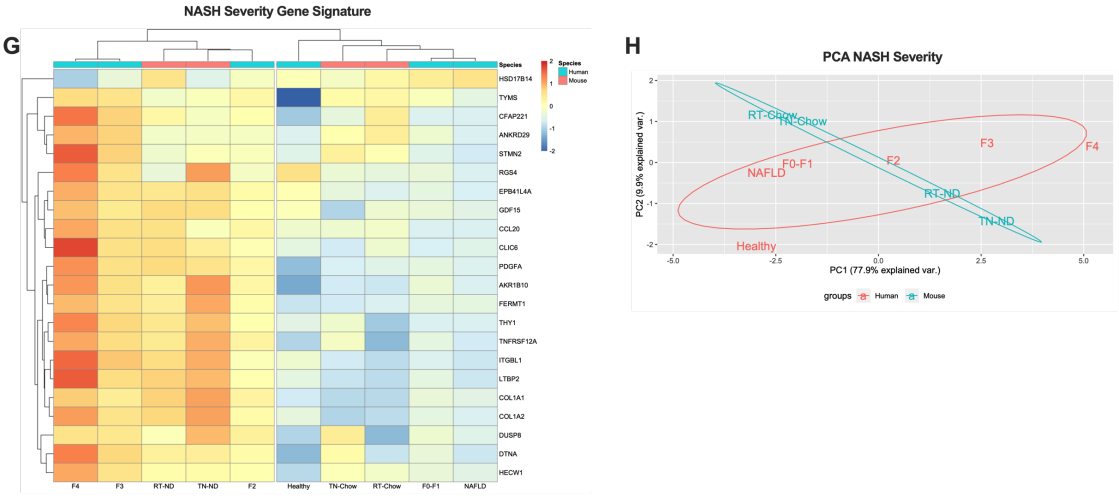
G
NASH Severity Gene Signature
Species
Human
Mouse
HSD17B14
TYMS
CFAP221
ANKRD29
STMN2
RGS4
EPB41L4A
GDF15
CCL20
CLIC6
PDGFA
AKR1B10
FERMT1
THY1
TNFRSF12A
ITGBL1
LTBP2
COL1A1
COL1A2
DUSP8
DTNA
HECW1
F4
F3
RT-ND
TN-ND
F2
Healthy
TN-Chow
RT-Chow
F0-F1
NAFLD
H
PCA NASH Severity
PC2 (9.9% explained var.)
PC1 (77.9% explained var.)
groups
Human
Mouse

Figure 3.2. Housing mice fed a high-fat, high-fructose diet at thermoneutrality promotes histological and molecular characteristics similar to advanced human NASH

(A) Representative photomicrographs of H&E-stained liver sections taken at 20X.
(B) NAS and individual histological scores for steatosis grade, hepatocellular ballooning, and lobular inflammation.
(C-D) Representative photomicrographs of **(C)** Masson's trichrome (MTC) and **(D)** picrosirius red (PSR)-stained liver sections taken at 4X.
(E) % positive PSR area measured on ImageJ.
(F) Representative photomicrographs of H&E-stained liver sections from TN-ND mice taken at 20X highlighting key histological features of NASH.
(G) Gene expression heatmap of 22 murine orthologous genes identified from the 25-gene signature characterizing human NASH severity (n=6/group, mice; n=10-54, human).
(H) PCA coordinates disease progression in human and mice samples according to average gene signature expression values (n=6/group for mouse, n=10-54/group for human).
Data are presented as mean ± SEM. Statistical significance within each dietary condition (*$p < 0.05$, **$p < 0.01$, ***$p < 0.001$, ****$p < 0.0001$) by unpaired t-test or by unpaired Mann-Whitney test (for histological scores) (n=8 for RT, n=10 for TN unless stated otherwise).

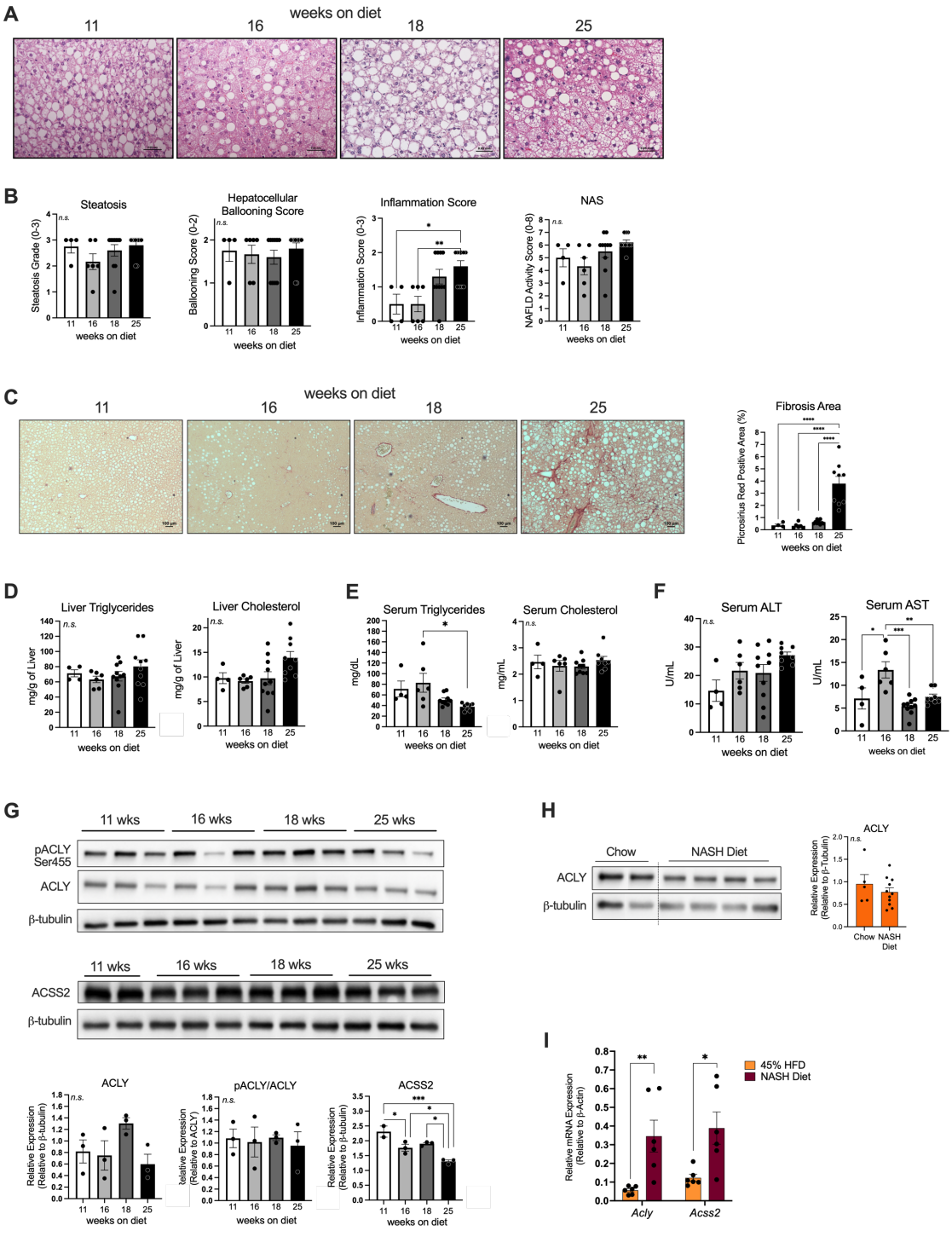
A
weeks on diet
11
16
18
25
B
Steatosis
Steatosis Grade (0-3)
Hepatocellular Ballooning Score
Ballooning Score (0-2)
Inflammation Score
Inflammation Score (0-3)
NAS
NAFLD Activity Score (0-8)
n.s.
weeks on diet
C
Fibrosis Area
Picrosirius Red Positive Area (%)
D
Liver Triglycerides
mg/g of Liver
Liver Cholesterol
E
Serum Triglycerides
mg/dL
Serum Cholesterol
mg/mL
F
Serum ALT
U/mL
Serum AST
G
11 wks
16 wks
18 wks
25 wks
pACLY Ser455
ACLY
β-tubulin
ACSS2
pACLY/ACLY
Relative Expression (Relative to β-tubulin)
Relative Expression (Relative to ACLY)
H
Chow
NASH Diet
I
45% HFD
NASH Diet
Relative mRNA Expression (Relative to β-Actin)
Acly
Acss2

Figure 3.3. Progression of disease over time in a metabolically induced mouse model of NASH and liver fibrosis

(A) Representative photomicrographs of H&E-stained liver sections taken at 20X.
(B) NAS and corresponding individual histological scores for steatosis grade, hepatocellular ballooning, and lobular inflammation from mice on ND and housed at TN for 11, 16, 18, or 25 weeks.
(C) Representative photomicrographs of PSR-stained liver sections taken at 4X and % positive PSR area measured on ImageJ.
(D-E) Liver and serum triglycerides and cholesterol measured at sacrifice.
(F) Serum ALT and AST measured at sacrifice.
(G-H) Relative liver protein expression measured by Western blot densitometry in mice housed at TN (n=3/group in (G), n=5 for chow and n=11 for ND in (H)).
(I) Liver mRNA expression of *Acly* and *Acss2* was measured using RT-qPCR and expressed relative to *Actb* (n=6/group).
Data are presented as mean ± SEM. Statistical significance ($p < 0.05$) by one-way ANOVA and * for Tukey's post hoc test or by unpaired Kruskal-Wallis test (for histological scores) and * for Dunn's multiple comparisons (n=4 for 11 weeks, n=6 for 16 weeks, n=8-10 for 18 weeks and 25 weeks unless stated otherwise).

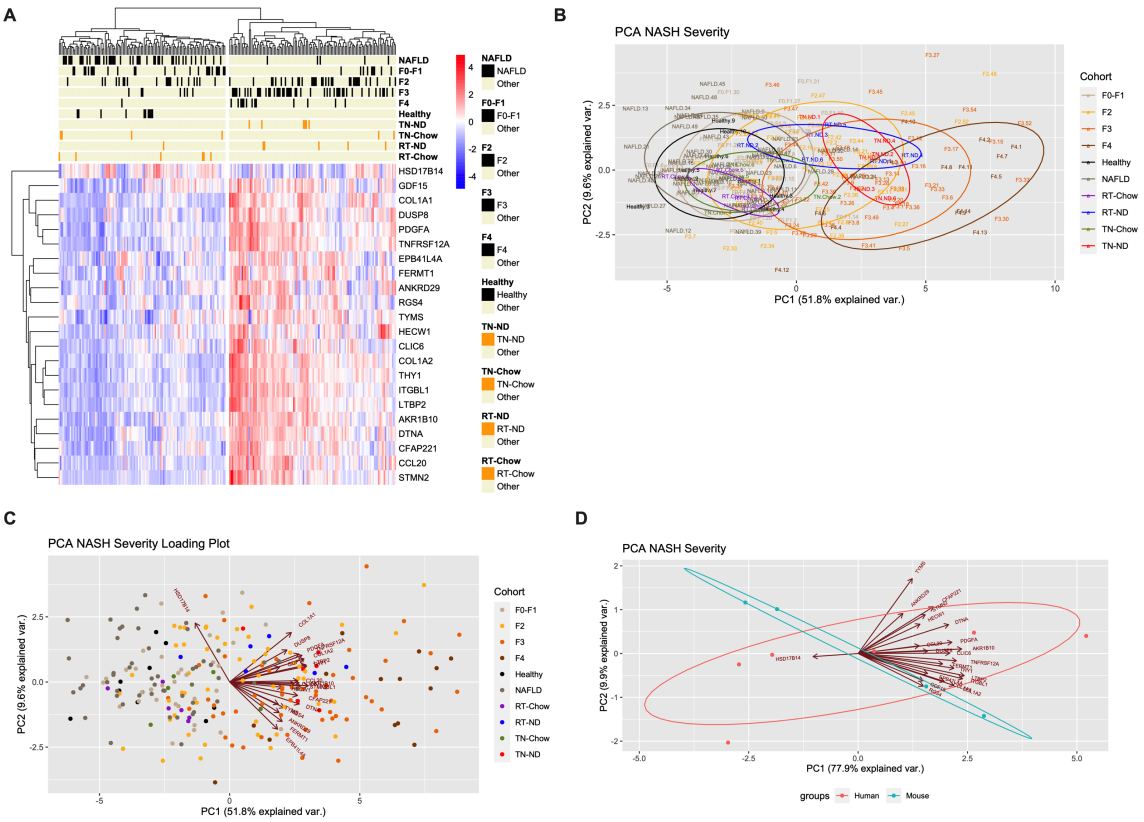

Figure 3.4. Supplementary gene expression data for mouse model validation
(A) Hierarchical clustering of individual human and mouse samples based on normalized gene expression values.
(B) PCA analysis of individual human and mouse samples based on gene expression values.
(C-D) PCA loading plots showing the positive or negative correlation between individual genes and principal components for aggregate and individual sample PCA.

3.1.5 Hepatocyte-specific deletion of ACLY reduces liver fatty acid and sterol synthesis and increases fatty acid oxidation

To investigate the role of ACLY in hepatocytes, ACLY floxed (*Acly$^{f/f}$*) mice (Zhao *et al.*, 2016) were injected with adeno-associated virus AAV8-Ttr-eYFP (wildtype (WT)) or AAV8-Ttr-Cre (ACLY hKO). Consistent with previous studies showing the efficiency and specificity of this promoter (Malato *et al.*, 2011), we saw that after one-week ACLY was almost undetectable in hepatocytes of *Acly$^{f/f}$* mice injected with AAV8-Ttr-Cre (Figure 3.5A). Primary hepatocytes from ACLY hKO mice had lower fatty acid and sterol synthesis (Figure 3.5B) and increased fatty acid oxidation (Figure 3.5C) compared to WT hepatocytes. In separate experiments completed one week following injection, mice were placed in metabolic cages and monitored for 24 hours. ACLY hKO mice had a small increase in food intake but no change in energy expenditure or ambient activity (Figure 3.6A). Consistent with observations in isolated hepatocytes, ACLY hKO mice had decreased whole body respiratory exchange ratio (RER) indicative of increased fatty acid oxidation and decreased carbohydrate oxidation and/or decreased DNL compared to WT mice (Figure 3.5D-E). To directly assess the impact on the liver, mice were injected with a bolus of [$^{13}C_6$]-D-glucose with livers collected after 15 minutes or 2 hours. ACLY hKO mice had increased ^{13}C incorporation into liver citrate 15 minutes post [$^{13}C_6$]-D-glucose-injection (Figure 3.5F-G). At 2 hrs post injection, ^{13}C incorporation into liver citrate was not different (Figure 3.5H), however, [$^{13}C_6$]-D-glucose incorporation into palmitate, stearate, and oleate was significantly reduced in ACLY hKO mice (Figure 3.5F-I). This occurred despite similar serum [$^{13}C_6$]-glucose levels between genotypes at both 15 minutes and 2 hours post-$^{13}C_6$-D-glucose injection (Figure 3.6B). These data indicate that

hepatocyte-specific inhibition of ACLY reduces fatty acid and sterol synthesis while increasing fatty acid oxidation, suggesting that inhibition may be beneficial for NASH.

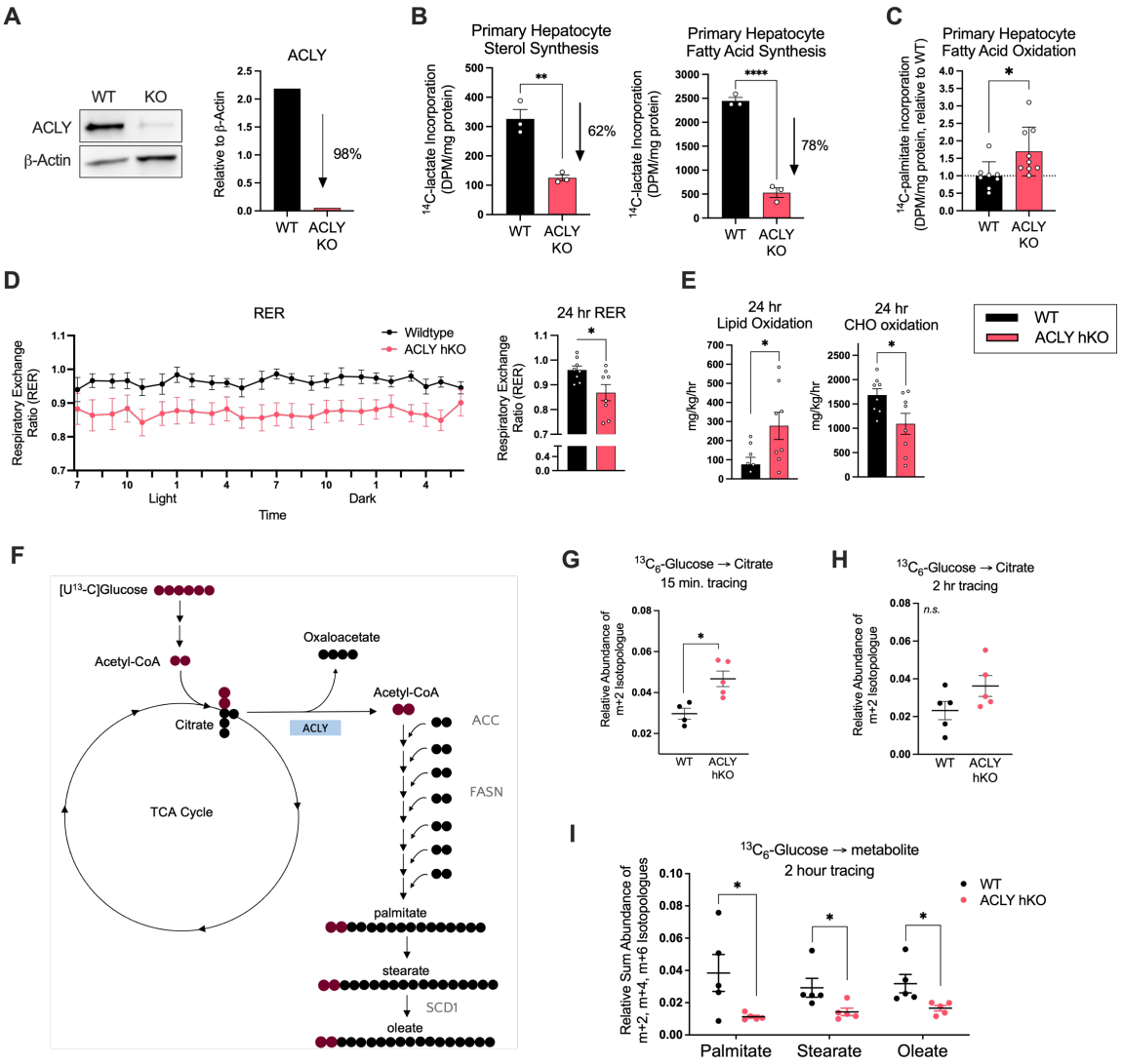

Figure 3.5. Hepatocyte-specific deletion of ACLY reduces liver fatty acid and sterol synthesis and increases fatty acid oxidation

(A) Relative ACLY expression in isolated hepatocytes determined by Western blot densitometry (n=1/group).
(B) Incorporation of [^{14}C]-lactate into non-saponifiable (sterols) and saponifiable (fatty acids) lipid fractions in primary mouse hepatocytes expressed relative to mg of protein (n=3 in triplicate).
(C) Incorporation of [^{14}C]-palmitate into CO_2 and acid-soluble β-oxidation intermediates in primary mouse hepatocytes expressed relative to mg of protein (n=8-9/group).

(D-E) Metabolic cage data in chow-fed mice represented as averages over two days (n=8/group). **(D)** Respiratory exchange ratio (RER). **(E)** Lipid oxidation and carbohydrate (CHO) oxidation calculated from VO_2 and VCO_2.
(F-I) Mice from (D) and (E) were intraperitoneally (IP) injected with 1g/kg [$^{13}C_6$]-D-glucose in a fed-state and sacrificed 2 hours post-injection. **(F)** Visual representation of ^{13}C flux (labelled red) through *de novo* lipogenesis (DNL). Relative m+2 isotopologue abundance of citrate **(G)** 15 minutes and **(H)** 2 hours following [$^{13}C_6$]-D-glucose injection, and **(I)** palmitate, stearate, and oleate, was measured in the liver of mice by GC/MS (n=4-5/group).
Data are presented as mean ± SEM. Statistical significance (*p < 0.05, **p < 0.01, ***p < 0.001, ****p < 0.0001, *n.s.*, not significant) by unpaired t-test.

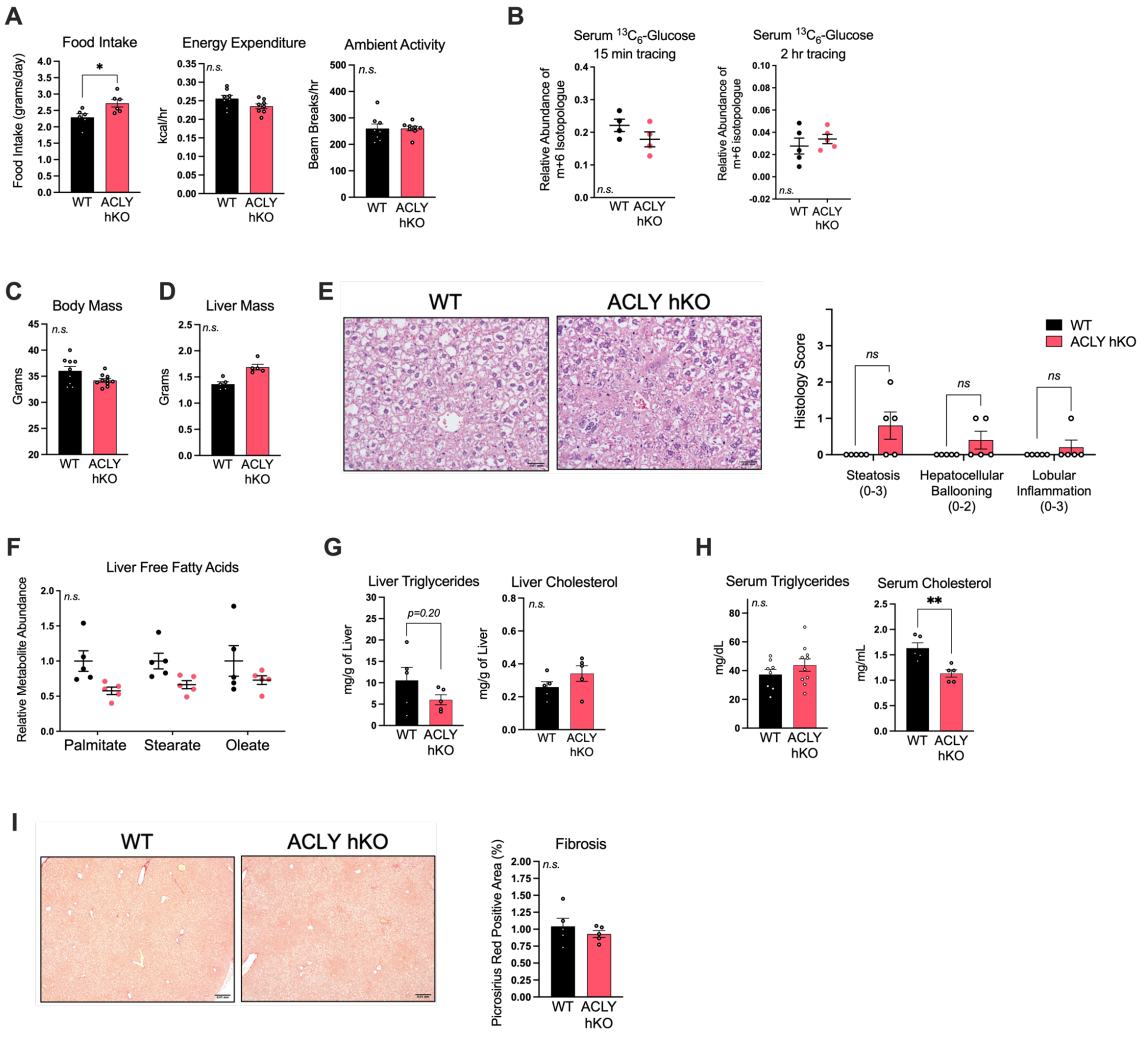

Figure 3.6. The effect of hepatocyte-ACLY knockout on whole body energy metabolism, NASH, and fibrosis in chow-fed mice

(A) At 30 weeks of age, mice were placed in metabolic cages and energy expenditure, ambient activity, and food intake was measured and represented as averages over two days (n=7-8/group).
(B) Serum glucose levels measured by GC/MS and expressed relative to volume.
(C) Body mass at sacrifice (n=9-10/group).
(D) Liver mass in grams at sacrifice (n=9-10/group).
(E) Representative photomicrographs of H&E-stained liver sections along with NAS and corresponding individual histological scores for steatosis grade, hepatocellular ballooning, and lobular inflammation.

(F) Liver metabolite abundance of palmitate, stearate, and oleate measured at sacrifice 2 hours post-glucose injection by GC/MS and expressed relative to protein.
(G-H) Liver and serum triglycerides and cholesterol measured at sacrifice (n=8-10/group for serum triglycerides).
(I) Representative photomicrographs of PSR-stained liver sections taken at 4X along with % PSR red area measured on ImageJ.
Data are presented as mean ± SEM. Statistical significance * ($p < 0.05$) by unpaired t-test or unpaired Mann-Whitney U test (for histological scores). (n=5/group unless stated otherwise).

3.1.6 Hepatocyte-specific deletion of ACLY reduces liver steatosis and intracellular ballooning without affecting inflammation and fibrosis

To examine the effects of genetic inhibition of ACLY in hepatocytes on liver histology and steatosis, *Acly*$^{f/f}$ mice were housed at TN and fed a chow or ND starting at 8 weeks of age for 16 weeks (the time point as described in Figure 3.1 and 3.2. at which significant NASH has developed) before being injected via the tail vein with AAV8-Ttr-eYFP (WT) or AAV8-Ttr-Cre (ACLY hKO) (Figure 3.7A).

In mice fed a chow diet there were no differences in body mass (Figure 3.6C), liver mass (Figure 3.6D), histological assessment of steatosis, hepatocellular ballooning, or lobular inflammation (Figure 3.6E). Consistent with these findings, liver fatty acids, triglycerides and cholesterol were not significantly altered between WT and ACLY hKO mice (Figure 3.6F-G). There was also no change in serum triglycerides, but serum cholesterol was reduced in ACLY hKO mice (Figure 3.6H). Consistent with low levels of steatosis and inflammation, fibrosis was nearly undetectable and unaltered between genotypes (Figure 3.6I).

When fed the ND ACLY hKO mice had no change in body or liver mass (Figure 3.7B). Liver histological assessments revealed reductions in steatosis and ballooning without changes in inflammation or NAS (Figure 3.7C). Consistent with reductions in the steatosis score, ACLY hKO mice had reduced liver free-fatty acids (Figure 3.7D) and triglycerides (Figure 3.7E) but no change in liver cholesterol (Figure 3.7E). However, in contrast to findings with ACC inhibitors, ACLY hKO mice had reduced serum triglycerides and cholesterol (Figure 3.7F). Consistent with similar levels of inflammation between

genotypes, there were no differences in serum ALT and AST (Figure 3.7G), or fibrosis (Figure 3.7H) between WT and ACLY hKO mice. Reductions in ACLY would be expected to reduce acetyl-CoA which is utilized by ACC to generate malonyl-CoA, the first committed step in DNL and an allosteric inhibitor of fatty acid oxidation (Batchuluun, Pinkosky and Steinberg, 2022). Consistent with this concept, liver malonyl-CoA was reduced in ACLY hKO mice compared to controls (Figure 3.7I). These data indicate that genetic inhibition of ACLY in hepatocytes reduces liver malonyl-CoA, liver and serum lipids and hepatocellular ballooning but does not affect liver fibrosis.

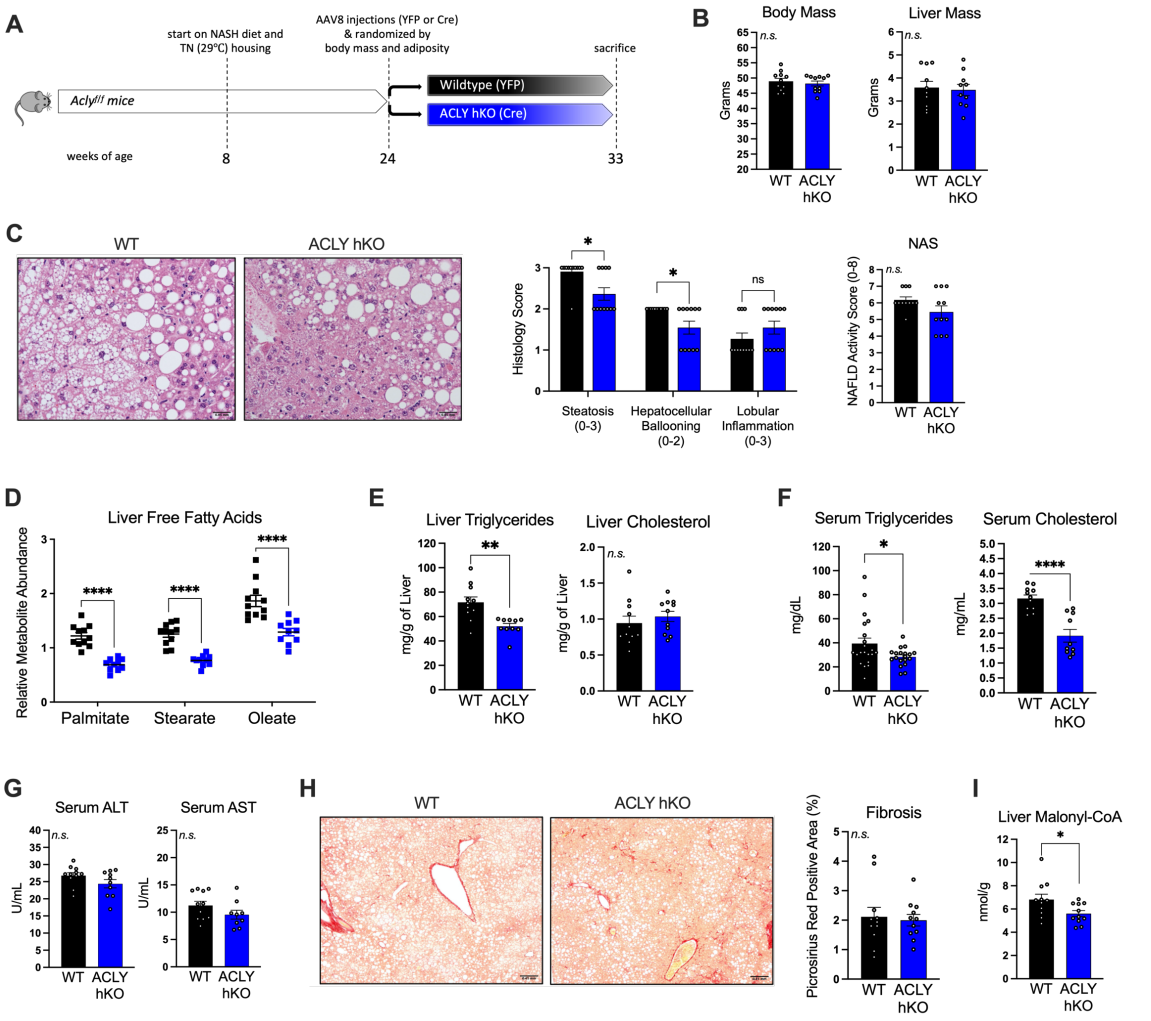

Figure 3.7. ACLY hepatocyte-specific knockout mice have reduced liver steatosis and intracellular ballooning without affecting inflammation and fibrosis

(A) Study design.
(B) Body and liver mass in grams at sacrifice.
(C) Representative photomicrographs of H&E-stained liver sections taken at 20X along with NAS and corresponding individual histological scores for steatosis grade, hepatocellular ballooning, and lobular inflammation.
(D) Liver metabolite abundance of palmitate, stearate, and oleate measured at sacrifice 2 hours post-glucose injection by GC/MS and expressed relative to protein.
(E-F) Liver and serum triglycerides and cholesterol measured at sacrifice (n=19-21/group for liver triglycerides).
(G) Serum ALT and AST measured at sacrifice.

(H) Representative photomicrographs of PSR-stained liver sections taken at 4X along with % positive PSR area measured on ImageJ.
(I) Liver malonyl-CoA measured at sacrifice by UPLC-MRM mass spectrometry (UPLC-MRM MS).
Data are presented as mean ± SEM. Statistical significance (*$p < 0.05$, **$p < 0.01$, ***$p < 0.001$, ****$p < 0.0001$, *n.s.,* not significant) by unpaired t-test or by unpaired Mann-Whitney test (for histological scores) (n=10-12/group unless stated otherwise).

3.1.7 Bempedoic acid lowers steatosis, ballooning, and fibrosis

The pro-drug bempedoic acid is converted to bempedoyl-CoA in the liver where it inhibits ACLY in a CoA competitive, citrate and ATP non-competitive manner (Pinkosky *et al.*, 2013, 2016). Consistent with observations in hepatocytes of ACLY hKO mice, bempedoic acid suppressed fatty acid and sterol synthesis while enhancing fatty acid oxidation (Figure 3.8A-B). We next investigated the therapeutic potential of pharmacologically inhibiting ACLY using bempedoic acid at a dose (10 mg/kg) that was selected based on its ability to reduce serum LDL-c and atherosclerosis in ApoE null mice (Pinkosky *et al.*, 2016). Importantly, to closely parallel the studies in ACLY hKO mice, *Acly*$^{f/f}$ mice were housed at TN and fed the ND before being injected with AAV8-Ttr-eYFP (WT) (Figure 3.8C). Similar to findings in the ACLY hKO mice, bempedoic acid did not alter body mass (Figure 3.8D) but did reduce steatosis and hepatocellular ballooning (Figure 3.8E). However, in contrast to ACLY hKO mice bempedoic acid also lowered lobular inflammation (Figure 3.8E). Consistent with reductions in the steatosis score bempedoic acid lowered liver fatty acids (Figure 3.8F) and triglycerides (Figure 3.8G) without significantly altering liver cholesterol (Figure 3.8G). Serum triglycerides and cholesterol (Figure 3.8H) and serum ALT and AST (Figure 3.8J) were all reduced with bempedoic acid. Bempedoic acid significantly increased serum ketone bodies (Figure 3.8I), consistent with findings in primary hepatocytes and changes in RER, indicating there were likely increases in liver fatty acid oxidation. Importantly and in contrast to ACLY hKO mice, bempedoic acid also lowered liver fibrosis (Figure 3.8K). These data indicate that

despite similar reductions in steatosis and hepatocellular ballooning as observed in ACLY hKO mice, bempedoic acid also reduces liver inflammation and fibrosis.

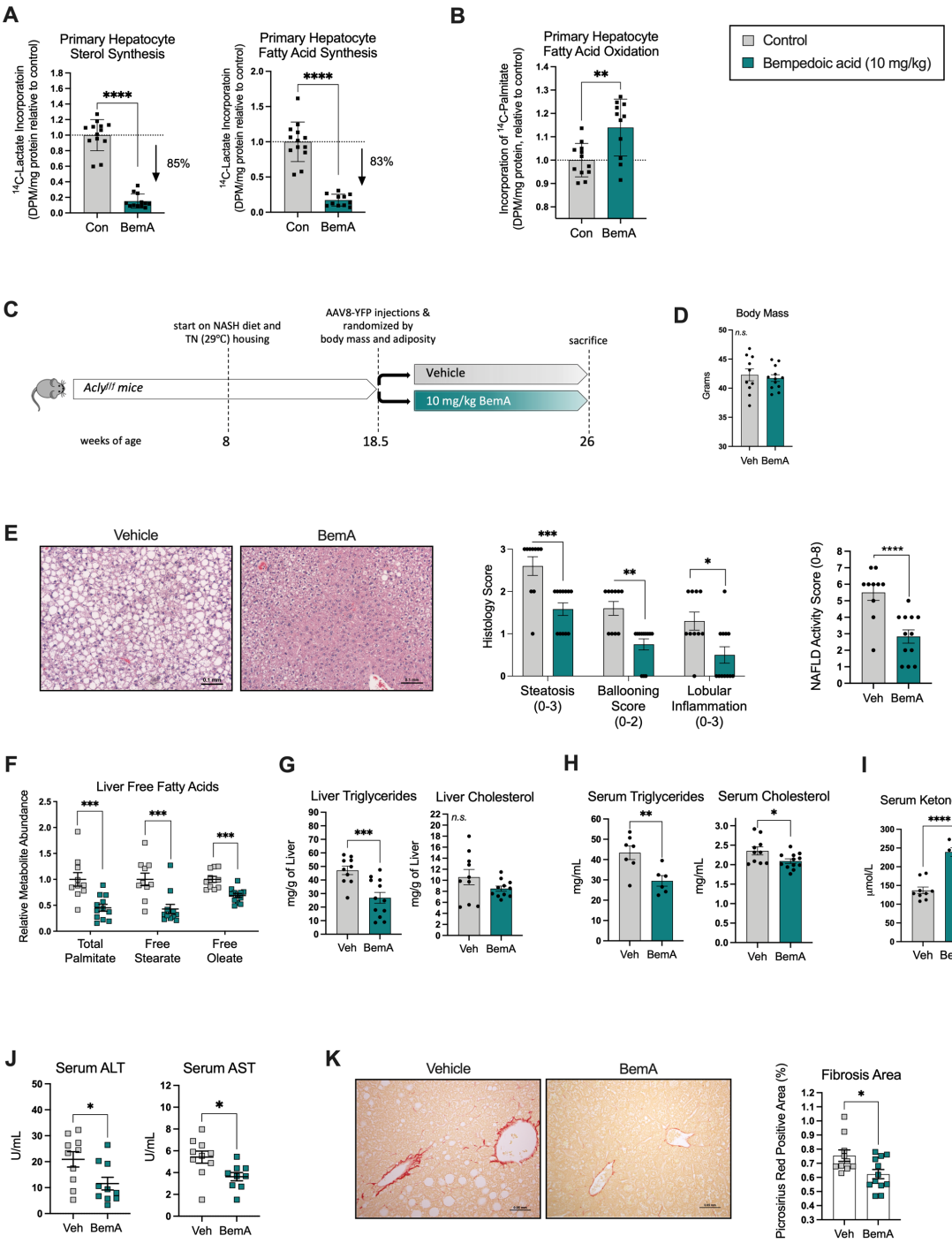
A
Primary Hepatocyte Sterol Synthesis
^{14}C-Lactate Incorporatoin (DPM/mg protein relative to control)
****
85%
Con BemA
Primary Hepatocyte Fatty Acid Synthesis
^{14}C-Lactate Incorporatoin (DPM/mg protein relative to control)
****
83%
Con BemA
B
Primary Hepatocyte Fatty Acid Oxidation
Incorporation of ^{14}C-Palmitate (DPM/mg protein, relative to control)
**
Con BemA
Control
Bempedoic acid (10 mg/kg)
C
start on NASH diet and TN (29°C) housing
AAV8-YFP injections & randomized by body mass and adiposity
sacrifice
Acly$^{f/f}$ mice
Vehicle
10 mg/kg BemA
weeks of age
8
18.5
26
D
Body Mass
n.s.
Grams
Veh BemA
E
Vehicle
BemA
Histology Score
***
**
*
Steatosis (0-3)
Ballooning Score (0-2)
Lobular Inflammation (0-3)
NAFLD Activity Score (0-8)
****
Veh BemA
F
Liver Free Fatty Acids
Relative Metabolite Abundance
***
***
***
Total Palmitate
Free Stearate
Free Oleate
G
Liver Triglycerides
mg/g of Liver
***
Veh BemA
Liver Cholesterol
mg/g of Liver
n.s.
Veh BemA
H
Serum Triglycerides
mg/mL
**
Veh BemA
Serum Cholesterol
mg/mL
*
Veh BemA
I
Serum Ketone Bodies
µmol/L
****
Veh BemA
J
Serum ALT
U/mL
*
Veh BemA
Serum AST
U/mL
*
Veh BemA
K
Vehicle
BemA
Fibrosis Area
Picrosirius Red Positive Area (%)
*
Veh BemA

Figure 3.8. Bempedoic acid lowers steatosis, ballooning, and fibrosis

(A) Incorporation of [^{14}C]-lactate into non-saponifiable (sterols) and saponifiable (fatty acids) lipid fractions in primary mouse hepatocytes (n=12-13/group).
(B) Incorporation of [^{14}C]-palmitate released into CO_2 and acid-soluble β-oxidation intermediates in primary mouse hepatocytes (n=11-12/group).
(C) Study design.
(D) Body mass in grams at sacrifice.
(**E)** Representative photomicrographs of H&E-stained liver sections taken at 20X along with NAS and corresponding individual histological scores for steatosis grade, hepatocellular ballooning, and lobular inflammation.
(F) Liver metabolite abundance of palmitate, stearate, and oleate measured at sacrifice 2 hours post-glucose injection by GC/MS and expressed relative to protein.
(G-H) Liver and serum triglycerides and cholesterol measured at sacrifice.
(I) Serum ketone bodies (acetoacetone + 3-hydroxybutyrate) measured at sacrifice**.**
(J) Serum ALT and AST measured at sacrifice.
(K) Representative photomicrographs of PSR-stained liver sections taken at 20X along with % positive PSR area measured on ImageJ.
Data are presented as mean ± SEM. Statistical significance (*p < 0.05, **p < 0.01, ***p < 0.001, ****p < 0.0001, *n.s.*, not significant) by unpaired t-test or unpaired Mann-Whitney U test (for histological scores) (n=10-12/group).

3.1.8 Genetic and pharmacological inhibition of ACLY lowers liver oxaloacetate and glucose intolerance

Liver steatosis promotes the development of insulin resistance (Samuel and Shulman, 2018). Consistent with reductions in steatosis we found that glucose tolerance was significantly improved in ACLY hKO mice (Figure 3.9A) and tended to be improved in mice treated with bempedoic acid (Figure 3.9B). To examine whether this was attributed to reductions in liver gluconeogenesis we conducted pyruvate tolerance tests and found that ACLY hKO mice had improved pyruvate tolerance (Figure 3.9C). Similarly, mice treated with bempedoic acid also had a tendency towards improved pyruvate tolerance (Figure 3.9D). Fasting serum insulin was lower in ACLY hKO (Figure 3.9E), however, this was not accompanied by substantial improvements in whole-body insulin tolerance in either ACLY hKO or bempedoic acid treated mice (Figure 3.9F-G) suggesting that ACLY inhibition may directly inhibit hepatic gluconeogenesis. Consistent with this hypothesis, hepatocyte glucose production, independent of insulin, was significantly lower in ACLY KO compared to WT controls (Figure 3.9H) was reduced with bempedoic acid (Figure 3.9I). Oxaloacetate is a metabolic intermediate generated by ACLY that is used for gluconeogenesis and we found that it was lower in the liver of ACLY hKO and bempedoic acid treated mice (Figure 3.9J-K). These data indicate that inhibiton of ACLY exerts favourable effects on glycemic control, potentially by reducing oxaloacetate and gluconeogenesis.

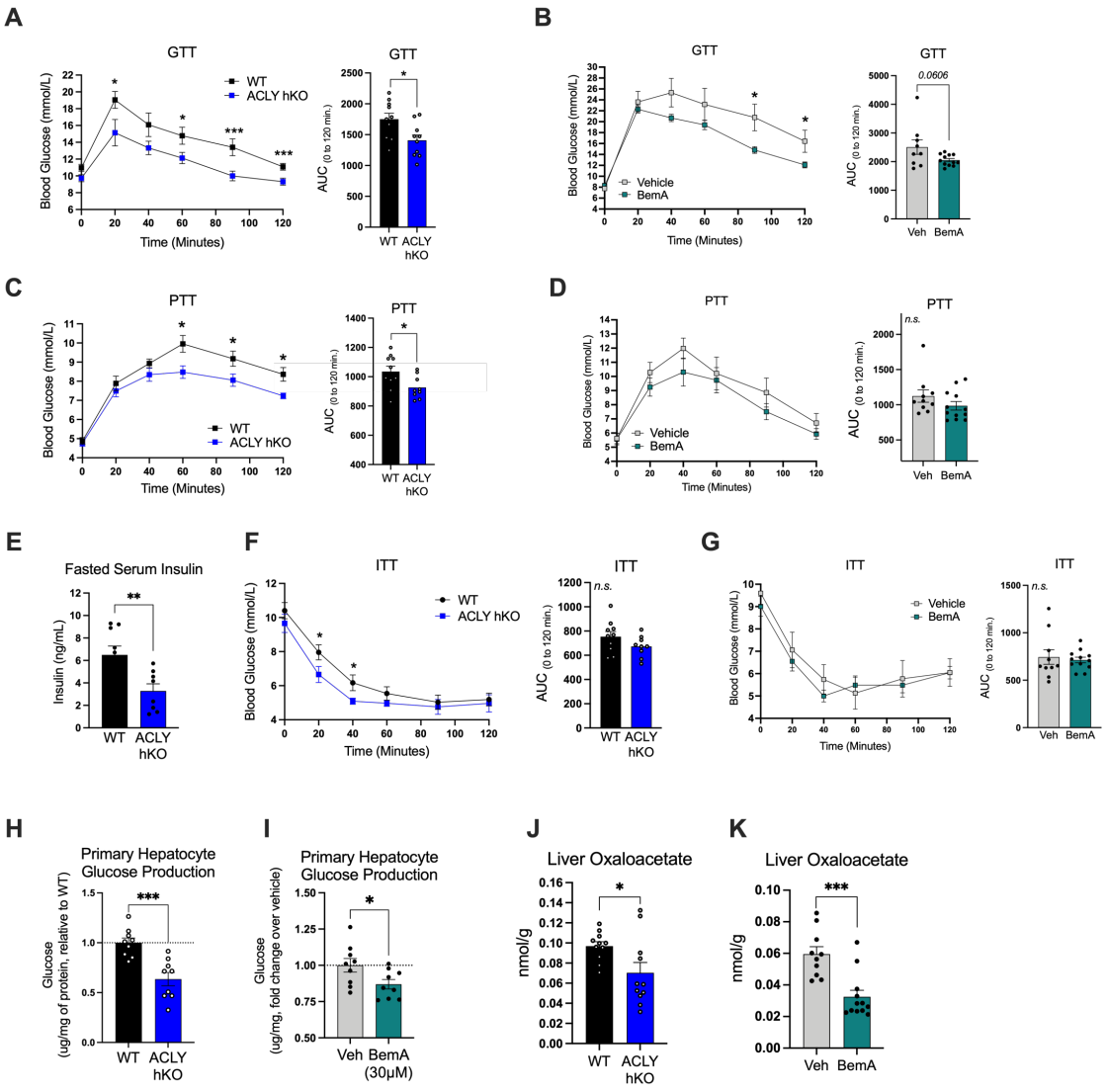

Figure 3.9. Genetic and pharmacological inhibition of ACLY lowers blood glucose

(A-B) GTT performed via IP injections of 1 g/kg D-glucose at **(A)** 21 weeks on ND for ACLY hKO cohort (n=10/group) and **(B)** 14 weeks on ND for bempedoic acid cohort (n=9-12/group), and $AUC_{0\text{-}120\ min}$ was calculated.
(C-D) Pyruvate tolerance test (PTT) via IP injections of 1.5 g/kg Na-pyruvate following a 15-hour fast to capture gluconeogenic rates and $AUC_{0\text{-}120\ min}$ was calculated (n=9-10/group for ACLY hKO cohort, n=10-12 for bempedoic acid cohort).
(E) Serum insulin measured following a 6-hour fast (n=8/group).

(F-G) ITT performed via IP injections of 1.3 U/kg of insulin at **(F)** 24 weeks on ND for ACLY hKO cohort (n=9-10/group), and **(G)** 16 weeks on ND for bempedoic acid cohort and area under the curve ($AUC_{0\text{-}120\ min}$) was calculated (n=10-12/group).
(H-I) Glucose production from primary mouse hepatocytes (n=9/group).
(J-K) Liver oxaloacetate measured at sacrifice by GC/MS (n=11/group for ACLY hKO cohort, n=10-12/group for bempedoic acid cohort).
Data are presented as mean ± SEM. Statistical significance * ($p < 0.05$) by unpaired t-test.

3.1.9 Bempedoic acid lowers ballooning and fibrosis in a mouse model not characterized by obesity and hyperinsulinemia

Given the positive effects of bempedoic acid on inflammation and fibrosis we next examined whether bempedoic acid may be beneficial in a mouse model of NASH not characterized by obesity and hyperinsulinemia; the STAM™ model of HFD-induced type 1 diabetes. Following low-dose injection of streptozotocin and 1 week of high fat feeding, STAM™ mice were treated at 5 weeks of age for 4 weeks with vehicle, or 3, 10, or 30 mg/kg bempedoic acid. Disease baseline was determined at 5 weeks such that comparisons made between baseline and the vehicle group at the end of the study (week 9) represent disease progression (Figure 3.10A). Bempedoic acid did not affect body weight (Figure 3.10B). Both baseline and vehicle groups exhibited steatosis, hepatocellular ballooning and inflammatory cell infiltration indicating that animals had pre-established NASH at the initiation of treatment (Figure 3.10C). Bempedoic acid lowered steatosis and hepatocyte ballooning but did not alter inflammation (Figure 3.10C). Serum triglycerides were also reduced in bempedoic acid treated mice (Figure 3.10D). However, in contrast to the metabolic model of NASH (Figure 3.9) there was no change in glucose tolerance (Figure 3.10E) suggesting that improvements in liver histology in STAM™ mice were independent of alterations in glycemic control. Importantly, bempedoic acid still attenuated collagen deposition such that a -57% ($p = 0.0504$), -68% ($p = 0.0120$) and -75% ($p = 0.0058$) inhibition of picrosirius red positive area (%) was observed at 3, 10, and 30 mg/kg of bempedoic acid treatment, respectively (Figure 3.10F). These data indicate that bempedoic

acid reduces liver steatosis, ballooning and fibrosis as well as serum triglycerides in two distinct mouse models.

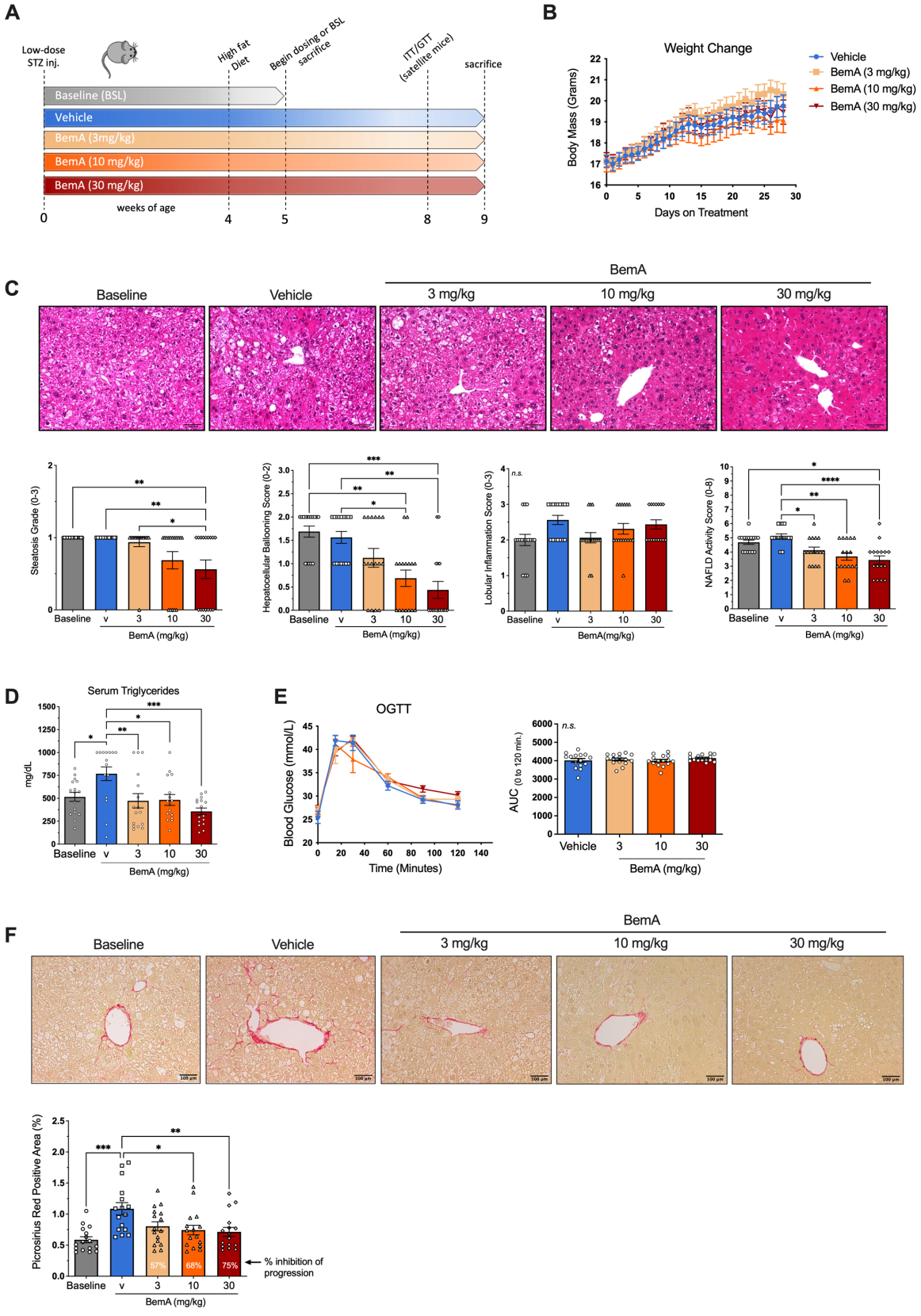
A
Low-dose STZ inj.
High fat Diet
Begin dosing or BSL sacrifice
ITT/GTT (satellite mice)
sacrifice
Baseline (BSL)
Vehicle
BemA (3mg/kg)
BemA (10 mg/kg)
BemA (30 mg/kg)
weeks of age
0
4
5
8
9
B
Weight Change
Body Mass (Grams)
Days on Treatment
Vehicle
BemA (3 mg/kg)
BemA (10 mg/kg)
BemA (30 mg/kg)
C
Baseline
Vehicle
BemA
3 mg/kg
10 mg/kg
30 mg/kg
Steatosis Grade (0-3)
Hepatocellular Ballooning Score (0-2)
Lobular Inflammation Score (0-3)
NAFLD Activity Score (0-8)
BemA (mg/kg)
D
Serum Triglycerides
mg/dL
E
OGTT
Blood Glucose (mmol/L)
Time (Minutes)
AUC (0 to 120 min.)
n.s.
F
Picrosirius Red Positive Area (%)
57%
68%
75%
% inhibition of progression

Figure 3.10. Bempedoic acid lowers ballooning and fibrosis in a mouse model not characterized by obesity and hyperinsulinemia

(A) Study design.
(B) Body mass over time.
(C) Representative photomicrographs of H&E-stained liver sections taken at 20X along with NAS and corresponding individual histological scores for steatosis grade, hepatocellular ballooning, and lobular inflammation.
(D) Serum triglycerides measured at sacrifice.
(E) Oral glucose tolerance test (OGTT) performed via oral gavage of 50 mg glucose/mouse at 8 weeks of age and area under the curve ($AUC_{0\text{-}120\ min}$) was calculated (n=15/group).
(F) Representative photomicrographs of PSR-stained liver sections taken at 20X along with % positive PSR area measured on ImageJ.
Data are presented as mean ± SEM. Statistical significance (*p < 0.05, **p < 0.01, ***p < 0.001, ****p < 0.0001, *n.s.*, not significant) by one-way ANOVA followed by Tukey's multiple comparison test or Kruskal-Wallis test followed by Dunn's multiple comparisons test (for histological scores) (n=16/group unless stated otherwise).

3.1.10 Bempedoic acid reduces molecular signatures of fibrosis important in human NASH

To explore the anti-fibrotic effects observed with bempedoic acid, we performed targeted transcriptome analysis of genes involved in fibrosis pathways using the Nanostring nCounter Fibrosis v2 Panel. Nanostring technology uses mRNA probes and hybridization to multiplex the expression of pre-defined gene targets in a sample. Comparison of pathway scores found that bempedoic acid markedly downregulated pathways associated with inflammation and fibrosis (TLR signalling, TGF-β signalling, adenosine pathway, PDGF signalling, *etc*.) (Figure 3.11A). False-discovery rate adjusted statistically significant pathways downregulated by bempedoic acid to levels comparable to age-matched chow controls included collagen biosynthesis and modification, extracellular matrix synthesis, and myofibroblast regulation while upregulated pathways included fatty acid metabolism, DNL, and gluconeogenesis (Figure 3.11A and Figure 3.12A).

To contextualize the clinical relevance of the transcriptional modulations associated with bempedoic acid treatment, we compared gene expression data derived from mice experimental cohorts with matching orthologous genes derived from 216 human liver biopsy samples grouped by NAFLD/NASH disease and fibrosis stage (Govaere *et al.*, 2020). Previous studies identified improved comparability between species and transcriptomic platforms by using gene set analytical methods (Nakagawa *et al.*, 2016; Teufel *et al.*, 2016; Kloet *et al.*, 2020). We computed Gene Set Enrichment Index (GSEI) to determine similarity between mice and human with respect to fibrosis related pathways. Out of 26 significantly altered pathways in bempedoic acid treated mice, we identified the

suppression of pathways in clusters II and III to thresholds at or below that of pre-fibrotic, NAFLD biopsies (Figure 3.12B). These pathways include critical processes involved in NASH pathophysiology such as collagen biosynthesis and modification, chemokine and cytokine signalling, and myofibroblast regulation. Both Euclidean distance and Pearson correlation metrics suggest that bempedoic acid treated mice more closely resemble pre-fibrotic NAFLD and F0-F1 biopsies compared to other disease stages and are most dissimilar to advanced F4 stage biopsies (Figure 3.11B and Figure 3.12B). PCA shows that NASH severity is coordinated by PC1 where the normalized component scores increase as disease progressively reverse from the cirrhotic F4 stage to pre-fibrotic NAFLD (Figure 3.11C). Bempedoic acid treatment exhibits the largest PC1 component score, supporting the similarity between treatment and pre-fibrotic stages of disease and demonstrating the efficacy of the treatment at reversing fibrosis related gene signatures.

With respect to specific pro-fibrotic pathways, single sample GSEA (ssGSEA) (Subramanian *et al.*, 2005) analyses demonstrated the downregulation of pathways in cluster II and III relative to the most advanced human NASH phenotypes (Figure 3.12C-E). On the gene level, bempedoic acid markedly reduced expression of several markers of fibrosis and NASH severity (*Tgfβ1, Col1a1, Col1a2, Col3a1, Col4a1, Col4a2, Col5a1 Col5a3, Col6a3*) to levels at or below those seen in chow-fed control mice and NAFLD patients (Figure 3.12C-E). Interestingly, significantly upregulated genes in bempedoic acid treated mice included genes and pathways involved in DNL (*Elovl6, Acaca, Fasn),* a transcriptional compensatory effect observed previously with DNL inhibition via ACC (Kim *et al.*, 2017; Goedeke *et al.*, 2018; Bates *et al.*, 2020) (Figure 3.11D). Other

upregulated genes included those involved in gluconeogenesis and fatty acid metabolism, likely also compensatory effects following ACLY and DNL inhibition (Figure 3.12A). Importantly, the pro-fibrotic pathways (collagen biosynthesis & modification, extracellular matrix synthesis and myofibroblast regulation) were not downregulated in ACLY hKO mice (Figure 3.11E-G). These data suggest that despite ACLY hKO and bempedoic acid eliciting similar changes in hepatocyte fatty acid metabolism and reductions in steatosis, only bempedoic acid inhibits fibrosis. Consistent with this concept, while there was a moderate positive correlation between steatosis and fibrosis in WT and ACLY hKO mice (R^2=0.4134), this relationship was not observed in mice treated with vehicle or bempedoic acid (R^2=0.09) (Figure 3.11H). Further, treatment of ACLY hKO mice with bempedoic acid still lowered liver fibrosis (Figure 3.11I). These data strongly suggest that the anti-fibrotic effects of bempedoic acid may be independent of hepatocyte ACLY and reductions in steatosis.

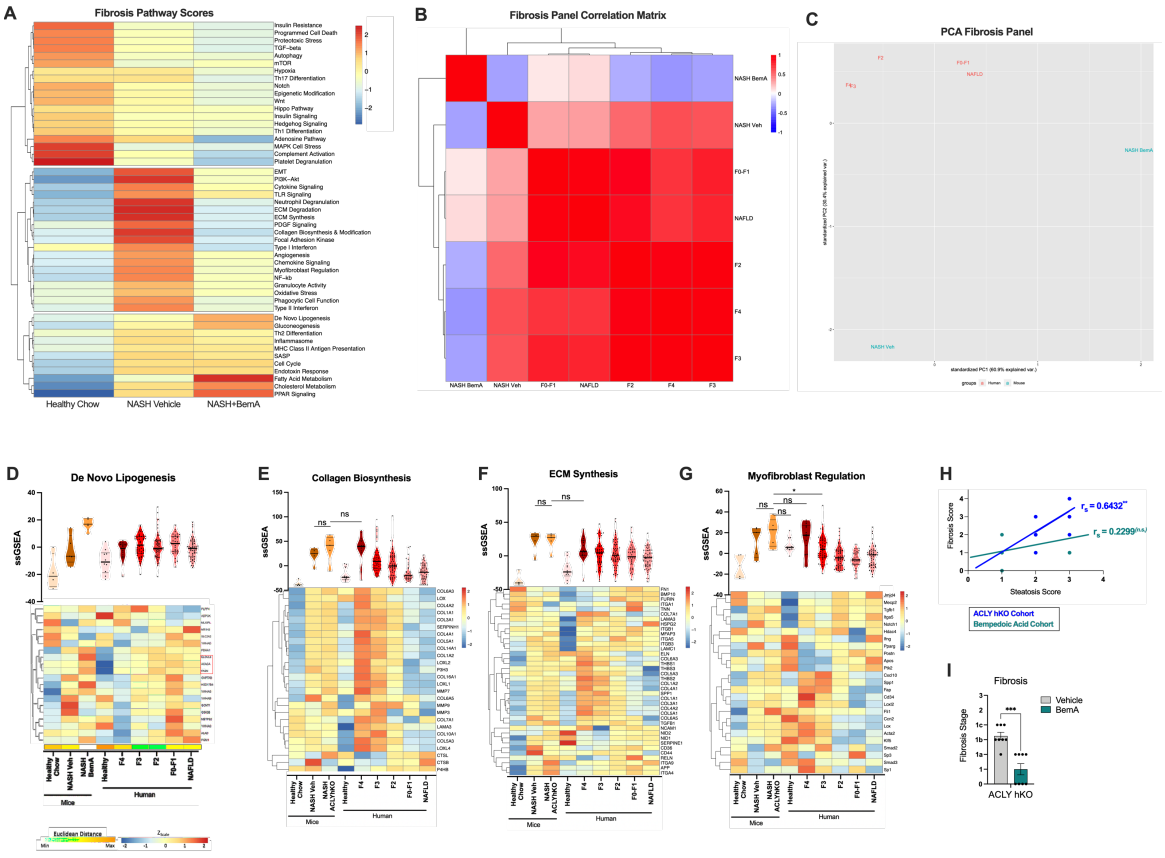

Figure 3.11. Effects of bempedoic acid and hepatocyte ACLY knockout on molecular signatures of *de novo* lipogenesis or fibrosis pathways relative to human NASH

(A) Heatmap of Nanostring nCounter Fibrosis v2 Panel pathway scores (n=4-5/group).
(B) Heatmap depicting pairwise Pearson correlation matrix between human biopsies at varying disease stages of NASH severity and mice experimental cohorts.
(C) PCA coordinates varying stages of human NASH biopsies and mice experimental cohorts according to GSEI.
(D-G) Violin plots of ssGSEA scores with accompanying heatmap showing gene-expression values of genes in the nCounter Fibrosis v2 Panel pathways in mice cohorts (n=4-5/group) and human biopsies (n=10-54/group). Violin plot data are presented with all data points shown and medians/quartiles denoted by straight line.
(H) Spearman's correlation of fibrosis score and steatosis grade in the ACLY hKO cohort and bempedoic acid cohort.
(I) ACLY hKO mice were housed at TN and fed the ND for 10.5 weeks and either switched to vehicle or 10 mg/kg bempedoic acid for an additional 7.5 weeks and representation of fibrosis scores were obtained from liver MTC- and PSR-stained liver sections (n=8/group). Data are presented as mean ± SEM. Statistical significance * ($p < 0.05$) by unpaired t-test.

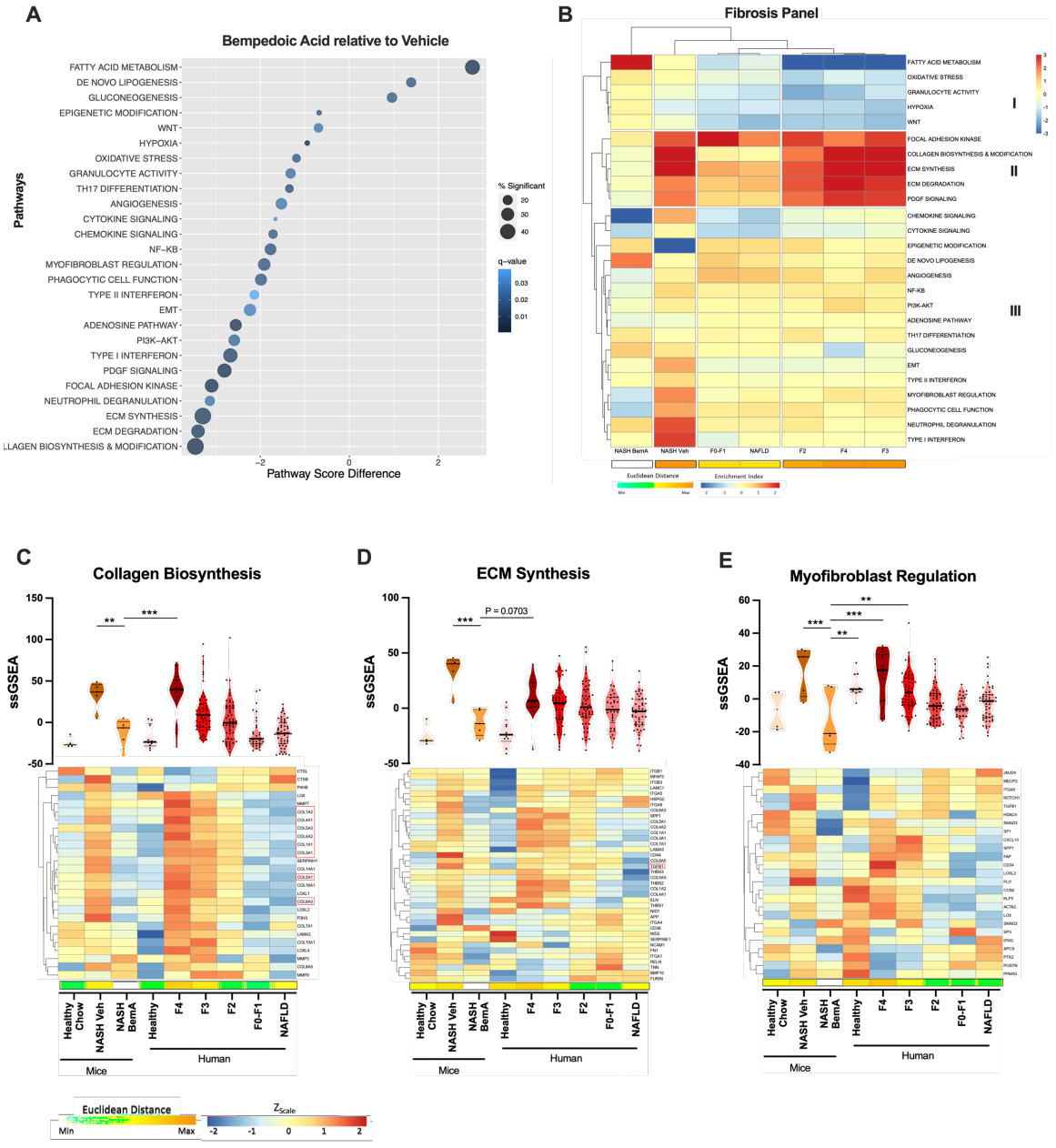

Figure 3.12. Bempedoic acid reduces molecular signatures of fibrosis important in human NASH

(A) Scatter plot of statistically significant (Benjamini-Hochberg FDR < 0.05) differentially regulated pathways in mice treated with bempedoic acid relative to NASH vehicle mice (n=4-5/group).

(B) Heatmap of GSEI between mice cohorts compared to NASH F0 – F4 stage patients (n=10-54/group). Enrichment index is computed as the logarithmic transformation of p-value. Pathways are clustered according to Pearson correlation and are grouped into clusters I – III.
(C-E) Violin plots showing ssGSEA scores with accompanying heatmaps showing gene-expression values of genes in the nCounter Fibrosis v2 Panel pathways in mice (n=4-5/group) and human biopsies (n=10-54/group). Violin plots are presented with all data points shown. Medians/quartiles are denoted by straight lines.

3.1.11 Bempedoic acid reduces the activation of primary mouse and human hepatic stellate cells.

Hepatocytes are just one of over a dozen distinct cell types in the liver (Loomba, Friedman and Shulman, 2021). We observed that while ACLY expression was undetectable in the livers of chow-fed ACLY hKO mice there was an increase in expression of ACLY in ACLY hKO mice fed the ND (Figure 3.13A). Consistent with previous reports (Malato *et al*., 2011), injection of the mice with the AAV8-Ttr-Cre virus led to undetectable ACLY in isolated hepatocytes (Figure 3.5A). This suggests that non-hepatocyte ACLY expression may increase with disease progression, and this may be the important differentiating factor between the lack of effect in the ACLY hKO compared to bempedoic acid treated mice.

Inflammation is critical for driving fibrosis and macrophages play an important role in the liver microenvironment in promoting this effect. Transcriptionally, bempedoic acid significantly lowered key pathways involved in inflammation (e.g., cytokine signalling, TLR signalling, chemokine signalling) (Figure 3.11A) suggesting it may be inhibiting fibrosis through actions on macrophages. To directly evaluate this possibility, we treated primary mouse bone-marrow derived macrophages (BMDMs) with bempedoic acid and found that in contrast to observations in hepatocytes and with the positive control salicylate (activates lipogenesis by mitochondrial uncoupling and AMPK activation) (Smith *et al*., 2016), bempedoic acid did not reduce lipogenesis or increase fatty acid oxidation (Figure 3.14A). It also did not reduce the production of TNF (Figure 3.14B). These data suggest that bempedoic acid is inactive in macrophages consistent with the low expression of

SLC27a2/ACSVL1 (Uhlén *et al.*, 2015), which is required for activation of the pro-drug bempedoic acid to its active CoA metabolite (Pinkosky *et al*., 2016).

Hepatic stellate cells are critical for driving liver fibrosis (Loomba, Friedman and Shulman, 2021), therefore, we hypothesized that the anti-fibrotic effects observed with bempedoic acid could be mediated by inhibiting stellate cell activation. *In situ* hybridization found that *Acly* was colocalized with *Acta2* (a marker of hepatic stellate cells) in ACLY hKO ND-fed mice (Figure 3.13B); confirming previous studies that AAV8-Ttr-Cre does not affect this cell type. Subsequent analysis showed that mouse hepatic stellate cells express both *Acly*/ACLY and *Slc27a2*/ACSVL1 (Figure 3.13C-D). This is consistent with Human Protein Atlas (www.proteinatlass.org) RNA-seq data showing that in human livers, after hepatocytes, myofibroblasts have the highest expression levels of *ACLY* and *SLC27A2* (Uhlén *et al.*, 2015). Studies by Wellen and colleagues have shown that the upregulation of ACSS2 is a biomarker of ACLY inhibition in the liver (Zhao *et al.*, 2020). Consistent with these findings, we observed an increase in *Accs2* expression in the whole liver and hepatic stellate cells isolated from WT mice chronically treated with bempedoic acid compared to vehicle (Figure 3.13E). Importantly, bempedoic acid blunted TGF-β induced activation of primary mouse and human hepatic stellate cells as indicated by suppression of *Acta2* and *Col1a1* expression (Figure 3.13F). Bempedoic acid also lowered human hepatic stellate cell expression of SMA (Figure 3.13G and Figure 3.15A), and procollagen 1a1 secretion into the media (Figure 3.13H). Two key pathways that regulate hepatic stellate cell activation are the TGF-β-SMAD and the hippo-YAP/TAZ signalling pathways (Mannaerts *et al*., 2015). Bempedoic acid however did not impact the phosphorylation of proteins in

these pathways or the expression of downstream targets of these pathways (Figure 3.14C-G), indicating that these are not the mechanisms responsible for bempedoic acid's ability to blunt cell activation. Studies in cancers cells have shown that inhibition of ACLY reduces proliferation by blocking the fatty acid and sterol synthesis required for generation of new cell membranes (Zaidi *et al.*, 2012). Consistent with findings in cancer cells, bempedoic acid increased fatty acid oxidation (Figure 3.13I) and trended to suppress fatty acid and cholesterol synthesis (Figure 3.13J), effects that were accompanied by significant reductions in hepatic stellate cell proliferation (Figure 3.13K) and the expression of the proliferation marker Ki67 (Figure 3.13L and Figure 3.15B).

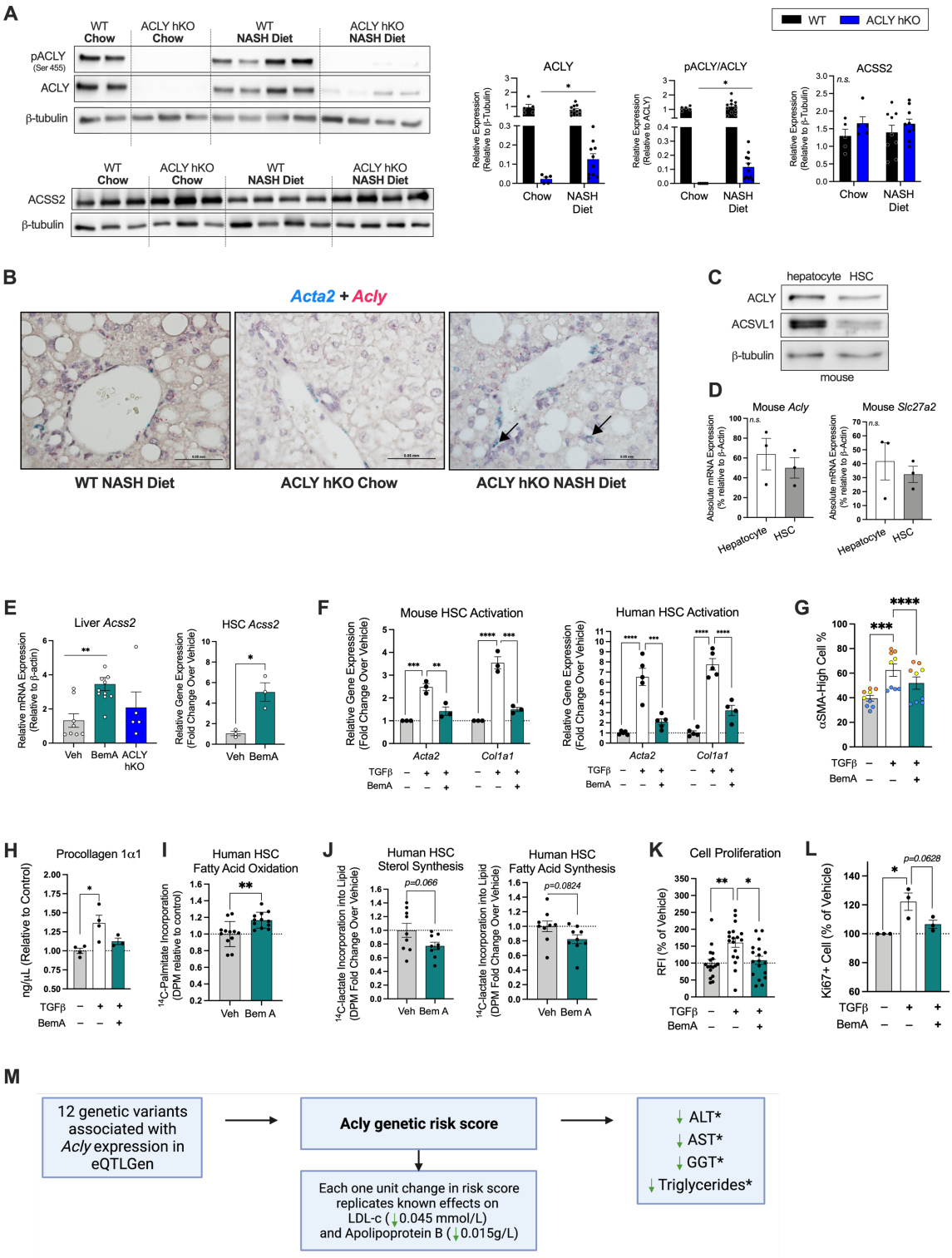
A
WT Chow
ACLY hKO Chow
WT NASH Diet
ACLY hKO NASH Diet
pACLY (Ser 455)
ACLY
β-tubulin
ACSS2
WT
ACLY hKO
Relative Expression (Relative to β-Tubulin)
Relative Expression (Relative to ACLY)
Chow
NASH Diet
n.s.
B
Acta2 + Acly
WT NASH Diet
ACLY hKO Chow
ACLY hKO NASH Diet
C
hepatocyte
HSC
ACLY
ACSVL1
β-tubulin
mouse
D
Mouse Acly
Mouse Slc27a2
Absolute mRNA Expression (% relative to β-Actin)
Hepatocyte
HSC
E
Liver Acss2
HSC Acss2
Relative mRNA Expression (Relative to β-actin)
Relative Gene Expression (Fold Change Over Vehicle)
Veh
BemA
ACLY hKO
F
Mouse HSC Activation
Human HSC Activation
Acta2
Col1a1
TGFβ
BemA
G
αSMA-High Cell %
H
Procollagen 1α1
ng/μL (Relative to Control)
I
Human HSC Fatty Acid Oxidation
14C-Palmitate Incorporation (DPM relative to control)
J
Human HSC Sterol Synthesis
Human HSC Fatty Acid Synthesis
p=0.066
p=0.0824
14C-lactate Incorporation into Lipid (DPM Fold Change Over Vehicle)
K
Cell Proliferation
RFI (% of Vehicle)
L
Ki67+ Cell (% of Vehicle)
p=0.0628
M
12 genetic variants associated with Acly expression in eQTLGen
Acly genetic risk score
Each one unit change in risk score replicates known effects on LDL-c (↓0.045 mmol/L) and Apolipoprotein B (↓0.015g/L)
↓ ALT*
↓ AST*
↓ GGT*
↓ Triglycerides*

Figure 3.13. Bempedoic acid reduces the activation of primary mouse and human hepatic stellate cells

(A) Relative expression of phosphorylated ACLY (Ser 455), total ACLY, β-tubulin, and ACSS2 in whole liver lysates measured by Western blot densitometry (n=5/group for chow, n=10-11/group for ND). Statistical significance by unpaired t-test between chow ACLY hKO and ND ACLY hKO groups.
(B) Colocalization of *Acly* (red) and *Acta2* (blue) on liver sections using *in situ* hybridization.
(C) Protein expression of ACLY and ACSVL1 in primary mouse hepatocytes and hepatic stellate cells (n=3/group).
(D) mRNA expression *Acly* and *Slc27a2* in primary mouse hepatocytes and hepatic stellate cells (n=3/group).
(E) mRNA expression of *Acss2* in liver and hepatic stellate cells isolated from WT and ACLY hKO mice on ND for 16 weeks +/- bempedoic acid (30 mg/kg) for an additional 9 weeks (n=5-11/group).
(F-H) Mouse and human hepatic stellate cells were treated with vehicle, TGF-β, or TGF-β+bempedoic acid (30 μM) for 48 hours. **(F)** mRNA expression of hepatic stellate cell activation markers *Acta2* and *Col1a1* was measured using RT-qPCR and expressed relative to *Hprt1* and as fold change over control (n=3/group for mouse, n=5/group for human). **(G)** Flow cytometry for αSMA protein expression. Different colour symbols denote different hepatic stellate cell donors (n=9/group). **(H)** Procollagen 1a1 measured in the media (n=4 in triplicate).
(I) Human hepatic stellate cells were treated with [^{14}C]-palmitate for 4 hours. Incorporation of [^{14}C]-palmitate into released CO_2 and acid-soluble β-oxidation intermediates was measured and expressed relative to protein and to control group (n=12/group).
(J) Human hepatic stellate cells were treated with [^{14}C]-lactate for 4 hours. Incorporation of [^{14}C]-lactate into non-saponifiable (sterols) and saponifiable (fatty acids) lipid fractions was measured and expressed relative to mg of protein (n=9/group).
(K-L) Cell proliferation measured by **(K)** PrestoBlue fluorescence (n=17-18/group) and **(L)** flow cytometry for Ki67 protein expression (n=3/group).
(M) Schematic of Mendelian randomization analysis of genetic variants associated with decreased *ACLY* gene expression. Associations with NASH outcomes were tested using linear regression. Statistical significance (*p < 0.05) by Benjamini-Hochberg FDR correction (results in Table 3.2).
Data are presented as mean ± SEM. Statistical significance (*p < 0.05, **p < 0.01, ***p < 0.001, ****p < 0.0001, *n.s.*, not significant) by unpaired t-test or one-way ANOVA followed by Tukey's multiple comparison test unless stated otherwise.

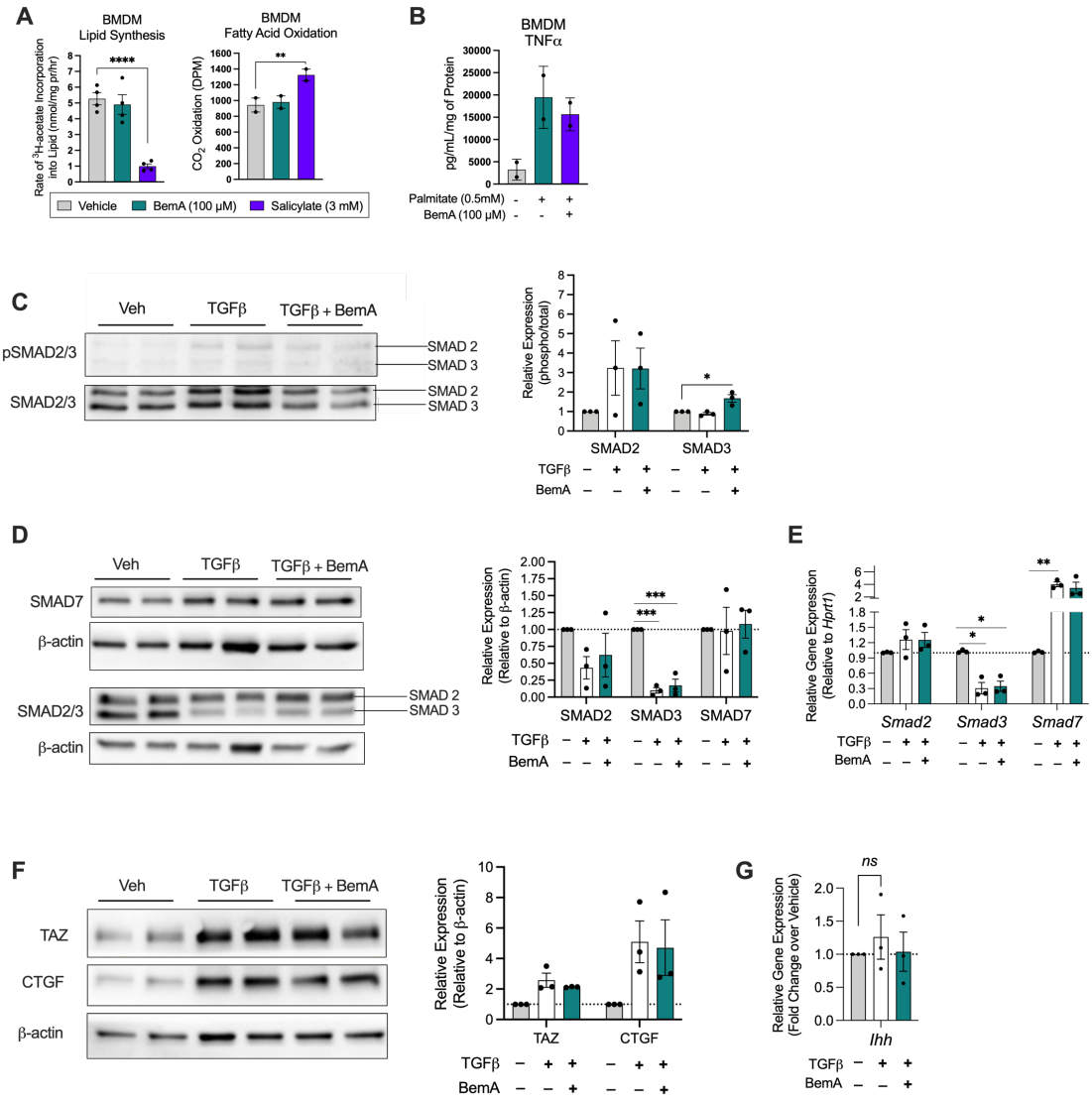

Figure 3.14. Effects of bempedoic acid in primary bone marrow derived macrophages and on SMAD and TAZ pathways in hepatic stellate cells

(A-B) Primary bone marrow derived macrophages (BMDM) were isolated from mice and treated with bempedoic acid or salicylate (positive control) (n=4 in triplicate). **(A)** Incorporation of [^{3}H]-acetate into lipid was determined and expressed relative to mg of protein per hour (n=4 in triplicate). Human hepatic stellate cells were treated with [^{14}C]-palmitate for 4 hours. Incorporation of [^{14}C]-palmitate into released CO_2 from β-oxidation was measured and expressed as DPM (n=3 in triplicate). **(B)** BMDM's were treated with

palmitate +/- bempedoic acid for 24 hours and TNFα expression was measured (n=2 in duplicate).
(C) Human hepatic stellate cells were treated with vehicle, TGF-β, or TGF-β+bempedoic acid (30 μM) for 30 minutes and phosphorylation of SMAD2 (Ser465/467) and SMAD3 (Ser423/425) was measured by Western blot densitometry and expressed relative to total SMAD2 and SMAD3 protein expression.
(D-G) Human hepatic stellate cells were treated with vehicle, TGF-β, or TGF-β+bempedoic acid (30 μM) for 48 hours. **(D)** Relative SMAD7 and SMAD2/3 protein expression was measured by Western blot densitometry. **(E)** mRNA expression of *Smad2*, *Smad3*, and *Smad7* was measured using RT-qPCR and expressed relative to *Hprt1*. **(F)** Relative TAZ and CTGF protein expression was measured by Western blot densitometry. **(G)** mRNA expression of *Ihh* was measured using RT-qPCR and expressed relative to *Hprt1*.
Data are presented as mean ± SEM. Statistical significance ($p < 0.05$) by one-way ANOVA and * * for Tukey's post hoc test (n=3 in triplicate unless stated otherwise).

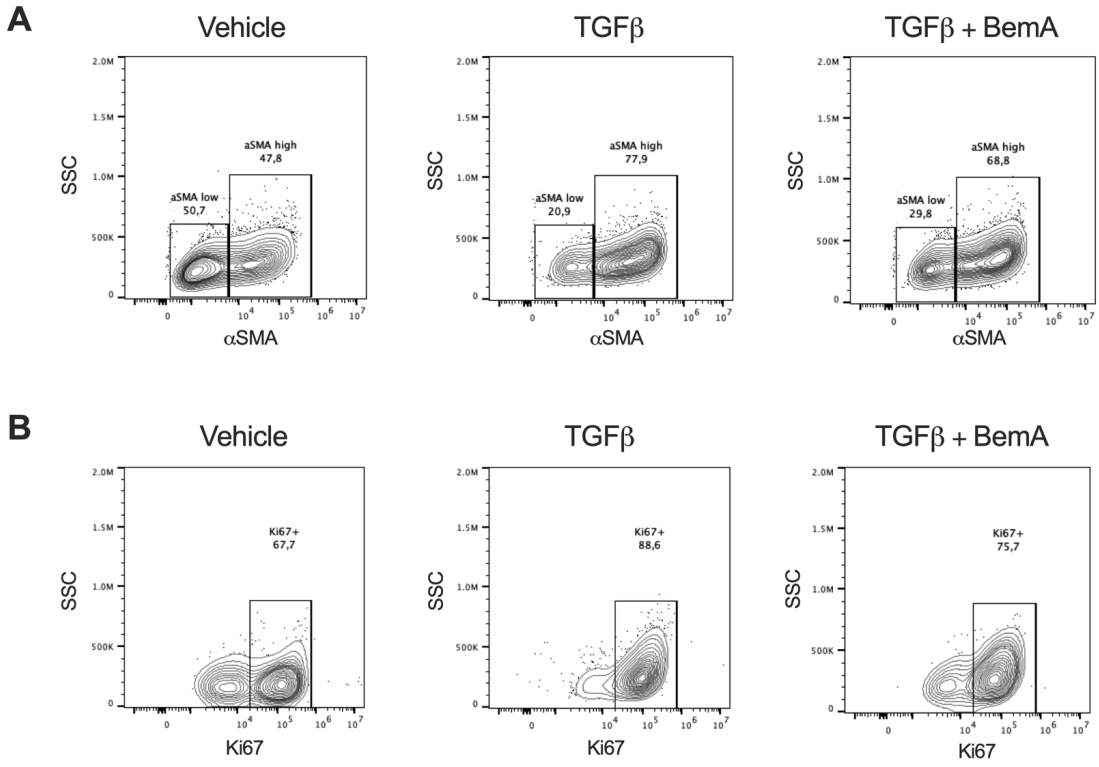

Figure 3.15. Flow cytometry plots for αSMA and Ki67+ expression in hepatic stellate cells

(A) Representative flow cytometry plots of αSMA cells from human hepatic stellate cells treated with vehicle, TGF-β, or TGF-β+30 μM bempedoic acid for 48 hours.
(B) Representative flow cytometry plots of Ki67+ cells from human hepatic stellate cells treated with vehicle, TGF-β, or TGF-β+30 μM bempedoic acid for 48 hours.

3.1.12 Association of ACLY genetic scores with human markers of NASH and liver injury

To assess whether inhibition of ACLY may also be important in preventing NASH in humans, we performed Mendelian randomization studies. Mendelian randomization is an epidemiological tool that uses natural variations in genes of known functions to study the causal effect of an exposure to an outcome. Mendelian randomization has been previously used to study ACLY inhibition on cholesterol as observed in the CLEAR Harmony trial (Ference *et al.*, 2019). Similarly, we used a genetic risk score comprising genetic variants associated with *ACLY* gene expression to infer the lifelong effects of (whole-body) ACLY inhibition on NASH and related metabolic markers.

In the eQTLGen consortium, there were 12 independent genetic variants associated with *ACLY* gene expression in the blood that comprised the *ACLY* genetic risk score (Table 3.1). As expected, the genetic risk score created for blood expression of *ACLY* was directionally concordant with known effects of ACLY inhibition on apolipoprotein B (0.015 g/L per unit increase in *ACLY*; 95% CI = -0.027 to -0.0038; $p=9.17x10^{-3}$) and LDL-c (0.045 mmol/L per unit increase in *ACLY*; 95%CI = -0.085 to -0.006; p=0.02) (Figure 3.13M, Table 3.2). We subsequently used this genetic risk score for downstream analyses of ACLY associations with serum triglycerides and commonly used serum biomarkers of NAFLD, ALT, AST, and GGT. After Bonferroni correction there were no significant associations between ACLY and serum ALT, AST, GGT and triglycerides (Table 3.2). However, there were significant associations using the FDR-corrected p-values that were directionally concordant with our findings from animal models. Altogether these data

suggest that similar to observations in mice, ACLY inhibition may be associated with reductions in serum triglycerides and serum biomarkers of NAFLD in humans, however, clinical trials with ACLY inhibitors will be required to further validate these findings.

Table 3.1. List of 12 independent genetic variants associated with *ACLY* gene expression in blood from eQTLGen consortium.

SNP	EA/OA	EAF	Effect Size (SE)	P-value
rs1378496	A/G	0.278	-0.017 (0.278)	0.025
rs148029598	T/C	0.037	0.049 (0.037)	0.021
rs80313087	G/A	0.107	-0.036 (0.107)	0.0038
rs142356140	T/C	0.019	0.09 (0.019)	0.0023
rs117889290	C/T	0.031	0.079 (0.031)	0.0020
rs149039453	A/G	0.051	0.064 (0.051)	0.0018
rs148395774	T/C	0.013	-0.145 (0.013)	0.0017
rs2354155	G/A	0.476	0.026 (0.476)	6.62E-04
rs4273091	T/G	0.456	0.03 (0.456)	3.10E-04
rs35967904	A/G	0.095	0.061 (0.095)	8.54E-05
rs79995639	C/T	0.063	0.076 (0.063)	6.67E-06
rs34200091	A/G	0.157	-0.195 (0.157)	1.86E-72

EA, effect allele; EAF, effect allele frequency; OA, other allele; SE, standard error; SNP, single nucleotide polymorphism

Table 3.2. Associations of human *ACLY* genetic risk scores (GRS) with NASH blood markers.

Outcome	Effect per unit decreased *ACLY*[e] expression (95% CI)	P-value	FDR[f]	Sample Size
Apolipoprotein B	-0.015 g/L (-0.026 to -0.003)	9.17e-03	0.046	326,020
LDL[a]	-0.045 mmol/L (-0.0846 to -0.006)	0.0237	0.046	326,020
Log-transformed ALT[b]	-0.014 units (-0.027 to -0.002)	0.0251	0.046	327,009
Log-transformed AST[c]	-0.013 units (-0.024 to -0.001)	0.0364	0.046	327,009
Log-transformed GGT[d]	-0.029 units (-0.057 to -0.002)	0.0380	0.046	326,431
Log-transformed triglycerides	-0.015 units (-0.031 to 0)	0.0496	0.05	327,444

[a]LDL=low density lipoprotein, [b]ALT=alanine transaminase, [c]AST=aspartate transaminase, [d]GGT=gamma-glutamyl transferase, [e]ACLY=ATP-citrate lyase, [f]FDR=false discovery rate corrected p-value.

3.2 Discussion

NAFLD has emerged as a leading cause of chronic liver disease that represents a global health challenge. High rates of DNL are associated with hepatic steatosis in mice and humans (Knebel *et al*., 2012; Fullerton *et al.*, 2013; Lambert *et al*., 2014; Cordoba-Chacon *et al*., 2015; Samuel and Shulman, 2018; Sanders *et al*., 2018). Recently, a new class of drugs that inhibit DNL by targeting ACC have been found to reduce NASH in clinical populations, however, the concomitant induction of hypertriglyceridemia associated with these agents has limited their development as a monotherapy (Kim *et al.*,

2017; Goedeke *et al*., 2018; Loomba *et al*., 2018), suggesting alternative strategies may be needed. In the current study, we demonstrate that genetic inhibition of ACLY in hepatocytes suppresses fatty acid and cholesterol synthesis and increases fatty acid oxidation, while reducing glucose intolerance, liver steatosis and ballooning, without increasing circulating triglycerides. Importantly, pharmacological inhibition of ACLY using bempedoic acid mimics the effects of genetic inhibition but also reduces fibrosis. Subsequent studies in primary mouse and human stellate cells demonstrate that bempedoic acid also increases fatty acid oxidation and suppresses lipid synthesis in this cell type and this is associated with reduced activation and proliferation. Importantly, Mendelian randomization of *ACLY* genetic variants in the UK biobank indicate that reductions in *ACLY* lower circulating triglycerides and serum biomarkers associated with NAFLD. These data suggest that inhibiting ACLY may be beneficial for reducing NASH while having favourable effects on glycemic control, and dyslipidemia.

To study the effects of ACLY inhibition we first characterized a mouse model of NASH that develops metabolically driven liver fibrosis, as observed in human NASH. NAFLD research often involves use of mouse models that do not recapitulate all arms of human disease development. Metabolically induced steatosis models such as feeding a HFD do not develop inflammation or fibrosis, and models that use liver injury insults (*e.g*., CCL4, methionine- or choline deficient diets), do not allow for the study of the interplay between obesity, insulin resistance and NASH. Giles and colleagues demonstrated that housing mice at TN accelerates the development of HFD-induced NASH such that after 24 weeks, mice display similar inflammatory and immune responses as observed in humans

with NASH (Giles *et al.*, 2017). However, a concern with the HFD-TN model is, while pathologically similar to human NASH, the mechanisms driving disease development differ as a HFD blunts DNL (Leite *et al.*, 2009; Softic, Cohen and Kahn, 2016). The inclusion of fructose to a HFD accelerates NASH development in 30 weeks (Clapper *et al.*, 2013). Another important dietary variable is cholesterol content, which is often increased to promote liver damage, however, this suppresses cholesterol synthesis, which contrasts the development of NASH in humans where cholesterol synthesis is elevated (Tsuchida *et al.*, 2018). In the current study we have fed mice a diet high in fat and fructose with lower levels of cholesterol. We find that when housed at TN, significant steatosis, hepatocellular ballooning, and histological markers of human NASH, and modest inflammation and fibrosis occurs within 16 weeks. Importantly, using a 25-gene signature established by Govaere and colleagues (Govaere *et al.*, 2020) we identified that this model develops NASH and liver fibrosis by activating similar genes as observed in human disease. Thus, the NASH model utilized in this study mirrors both the pathological and molecular drivers consistent with human disease within a reasonable time frame to conduct intervention studies.

Using several distinct methodologies, we demonstrate that genetic inhibition of ACLY in hepatocytes of adult mice reduces DNL and increases fatty acid oxidation. In mice fed a control diet this does not impact liver histology. This is likely because ACLY and DNL are not upregulated in healthy chow mice, and therefore inhibiting ACLY, an essential metabolic enzyme in the healthy state, may not be beneficial. However, when NASH is induced before inhibiting ACLY we find marked reductions in liver steatosis and

ballooning. This is consistent with a previous study showing reduced liver steatosis with liver directed ACLY siRNA in *db/db* mice (Wang *et al.*, 2009). However, our findings contrast a study demonstrating that lifelong genetic inhibition of liver ACLY in mice fed a diet high in fructose does not reduce liver lipids due to microbiome derived acetate uptake by ACCS2 (Zhao *et al.*, 2020). There are many differences between our study and this report. First, in our study, rather than from birth, we genetically inhibited ACLY in hepatocytes of adult mice with established disease. This difference may explain why we only observed modest increases in ACSS2 expression. Secondly, in contrast to the delivery of high concentrations of fructose via oral gavage or in the drinking water we used lower doses of fructose that were mixed with a HFD. While there may be some situations where microbiome derived acetate is the primary carbon source for DNL, our studies along with those indicating the effectiveness of ketohexokinase inhibitors to reduce steatosis in mice and humans, suggest that it is unlikely to be the primary pathway regulating DNL in NASH (Futatsugi *et al.*, 2020; Gutierrez *et al.*, 2021; Kazierad *et al.*, 2021).

Bempedoic acid is a pro-drug that when activated to bempedoyl-CoA in the liver inhibits ACLY activity. We find that consistent with observations in ACLY hKO mice, bempedoic acid increased fatty acid oxidation and reduced lipogenesis, steatosis, glucose intolerance and serum triglycerides. However, in contrast to findings in ACLY hKO mice, bempedoic acid also lowered liver fibrosis in two distinct mouse models. Subsequent molecular analysis revealed that the top pathways downregulated by bempedoic acid were those involved with collagen biosynthesis and extracellular matrix degradation and synthesis, with marked reductions in several markers of fibrosis (*Tgfβ1, Col1a1 Col1a2,*

etc.) to levels at or below those seen in healthy chow-fed mice or healthy human livers. These data suggested that bempedoic acid may be exerting effects in cell types beyond hepatocytes.

Hepatic stellate cells are critical for driving the development of fibrosis (Loomba, Friedman and Shulman, 2021). Previous studies have indicated that the AAV8-Ttr-Cre used to induce deletion of hepatocyte ACLY does not affect hepatic stellate cells (Malato *et al.*, 2011), suggesting that bempedoic acid may be reducing fibrosis by acting in stellate cells. We found that mouse and human hepatic stellate cells express ASCVL1 which is required for activation of bempedoic acid, and consistent with inhibition of ACLY, bempedoic acid upregulated ACCS2 expression. TGF-β activates hepatic stellate cells and we found that bempedoic acid inhibited the induction of aSMA and collagen biosynthesis. These inhibitory effects of bempedoic acid on the activation of hepatic stellate cells were not associated with changes in SMAD or YAP/TAZ signaling but instead were linked to reductions in fatty acid and cholesterol biosynthesis and cellular proliferation. These effects are similar to those recently observed with ACC inhibitors (Bates *et al*., 2020) and are consistent with studies in cancer cells treated with ACLY inhibitors (Zaidi *et al.*, 2012). Recently, short hairpin RNA (shRNA) targeting of *Acly* demonstrated that ACLY is required to maintain the TCA cycle flux and redox balance required for cell viability and proliferation in dividing cells, including myoblasts (Arnold *et al.*, 2022). Although not yet studied with bempedoic acid, this mechanism may similarly contribute to our observed reductions in cell proliferation in hepatic stellate cells. Collectively, these data indicate that

bempedoic acid inhibits ACLY not only in hepatocytes, but also hepatic stellate cells and the latter activity is potentially critical for mediating the anti-fibrotic effects.

To determine whether our observations in rodents might be extended to humans, we conducted a Mendelian randomization study. Mendelian randomization uses natural genetic variation as instruments for causal inference and is thus resistant to common sources of epidemiological bias such as confounding and reverse causation. Our results recapitulate the known effects of bempedoic acid on serum lipids while supporting an effect on decreased liver injury, as evidenced by decreased concentrations of circulating AST, ALT and GGT. Although results did not meet the pre-specified significance threshold using Bonferroni correction, there were significant associations using the FDR-corrected p-values, and directionally concordant findings from animal models that provided *a priori* evidence for these analyses. Importantly, genetic effects likely reflect inhibition of ACLY expression in multiple tissues or cells, including hepatocytes and hepatic stellate cells, as this type of analysis does not lend itself easily to tissue-specific effects.

In summary, the current study provides evidence in both mice and humans that inhibition of ACLY may be effective in reducing NAFLD, glucose intolerance and serum triglycerides. Given the overlapping morbidity and mortality of NAFLD, type 2 diabetes and CVD (Younossi *et al.*, 2016), these findings strongly support further clinical development of ACLY inhibitors for the treatment of NASH.

CHAPTER 4: CONCLUDING REMARKS AND FUTURE DIRECTIONS

4. Concluding remarks and future directions

4.1 Introduction

ACLY is a key enzyme in the communication between nutrient catabolism and lipid biosynthesis, via its product, acetyl-CoA. It has been studied as a viable target to treat dyslipidemia for several decades, however, in this dissertation, new insights into its role in NASH and hepatic fibrosis are revealed. To investigate this role, and to help address the current gap in translatable and feasible animal models in this field, a mouse model of human-relevant NASH was developed and characterized.

4.2 Thermoneutral housing and a high-fat, high-fructose diet (TN-ND) as a mouse model for human NASH

The value of adding fructose to a HFD to exacerbate liver steatosis and inflammation development has been well established. However, these high-fat, high-fructose diet models still take upwards of 24-30 weeks to develop fibrosis (Appendix A) (Clapper *et al*., 2013; Im *et al*., 2021). Thermoneutral housing has emerged as an important tool to more accurately model human disease as chronic cold housing temperatures impart metabolic and immune changes that are not akin to human physiology (Ganeshan and Chawla 2017; James, Olejniczak, and Repasky, 2022). Using the combination of these dietary and environmental conditions, we developed the TN-ND mouse model. This model developed accelerated NASH and fibrosis and is amenable to genetic manipulations or pharmacological interventions.

Consistent with the criteria for modelling NASH in mice, described in the introduction of this dissertation (Chapter 1.6.2) (Brenner, 2018; Santhekadur, Kumar and

Sanyal, 2018), we validated that the TN-ND model developed histological markers of human NASH and similar transcriptomic profiles to human disease. In line with these recommendations, we used a diet similar to human obesogenic diets, that did not have unnatural levels of fat, fructose, or cholesterol. As noted in chapter one, a recent systematic review concluded that high-fat, high-fructose diets most closely replicate human NAFLD (Im *et al.*, 2021). However, a key component of current high-fat, high-fructose diets (i.e., AMLN/GAN diets), and other high-fat, high-cholesterol "Western" diets, is the addition of supraphysiological levels of cholesterol to promote liver damage and inflammation. The cholesterol content of these diets' ranges from 1.5-2%, which when scaled to humans is roughly 60-fold higher (20,000 mg/day) than normal consumption (Vinué, Herrero-Cervera and González-Navarro, 2018). In the TN-ND model, the commonly used high-fat, high-fructose (40% fat, 20% fructose) AMLN/GAN diet was modified to include a lower level of cholesterol (0.02% cholesterol). When combined with thermoneutral housing, this ND still effectively induced NASH, while still developing metabolic parameters that present in human NASH, including obesity, glucose intolerance, and hypercholesterolemia (Figure 3.1). Utilizing a higher, but still physiological, dose of 0.2% cholesterol, would likely also be appropriate for modelling NASH, and may even induce disease further.

One outstanding criterion listed by Santhekadur and colleagues, that has not yet been explored in the TN-ND model, is the occurrence of liver cirrhosis and/or HCC (Brenner, 2018; Santhekadur, Kumar and Sanyal, 2018). Designing models that mimic the progression of NASH toward liver cirrhosis and HCC observed in humans is important for testing translatable treatments. The TN-ND model has not been studied yet for long enough

periods to determine whether these liver pathologies develop. Diet-induced models using HFD (42% fat, 0.2%% cholesterol, 42.7% sucrose) with fructose in the drinking water (23.1 g/L) induce HCC in 75% of mice after 54 weeks, without the use of an unnatural toxin (Green *et al.*, 2022). This suggests that the TN-ND model, which uses similar dietary components, would develop HCC after a prolonged period, however, this should be confirmed with lengthier studies. Lastly, future studies are needed in this model to examine the effects of therapies in people with NASH that are known to exert no effect (i.e., metformin) or positive effects (OCA, GLP1R agonists, pioglitazone) to determine how accurately the model predicts disease outcomes.

4.2.1 The importance of fructose in NASH mouse models

The use of fructose in the diets of many people, particularly in North America, has substantially increased over the last two decades. Paralleling these increases there have been numerous epidemiological (Ouyang *et al.*, 2008; Ma *et al.*, 2015), clinical (Schwarz *et al.*, 2015), and animal studies (Jürgens *et al.*, 2005; Kawasaki *et al.*, 2009; De Castro *et al.*, 2013) linking fructose to increased DNL, liver steatosis, mitochondrial dysfunction, and microbiome disruption. Many of the mechanisms linking fructose to DNL and mitochondrial dysfunction (e.g., serum uric acid, microbiome-derived factors, gut-epithelial barrier function) were not explored in this dissertation and represent avenues for future work in the TN-ND model.

A longstanding question with the association between fructose and NAFLD is whether it is an effect confounded by excess calories and weight gain. It is difficult to

separate the effects of excess calories versus the individual effects of different carbohydrates, but several isocaloric or hypercaloric studies have been performed to provide insight. A meta-analysis performed on controlled feeding studies found that compared to other carbohydrate sources, isocaloric fructose did not induce NAFLD to a greater degree (Chiu *et al.*, 2014). However, additional trials have been performed since suggesting that short-term isocaloric fructose intake is associated with higher rates of DNL and hepatic fat content (Schwarz *et al.*, 2015). Recently, short-term fructose restriction was also shown to decrease DNL and lower ceramides, which was associated with decreased composite insulin sensitivity index (CSI) in children with obesity (Olsen *et al*., 2022). Large, long-term trials are needed to delineate whether the increased fructose intake in our populations is contributing to NAFLD.

Despite the lack of definitive human trials, the mechanistic data linking fructose to gut dysbiosis, hepatic DNL, and mitochondrial dysfunction, suggests that high fructose consumption contributes, to some degree, to NASH. It is still important, however, to use animal models that use physiological levels of fructose when testing these mechanisms. In addition to experiments described in Figures 3.1-3.4, we tested the effects of more human-relevant doses of high fat (40 kcal%) and high fructose (20 kcal%) on NAFLD development, compared to a high fat (45 kcal%) alone (Appendix B). In mice housed at thermoneutrality, the high-fat, high-fructose diet (NASH diet: ND) significantly exacerbates NASH and fibrosis relative to a standard HFD (Appendix B). The standard HFD was matched in micronutrient composition and closely matched in macronutrient composition to the ND (HFD: 45% fat (high in saturated fat), 0.02% cholesterol, 40.7%

carbohydrates (~7.5% fructose); ND: 40% fat (high in saturated fat), 0.02% cholesterol, 55% carbohydrates (20% fructose). Therefore, the main difference between these diets is the added fructose. This indicates that at thermoneutrality, the addition of fructose to a HFD accelerates NAFLD development, which is similar to previous observations at room temperature (Clapper *et al*., 2013). These changes in liver pathologies seem to be independent of body weight and glucose tolerance, suggesting fructose specifically targets liver damage (Appendix B). The addition of fructose is also able to overcome any reductions in ACLY that are typically observed with a HFD (Figure 3.3H) (Jiang *et al*, 2009; Fukuda, Katsurada and Iritani, 1992). The ND significantly increased *Acly* and *Acss2* gene expression relative to a standard HFD (Figure 3.3I), and therefore better reflects human NAFLD, where ACLY is elevated (Ahrens *et al.*, 2013; Muir *et al.*, 2013; Ryaboshapkina and Hammar, 2017; Ma *et al.*, 2018).

4.2.2 Further characterization of the TN-ND mouse model

This dissertation discusses the preliminary characterization of important features and criteria for human disease development in the TN-ND model. However, there is extensive room for additional characterization. For example, further quantification of histological markers not defined in the NASH diagnostic criteria, but observed in human disease (Kleiner *et al.*, 2005), including those in Figure 3.2, should be performed. For example, Mallory bodies, acidophil bodies, and pigmented macrophages are common histological features in NASH that were observed in liver sections from the TN-ND but were not quantified (Kleiner *et al.*, 2005). Additionally, a more comprehensive analysis of

histological steatosis could be performed. The presence of microvesicular steatosis is associated with advanced histological features, such as ballooning, inflammation, and fibrosis (Tandra *et al*., 2010). Qualitatively, earlier time points in the TN-ND model seem to be characterized by macrovesicular steatosis, whereas later time points (i.e., 25 weeks) seem to be characterized by microvesicular steatosis. (Figure 3.3A). This should be quantified to confirm this finding. A complete RNA-seq analysis should be performed on TN-ND livers and compared to datasets from human disease stages as well as other mouse models. This direct comparison can help conclude that our model more closely resembles human gene signatures compared to other models.

One additional limitation in the development of this mouse model is the exclusion of female mice. The historical underrepresentation of females in animal research has been brought to attention in recent years. Studies in females reveal significant sex differences in many biological processes, including response to treatment. The lack of incorporation of female mice in preclinical studies likely translates to inaccurate or poorer treatment outcomes for women (Beery, 2018). This has led federal research agencies, such as the Canadian Institutes of Health Research (CIHR) and the National Institutes of Health (NIH) to institute policies to encourage animal research to include both males and females. A reason, albeit not a justified one, for the lack of female subject inclusion in metabolic disease and NAFLD research, is that they are often resistant to diet-induced metabolic disease and NAFLD (Hart-Unger *et al.*, 2017; Lee *et al.*, 2022). The prevalence of human obesity and NAFLD, however, is similar between males and females and it is therefore important to determine whether therapies in development work equally as well in both

sexes. This will ensure that the most promising drug candidates are advanced to clinical trials (Pan and Fallon, 2014). Previous studies by Giles et al. show that thermoneutral housing of mice fed a HFD overcomes this sex-dependent resistance to NAFLD (Giles *et al.*, 2017). This suggests our model involving thermoneutral housing may also induce exacerbated NASH in female mice, however, this should be tested in future studies.

Fibrosis typically progresses in a zone-specific manner and more research in comparing the progression of fibrosis in humans and mice is needed and could be achieved with the TN-ND model. To further examine whether the model mimics fibrosis progression in humans, it will be important to perform a more intricate liver zonation analysis. Liver zonation analysis is becoming a valuable tool in improving disease stage determinations and the efficacy of a treatment. Zonation analysis in NAFLD research, however, is in its infancy and thus information on the importance of zone-specific differences in NAFLD progression is limited. In different zones of the liver, there are differential supplies of oxygen and nutrients and thus differences in glucose and fatty acid metabolism (Hall *et al.*, 2017). Zone, 1, 2, and 3 are the respective areas between the portal tracts and the central vein. Steatosis and oxidative damage to cells in adult NASH are mainly localized to pericentral regions (zone 3) and zonal distributions of phospholipids in NAFLD have been reported (Hall *et al.*, 2017). Fibrosis in adult NASH typically develops first in zone 3, expands to periportal and portal areas (zone 1), and then progresses to bridging fibrosis and eventually, cirrhosis (Table 1.1). Additional work on deciphering whether steatotic, inflammatory, and fibrotic disease patterns present similarly in the TN-ND model should be performed.

Spatial transcriptomics is a rapidly growing field used to assess zone-specific and location-specific changes. New spatial transcriptomics technologies are becoming more accessible and feasible (Williams *et al.*, 2022). Spatial transcriptomics allows for the locational mapping of gene expression in a tissue sample. This can determine whether transcriptomic changes overlap with functional changes (i.e., disease phenotypes on a tissue section). For example, spatial transcriptomics on liver tissue from end-stage liver disease patients has revealed that there are distinct areas of gene expression that correlate with fibrotic areas (Chung *et al.*, 2022). scRNA-seq can be combined with spatial transcriptomics to identify cell-specific changes in specific locations of the liver (Chung *et al.*, 2022). New advancements in artificial intelligence applications for spatial transcriptomics computation have also been developed (Li, Stanojevic and Garmire, 2022). Spatial transcriptomic applications could allow for zone-targeted treatments to specific areas in which fibrosis is developing, making for an exciting avenue as new technologies and techniques become available. It could also allow for testing of zonal changes in response to treatment and whether changes in certain areas of the liver correlate with better outcomes.

4.2.3 Applications of the TN-ND mouse model

If this model is systematically validated as a human-relevant model by the suggestions discussed, it has a large potential to lay the foundation for many exploratory and mechanistic questions in NASH. For example, available liver sections from TN-ND

mice can be utilized to further the understanding of NASH progression and the mechanisms driving it.

One area that has significant potential for human implications, is the discovery of novel non-invasive biomarkers for fibrosis. Given the fact that hepatic stellate cells are the critical drivers of fibrosis in NASH, the TN-ND mouse model could be used to reveal a hepatic stellate cell-specific circulating biomarker (i.e., a secreted factor). To explore this, hepatic stellate cells could be isolated using techniques described in this dissertation (Mederacke *et al*., 2015), and proteomics and secretomics analysis could be performed. Considering it is very difficult to accurately detect human fibrosis in the absence of a liver biopsy, this could help identify a novel non-invasive biomarker for liver fibrosis.

In summary, the work in this dissertation lays the foundation for further characterization and validation of the TN-ND mouse model, however additional studies in this model are needed. This includes examining disease development in female mice, carrying out longer studies to examine whether hepatic cirrhosis and HCC occur, and completing more detailed disease characterization, such as using spatial transcriptomics for liver zone analysis.

4.3 Insights into targeting DNL in NASH and metabolic disorders

Several DNL inhibitors have reached the clinical stage or have been approved for the treatment of hyperlipidemia (Markham, 2020; X. Wang *et al.,* 2020), NAFLD (clinicaltrials.gov identifier: NCT03248882, NCT02856555, NCT01431521,

NCT04906421, and NCT04004325), and T2D (clinicaltrials.gov identifier: NCT01792635, NCT01238887, and NCT00699413). This dissertation shows that inhibiting DNL by ACLY genetic manipulation in hepatocytes or pharmacologically, with bempedoic acid, can reduce lipid synthesis and liver lipids. Similar findings have been observed in ACC KO mice and with ACC inhibitors in humans (Kim *et al.*, 2017; Stiede *et al.*, 2017; Goedeke *et al.*, 2018; Bates *et al.*, 2020; Loomba *et al.,* 2018; Calle *et al.,* 2021). However, as mentioned, ACC inhibition increases circulating triglycerides (Kim *et al.*, 2017; Loomba *et al.*, 2018; Calle *et al.*, 2021). The reduction in hepatic polyunsaturated fats following ACC inhibition triggers compensatory upregulation of SREBP1c and glycerol-3-phosphate acyltransferase (GPAT). GPAT, the rate-limiting enzyme in triglyceride synthesis, drives the incorporation of triglycerides into VLDLs, which when released into circulation, increases blood triglycerides.

ACLY sits one step upstream of ACC in DNL, and therefore, following inhibition, there is no buildup of acetyl-CoA. This likely prevents any consequences of increased acetyl-CoA. Acetyl-CoA is a critical molecule in linking nutrient signals to energy signals, and manipulating its levels, could, therefore, have a greater impact on compensatory mechanisms. Whether the same is true of the buildup of citrate with ACLY inhibition by bempedoic acid is unknown but does not seem to translate to any measurable negative phenotypes in mice or humans. Consistent with clinical studies with bempedoic acid, compensatory increases in liver or serum lipids were not observed in TN-ND mice. The position of ACLY in lipid metabolism enables it to impact not only lipid synthesis but also cholesterol synthesis. ACLY inhibition by bempedoic acid reduces cholesterol synthesis in

hepatocytes (Pinkosky *et al.*, 2016), and lowers LDL-c in mice and humans (Thompson *et al*., 2015; Ballantyne *et al*., 2016; Pinkosky *et al*., 2016; Goldberg *et al.*, 2019), which is a significant benefit in a population where CVD risk is high. This differential effect on cytosolic acetyl-CoA levels with ACLY inhibition compared to ACC inhibition does not however explain all differential responses to inhibiting DNL. ACLY inhibition reduces polyunsaturated fatty acids in the same way that ACC inhibition does, without triggering compensatory SREBP1c upregulation. A greater understanding of these mechanisms is therefore still needed.

One possible explanation, however, is the notion that acetyl-CoA not only communicates cellular nutrient and energy status via substrate activity but also through its ability to acetylate histones and proteins, thus affecting gene expression and protein function respectively (Shi and Tu, 2015). Changes in cellular acetylation status and acetylation of various proteins and histones can impact numerous cellular processes, involved in metabolism, mitochondrial function, and energy homeostasis (Wellen *et al.*, 2009; Shi and Tu, 2015; Pinkosky *et al.*, 2017). ACLY-regulated acetylation events may contribute to changes in lipid metabolism, autophagy, mitochondrial biogenesis, inflammation, and oxidative stress in NASH (Wellen *et al.*, 2009; Shi and Tu, 2015; Pinkosky *et al.*, 2017). Dissimilar to ACLY inhibition, ACC inhibition would increase acetylation, which may negatively affect various changes to metabolic and inflammatory pathways (Batchuluun, Pinkosky and Steinberg, 2022). Reducing acetyl-CoA levels by ACLY inhibition, however, reduces global acetylation in the cell, and may reduce some of

the negative consequences of hyperacetylation. This could also be another interesting avenue to explore in future studies.

4.3.1 DNL inhibitors and glucose homeostasis

The bidirectional relationship between insulin sensitivity and hepatic lipid accumulation suggests that reductions in hepatic lipids following DNL inhibition would simultaneously improve insulin sensitivity and glucose homeostasis. In rodent studies, improvements in blood glucose and/or glucose tolerance have been observed following genetic or pharmacological suppression of CIC (Tan *et al.*, 2020) and ACLY (Wang *et al.*, 2009). ACC inhibition in preclinical models shows improvements in blood glucose, glucose uptake and insulin sensitivity (Schreurs *et al.*, 2009; Glund *et al.*, 2012; Harriman *et al.*, 2016; Liu *et al.*, 2020). The ACC inhibitor PF-05221304 lowers HbA_{1c}, (Calle *et al.*, 2021), and in a meta-analysis of randomized control trials, bempedoic acid was shown to reduce the new incidence or worsening of diabetes and reduce HbA_{1c} in patients with diabetes or prediabetes (X. Wang *et al.*, 2020). Consistent with this, improvements in liver lipids and glucose homeostasis were observed in ACLY hKO mice and bempedoic acid treated mice (Figure 3.9). There were modest or null improvements in insulin tolerance following an insulin tolerance test in ACLY hKO mice and bempedoic acid treated mice respectively, (Figure 3.9), and lower fasting serum insulin in ACLY hKO mice. Future studies using hyperinsulinemic-euglycemic clamps and metabolic tracers should also be performed to make conclusions on changes in insulin sensitivity specifically.

ACLY deletion or inhibition with bempedoic acid, also improved pyruvate tolerance, suggesting reduced hepatic glucose output. As expected, there were lower hepatic oxaloacetate levels in ACLY hKO and bempedoic acid treated mice; oxaloacetate is a gluconeogenic substrate and this may be the link behind lower hepatic glucose output. Further substrate tracing studies are also needed to solidify this connection. Overall, there is some evidence to support a role for ACLY and DNL inhibition in improved glucose homeostasis, and whether this is due to improvements in insulin sensitivity or hepatic glucose production directly still warrants further investigation. Interestingly, in STAM™ mice, bempedoic acid showed no change in glucose tolerance (Figure 3.10), suggesting that improvements in liver histology are independent of blood glucose levels.

4.4 Targeting fibrosis and hepatic stellate cells in NASH

Hepatic lipid accumulation and the activation of downstream pro-fibrogenic pathways is indeed a known contributor to hepatic stellate cell activation and fibrosis development. Studies in preclinical models and humans support the role of hepatic lipid accumulation and lipotoxicity in fibrogenesis and hepatic stellate cell activation (Reeves *et al.*, 1996; Wobser *et al.*, 2009; Yu *et al.*, 2021). The association between steatosis and fibrosis (Chalasani *et al.*, 2008) and steatosis and HCC development (Alexander *et al.*, 2013) in humans, has also been previously reported. Therefore, it can be hypothesized that inhibiting ACLY and DNL, and increasing fat oxidation, would remove a "root cause" of NASH and therefore reduce fibrosis development. Contrary to this, it was shown that bempedoic acid lowers hepatic inflammation and fibrosis, while ACLY hKO does not,

despite both lowering steatosis. Additionally, bempedoic acid decreased fibrosis in the STAM™ model of hepatic fibrosis, which does not develop significant steatosis (Figure 3.9). Consistent with this, while there was a moderate positive correlation between steatosis and fibrosis in WT and ACLY hKO mice ($R^2 = 0.4134$), this relationship was not observed in mice treated with vehicle or bempedoic acid ($R^2 = 0.09$) (Figure 3.11). Interestingly, meta-analyses have also shown that steatosis in humans does not predict disease progression in NASH, rather it is hepatic inflammation that is associated with the progression to advanced fibrosis (Singh *et al.*, 2015). Bempedoic acid still lowered fibrosis in ACLY hKO mice, indicating anti-fibrotic effects independent of hepatocyte ACLY and DNL. This indicates that 1) reversing steatosis may not be sufficient to reverse fibrosis, and 2) bempedoic acid targets a mechanism independent of hepatocyte ACLY to reduce fibrosis.

Subsequent studies (Figure 3.13) revealed that this additional benefit may in part be mediated by ACLY inhibition in hepatic stellate cells. This revealed a novel cell type target for bempedoic acid. Bempedoic acid increased fatty acid oxidation, reduced fatty acid and cholesterol biosynthesis, and blocked TGF-β-induced cellular proliferation in hepatic stellate cells. Although the mechanisms linking these outcomes have not yet been elucidated, some potential ones will be proposed below.

4.4.1 Potential mechanisms of ACLY inhibition in hepatic stellate cells

Rapidly dividing cells, such as cancer cells, or hepatic stellate cells, have high anabolic demands due to their accelerated proliferation, and protein, nucleotide, and lipid synthesis (Zaidi *et al.*, 2012; Zhu and Thompson, 2019). These cells, therefore, have a high glycolytic activity and high rates of DNL, and hepatic stellate cell activation seems to be reliant on these activities (Chen *et al.*, 2012; Lian *et al.*, 2016; Bates *et al.,* 2020). Blocking this metabolic shift is thought to inhibit hepatic stellate cell activation (Smith-Cortinez *et al*., 2020; Trivedi *et al*., 2021).

One key cytokine mediating this "shift" to a proliferative and anabolic state is TGF-β, which activates gene expression of pro-fibrotic genes, including *Acta2* and *Col1a1* (Figure 3.13), via the SMAD signalling pathway (Dewidar *et al.*, 2019). TGF-β however, activates several other signalling pathways in hepatic stellate cells, including PI3K/Akt (Son *et al*., 2009; Liu *et al*., 2009; Lechuga *et al*., 2004). TGF-β signalling in hepatic stellate cells through the PI3K/Akt pathway, increases glycolysis (Tu *et al*., 2016; Zhou *et al*., 2021), and promotes this shift to an anabolic and proliferative growth state (Liu *et al*., 2009; Reif *et al*., 2003). As discussed in chapter one, Akt activates ACLY via phosphorylation. In preliminary experiments, TGF-β was found to increase Ser 455 (Akt site) phosphorylation on ACLY (Appendix C). This data is from one experiment and thus needs to be replicated. It does, however, suggest that phosphorylation of ACLY could be the main link between TGF-β and hepatic stellate cell activation and proliferation, and blocking this contributes to lower levels of cell activation.

As proposed by Arnold et al., hepatic stellate cells may also adopt a non-canonical TCA cycle driven by ACLY, where acetyl-CoA produced from glycolysis is converted to citrate and transported back into the mitochondria by *Slc25a1*, rather than being fully oxidized to CO_2. Mitochondrial citrate is then converted to oxaloacetate and acetyl-CoA by ACLY. Acetyl-CoA is used to serve the high rates of lipid and cholesterol synthesis (required for the biosynthesis of new cellular components and membranes) and acetylation events (required for cell growth signals). The resulting cytosolic oxaloacetate is converted to malate, transported back into the mitochondria by *Slc25a1*, and used to regenerate mitochondrial oxaloacetate and subsequently citrate. This transition of the TCA cycle from carbohydrate and lipid consumption to preserving carbon metabolites, while regenerating redox balance (i.e., NAD+) required to sustain glycolysis, allows for more efficient production of acetyl-CoA for lipid biosynthesis and histone acetylation. These mechanisms are likely mediated by several cytokines and signalling pathways, one of which being TGF-β. Arnold et al. also showed that ACLY blockage in myoblasts, embryonic stem cells, and lung cancer cell lines impaired cell viability and proliferation, and increased citrate regeneration through the oxidative canonical TCA cycle (Arnold *et al.*, 2022). Similarly, ACLY inhibition in cancer cells reduces cell proliferation (Zaidi *et al.*, 2012). ACC inhibition was shown to shift activated hepatic stellate cells away from a high glycolytic state by decreasing lipid synthesis and increasing fatty acid oxidation, and this was associated with reduced cell activation (Bates *et al.*, 2020). The intricacies of these described metabolic shifts have not been studied with ACLY inhibition by bempedoic acid in hepatic stellate cells. However, these same mechanisms are likely contributing to the

observed reductions in lipid synthesis, increases in fat oxidation, and reductions in cell proliferation.

These mechanisms of reducing an otherwise high concentration of cytosolic acetyl-CoA may also explain the observations of reduced hepatic stellate cell activation markers *Acta2* and *Col1a1* following bempedoic acid treatment. It is thought that acetyl-CoA signals to the cell that it is in a growth and proliferative state, potentially through histone acetylation (Shi and Tu, 2015; Cai *et al.,* 2011). Genome-wide acetylation is increased in the livers of high-fat or high-fructose-fed mice with hepatic steatosis (Assante *et al*., 2022). Studies in mesangial cells demonstrate that exposures to high-glucose, TNF, or palmitate, induce genome-wide hyperacetylation, and specifically, increase acetylation of lipogenic and fibrogenic genes, including *Tgfb*, *Acaca, Fasn,* and *Hmgcr* (Y. Chen *et al*., 2019; Deb *et al*., 2017). Silencing ACLY with siRNAs blocks hyperacetylation and expression of pro-fibrotic genes (Y. Chen *et al*., 2019; Deb *et al*., 2017). Considering this, it is possible that ACLY inhibition in stellate cells is reducing acetylation events that control the expression of *Acta2, Col1a1,* as well as other fibrogenic genes. This could be another key link between ACLY inhibition and reduced cell activation markers. The direct mechanisms occurring in hepatic stellate cells, however, again, require further exploration and confirmation.

More studies are needed to directly connect dysregulated metabolism to activated hepatic stellate cells and how targeting this may help halt hepatic stellate cell activation and proliferation. It might be interesting to explore whether this anti-proliferative mechanism of ACLY inhibition extends to other highly proliferative and activated cells.

For example, ACLY activity has been associated with CKD, and therefore it would be interesting to study this mechanism in the activated myofibroblasts that drive kidney fibrosis (Mohammadi-Shemirani *et al.*, 2022).

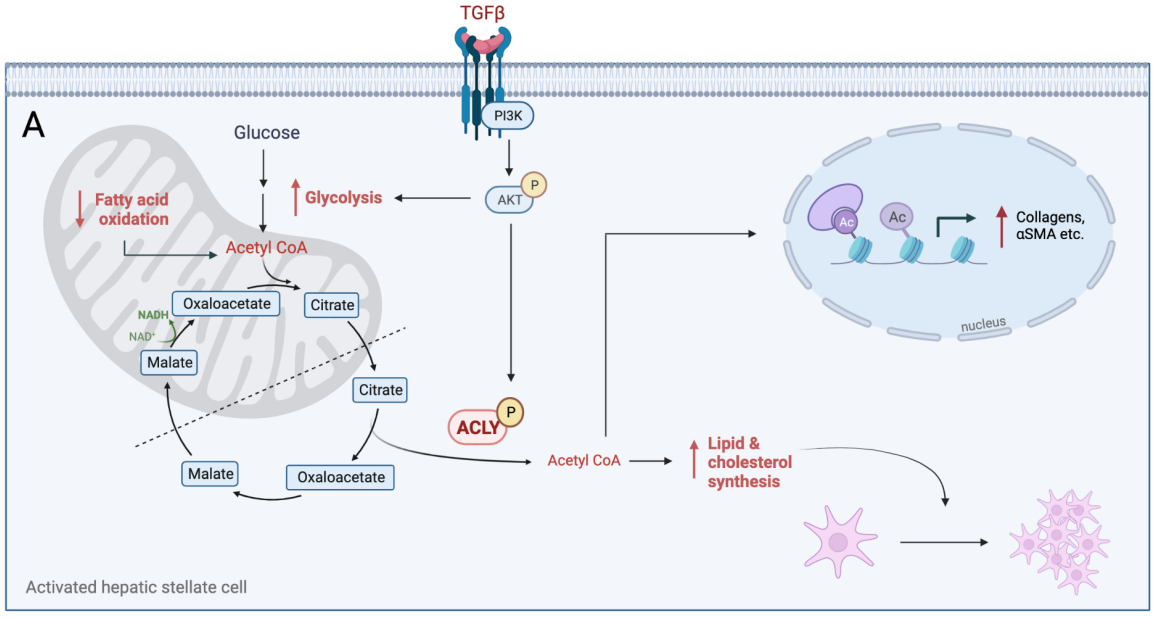

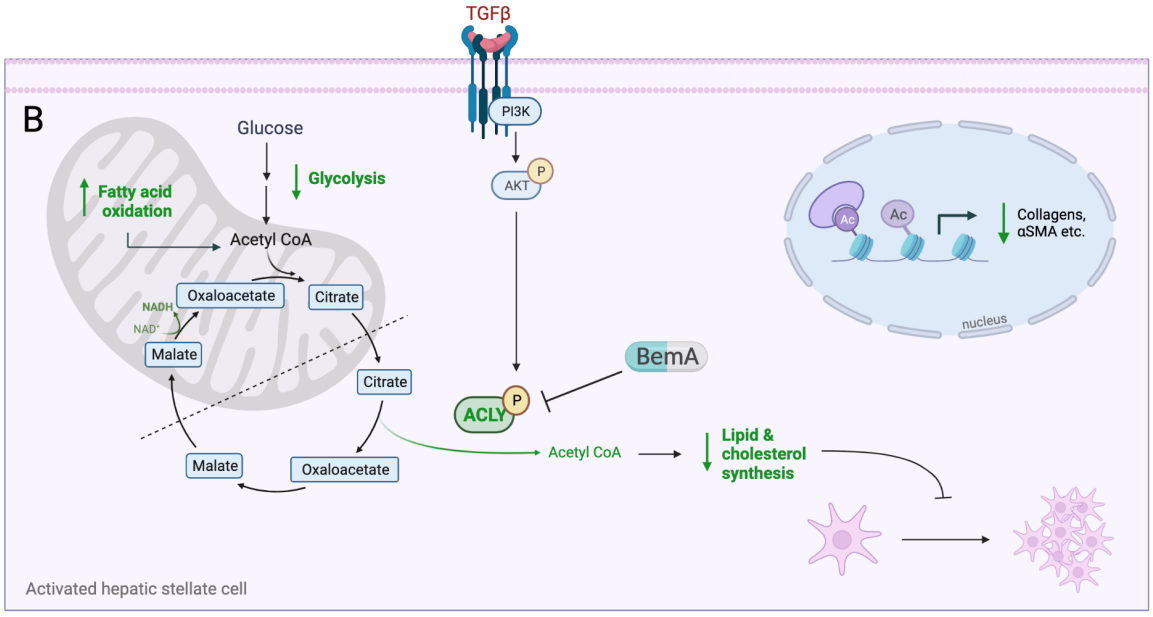

Figure 4.1. Proposed mechanism of ACLY inhibition in activated hepatic stellate cells

A) A proposed non-canonical TCA cycle in highly proliferative cells such as hepatic stellate cells. Mitochondrial acetyl-CoA and citrate are used to fuel cytosolic acetyl-CoA production via high ACLY activity. High glycolytic and ACLY activity is in part regulated by TGF-β-Akt signalling. The resulting elevated production of acetyl-CoA is used to fuel lipid and cholesterol biosynthesis required for cell viability and proliferation, and for histone acetylation events which are thought to further sustain cell growth signals (Arnold *et al.*, 2022). Metabolic pathways or metabolites highlighted in red are upregulated or highly active.
B) In activated hepatic stellate cells, ACLY inhibition by bempedoic acid reduces lipid and cholesterol synthesis and increases fatty acid oxidation. This translates to decreased cell proliferation and decreased expression of cell activation markers collagen and αSMA. Although not measured in our studies, ACLY inhibition may be reducing the high glycolytic activity and histone acetylation required to sustain hepatic stellate cell activation and proliferation. Metabolic pathways or metabolites highlighted in green are downregulated or have low activity. αSMA: alpha-smooth muscle actin.

In addition to TCA flux and lipid load impacting hepatic stellate cell activity, free cholesterol accumulation in hepatic stellate cells has been linked to cell activation and fibrogenesis (Schwabe and Maher, 2012; Teratani *et al.*, 2012; Tomita *et al.*, 2014; Furuhashi *et al.*, 2018). Free cholesterol increases TLR4 levels and sensitization to TGF-β signalling. In a mouse model of liver fibrosis, the reduction of free cholesterol in activated hepatic stellate cells downregulated TLR4 signalling and reduced liver fibrosis (Furuhashi *et al.*, 2018). Interestingly, statins, which inhibit HMGCR thereby reducing cholesterol synthesis, have been shown to have antifibrotic effects (Trebicka *et al.*, 2010; Yang *et al.*, 2010; Klein *et al.*, 2012; Wang *et al.*, 2013; Chong *et al.*, 2015; Ying *et al.*, 2017; Y. Jang *et al.*, 2018). It is possible that the reductions seen with bempedoic acid in hepatic stellate cells *in vitro* would reduce free cholesterol accumulation and TLR4 signalling, however, this was never assessed in our studies. This may, however, be another viable mechanism of ACLY inhibition in hepatic stellate cells, and one that would not occur following ACC inhibition.

It is possible that in addition to hepatocytes and hepatic stellate cells bempedoic acid is targeting other cell types in the liver or outside of the liver. Although, the expression of *ACLY* and *SLC27A2* in non-hepatocyte and non–hepatic stellate cell liver cell types seem negligible based on scRNA-seq data (Human Protein Atlas (www.proteinatlass.org), it is still possible that bempedoic acid is being activated and inhibiting ACLY in another cell type. Although hepatic Kupffer cells were not specifically explored, bempedoic acid had no effect when tested in bone marrow-derived macrophages, even at high doses, suggesting

it is not active in macrophages (Figure 3.14A). Whether bempedoic acid was acting in other immune cells or LSECs was also not explored. Due to increasing evidence supporting the role of multiple cell types in the pro-inflammatory and pro-fibrotic environment, this is important to address in future studies.

In addition to effects in hepatic stellate cells, it is possible that bempedoic acid is having effects independent of ACLY that are contributing to the reductions in hepatic inflammation and fibrosis. For example, bempedoic acid has been shown to activate AMPK at the β1 subunit, subsequently inhibiting ACC, and thus could be reducing fatty acid synthesis by simultaneously inhibiting ACLY and ACC (Pinkosky *et al*., 2013). Future experiments with bempedoic acid in AMPKβ1 knockout hepatocytes could help delineate whether this mechanism is responsible for any observed reductions in lipid synthesis. AMPK activation has several other beneficial metabolic effects and been shown to decrease liver fat in rodents (Boudaba *et al.*, 2018; Esquejo *et al.,* 2018). PXL770, an AMPKβ1 activation, suppresses hepatic inflammation and fibrosis in mice, and is currently in clinical development for NASH (Gluais-Dagorn *et al*., 2022). Whether AMPK activation by bempedoic acid is contributing to the reduced hepatic inflammation and fibrosis in our mice is currently unknown and requires further investigation. It is also possible that bempedoic acid is acting in the kidneys, where ACSVL1 is also expressed. This may contribute to differential effects observed in ACLY hKO mice and bempedoic acid treated mice. In general, whether bempedoic acid is having extra-hepatic effects that are contributing to our observed phenotypes requires further exploration.

4.4.2 Targeting hepatic stellate cells to reverse fibrosis

This dissertation provides insight into the potential importance of targeting activated hepatic stellate cells in NASH. Although the relationship between steatosis and fibrosis is still not fully established, this work supports the notion that once fibrosis has developed, removing one of the initial hits (i.e., steatosis) may not be sufficient to reverse inflammation and fibrosis. Fibrosis is the number one predictor of mortality in NASH patients and thus targeting it is important in this population with end-stage liver disease. To reverse fibrosis once developed, it may be necessary to target the fibrotic cells themselves (i.e., hepatic stellate cells).

The benefits of targeting hepatic stellate cells directly have been demonstrated with ACC inhibition, where inhibiting cell activation *in vitro* translates to reduced fibrosis in preclinical NASH models (Bates *et al.*, 2020). These findings were replicated in this dissertation with ACLY inhibition. Many other drugs currently in clinical trials for NASH indirectly or directly target hepatic stellate cells, further supporting this theory (Romero *et al.*, 2020; Wang *et al.*, 2022). For example, inhibition of lysyl oxidase-like 2 (LOXL2), an enzyme upregulated in fibrotic tissue and NASH, that is involved in remodelling collagen and elastin in the extracellular matrix reverses NASH and fibrosis in mice (Romero *et al.*, 2020). Phase I and II clinical trials are ongoing. Pirfenidone, a drug approved for idiopathic pulmonary fibrosis that inhibits TGF−β signalling, is also being investigated for its repurposing for the treatment of hepatic fibrosis (Philips *et al*., 2020; Xi *et al*., 2021; Komiya *et al*., 2017).

With single-cell analysis, an exciting avenue of research focusing on cell type targeting has emerged. Several new technologies for direct targeting and drug delivery of molecules to hepatic stellate cells are emerging, and reviewed here (Z. Chen *et al.*, 2019; Ezhilararasan, Lakshmi and Raut, 2021). This may lead to new insight into whether upregulated DNL, and subsequent decreased fatty acid oxidation in certain cell types contribute specifically to disease progression. Cell type targeting could also be a promising mode to improve specificity and reduce side effects in cell types in which inhibiting DNL may be unfavourable. This ideology translates to several other disease areas with advantages such as targeting specific arms (i.e., specific cell types) of complex pathologies, while reducing unwanted side effects in other cell types. NASH for example is caused by the engagement of several different cell types and pathways, and it is unlikely that one target will be effective in treating this complex disease.

4.5 Human translation of ACLY inhibition

Despite the vast advancements in drug development for NAFLD and NASH, there are still no approved therapeutics. Several drugs that have shown preclinical benefits do not translate to human disease, which puts the translatability of mouse work to human disease into question. When designing the studies in this dissertation, adopting a translational approach was at the forefront. This was in part why a novel, more accurate mouse model of disease was characterized, and validated transcriptionally compared to human disease. The efficacy of bempedoic acid was also confirmed by comparing its transcriptional fibrotic changes to human datasets from healthy and NASH patients. Many

compounds in clinical trials lack efficacy in improving primary endpoints in humans, specifically in reducing or preventing the worsening of fibrosis, an FDA requirement for approval. This is partly due to the lack of testing in severe enough NASH and fibrosis models (Omokaro and Golden, 2020).

The discontinuation of clinical trials has also been fueled by safety concerns in humans that were not present or detectable in preclinical models. The benefit of targeting ACLY with bempedoic acid is that bempedoic acid is FDA approved for the treatment of hyperlipidemia. Drug repurposing is a great strategy to avoid roadblocks in early-phase clinical trials and can accelerate drug development. With early phases of safety and bioavailability testing passed, repurposed drugs have the potential to gain FDA approvals in less than half the time and one quarter of the cost (Scannell *et al.*, 2012; Nosengo, 2016; Seyhan, 2019). Drugs that have failed to meet FDA-approval as monotherapies, have safety concerns of increasing risk factors for CVD, such as hypertriglyceridemia by ACC inhibition, or elevated circulating cholesterol for FXR agonism by OCA (Younossi, Ratziu, *et al.*, 2019). As mentioned, bempedoic acid is in advanced phase III trials for cardiovascular event reduction (clinicaltrials.gov identifier: NCT02993406) (Nicholls *et al.*, 2021) and is effective at reducing adult hypercholesterolemia (Thompson *et al.*, 2015, 2016; Ballantyne *et al.*, 2016; Goldberg *et al.*, 2019). This is an important consideration as cardiovascular events are the leading cause of death in NASH patients (Fraile *et al.*, 2021). The work in this dissertation, therefore, supports the development of clinical trials testing the efficacy of bempedoic acid on liver fat reduction, and subsequently on NASH reduction in biopsy-proven patients.

To further test the translatability of observations in rodents, Mendelian randomization was performed. We replicated previous associations of *ACLY* with LDL-c and ApoB and additionally showed that reduced *ACLY* expression is associated with lower circulating triglycerides, AST, ALT, and GGT (Figure 3.13). At the time of performing these analyses, available UK Biobank liver fat data was limited, and therefore the analysis associating *ACLY* expression with liver fat was highly underpowered. When more data on liver fat, as well as liver outcomes, such as liver cancer or cirrhosis, becomes available, additional analysis into the relationship of these with *ACLY* expression should be performed.

4.6 Additional future directions and insights

The findings in this thesis provide insight into the role of ACLY in hepatocyte and hepatic stellate cell lipid metabolism and the impact this has in the setting of NASH. However, there are still several unanswered questions that were not addressed in this thesis that have been described throughout the concluding remarks. One additional limitation of this work was the inability to perform dual hepatocyte and hepatic stellate cell ACLY deletion. This would definitively confirm whether hepatic stellate cell ACLY inhibition is the main contributor to the improvements in fibrosis and inflammation observed with bempedoic acid treatment, relative to ACLY hKO mice. Currently, the most efficient AAV system to transiently transduce hepatic stellate cells is the AAV6 delivery system, which only transduces 30% of hepatic stellate cells (Rezvani *et al.*, 2016). Alternative gene transfer methods have been made (Schoemaker *et al.*, 2008; Reetz *et al.*, 2013),

demonstrating the promise of this avenue, but these are still not extensively used (or commercially available). Hepatic stellate cell specific promoters, such as lecithin retinol acyltransferase (LRAT), have been characterized and used to generate cell-specific Cre expression from birth (Mederacke *et al.,* 2013). Future studies crossing LRAT-Cre mice with *Acly*$^{f/f}$ mice to generate hepatic stellate cell-specific ACLY knockouts from birth could be performed. However, this will not answer the proposed hypothesis of bempedoic acid in a NASH intervention setting. Hopefully, AAV technology advances will allow for the dual and selective deletion of ACLY in hepatic stellate cells and hepatocytes to allow for intervention testing. This will help confirm whether the genetic ACLY deletion phenotype is consistent with the phenotype in bempedoic acid treated mice and will determine whether the proposed mechanisms are accurate.

4.7 Summary

This dissertation provides several key insights into the role of ACLY in NASH. In both mice and humans, we demonstrate that ACLY inhibition may be effective in improving NASH, glucose intolerance, and serum lipids. A diet-induced mouse model that recapitulates human disease conditions was developed and characterized. This model can be used for future studies investigating NAFLD, which has emerged as a leading cause of chronic liver disease. ACLY inhibition in hepatocytes lowers lipid and cholesterol synthesis and increases fatty acid oxidation *in vitro,* which translates to improved hepatic steatosis, glucose tolerance, and serum lipids in mice with NASH. ACLY inhibition in hepatic stellate cells, lowers lipid and cholesterol synthesis and increases fatty acid

oxidation *in vitro,* and inhibits cell activation and proliferation. This translates to improved inflammation and fibrosis in mice with NASH. Translation of these findings to humans was supported by Mendelian randomization analysis, which demonstrates that reductions in *ACLY* are associated with lower circulating triglycerides and serum liver injury markers. These findings, indicate a role for ACLY inhibition in NASH and suggest that the hepatic stellate cell is an important target for fibrosis reversal. Importantly, ACLY inhibition provides benefits not only to NASH, but also to key risk factors of T2D and CVDs, (glucose intolerance and dyslipidemia respectively). Given the interconnectivity of these diseases in patient populations, this work strongly supports further development of ACLY inhibition in the treatment of NASH.

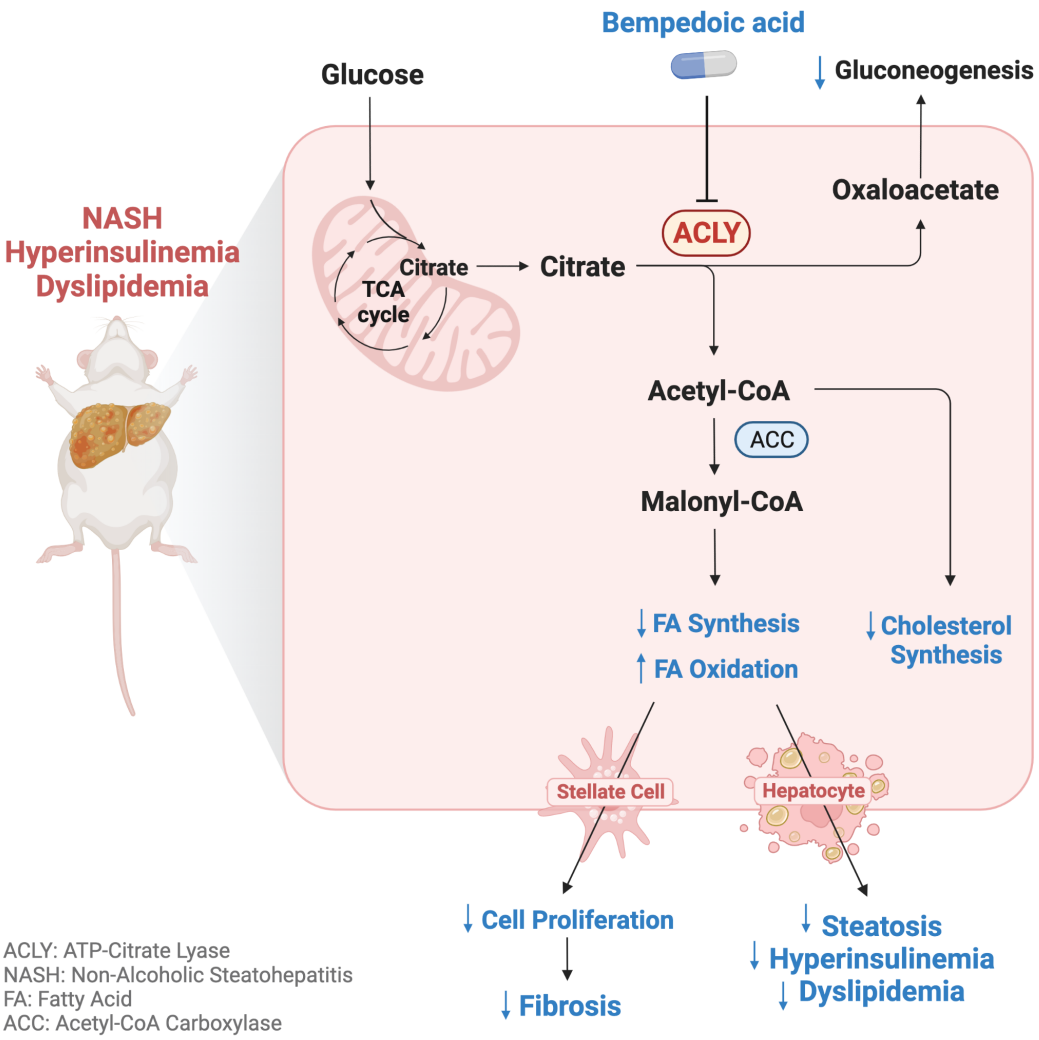

Figure 4.2. Summary of ACLY inhibition in a mouse model of NASH and fibrosis

A TN-ND mouse model elicited genomic and histological features of NASH, dyslipidemia, and hepatic fibrosis. Inhibiting ACLY in hepatocytes and stellate cells decreases fatty acid and cholesterol synthesis and increases fatty acid oxidation. In the TN-ND mouse model, inhibiting hepatocyte ACLY by bempedoic acid or genetic deletion reduces hepatic steatosis, hyperinsulinemia, and dyslipidemia. Inhibition of ACLY in stellate cells by bempedoic acid reduces cell proliferation, which in the TN-ND mice translated to decreased hepatic fibrosis. TN-ND: thermoneutral NASH diet; FA: fatty acid.

CHAPTER 5: REFERENCES

5. References

Achiwa, K. *et al.* (2016) 'DSS colitis promotes tumorigenesis and fibrogenesis in a choline-deficient high-fat diet-induced NASH mouse model', *Biochemical and Biophysical Research Communications*, 470(1), pp. 15–21. Available at: https://doi.org/10.1016/j.bbrc.2015.12.012.
Ahrens, M. *et al.* (2013) 'DNA methylation analysis in nonalcoholic fatty liver disease suggests distinct disease-specific and remodeling signatures after bariatric surgery', *Cell Metabolism*, 18(2), pp. 296–302. Available at: https://doi.org/10.1016/j.cmet.2013.07.004.
Alam, Dr.S. *et al.* (2019) 'Effect of weight reduction on histological activity and fibrosis of lean nonalcoholic steatohepatitis patient', *Journal of Translational Internal Medicine*, 7(3), p. 106. Available at: https://doi.org/10.2478/jtim-2019-0023.
Alexander, J. *et al.* (2013) 'Non-alcoholic fatty liver disease contributes to hepatocarcinogenesis in non-cirrhotic liver: a clinical and pathological study', *Journal of Gastroenterology and Hepatology*, 28(5), pp. 848–854. Available at: https://doi.org/10.1111/jgh.12116.
Alkhouri, N. and McCullough, A.J. (2012) 'Noninvasive diagnosis of NASH and liver fibrosis within the spectrum of NAFLD', *Gastroenterology & Hepatology*, 8(10), p. 661.
Altshuler, D.M. *et al.* (2012) 'An integrated map of genetic variation from 1,092 human genomes', *Nature*, 491(7422), pp. 56–65. Available at: https://doi.org/10.1038/nature11632.
Angulo, P. *et al.* (2015) 'Liver fibrosis, but no other histologic features, is associated with long-term outcomes of patients with nonalcoholic fatty liver disease', *Gastroenterology*, 149(2), pp. 389-397.e10. Available at: https://doi.org/10.1053/j.gastro.2015.04.043.
Arnold, P.K. *et al.* (2022) 'A non-canonical tricarboxylic acid cycle underlies cellular identity', *Nature*, 603, p. 477. Available at: https://doi.org/10.1038/s41586-022-04475-w.
Asahina, K. (2012) 'Hepatic stellate cell progenitor cells', *Journal of Gastroenterology and Hepatology*, 27(Suppl 2), p. 80. Available at: https://doi.org/10.1111/j.1440-1746.2011.07001.x.
Asipu, A. *et al.* (2003) 'Properties of normal and mutant recombinant human ketohexokinases and implications for the pathogenesis of essential fructosuria', *Diabetes*, 52(9), pp. 2426–2432. Available at: https://doi.org/10.2337/diabetes.52.9.2426.
Assante, G. *et al.* (2022) 'Acetyl-CoA metabolism drives epigenome change and contributes to carcinogenesis risk in fatty liver disease', *Genome Medicine*, 14(1), pp. 1–16. Available at: https://doi.org/10.1186/s13073-022-01071-5
Ballantyne, C.M. *et al.* (2012) 'ETC-1002 lowers LDL-c and beneficially modulates other cardio-metabolic risk factors in hypercholesterolemic subjects with either normal or elevated triglycerides', *Journal of the American College of Cardiology*, 59(13), p. e1625. Available at: https://doi.org/10.1016/s0735-1097(12)61626-x.
Ballantyne, C.M. *et al.* (2013) 'Efficacy and safety of a novel dual modulator of adenosine triphosphate-citrate lyase and adenosine monophosphate-activated protein kinase in patients with hypercholesterolemia: results of a multicenter, randomized,

double-blind, placebo-controlled, parallel-group trial', *Journal of the American College of Cardiology*, 62(13), pp. 1154–1162. Available at: https://doi.org/10.1016/j.jacc.2013.05.050.
Ballantyne, C.M. *et al.* (2016) 'Effect of ETC-1002 on serum low-density lipoprotein cholesterol in hypercholesterolemic patients receiving statin therapy', *American Journal of Cardiology*, 117(12), pp. 1928–1933. Available at: https://doi.org/10.1016/j.amjcard.2016.03.043.
Barrows, B.R. and Parks, E.J. (2006) 'Contributions of different fatty acid sources to very low-density lipoprotein-triacylglycerol in the fasted and fed states', *The Journal of Clinical Endocrinology & Metabolism*, 91(4), pp. 1446–1452. Available at: https://doi.org/10.1210/jc.2005-1709.
BasuRay, S. *et al.* (2017) "The PNPLA3 variant associated with fatty liver disease (I148M) accumulates on lipid droplets by evading ubiquitylation," *Hepatology*, 66(4), pp. 1111–1124. Available at: https://doi.org/10.1002/hep.29273.
Batchuluun, B., Pinkosky, S.L. and Steinberg, G.R. (2022) 'Lipogenesis inhibitors: therapeutic opportunities and challenges', *Nature Reviews Drug Discovery*, pp. 1–23. Available at: https://doi.org/10.1038/s41573-021-00367-2.
Bates, J. *et al.* (2020) 'Acetyl-CoA carboxylase inhibition disrupts metabolic reprogramming during hepatic stellate cell activation', *Journal of Hepatology*, 73(4), pp. 896–905. Available at: https://doi.org/10.1016/j.jhep.2020.04.037.
Beery, A.K. (2018) 'Inclusion of females does not increase variability in rodent research studies', *Current Opinion in Behavioral Sciences*, 23, pp. 143–149. Available at: https://doi.org/10.1016/j.cobeha.2018.06.016.
Beigneux, A.P. *et al.* (2004) 'ATP-citrate lyase deficiency in the mouse', *Journal of Biological Chemistry*, 279(10), pp. 9557–9564. Available at: https://doi.org/10.1074/jbc.m310512200.
Boudaba, N. *et al.* (2018) 'AMPK re-activation suppresses hepatic steatosis but its downregulation does not promote fatty liver development' *EBioMedicine,* 28, pp. 194-209.
Brenner, D.A. (2018) 'Of mice and men and nonalcoholic steatohepatitis', *Hepatology*, 68(6), p. 2059. Available at: https://doi.org/10.1002/hep.30186.
Burgess, S.C. *et al.* (2005) 'Effect of murine strain on metabolic pathways of glucose production after brief or prolonged fasting', *American Journal of Physiology. Endocrinology and Metabolism*, 289(1). Available at: https://doi.org/10.1152/ajpendo.00601.2004.
Calle, R.A. *et al.* (2021) 'ACC inhibitor alone or co-administered with a DGAT2 inhibitor in patients with non-alcoholic fatty liver disease: two parallel, placebo-controlled, randomized phase 2a trials.', *Nature Medicine*, 27(10), pp. 1836–1848. Available at: https://doi.org/10.1038/s41591-021-01489-1.
Cai, L. *et al.* (2011) 'Acetyl-CoA induces cell growth and proliferation by promoting the acetylation of histones at growth genes', *Molecular Cell*, 42(4), p. 426. Available at: https://doi.org/10.1016/j.molcel.2011.05.004.

Cao, Y. *et al.* (2021) 'The association between NAFLD and risk of chronic kidney disease: a cross-sectional study', *Therapeutic Advances in Chronic Disease*, 12. Available at: https://doi.org/10.1177/20406223211048649.
De Castro, U.G.M. *et al.* (2013) 'Age-dependent effect of high-fructose and high-fat diets on lipid metabolism and lipid accumulation in liver and kidney of rats', *Lipids in Health and Disease*, 12(1), p. 136. Available at: https://doi.org/10.1186/1476-511x-12-136.
Cha, J.Y. and Repa, J.J. (2007) 'The liver X receptor (LXR) and hepatic lipogenesis. The carbohydrate-response element-binding protein is a target gene of LXR', *The Journal of Biological Chemistry*, 282(1), pp. 743–751. Available at: https://doi.org/10.1074/jbc.m605023200.
Chalasani, N. *et al.* (2008) 'Relationship of steatosis grade and zonal location to histological features of steatohepatitis in adult patients with non-alcoholic fatty liver disease', *Journal of Hepatology*, 48(5), p. 829. Available at: https://doi.org/10.1016/j.jhep.2008.01.016.
Chalasani, N. *et al.* (2018) 'The diagnosis and management of nonalcoholic fatty liver disease: Practice guidance from the American Association for the Study of Liver Diseases', *Hepatology*, 67(1), pp. 328–357. Available at: https://doi.org/10.1002/hep.29367.
Chen, Y. *et al.* (2019) 'ATP-citrate lyase is an epigenetic regulator to promote obesity-related kidney injury.', *The FASEB Journal*, 33(8), pp. 9602–9615. Available at: https://doi.org/10.1096/fj.201900213r.
Chen, Y. *et al.* (2012) 'Hedgehog controls hepatic stellate cell fate by regulating metabolism', *Gastroenterology*, 143(5), pp. 1319-1329.e11. Available at: https://doi.org/10.1053/j.gastro.2012.07.115.
Chen, Z. *et al.* (2019) 'Targeted drug delivery to hepatic stellate cells for the treatment of liver fibrosis', *The Journal of Pharmacology and Experimental Therapeutics*, 370(3), p. 695. Available at: https://doi.org/10.1124/jpet.118.256156.
Cheng, T. *et al.* (2011) 'Pyruvate carboxylase is required for glutamine-independent growth of tumor cells', *Proceedings of the National Academy of Sciences of the United States of America*, 108(21), pp. 8674–8679. Available at: https://doi.org/10.1073/pnas.1016627108.
Cheng, W.-L. *et al.* (2021) 'Sugar fructose triggers gut dysbiosis and metabolic inflammation with cardiac arrhythmogenesis', *Biomedicines*, 9(7), p. 728. Available at: https://doi.org/10.3390/biomedicines9070728.
Chiu, S. *et al.* (2014) 'Effect of fructose on markers of non-alcoholic fatty liver disease (NAFLD): a systematic review and meta-analysis of controlled feeding trials', *European Journal of Clinical Nutrition*, 68(4), pp. 416–423. Available at: https://doi.org/10.1038/ejcn.2014.8.
Choi, W.G. *et al.* (2017) 'EIF2α phosphorylation is required to prevent hepatocyte death and liver fibrosis in mice challenged with a high fructose diet', *Nutrition and Metabolism*, 14(1), pp. 1–21. Available at: https://doi.org/10.1186/s12986-017-0202-s6
Chong, L.W. *et al.* (2015) 'Fluvastatin attenuates hepatic steatosis-induced fibrogenesis in rats through inhibiting paracrine effect of hepatocyte on hepatic stellate cells', *BMC Gastroenterology*, 15(1). Available at: https://doi.org/10.1186/s12876-015-0248-8.

Chung, B.K. *et al.* (2022) 'Spatial transcriptomics identifies enriched gene expression and cell types in human liver fibrosis', *Hepatology Communications*, 6(9), pp. 2538–2550. Available at: https://doi.org/10.1002/hep4.2001.
Chypre, M., Zaidi, N. and Smans, K. (2012) 'ATP-citrate lyase: A mini-review', *Biochemical and Biophysical Research Communications*, 422(1), pp. 1–4. Available at: https://doi.org/10.1016/j.bbrc.2012.04.144.
Clapper, Jason R. *et al.* (2013) 'Diet-induced mouse model of fatty liver disease and nonalcoholic steatohepatitis reflecting clinical disease progression and methods of assessment', *American Journal of Physiology - Gastrointestinal and Liver Physiology*, 305(7). Available at: https://doi.org/10.1152/ajpgi.00079.2013.
Cordoba-Chacon, J. *et al.* (2015) 'Growth hormone inhibits hepatic de novo lipogenesis in adult mice', *Diabetes*, 64(9), pp. 3093–3103. Available at: https://doi.org/10.2337/db15-0370.
Deb, D.K. *et al.* (2017) 'ATP-citrate lyase is essential for high glucose-induced histone hyperacetylation and fibrogenic gene upregulation in mesangial cells', *American Journal of Physiology Renal Physiology*, 313(2), pp. 423–429. Available at: https://doi.org/10.1152/ajprenal.00029.2017.
Dewidar, B. *et al.* (2019) 'TGF-β in hepatic stellate cell activation and liver fibrogenesis', *Cells*, 8(11). Available at: https://doi.org/10.3390/cells8111419.
Ding, C. *et al.* (2016) 'A cell-type-resolved liver proteome', *Molecular & Cellular Proteomics*, 15(10), p. 3190. Available at: https://doi.org/10.1074/mcp.m116.060145.
Diraison, F. *et al.* (2002) 'Increased hepatic lipogenesis but decreased expression of lipogenic gene in adipose tissue in human obesity', *American Journal of Physiology. Endocrinology and Metabolism*, 282(1). Available at: https://doi.org/10.1152/ajpendo.2002.282.1.e46.
Diraison, F., Pachiaudi, C. and Beylot, M. (1996) 'In vivo measurement of plasma cholesterol and fatty acid synthesis with deuterated water: determination of the average number of deuterium atoms incorporated', *Metabolism: Clinical and Experimental*, 45(7), pp. 817–821. Available at: https://doi.org/10.1016/s0026-0495(96)90152-3.
Diraison, F., Pachiaudi, C. and Beylot, M. (1997) 'Measuring lipogenesis and cholesterol synthesis in humans with deuterated water: use of simple gas chromatographic/mass spectrometric techniques', *Journal of Mass Spectrometry*, 32(1), pp. 81–86. Available at: https://doi.org/10.1002/(SICI)1096-9888(199701)32:1<81::AID-JMS454>3.0.CO;2-2.
Do, M.H. *et al.* (2018) 'High-glucose or -fructose diet cause changes of the gut microbiota and metabolic disorders in mice without body weight change', *Nutrients*, 10(6), p. 761. Available at: https://doi.org/10.3390/nu10060761.
Donnelly, K.L. *et al.* (2005) 'Sources of fatty acids stored in liver and secreted via lipoproteins in patients with nonalcoholic fatty liver disease', *The Journal of Clinical Investigation*, 115. Available at: https://doi.org/10.1172/jci200523621.
Duarte, J.A.G. *et al.* (2014) 'A high-fat diet suppresses de novo lipogenesis and desaturation but not elongation and triglyceride synthesis in mice', *Journal of Lipid Research*, 55(12), pp. 2541–2553. Available at: https://doi.org/10.1194/jlr.M052308.

Eissing, L. *et al.* (2013) 'De novo lipogenesis in human fat and liver is linked to ChREBP-β and metabolic health', *Nature Communications*, 4(1), pp. 1–11. Available at: https://doi.org/10.1038/ncomms2537.
Ekstedt, M. *et al.* (2006) 'Long-term follow-up of patients with NAFLD and elevated liver enzymes', *Hepatology*, 44(4), pp. 865–873. Available at: https://doi.org/10.1002/hep.21327.
Ekstedt, M. *et al.* (2015) 'Fibrosis stage is the strongest predictor for disease-specific mortality in NAFLD after up to 33 years of follow-up', *Hepatology,* 61(5), pp. 1547–1554. Available at: https://doi.org/10.1002/hep.27368.
Endo, Y. *et al.* (2015) 'Obesity drives Th17 cell differentiation by inducing the lipid metabolic kinase, ACC1', *Cell Reports*, 12(6), pp. 1042–1055. Available at: https://doi.org/10.1016/J.celrep.2015.07.014.
Enjoji, M., Kohjima, M. and Nakamuta, M. (2016) 'Lipid metabolism and the liver', *The Liver in Systemic Diseases*, pp. 105–122. Available at: https://doi.org/10.1007/978-4-431-55790-6_6.
Entenman, C. (1957) 'General procedures for separating lipid components of tissue', *Methods in Enzymology*, 3, pp. 299–317. Available at: https://doi.org/10.1016/s0076-6879(57)03395-9.
Esquejo, R.M. (2018) 'Activation of liver AMPK with PF-06409577 corrects NAFLD and lowers cholesterol in rodent and primate preclinical models' *EBioMedicine,* 31, 122-132. Available at: https://doi.org/10.1016/j.ebiom.2018.04.009.
Ezhilararasan, D., Lakshmi, T. and Raut, B. (2021) 'Novel nano-based drug delivery systems targeting hepatic stellate cells in the fibrotic liver', *Journal of Nanomaterials*, 8, pp. 804396. Available at: https://doi.org/10.1155/2021/4674046.
Farrell, G. *et al.* (2019) 'Mouse models of nonalcoholic steatohepatitis: toward optimization of their relevance to human nonalcoholic steatohepatitis', *Hepatology*, 69(5), pp. 2241–2257. Available at: https://doi.org/10.1002/hep.30333.
Febbraio, M.A. and Karin, M. (2021) '"Sweet death": fructose as a metabolic toxin that targets the gut-liver axis', *Cell Metabolism*, 33(12), p. 2316. Available at: https://doi.org/10.1016/J.cmet.2021.09.004.
Federico, A. *et al.* (2021) 'The role of fructose in non-alcoholic steatohepatitis: old relationship and new insights', *Nutrients,* 13(4), p. 1314. Available at: https://doi.org/10.3390/nu13041314.
Ference, B.A. *et al.* (2019) 'Mendelian randomization study of *ACLY* and cardiovascular disease', *New England Journal of Medicine*, 380(11), pp. 1033–1042. Available at: https://doi.org/10.1056/nejmoa1806747.
Folch, J., Lees, M., and Sloane Stanley, G.H. (1957) 'A simple method for the isolation and purification of total lipides from animal tissues.', *The Journal of Biological Chemistry*, 226(1), pp. 497–509. Available at: https://doi.org/10.3989/scimar.2005.69n187.
Fonseca, V.A. (2009) 'Defining and characterizing the progression of type 2 diabetes', *Diabetes Care*, 32(suppl 2), pp. S151–S156. Available at: https://doi.org/10.2337/dc09-s301.

Fraile, J.M. *et al.* (2021) 'Non-alcoholic steatohepatitis (NASH)-a review of a crowded clinical landscape, driven by a complex disease', *Drug Design, Development and Therapy,* 15, pp. 3997-4009. Available at: https://doi: 10.2147/dddt.s315724.
Friedman, S.L. (2013) 'Convergent pathways that cause hepatic fibrosis in NASH', *Nature Reviews Gastroenterology & Hepatology,* 10(2), pp. 71–72. Available at: https://doi.org/10.1038/nrgastro.2012.256.
Friedman, S.L. *et al.* (2018) 'Mechanisms of NAFLD development and therapeutic strategies', *Nature Medicine,* 24(7), pp. 908–922. Available at: https://doi.org/10.1038/s41591-018-0104-9.
Fullerton, M.D. *et al.* (2013) 'Single phosphorylation sites in Acc1 and Acc2 regulate lipid homeostasis and the insulin-sensitizing effects of metformin', *Nature Medicine*, 19(12), pp. 1649–1654. Available at: https://doi.org/10.1038/nm.3372.
Furuhashi, H. *et al.* (2018) 'Vitamin A-coupled liposome system targeting free cholesterol accumulation in hepatic stellate cells offers a beneficial therapeutic strategy for liver fibrosis', *Hepatology Research: The Official Journal of the Japan Society of Hepatology*, 48(5), pp. 397–407. Available at: https://doi.org/10.1111/hepr.13040.
Futatsugi, K. *et al.* (2020) 'Discovery of PF-06835919: A potent inhibitor of ketohexokinase (KHK) for the treatment of metabolic disorders driven by the overconsumption of fructose', *Journal of Medicinal Chemistry*, 63(22), pp. 13546–13560. Available at: https://doi.org/10.1021/acs.jmedchem.0c00944.
Galic, S. *et al.* (2011) 'Hematopoietic AMPK β1 reduces mouse adipose tissue macrophage inflammation and insulin resistance in obesity', *Journal of Clinical Investigation*, 121(12), pp. 4903–4915. Available at: https://doi.org/10.1172/jci58577.
Galsgaard, K.D. *et al.* (2019) 'Glucagon receptor signaling and lipid metabolism', *Frontiers in Physiology*, 10, p. 413. Available at: https://doi.org/10.3389/fphys.2019.00413/bibtex.
Ganeshan, K. and Chawla, A. (2017) 'Warming the mouse to model human diseases', *Nature Reviews Endocrinology*, 13(8), pp. 458–465. Available at: https://doi.org/10.1038/nrendo.2017.48.
Geng, Y. *et al.* (2021) 'How does hepatic lipid accumulation lead to lipotoxicity in non-alcoholic fatty liver disease?', *Hepatology International,* 15(1), pp. 21–35. Available at: https://doi.org/10.1007/S12072-020-10121-2.
Giles, D.A. *et al.* (2017) 'Thermoneutral housing exacerbates nonalcoholic fatty liver disease in mice and allows for sex-independent disease modeling', *Nature Medicine*, 23(7), pp. 829–838. Available at: https://doi.org/10.1038/nm.4346.
Glass, L.M. *et al.* (2019) 'Comorbidities and nonalcoholic fatty liver disease: the chicken, the egg, or both?', *Federal Practitioner,* 36(2), pp. 64–71.
Glen, J. *et al.* (2016) 'Non-alcoholic fatty liver disease (NAFLD): summary of NICE guidance', *The British Medical Journal*. Available at: https://doi.org/10.1136/bmj.i4428.
Gluais-Dagorn *et al.,* (2022) 'Direct AMPK activation corrects NASH in rodents through metabolic effects and direct action on inflammation and fibrogenesis', *Hepatology Communications,* 6(1), pp. 101-119. Available at: https://doi.org/10.1002/hep4.1799.
Glund, S. *et al.* (2012) 'Inhibition of acetyl-CoA carboxylase 2 enhances skeletal muscle fatty acid oxidation and improves whole-body glucose homeostasis in db/db mice',

Diabetologia, 55(7), pp. 2044–2053. Available at: https://doi.org/10.1007/s00125-012-2554-9.
Goedeke, L. *et al.* (2018) 'Acetyl-CoA carboxylase inhibition reverses NAFLD and hepatic insulin resistance but promotes hypertriglyceridemia in rodents', *Hepatology*, 68(6), pp. 2197–2211. Available at: https://doi.org/10.1002/hep.30097.
Goldberg, A.C. *et al.* (2019) 'Effect of bempedoic acid vs placebo added to maximally tolerated statins on low-density lipoprotein cholesterol in patients at high risk for cardiovascular disease: The CLEAR wisdom randomized clinical trial', *Journal of the American Medical Association*, 322(18), pp. 1780–1788. Available at: https://doi.org/10.1001/jama.2019.16585.
Govaere, O. *et al.* (2020) 'Transcriptomic profiling across the nonalcoholic fatty liver disease spectrum reveals gene signatures for steatohepatitis and fibrosis', *Science Translational Medicine*, 12(572). Available at: https://doi.org/10.1126/scitranslmed.aba4448.
Green, C.D. *et al.* (2022) 'A new preclinical model of western diet-induced progression of non-alcoholic steatohepatitis to hepatocellular carcinoma', *The FASEB Journal*, 36(7), p. e22372. Available at: https://doi.org/10.1096/fj.202200346r.
Gutierrez, J.A. *et al.* (2021) 'Pharmacologic inhibition of ketohexokinase prevents fructose-induced metabolic dysfunction', *Molecular Metabolism*, 48, p. 101196. Available at: https://doi.org/10.1016/j.molmet.2021.101196.
Haas, J.T. *et al.* (2012) 'Hepatic insulin signaling is required for obesity-dependent expression of SREBP-1c mRNA but not for feeding-dependent expression', *Cell Metabolism*, 15(6), pp. 873–884. Available at: https://doi.org/10.1016/j.cmet.2012.05.002.
Hall, Z. *et al.* (2017) 'Lipid zonation and phospholipid remodeling in nonalcoholic fatty liver disease', *Hepatology*, 65(4), pp. 1165–1180. Available at: https://doi.org/10.1002/hep.28953/suppinfo.
Hammoutene, A. and Rautou, P.E. (2019) 'Role of liver sinusoidal endothelial cells in non-alcoholic fatty liver disease', *Journal of Hepatology*, 70(6), pp. 1278–1291. Available at: https://doi.org/10.1016/j.jhep.2019.02.012.
Harriman, G. *et al.* (2016) 'Acetyl-CoA carboxylase inhibition by ND-630 reduces hepatic steatosis, improves insulin sensitivity, and modulates dyslipidemia in rats', *Proceedings of the National Academy of Sciences of the United States of America*, 113(13), pp. e1796–e1805. Available at: https://doi.org/10.1073/pnas.1520686113.
Hart-Unger, S. *et al.* (2017) 'Hormone signaling and fatty liver in females: analysis of estrogen receptor α mutant mice', *International Journal of Obesity,* 41(6), pp. 945–954. Available at: https://doi.org/10.1038/ijo.2017.50.
Herck, M.A.V. *et al.* (2019) 'The differential roles of T cells in non-alcoholic fatty liver disease and obesity', *Frontiers in Immunology*, 10. Available at: https://doi.org/10.3389/fimmu.2019.00082.
Herman, M.A. and Birnbaum, M.J. (2021) 'Molecular aspects of fructose metabolism and metabolic disease', *Cell metabolism*, 33(12), pp. 2329–2354. Available at: https://doi.org/10.1016/j.cmet.2021.09.010.

Heyens, L.J.M. *et al.* (2021) 'Liver Fibrosis in Non-alcoholic Fatty Liver Disease: From Liver Biopsy to Non-invasive Biomarkers in Diagnosis and Treatment', *Frontiers in Medicine*, 8, p. 476. Available at: https://doi.org/10.3389/fmed.2021.615978/bibtex.
Higuchi, N. *et al.* (2008) 'Liver X receptor in cooperation with SREBP-1c is a major lipid synthesis regulator in nonalcoholic fatty liver disease', *Hepatology Research*, 38(11), pp. 1122–1129. Available at: https://doi.org/10.1111/j.1872-034x.2008.00382.x.
H'ng, M.W.C. and Kwek, J.W. (2010) 'Imaging appearance of severe subcapsular hepatic steatosis: mimicking hepatic embolic infarcts', *The British Journal of Radiology*, 83(989), p. e098. Available at: https://doi.org/10.1259/bjr/62944791.
Hodson, L. *et al.* (2007) 'The contribution of splanchnic fat to VLDL triglyceride is greater in insulin-resistant than insulin-sensitive men and women studies in the postprandial state', *Diabetes*, 56(10), pp. 2433–2441. Available at: https://doi.org/10.2337/db07-0654.
Hodson, L., Rosqvist, F. and Parry, S.A. (2020) 'The influence of dietary fatty acids on liver fat content and metabolism', *Proceedings of the Nutrition Society*, 79(1), pp. 30–41. Available at: https://doi.org/10.1017/s0029665119000569.
Ter Horst, K.W. *et al.* (2021) 'Hepatic insulin resistance is not pathway selective in humans with nonalcoholic fatty liver disease', *Diabetes Care*, 44(2), p. 489. Available at: https://doi.org/10.2337/dc20-1644.
Ter Horst, K.W. and Serlie, M.J. (2017) 'Fructose consumption, lipogenesis, and non-alcoholic fatty liver disease', *Nutrients*, 9(9), pp. 1–20. Available at: https://doi.org/10.3390/nu9090981.
Hughes, K. *et al.* (1992) 'Identification of multifunctional ATP-citrate lyase kinase as the alpha-isoform of glycogen synthase kinase-3', *The Biochemical Journal*, 288, pp. 309–314. Available at: https://doi.org/10.1042/bj2880309.
Hughey, C.C. *et al.* (2014) 'Approach to assessing determinants of glucose homeostasis in the conscious mouse', *Mammalian Genome*, 25(9-10), pp. 522–538. Available at: https://doi.org/10.1007/s00335-014-9533-z.
Huynh, F.K. *et al.* (2014) 'Measurement of fatty acid oxidation rates in animal tissues and cell lines', *Methods in Enzymology*, 542, pp. 391–405. Available at: https://doi.org/10.1016/b978-0-12-416618-9.00020-0.
Im, Y.R. *et al.* (2021) 'A Systematic review of animal models of NAFLD finds high-fat, high-fructose diets most closely resemble human NAFLD', *Hepatology*, 74(4), pp. 1884–1901. Available at: https://doi.org/10.1002/hep.31897.
Imamura, F. *et al.* (2020) 'Fatty acids in the de novo lipogenesis pathway and incidence of type 2 diabetes: a pooled analysis of prospective cohort studies', *PLoS Medicine*, 17(6). Available at: https://doi.org/10.1371/journal.pmed.1003102.
Isaev, N.K., Stelmashook, E. V. and Genrikhs, E.E. (2019) 'Neurogenesis and brain aging', *Reviews in the Neurosciences*, 30(6), pp. 573–580. Available at: https://doi.org/10.1515/revneuro-2018-0084.
Ishii, S. *et al.* (2004) 'Carbohydrate response element binding protein directly promotes lipogenic enzyme gene transcription', *Proceedings of the National Academy of Sciences of the United States of America*, 101(44), pp. 15597–15602. Available at: https://doi.org/10.1073/pnas.0405238101

James, C.M., Olejniczak, S.H. and Repasky, E.A. (2022) 'How murine models of human disease and immunity are influenced by housing temperature and mild thermal stress'. Available at: https://doi.org/10.1080/23328940.2022.2093561.
Jang, C. *et al.* (2018) 'The small intestine converts dietary fructose into glucose and organic acids', *Cell Metabolism*, 27(2), p. 351. Available at: https://doi.org/10.1016/j.cmet.2017.12.016.
Jang, Y.O. *et al.* (2018) 'Synergistic effects of simvastatin and bone marrow-derived mesenchymal stem cells on hepatic fibrosis', *Biochemical and Biophysical Research Communications*, 497(1), pp. 264–271. Available at: https://doi.org/10.1016/j.bbrc.2018.02.067.
Jegatheesan, P. and De Bandt, J.P. (2017) 'Fructose and NAFLD: the multifaceted aspects of fructose metabolism', *Nutrients*, 9(3). Available at: https://doi.org/10.3390/nu9030230.
Jensen, V.S. *et al*. (2021). 'Insulin treatment improves liver histopathology and decreases expression of inflammatory and fibrogenic genes in a hyperglycemic, dyslipidemic hamster model of NAFLD
Jiang, Z.Y. *et al.* (2021) 'Identification of key genes and immune infiltrate in nonalcoholic steatohepatitis: a bioinformatic analysis', *BioMed Research International*, p. 7561645. Available at: https://doi.org/10.1155/2021/7561645.
Jin, E.S. *et al.* (2005) 'Differing mechanisms of hepatic glucose overproduction in triiodothyronine-treated rats vs. Zucker diabetic fatty rats by NMR analysis of plasma glucose', *American Journal of Physiology-Endocrinology and Metabolism*, 288(4), pp. e654-62. Available at: https://doi.org/10.1152/ajpendo.00365.2004.
Jones, J.G. *et al.* (1998) '13C NMR measurements of human gluconeogenic fluxes after ingestion of [U-13C]propionate, phenylacetate, and acetaminophen', *The American Journal of Physiology*, 275(5), pp. e843-52. Available at: https://doi.org/10.1152/ajpendo.1998.275.5.e843.
Jones, J.G. *et al.* (2001) 'An integrated (2)H and (13)C NMR study of gluconeogenesis and TCA cycle flux in humans', *American Journal of Physiology-Endocrinology and Metabolism*, 281(4), pp. e848-56. Available at: https://doi.org/10.1152/ajpendo.2001.281.4.e848.
Jones, J.G. (2016) 'Hepatic glucose and lipid metabolism', *Diabetologia*, 59(6), pp. 1098–1103. Available at: https://doi.org/10.1007/s00125-016-3940-5.
Jürgens, H. *et al.* (2005) 'Consuming fructose-sweetened beverages increases body adiposity in mice', *Obesity Research*, 13(7), pp. 1145–1156. Available at: https://doi.org/10.1038/oby.2005.136.
Kawasaki, T. *et al.* (2009) 'Rats fed fructose-enriched diets have characteristics of nonalcoholic hepatic steatosis', *The Journal of Nutrition*, 139(11), pp. 2067–2071. Available at: https://doi.org/10.3945/jn.109.105858.
Kazierad, D.J. *et al.* (2021) 'Inhibition of ketohexokinase in adults with NAFLD reduces liver fat and inflammatory markers: a randomized phase 2 trial', *Med*, 2, pp. 800-813. Available at: https://doi.org/10.1016/j.medj.2021.04.007.

Khalili, K. *et al.* (2003) 'Hepatic subcapsular steatosis in response to intraperitoneal insulin delivery: CT findings and prevalence', *American Journal of Roentgenology*, 180(6), pp. 1601–1604. Available at: https://doi.org/10.2214/ajr.180.6.1801601.
Khomich, O., Ivanov, A. V. and Bartosch, B. (2019) 'Metabolic hallmarks of hepatic stellate cells in liver fibrosis', *Cells*, 9(1), p. 24. Available at: https://doi.org/10.3390/cells9010024.
Kim, C.W. *et al.* (2017) 'Acetyl-CoA carboxylase inhibition reduces hepatic steatosis but elevates plasma triglycerides in mice and humans: a bedside to bench investigation', *Cell Metabolism*, 26(2), pp. 394-406.e6. Available at: https://doi.org/10.1016/j.cmet.2017.07.009.
Kishida, N. *et al.* (2016) 'Development of a novel mouse model of hepatocellular carcinoma with nonalcoholic steatohepatitis using a high-fat, choline-deficient diet and intraperitoneal injection of diethylnitrosamine', *BMC Gastroenterology*, 16(1), pp. 1–13. Available at: https://doi.org/10.1186/s12876-016-0477-5.
Klein, S. *et al.* (2012) 'Atorvastatin inhibits proliferation and apoptosis, but induces senescence in hepatic myofibroblasts and thereby attenuates hepatic fibrosis in rats', *Laboratory Investigation*, 92(10), pp. 1440–1450. Available at: https://doi.org/10.1038/labinvest.2012.106.
Kleiner, D.E. *et al.* (2005) 'Design and validation of a histological scoring system for nonalcoholic fatty liver disease', *Hepatology*, 41(6), pp. 1313–1321. Available at: https://doi.org/10.1002/hep.20701.
Kloet, F.M. van der *et al.* (2020) 'Increased comparability between RNA-Seq and microarray data by utilization of gene sets', *PLOS Computational Biology*, 16(9), p. e1008295. Available at: https://doi.org/10.1371/journal.pcbi.1008295.
Knebel, B. *et al.* (2012) 'Liver-specific expression of transcriptionally active SREBP-1c is associated with fatty liver and increased visceral fat mass', *PLoS ONE*, 7(2), p. e31812. Available at: https://doi.org/10.1371/journal.pone.0031812.
Knobloch, M. *et al.* (2012) 'Metabolic control of adult neural stem cell activity by FASN-dependent lipogenesis', *Nature,* 493(7431), pp. 226–230. Available at: https://doi.org/10.1038/nature11689.
Koliaki, C. *et al.* (2015) 'Adaptation of hepatic mitochondrial function in humans with non-alcoholic fatty liver is lost in steatohepatitis', *Cell Metabolism*, 21(5), pp. 739–746. Available at: https://doi.org/10.1016/j.cmet.2015.04.004.
Kozlitina, J. *et al.* (2014) "Exome-wide association study identifies a TM6SF2 variant that confers susceptibility to nonalcoholic fatty liver disease," *Nature Genetics*, 46(4), pp. 352–356. Available at: https://doi.org/10.1038/ng.2901.
Komiya, C. *et al.* (2017) 'Antifibrotic effect of pirfenidone in a mouse model of human nonalcoholic steatohepatitis', *Scientific Reports*, 7, p. 44754. Available at: https://doi.org/10.1038/srep44754.
Lai, H.T.M. *et al.* (2019) 'Serial plasma phospholipid fatty acids in the de novo lipogenesis pathway and total mortality, cause-specific mortality, and cardiovascular diseases in the cardiovascular health study', *Journal of the American Heart Association: Cardiovascular and Cerebrovascular Disease*, 8(22). Available at: https://doi.org/10.1161/jaha.119.012881.

Lambert, J.E. *et al.* (2014) 'Increased de novo lipogenesis is a distinct characteristic of individuals with nonalcoholic fatty liver disease', *Gastroenterology*, 146(3), pp. 726–735. Available at: https://doi.org/10.1053/j.gastro.2013.11.049.
Large, V. *et al.* (1997) 'Use of labeling pattern of liver glutamate to calculate rates of citric acid cycle and gluconeogenesis', *The American Journal of Physiology*, 272. Available at: https://doi.org/10.1152/ajpendo.1997.272.1.e51.
Lawitz, E.J. *et al.* (2018) 'Acetyl-CoA carboxylase inhibitor GS-0976 for 12 weeks reduces hepatic de novo lipogenesis and steatosis in patients with nonalcoholic steatohepatitis', *Clinical Gastroenterology and Hepatology*, 16(12), pp. 1983-1991.e3. Available at: https://doi.org/10.1016/j.cgh.2018.04.042.
Lechuga, C.G. *et al.* (2004) 'TGF-β1 modulates matrix metalloproteinase-13 expression in hepatic stellate cells by complex mechanisms involving p38MAPK, PI3-kinase, AKT, and p70S6k', *American Journal of Physiology - Gastrointestinal and Liver Physiology*, 287(5 50-5), pp. 974–987. Available at: https://doi.org/10.1152/ajpi.00264.2003.
LeCluyse, E.L., Norona, L.M. and Presnell, S.C. (2018) 'Liver—Structure and Microanatomy', *Reference Module in Biomedical Sciences* [Preprint]. Available at: https://doi.org/10.1016/B978-0-12-801238-3.05123-0.
Lee, C. *et al.* (2022) 'Formyl peptide receptor 2 determines sex-specific differences in the progression of nonalcoholic fatty liver disease and steatohepatitis', *Nature Communications,* 13(1), pp. 1–17. Available at: https://doi.org/10.1038/s41467-022-28138-6.
Lee, J.W. *et al.* (2008) 'Hepatic capsular and subcapsular pathologic conditions: demonstration with CT and MR Imaging', *Radiographics*, 28(5), pp. 1307–1323. Available at: https://doi.org/10.1148/rg.285075089.
Lefebvre, E. *et al.* (2016) 'Antifibrotic effects of the dual CCR2/CCR5 antagonist cenicriviroc in animal models of liver and kidney fibrosis', *PLOS ONE*, 11(6), p. e0158156. Available at: https://doi.org/10.1371/journal.pone.0158156.
Leite, N.C. *et al.* (2009) 'Prevalence and associated factors of non-alcoholic fatty liver disease in patients with type-2 diabetes mellitus', *Liver International*, 29(1), pp. 113–119. Available at: https://doi.org/10.1111/j.1478-3231.2008.01718.x.
Leung, C. *et al.* (2016) 'The role of the gut microbiota in NAFLD', *Nature Reviews Gastroenterology & Hepatology*, 13(7), pp. 412–425. Available at: https://doi.org/10.1038/nrgastro.2016.85.
Li, W.C., Ralphs, K.L. and Tosh, D. (2010) 'Isolation and culture of adult mouse hepatocytes.', *Methods in Molecular Biology,* 633, pp. 185–196. Available at: https://doi.org/10.1007/978-1-59745-019-5_13.
Li, Y., Stanojevic, S. and Garmire, L.X. (2022) 'Emerging artificial intelligence applications in spatial transcriptomics analysis', *Computational and Structural Biotechnology Journal*, 20, pp. 2895–2908. Available at: https://doi.org/10.1016/j.csbj.2022.05.056.
Lian, N. *et al.* (2016) 'Curcumin inhibits aerobic glycolysis in hepatic stellate cells associated with activation of adenosine monophosphate-activated protein kinase', *IUBMB Life*, 68(7), pp. 589–596. Available at: https://doi.org/10.1002/iub.1518.

Lin, Y.-C. *et al.* (2014) "Genetic variants in GCKR and PNPLA3 confer susceptibility to nonalcoholic fatty liver disease in obese individuals," *The American Journal of Clinical Nutrition*, 99(4), pp. 869–874. Available at: https://doi.org/10.3945/ajcn.113.079749.
Liu, T. *et al.* (2020) 'Inhibition of acetyl-CoA carboxylase by PP-7a exerts beneficial effects on metabolic dysregulation in a mouse model of diet-induced obesity', *Experimental and Therapeutic Medicine*, 20(1), p. 521. Available at: https://doi.org/10.3892/etm.2020.8700.
Liu, Y. *et al.* (2009) 'Therapeutic targeting of the PDGF and TGF-β-signaling pathways in hepatic stellate cells by PTK787/ZK22258', *Laboratory Investigation*, 89(10), pp. 1152–1160. Available at: https://doi.org/10.1038/labinvest.2009.77.
Lonardo, A. *et al.* (2006) 'Hepatic steatosis and insulin resistance: does etiology make a difference?', *Journal of Hepatology*, 44(1), pp. 190–196. Available at: https://doi.org/10.1016/j.jhep.2005.06.018.
Loomba, R. *et al.* (2018) 'GS-0976 reduces hepatic steatosis and fibrosis markers in patients with nonalcoholic fatty liver disease', *Gastroenterology*, 155(5), pp. 1463-1473.e6. Available at: https://doi.org/10.1053/j.gastro.2018.07.027.
Loomba, R., Friedman, S.L. and Shulman, G.I. (2021) 'Mechanisms and disease consequences of nonalcoholic fatty liver disease', *Cell*, 184(10), pp. 2537–2564. Available at: https://doi.org/10.1016/j.cell.2021.04.015.
Luo, F., Oldoni, F. and Das, A. (2021) "TM6SF2: A novel genetic player in nonalcoholic fatty liver and cardiovascular disease," *Hepatology Communications*, 6(3), pp. 448–460. Available at: https://doi.org/10.1002/hep4.1822.
Love, M.I., Huber, W. and Anders, S. (2014) 'Moderated estimation of fold change and dispersion for RNA-seq data with DESeq2', *Genome Biology*, 15(12), pp. 1–21. Available at: https://doi.org/10.1186/s13059-014-0550-8.
Ma, J. *et al.* (2015) 'Sugar-sweetened beverage, diet soda, and fatty liver disease in the Framingham Heart Study cohorts', *Journal of Hepatology*, 63(2), pp. 462–469. Available at: https://doi.org/10.1016/j.jhep.2015.03.032.
Ma, L., Robinson, L.N. and Towle, H.C. (2006) 'ChREBP*Mlx is the principal mediator of glucose-induced gene expression in the liver', *The Journal of Biological Chemistry*, 281(39), pp. 28721–28730. Available at: https://doi.org/10.1074/jbc.m601576200.
Ma, T.T. *et al.* (2018) 'ATP citrate lyase and LncRNA NONMMUT010685 play crucial role in nonalcoholic fatty liver disease based on analysis of microarray data', *Cellular Physiology and Biochemistry*, 51(2), pp. 871–885. Available at: https://doi.org/10.1159/000495384.
Magnussons, I. *et al.* (1991) 'The Journal of Biological Chemistry Noninvasive Tracing of Krebs Cycle Metabolism in Liver', *Journal of Biological Chemistry*, 266(11), pp. 6975–6984. Available at: https://doi.org/10.1016/s0021-9258(20)89598-2.
Malato, Y. *et al.* (2011) 'Fate tracing of mature hepatocytes in mouse liver homeostasis and regeneration', *Journal of Clinical Investigation*, 121(12), pp. 4850–4860. Available at: https://doi.org/10.1172/jci59261.
Mancina, R.M. *et al.* (2016) "The MBOAT7-TMC4 variant RS641738 increases risk of nonalcoholic fatty liver disease in individuals of European descent," *Gastroenterology*, 150(5), pp.1219-1230. Available at: https://doi.org/10.1053/j.gastro.2016.01.032.

Mannaerts, I. *et al.* (2015) 'The Hippo pathway effector YAP controls mouse hepatic stellate cell activation', *Journal of Hepatology*, 63(3), pp. 679–688. Available at: https://doi.org/10.1016/J.JHEP.2015.04.011.
Marinho, T. de S. *et al.* (2019) 'Beneficial effects of intermittent fasting on steatosis and inflammation of the liver in mice fed a high-fat or a high-fructose diet', *Nutrition*, 65, pp. 103–112. Available at: https://doi.org/10.1016/j.nut.2019.02.020.
Markham, A. (2020) 'Bempedoic acid: first approval', *Drugs*, 80(7), pp. 747–753. Available at: https://doi.org/10.1007/s40265-020-01308-w.
Marriott, B.P., Cole, N. and Lee, E. (2009) 'National estimates of dietary fructose intake increased from 1977 to 2004 in the United States', *The Journal of Nutrition*, 139(6), pp. 1228S-1235S. Available at: https://doi.org/10.3945/jn.108.098277.
Masson, W. *et al.* (2020) 'Effect of bempedoic acid on new onset or worsening diabetes: a meta-analysis', *Diabetes Research and Clinical Practice*, 168, p. 108369. Available at: https://doi.org/10.1016/j.diabres.2020.108369.
Matsuzaka, T. and Shimano, H. (2013) 'Insulin-dependent and -independent regulation of sterol regulatory element-binding protein-1c', *Journal of Diabetes Investigation*, 4(5), p. 411. Available at: https://doi.org/10.1111/jdi.12098.
Mederacke, I. *et al.* (2013) 'Fate tracing reveals hepatic stellate cells as dominant contributors to liver fibrosis independent of its aetiology', *Nature Communications*, 4(1), pp. 1–11. Available at: https://doi.org/10.1038/ncomms3823.
Mederacke, I. *et al.* (2015) 'High-yield and high-purity isolation of hepatic stellate cells from normal and fibrotic mouse livers', *Nature Protocols*, 10(2), pp. 305–315. Available at: https://doi.org/10.1038/nprot.2015.017.
Migita, T. *et al.* (2008) 'ATP citrate lyase: activation and therapeutic implications in non-small cell lung cancer', *Cancer Research*, 68(20), pp. 8547–8554. Available at: https://doi.org/10.1158/0008-5472.can-08-1235.
Mohammadi-Shemirani, P. *et al.* (2022) 'ACLY and CKD: A mendelian randomization analysis', *Kidney International Reports*, 7(7), pp. 1673–1681. Available at: https://doi.org/10.1016/j.ekir.2022.04.013.
Mudaliar, S. *et al.* (2013) 'Efficacy and safety of the farnesoid x receptor agonist Obeticholic acid in patients with type 2 diabetes and nonalcoholic fatty liver disease', *Gastroenterology*, 145(3). Available at: https://doi.org/10.1053/j.gastro.2013.05.042.
Muir, K. *et al.* (2013) 'Proteomic and lipidomic signatures of lipid metabolism in NASH-associated hepatocellular carcinoma', *Cancer Research*, 73(15), pp. 4722–4731. Available at: https://doi.org/10.1158/0008-5472.can-12-3797.
Musso, G. *et al.* (2011) 'Meta-analysis: natural history of non-alcoholic fatty liver disease (NAFLD) and diagnostic accuracy of non-invasive tests for liver disease severity', *Annals of Medicine*, 43(8), pp. 617–649. Available at: https://doi.org/10.3109/07853890.2010.518623.
Musso, G. *et al.* (2014) 'Association of non-alcoholic fatty liver disease with chronic kidney disease: a systematic review and meta-analysis', *PLOS Medicine*, 11(7), p. e1001680. Available at: https://doi.org/10.1371/journal.pmed.1001680.

Nakagawa, S. *et al.* (2016) 'Molecular liver cancer prevention in cirrhosis by organ transcriptome analysis and lysophosphatidic acid pathway inhibition', *Cancer Cell*, 30(6), p. 879. Available at: https://doi.org/10.1016/j.ccell.2016.11.004.
Nakamura, I. *et al.* (2014) 'Brivanib attenuates hepatic fibrosis in vivo and stellate cell activation in vitro by inhibition of FGF, VEGF and PDGF signaling', *PLOS ONE*, 9(4), p. e92273. Available at: https://doi.org/10.1371/journal.pone.0092273.
Nati, M., Chung, K.J. and Chavakis, T. (2022) 'The role of innate immune cells in nonalcoholic fatty liver disease', *Journal of Innate Immunity*, 14(1), p. 31. Available at: https://doi.org/10.1159/000518407.
Neuschwander-Tetri, B.A. *et al.* (2015) 'Farnesoid X nuclear receptor ligand obeticholic acid for non-cirrhotic, non-alcoholic steatohepatitis (FLINT): A multicentre, randomised, placebo-controlled trial', *The Lancet*, 385(9972), pp. 956–965. Available at: https://doi.org/10.1016/s0140-6736(14)61933-4.
Nicholls, S.J. *et al.* (2021) 'Rationale and design of the CLEAR-outcomes trial: evaluating the effect of bempedoic acid on cardiovascular events in patients with statin intolerance', *American Heart Journal*, 235, pp. 104–112. Available at: https://doi.org/10.1016/j.ahj.2020.10.060.
Nosengo, N. (2016) 'Can you teach old drugs new tricks?', *Nature*, 534(7607), pp. 314–316. Available at: https://doi.org/10.1038/534314a.
Olson, E. *et al.* (2022) 'Effects of isocaloric fructose restriction on ceramide levels in children with obesity and cardiometabolic risk: relation to hepatic de novo lipogenesis and insulin sensitivity', *Nutrients*, 14(7), p.1432. Available at: https://doi.org/10.3390/nu14071432.
Omokaro, S.O. and Golden, J.K. (2020) 'The regulatory state of nonalcoholic steatohepatitis and metabolism', *Endocrinology, Diabetes & Metabolism*, 3(4), p. e00113. Available at: https://doi.org/10.1002/edm2.113.
Ouyang, X. *et al.* (2008) 'Fructose consumption as a risk factor for non-alcoholic fatty liver disease', *Journal of Hepatology*, 48(6), pp. 993–999. Available at: https://doi.org/10.1016/j.jhep.2008.02.011.
Pan, J.J. and Fallon, M.B. (2014) 'Gender and racial differences in nonalcoholic fatty liver disease', *World Journal of Hepatology*, 6(5), pp. 274–283. Available at: https://doi.org/10.4254/wjh.v6.I5.274.
Pantano, L. *et al.* (2021) 'Molecular characterization and cell type composition deconvolution of fibrosis in NAFLD', *Scientific Reports,* 11(1), pp. 1–14. Available at: https://doi.org/10.1038/s41598-021-96966-5.
Parks, E.J. and Hellerstein, M.K. (2006) 'Recent advances in liver triacylglycerol and fatty acid metabolism using stable isotope labeling techniques', *Journal of Lipid Research*, 47(8), pp. 1651–1660. Available at: https://doi.org/10.1194/jlr.r600018-jlr200.
Parks, E., Yki-Järvinen, H. and Hawkins, M. (2017) 'Out of the frying pan: dietary saturated fat influences nonalcoholic fatty liver disease', *The Journal of Clinical Investigation*, 127(2), pp. 454–456. Available at: https://doi.org/10.1172/jci92407.

Peng, L. *et al.* (2021) 'Clinical characteristics and risk factors of nonalcoholic fatty liver disease in children with obesity', *BMC Pediatrics*, 21(1), pp. 1–8. Available at: https://doi.org/10.1186/s12887-021-02595-2
Perry, R.J. *et al.* (2014) 'The role of hepatic lipids in hepatic insulin resistance and type 2 diabetes', *Nature*, 510(7503), pp. 84–91. Available at: https://doi.org/10.1038/nature13478.
Philips, C.A. *et al.* (2020) 'Repurposing pirfenidone for nonalcoholic steatohepatitis-related cirrhosis: a case series', *Journal of Clinical and Translational Hepatology*, 8(1), p. 100. Available at: https://doi.org/10.14218/jcth.2019.00056.
Pierantonelli, I. and Svegliati-Baroni, G. (2019) 'Nonalcoholic fatty liver disease: basic pathogenetic mechanisms in the progression from NAFLD to NASH', *Transplantation*, 103(1), pp. E1–E13. Available at: https://doi.org/10.1097/tp.0000000000002480.
Pinkosky, S.L. *et al.* (2013) 'AMP-activated protein kinase and ATP-citrate lyase are two distinct molecular targets for ETC-1002, a novel small molecule regulator of lipid and carbohydrate metabolism', *Journal of Lipid Research*, 54(1), p. 134. Available at: https://doi.org/10.1194/jlr.m030528.
Pinkosky, S.L. *et al.* (2016) 'Liver-specific ATP-citrate lyase inhibition by bempedoic acid decreases LDL-C and attenuates atherosclerosis', *Nature Communications*, 7(1), p. 13457. Available at: https://doi.org/10.1038/ncomms13457.
Pinkosky, S.L. *et al.* (2017) 'Targeting ATP-citrate lyase in hyperlipidemia and metabolic disorders', *Trends in Molecular Medicine*, 23(11), pp. 1047–1063. Available at: https://doi.org/10.1016/j.molmed.2017.09.001.
Ramakrishna, S., D'Angelo, G. and Benjamin, W.B. (1990) 'Sequence of sites on ATP-citrate lyase and phosphatase inhibitor 2 phosphorylated by multifunctional protein kinase (a glycogen synthase kinase 3 like kinase)', *Biochemistry*, 29(33), pp. 7617–7624. Available at: https://doi.org/10.1021/bi00485a011.
Reetz, J. *et al.* (2013) 'Development of adenoviral delivery systems to target hepatic stellate cells in vivo', *PloS One*, 8(6). Available at: https://doi.org/10.1371/journal.prone.0067091.
Reeves, H.L. *et al.* (1996) 'Hepatic stellate cell activation occurs in the absence of hepatitis in alcoholic liver disease and correlates with the severity of steatosis', *Journal of Hepatology*, 25(5), pp. 677–683. Available at: https://doi.org/10.1016/s0168-8278(96)80238-8.
Reif, S. *et al.* (2003) 'The role of focal adhesion kinase-phosphatidylinositol 3-kinase-akt signaling in hepatic stellate cell proliferation and type I collagen expression', *The Journal of Biological Chemistry*, 278(10), pp. 8083–8090. Available at: https://doi.org/10.1074/jbc.m212927200.
Rezvani, M. *et al.* (2016) 'In vivo hepatic reprogramming of myofibroblasts with AAV vectors as a therapeutic strategy for liver fibrosis', *Cell Stem Cell*, 18(6), pp. 809–816. Available at: https://doi.org/10.1016/j.stem.2016.05.005.
Rinella, M.E. *et al.* (2008) 'Mechanisms of hepatic steatosis in mice fed a lipogenic methionine choline-deficient diet', *Journal of Lipid Research*, 49(5), p. 1068. Available at: https://doi.org/10.1194/jlr.m800042-jlr200.

Rinella, M.E. (2015) 'Nonalcoholic fatty liver disease a systematic review', *Journal of the American Medical Association*, 313(22), pp. 2263–2273. Available at: https://doi.org/10.1001/jama.2015.5370.
Romero, F.A. *et al.* (2020) 'The Race to bash NASH: emerging targets and drug development in a complex liver disease', *Journal of Medicinal Chemistry*, 63(10), pp. 5031-5073. Available at: https://doi.org/10.1021/acs.jmedchem.9b01701.
Romeo, S. *et al.* (2008) "Genetic variation in PNPLA3 confers susceptibility to nonalcoholic fatty liver disease," *Nature Genetics*, 40(12), pp. 1461–1465. Available at: https://doi.org/10.1038/ng.257.
Rosqvist, F. *et al.* (2019) 'Overeating saturated fat promotes fatty liver and ceramides compared with polyunsaturated fat: a randomized trial', *The Journal of Clinical Endocrinology and Metabolism*, 104(12), pp. 6207–6219. Available at: https://doi.org/10.1210/jc.2019-00160.
Rui, L. (2014) 'Energy metabolism in the liver', *Comprehensive Physiology*, 4(1), p. 177. Available at: https://doi.org/10.1002/cphy.c130024.
Ryaboshapkina, M. and Hammar, M. (2017) 'Human hepatic gene expression signature of non-alcoholic fatty liver disease progression, a meta-analysis', *Scientific Reports*, 7(1), p. 12361. Available at: https://doi.org/10.1038/s41598-017-10930-w.
Safari, Z. and Gérard, P. (2019) 'The links between the gut microbiome and non-alcoholic fatty liver disease (NAFLD)', *Cellular and Molecular Life Sciences*, 76(8), pp. 1541–1558. Available at: https://doi.org/10.1007/s00018-019-03011-w.
Saito, T. *et al.* (2017) 'Pathophysiological analysis of the progression of hepatic lesions in STAM mice', *Physiological Research*, 66(5), pp. 791–799. Available at: https://doi.org/10.33549/physiolres.933592.
Samsoondar, J.P. *et al.* (2017) 'Prevention of diet-induced metabolic dysregulation, inflammation, and atherosclerosis in Ldlr-/- mice by treatment with the ATP-citrate lyase inhibitor bempedoic acid', *Arteriosclerosis, Thrombosis, and Vascular Biology*, 37(4), pp. 647–656. Available at: https://doi.org/10.1161/atvbaha.116.308963.
Samuel, V.T. and Shulman, G.I. (2018) 'Nonalcoholic fatty liver disease as a nexus of metabolic and hepatic diseases', *Cell Metabolism*, 27(1), pp. 22–41. Available at: https://doi.org/10.1016/j.cmet.2017.08.002.
Sanders, F.W.B. *et al.* (2018) 'Hepatic steatosis risk is partly driven by increased de novo lipogenesis following carbohydrate consumption', *Genome Biology*, 19(1), p. 79. Available at: https://doi.org/10.1186/s13059-018-1439-8.
Santhekadur, P.K., Kumar, D.P. and Sanyal, A.J. (2018) 'Preclinical models of nonalcoholic fatty liver disease', *Journal of Hepatology*, 68(2), p. 230. Available at: https://doi.org/10.1016/j.jhep.2017.10.031.
Satapathy, S.K. *et al.* (2015) 'Drug-induced fatty liver disease: An overview of pathogenesis and management', *Annals of Hepatology*, 14(6), pp. 789–806. Available at: https://doi.org/10.5604/16652681.1171749.
Satapati, S. *et al.* (2012) 'Elevated TCA cycle function in the pathology of diet-induced hepatic insulin resistance and fatty liver', *Journal of Lipid Research*, 53(6), pp. 1080–1092. Available at: https://doi.org/10.1194/jlr.m023382.

Scannell, J.W. *et al.* (2012) 'Diagnosing the decline in pharmaceutical R&D efficiency', *Nature Reviews. Drug discovery*, 11(3), pp. 191–200. Available at: https://doi.org/10.1038/nrd3681.
Schoemaker, M.H. *et al.* (2008) 'PDGF-receptor beta-targeted adenovirus redirects gene transfer from hepatocytes to activated stellate cells', *Molecular Pharmaceutics*, 5(3), pp. 399–406. Available at: https://doi.org/10.1021/mp700118p.
Schreurs, M. *et al.* (2009) 'Soraphen, an inhibitor of the acetyl-CoA carboxylase system, improves peripheral insulin sensitivity in mice fed a high-fat diet', *Diabetes, Obesity & Metabolism*, 11(10), pp. 987–991. Available at: https://doi.org/10.1111/j.1463-1326.2009.01078.x.
Schultz, A. *et al.* (2013) 'Hepatic adverse effects of fructose consumption independent of overweight/obesity', *International Journal of Molecular Sciences*, 14(11), pp. 21873–21886. Available at: https://doi.org/10.3390/ijms141121873.
Schwabe, R.F. and Maher, J.J. (2012) 'Lipids in liver disease: looking beyond steatosis', *Gastroenterology*, 142(1), pp. 8–11. Available at: https://doi.org/10.1053/j.gastro.2011.11.004.
Schwarz, J.M. *et al.* (2015) 'Effect of a high-fructose weight-maintaining diet on lipogenesis and liver fat', *The Journal of Clinical Endocrinology and Metabolism*, 100(6), pp. 2434–2442. Available at: https://doi.org/10.1210/jc.2014-3678.
Severson, T.J., Besur, S. and Bonkovsky, H.L. (2016) 'Genetic factors that affect nonalcoholic fatty liver disease: A systematic clinical review', *World Journal of Gastroenterology*, 22(29), p. 6742. Available at: https://doi.org/10.3748/wjg.v22.i29.6742.
Seyhan, A.A. (2019) 'Lost in translation: the valley of death across preclinical and clinical divide – identification of problems and overcoming obstacles', *Translational Medicine Communications*, 4(1), pp. 1–19. Available at: https://doi.org/10.1186/s41231-019-0050-7.
Shepherd, E.L. *et al.* (2021) 'Ketohexokinase inhibition improves NASH by reducing fructose-induced steatosis and fibrogenesis', *JHEP Reports*, 3(2), p. 100217. Available at: https://doi.org/10.1016/j.jhepr.2020.100217.
Shi, L. and Tu, Benjamin P (2015) 'Acetyl-CoA and the regulation of metabolism: mechanisms and consequences', *Current Opinion in Cell Biology*, 33, pp. 125–31. Available at: https://doi.org/10.1016/j.ceb.2015.02.003.
Siddiqui, M.S. *et al.* (2020) 'Impact of obeticholic acid on the lipoprotein profile in patients with non-alcoholic steatohepatitis', *Journal of Hepatology*, 72(1), pp. 25–33. Available at: https://doi.org/10.1016/j.jhep.2019.10.006.
Singh, S. *et al.* (2015) 'Fibrosis progression in nonalcoholic fatty liver versus nonalcoholic steatohepatitis: a systematic review and meta-analysis of paired-biopsy studies', *Clinical Gastroenterology and Hepatology*, 13(4), p. 643. Available at: https://doi.org/10.1016/j.cgh.2014.04.014.
Sjöström, L. *et al.* (1998) 'Randomised placebo-controlled trial of orlistat for weight loss and prevention of weight regain in obese patients', *Lancet*, 352(9123), pp. 167–172. Available at: https://doi.org/10.1016/s0140-6736(97)11509-4.

Smith, B.K., *et al.* (2016) 'Salsalate (salicylate) uncouples mitochondria, improves glucose homeostasis, and reduces liver lipids independent of AMPK-β1', *Diabetes,* 65(11), pp. 3352-3361. Available at: https://doi.org/10.2337/db16-0564.
Smith-Cortinez, N. *et al.* (2020) 'Simultaneous induction of glycolysis and oxidative phosphorylation during activation of hepatic stellate cells reveals novel mitochondrial targets to treat liver fibrosis', *Cells*, 9(11). Available at: https://doi.org/10.3390/cells9112456.
Smith, G.I. *et al.* (2020) 'Insulin resistance drives hepatic de novo lipogenesis in nonalcoholic fatty liver disease', *The Journal of Clinical Investigation*, 130(3), pp. 1453–1460. Available at: https://doi.org/10.1172/jci134165.
Softic, S., Cohen, D.E. and Kahn, C.R. (2016) 'Role of dietary fructose and hepatic de novo lipogenesis in fatty liver disease', *Digestive Diseases and Sciences*, 61(5), pp. 1282–1293. Available at: https://doi.org/10.1007/s10620-016-4054-0.
Son, G. *et al.* (2009) 'Inhibition of phosphatidylinositol 3-kinase signaling in hepatic stellate cells blocks the progression of hepatic fibrosis', *Hepatology,* 50(5), p. 1512. Available at: https://doi.org/10.1002/hep.23186.
Staaf, J. *et al.* (2010) 'High-resolution genomic and expression analyses of copy number alterations in HER2-amplified breast cancer', *Breast Cancer Research*, 12, p. 25. Available at: https://doi.org/10.1186/bcr2568.
Stefan, N., Häring, H.-U. and Cusi, K. (2019) 'Non-alcoholic fatty liver disease: causes, diagnosis, cardiometabolic consequences, and treatment strategies', *The Lancet Diabetes & Endocrinology*, 7(4), pp. 313-324. Available at: https://doi.org/10.1016/s2213-8587(18)30154-2.
Stiede, K. *et al.* (2017) 'Acetyl-coenzyme A carboxylase inhibition reduces de novo lipogenesis in overweight male subjects: a randomized, double-blind, crossover study', *Hepatology*, 66(2), pp. 324–334. Available at: https://doi.org/10.1002/hep.29246.
Subramanian, A. *et al.* (2005) 'Gene set enrichment analysis: a knowledge-based approach for interpreting genome-wide expression profiles', *Proceedings of the National Academy of Sciences*, 102(43), pp. 15545–15550. Available at: https://doi.org/10.1073/pnas.0506580102.
Sudlow, C. *et al.* (2015) 'UK biobank: an open access resource for identifying the causes of a wide range of complex diseases of middle and old age', *PLoS Medicine*, 12(3), p. e1001779. Available at: https://doi.org/10.1371/journal.pmed.1001779.
Sunny, N.E. *et al.* (2011) 'Excessive hepatic mitochondrial TCA cycle and gluconeogenesis in humans with nonalcoholic fatty liver disease', *Cell Metabolism*, 14(6), pp. 804–810. Available at: https://doi.org/10.1016/j.cmet.2011.11.004.
Takahashi, Y. and Fukusato, T. (2014) 'Histopathology of nonalcoholic fatty liver disease/nonalcoholic steatohepatitis', *World Journal of Gastroenterology*, 20(42), p. 15539. Available at: https://doi.org/10.3748/wjg.v20.I42.15539.
Tan, M. *et al.* (2020) 'Inhibition of the mitochondrial citrate carrier, Slc25a1, reverts steatosis, glucose intolerance, and inflammation in preclinical models of NAFLD/NASH', *Cell Death & Differentiation*, 27(7), pp. 2143–2157. Available at: https://doi.org/10.1038/s41418-020-0491-6.

Tan, R. *et al.* (2021) 'Intestinal microbiota mediates high-fructose and high-fat diets to induce chronic intestinal inflammation', *Frontiers in Cellular and Infection Microbiology*, 11, p. 654074. Available at: https://doi.org/10.3389/fcimb.2021.654074.
Tandra, S. *et al.* (2011) 'Presence and significance of microvesicular steatosis in nonalcoholic fatty liver disease', *Journal of Hepatology*, 55(3), pp. 654–659. Available at: https://doi.org/10.1016/j.jhep.2010.11.021.
Taylor, R.S. *et al.* (2020) 'Association between fibrosis stage and outcomes of patients with nonalcoholic fatty liver disease: a systematic review and meta-analysis', *Gastroenterology*, 158(6), pp. 1611-1625.e12. Available at: https://doi.org/10.1053/j.gastro.2020.01.043.
Teratani, T. *et al.* (2012) 'A high-cholesterol diet exacerbates liver fibrosis in mice via accumulation of free cholesterol in hepatic stellate cells', *Gastroenterology*, 142(1), pp. 152-164.e10. Available at: https://doi.org/10.1053/j.gastro.2011.09.049.
Teufel, A. *et al.* (2016) 'Comparison of gene expression patterns between mouse models of nonalcoholic fatty liver disease and liver tissues from patients', *Gastroenterology*, 151(3), pp. 513-525.e0. Available at: https://doi.org/10.1053/j.gastro.2016.05.051.
Thompson, P.D. *et al.* (2015) 'Use of ETC-1002 to treat hypercholesterolemia in patients with statin intolerance', *Journal of Clinical Lipidology*, 9(3), pp. 295–304. Available at: https://doi.org/10.1016/j.jacl.2015.03.003.
Thompson, P.D. *et al.* (2016) 'Treatment with ETC-1002 alone and in combination with ezetimibe lowers LDL cholesterol in hypercholesterolemic patients with or without statin intolerance', *Journal of Clinical Lipidology*, 10(3), pp. 556–567. Available at: https://doi.org/10.1016/j.jacl.2015.12.025.
Tomita, K. *et al.* (2006) 'Tumour necrosis factor alpha signalling through activation of Kupffer cells plays an essential role in liver fibrosis of non-alcoholic steatohepatitis in mice', *Gut*, 55(3), pp. 415–424. Available at: https://doi.org/10.1136/gut.2005.071118.
Tomita, K. *et al.* (2014) 'Free cholesterol accumulation in hepatic stellate cells: Mechanism of liver fibrosis aggravation in nonalcoholic steatohepatitis in mice', *Hepatology*, 59(1), pp. 154–169. Available at: https://doi.org/10.1002/hep.26604.
Trebicka, J. *et al.* (2010) 'Atorvastatin attenuates hepatic fibrosis in rats after bile duct ligation via decreased turnover of hepatic stellate cells', *Journal of Hepatology*, 53(4), pp. 702–712. Available at: https://doi.org/10.1016/j.jhep.2010.04.025.
Trivedi, P., Wang, S. and Friedman, S.L. (2021) 'The power of plasticity—metabolic regulation of hepatic stellate cells', *Cell Metabolism*, 33(2), pp. 242–257. Available at: https://doi.org/10.1016/j.cmet.2020.10.026.
Tsuchida, T. and Friedman, Scott L. (2017) 'Mechanisms of hepatic stellate cell activation', *Nature Reviews Gastroenterology and Hepatology*, 14(7), pp. 397–411. Available at: https://doi.org/10.1038/nrgastro.2017.38.
Tu, W., Ye, J. and Wang, Z.J. (2016) 'Embryonic liver fordin is involved in glucose glycolysis of hepatic stellate cell by regulating PI3K/Akt signaling', *World Journal of Gastroenterology*, 22(38), p. 8519. Available at: https://doi.org/10.3748/wjg.v22.i38.8519.

Turyn, J. *et al.* (2003) 'Increased activity of glycerol 3-phosphate dehydrogenase and other lipogenic enzymes in human bladder cancer', *Hormone and Metabolic Research,* 35(10), pp. 565–569. Available at: https://doi.org/10.1055/s-2003-43500.
Uhlén, M. *et al.* (2015) 'Tissue-based map of the human proteome', *Science*, 347(6220). Available at: https://doi.org/10.1126/science.1260419.
De Vadder, F. *et al.* (2014) 'Microbiota-generated metabolites promote metabolic benefits via gut-brain neural circuits', *Cell*, 156(1–2), pp. 84–96. Available at: https://doi.org/10.1016/j.cell.2013.12.016.
Vedala, A. *et al.* (2006) 'Delayed secretory pathway contributions to VLDL-triglycerides from plasma NEFA, diet, and de novo lipogenesis in humans', *Journal of Lipid Research*, 47(11), pp. 2562–2574. Available at: https://doi.org/10.1194/jlr.m600200-jlr200.
Verschueren, K.H.G. *et al.* (2019) 'Structure of ATP citrate lyase and the origin of citrate synthase in the Krebs cycle', *Nature*, 568(7753), pp. 571–575. Available at: https://doi.org/10.1038/s41586-019-1095-5.
Vinué, Á., Herrero-Cervera, A. and González-Navarro, H. (2018) 'Understanding the impact of dietary cholesterol on chronic metabolic diseases through studies in rodent models', *Nutrients*, 10(7), p.939. Available at: https://doi.org/10.3390/nu10070939.
Vos, M.B. (2014) 'Nutrition, nonalcoholic fatty liver disease and the microbiome: recent progress in the field', *Current Opinion in Lipidology*, 25(1), pp. 61–66. Available at: https://doi.org/10.1097/mol.0000000000000043.
Võsa, U. *et al.* (2018) 'Unraveling the polygenic architecture of complex traits using blood eQTL metaanalysis', *BioRxiv*, p. 447367. Available at: https://doi.org/10.1101/447367.
Wang, M. *et al.* (2022) 'Roles of hepatic stellate cells in NAFLD: from the perspective of inflammation and fibrosis', *Frontiers in Pharmacology*, 13, p. 958428. Available at: https://doi.org/10.3389/fphar.2022.958428.
Wang, Q. *et al.* (2009) 'Abrogation of hepatic ATP-citrate lyase protects against fatty liver and ameliorates hyperglycemia in leptin receptor-deficient mice', *Hepatology*, 49(4), pp. 1166–1175. Available at: https://doi.org/10.1002/hep.22774.
Wang, W. *et al.* (2013) 'Simvastatin ameliorates liver fibrosis via mediating nitric oxide synthase in rats with non-alcoholic steatohepatitis-related liver fibrosis', *PLoS ONE*, 8(10), p. e76538. Available at: https://doi.org/10.1371/journal.pone.0076538.
Wang, X. *et al.* (2020) 'Efficacy and safety of bempedoic acid for prevention of cardiovascular events and diabetes: a systematic review and meta-analysis', *Cardiovascular Diabetology*, 19(1), p. 128. Available at: https://doi.org/10.1186/s12933-020-01101-9.
Wang, X.K. and Peng, Z.G. (2021) 'Targeting liver sinusoidal endothelial cells: an attractive therapeutic strategy to control inflammation in nonalcoholic fatty liver disease', *Frontiers in Pharmacology*, 12, p. 655557. Available at: https://doi.org/10.3389/fphar.2021.655557.
Wang, Z. *et al.* (2020) 'Chronic cold exposure enhances glucose oxidation in brown adipose tissue', *EMBO Reports*, 21(11), p. e50085. Available at: https://doi.org/10.15252/embr.202050085.

Wei, J. *et al.* (2019) 'An allosteric mechanism for potent inhibition of human ATP-citrate lyase', *Nature*, 568(7753), pp. 566–570. Available at: https://doi.org/10.1038/s41586-019-1094-6.
Wellen, K.E. *et al.* (2009) 'ATP-citrate lyase links cellular metabolism to histone acetylation', *Science*, 324(5930), pp. 1076–1080. Available at: https://doi.org/10.1126/science.1164097.
Williams, C.G. *et al.* (2022) 'An introduction to spatial transcriptomics for biomedical research', *Genome Medicine*, 14(1), pp. 1–18. Available at: https://doi.org/10.1186/S13073-022-01075-1.
Wilson, C.L. *et al.* (2014) 'Quiescent hepatic stellate cells functionally contribute to the hepatic innate immune response via TLR3', *PLoS ONE*, 9(1). Available at: https://doi.org/10.1371/journal.pone.0083391.
Wobser, H. *et al.* (2009) 'Lipid accumulation in hepatocytes induces fibrogenic activation of hepatic stellate cells', *Cell Research*, 19(8), pp. 996–1005. Available at: https://doi.org/10.1038/cr.2009.73.
Wong, R.J. *et al.* (2015) 'Nonalcoholic steatohepatitis is the second leading etiology of liver disease among adults awaiting liver transplantation in the United States', *Gastroenterology*, 148(3), pp. 547–555. Available at: https://doi.org/10.1053/j.gastro.2014.11.039.
Wong, V.W.S. *et al.* (2018) 'Noninvasive biomarkers in NAFLD and NASH — current progress and future promise', *Nature Reviews Gastroenterology & Hepatology*, 15(8), pp. 461–478. Available at: https://doi.org/10.1038/s41575-018-0014-9.
Xi, Y. *et al.* (2021) 'The anti-fibrotic drug pirfenidone inhibits liver fibrosis by targeting the small oxidoreductase glutaredoxin-1', *Science Advances*, 7(36). Available at: https://doi.org/10.1126/sciadv.abg9241.
Yancy, H.F. *et al.* (2007) 'Metastatic progression and gene expression between breast cancer cell lines from African American and Caucasian women', *Journal of Carcinogenesis*, 6, p.8. Available at: https://doi.org/10.1186/1477-3163-6-8.
Yang, J.I. *et al.* (2010) 'Synergistic antifibrotic efficacy of statin and protein kinase C inhibitor in hepatic fibrosis', *American Journal of Physiology Gastrointestinal and Liver Physiology*, 298(1), p. g126-32. Available at: https://doi.org/10.1152/ajpgi.00299.2009.
Yang, Z. *et al.* (2015) 'T-cell metabolism in autoimmune disease', *Arthritis Research and Therapy*, 17(1), pp. 1–10. Available at: https://doi.org/10.1186/s13075-015-0542-4.
Yenilmez, B. *et al.* (2022) 'Paradoxical activation of transcription factor SREBP1c and de novo lipogenesis by hepatocyte-selective ATP-citrate lyase depletion in obese mice', *Journal of Biological Chemistry*, 298, p. 102401. Available at: https://doi.org/10.1016/j.jbc.2022.102401.
Ying, L. *et al.* (2017) '(-)-Epigallocatechin-3-gallate and atorvastatin treatment down-regulates liver fibrosis-related genes in non-alcoholic fatty liver disease', *Clinical and Experimental Pharmacology & Physiology*, 44(12), pp. 1180–1191. Available at: https://doi.org/10.1111/1440-1681.12844.
Younossi, Z.M. *et al.* (2016) 'Global epidemiology of nonalcoholic fatty liver disease—Meta-analytic assessment of prevalence, incidence, and outcomes', *Hepatology*, 64(1), pp. 73–84. Available at: https://doi.org/10.1002/hep.28431.

Younossi, Z.M., Ratziu, V., *et al.* (2019) 'Obeticholic acid for the treatment of non-alcoholic steatohepatitis: interim analysis from a multicentre, randomised, placebo-controlled phase 3 trial', *The Lancet*, 394(10215), pp. 2184–2196. Available at: https://doi.org/10.1016/s0140-6736(19)33041-7.
Younossi, Z.M., Golabi, P., *et al.* (2019) 'The global epidemiology of NAFLD and NASH in patients with type 2 diabetes: A systematic review and meta-analysis', *Journal of Hepatology*, 71(4), pp. 793–801. Available at: https://doi.org/10.1016/j.jhep.2019.06.021.
Yu, H. *et al.* (2021) 'Lipid accumulation-induced hepatocyte senescence regulates the activation of hepatic stellate cells through the Nrf2-antioxidant response element pathway', *Experimental Cell Research*, 405(2). Available at: https://doi.org/10.1016/j.yexcr.2021.112689.
Zaidi, N. *et al.* (2012) 'ATP citrate lyase knockdown induces growth arrest and apoptosis through different cell- and environment-dependent mechanisms', *Molecular Cancer Therapeutics*, 11(9), pp. 1925–1935. Available at: https://doi.org/10.1158/1535-7163.mct-12-0095.
Zhang, H. *et al.* (2022) "HSD17B13: A potential therapeutic target for NAFLD," *Frontiers in Molecular Biosciences*, 8. Available at: https://doi.org/10.3389/fmolb.2021.824776.
Zhao, S. *et al.* (2016) 'ATP-citrate lyase controls a glucose-to-acetate metabolic switch', *Cell Reports*, 17(4), pp. 1037–1052. Available at: https://doi.org/10.1016/j.celrep.2016.09.069.
Zhao, S. *et al.* (2020) 'Dietary fructose feeds hepatic lipogenesis via microbiota-derived acetate', *Nature*, 579(7800), pp. 586–591. Available at: https://doi.org/10.1038/s41586-020-2101-7.
Zhou, M.Y. *et al.* (2021) 'Transforming growth factor beta-1 upregulates glucose transporter 1 and glycolysis through canonical and noncanonical pathways in hepatic stellate cells', *World Journal of Gastroenterology*, 27(40), p. 6908. Available at: https://doi.org/10.3748/wjg.v27.I40.6908.
Zhu, J. and Thompson, C.B. (2019) 'Metabolic regulation of cell growth and proliferation', *Nature Reviews Molecular Cell Biology*, 20(7), p. 436. Available at: https://doi.org/10.1038/s41580-019-0123-5.

Appendix A. A review of current NASH mouse models

	Diet	Time (wks)	Obes.	Dys. Lip.	Gluc. Intol.	Steat.	NASH	Fibrosis	HCC	E.g., of drugs tested in model	Comments on mod el	Ref.
Diet Models												
HFD	40-60% fat	Varies	✓	✓	✓	✓	×	Very mild	×	Sulforaphane, orlistat, emricasan (IDN-6556), GSK'872, necrostatin-1 (Nec-1)	NASH features around 16 weeks, but not severe; moderate fibrosis after prolonged feeding (80 weeks)	(1–6)
HFD + TN	60% fat	24	✓	✓	✓	✓	✓	×	?	N/A	Sex-independent NASH, no fibrosis in C57BL/6 mice, mild-moderate fibrosis in AKR mice	(4)
HF-HC	60% fat, 1.25% cholest.	6-42	✓	✓	✓	✓	✓	Very mild	×	Ezetimibe, sildenafil, leucine, metformin	Few mice show mild fibrosis	(7,8)
HF-FRUC	40-60% fat	14-18	✓	✓	✓	✓	✓	Mild - moderate	×	Liraglutide, BAR502	Increased NASH and fibrosis relative to HFD feeding alone	(9,10)
AMLN (HF-HC-FRUC)	40% fat (trans fat), 22% fructose, 2% cholest.	20-30	✓	✓	✓	✓	✓	Mild	×	AC3174, elafibranor, obeticholic acid, liraglutide, ipragliflozin, APD668, DPP4i	Commonly accepted for preclinical NASH therapeutic testing	(11–14)
GAN (new AMLN diet)	40% fat, 22% fructose, 2% cholest.	38-44	✓	✓	✓	✓	✓	Moderate	×	Semaglutide, lanifranor,	The ban of trans fat led to the modification of the AMLN diet to the GAN diet (trans fat in the AMLN diet has been substituted for palm oil)	(15,16)

Appendix A. A review of current NASH mouse models

	Diet	Time (wks)	Obes.	Dys. Lip.	Gluc. Intol.	Steat.	NASH	Fibrosis	HCC	E.g., of drugs tested in model	Comments on mod el	Ref.
*Wks: weeks; Obes.: Obesity; Dys. Lip.: dyslipidemia; Gluc. Intol.: glucose intolerance; HCC: hepatocellular carcinoma; Ref.: References												
HF-sucrose +FRUC water	42% fat, 0.2% cholest., 42.7% sucrose, 23.1 g/L fructose in drinking water	16-54	✓	✓	✓	✓	✓	Mild – severe	✓	N/A	Bridging fibrosis after 54 weeks; HCC developed in 75% of mice after 54 weeks	(17)
MCD	21% fat, 63% carb. (40% sucrose), 16% protein	5-8	×	×	×	✓	✓	Moderate	×	Wy-14,643, pentoxifylline,G49, rosiglitazone, bezafibrate, GW501516, sitagliptin, MCC950, WAY-362450, statins	Weight loss	(18–26)
CD	10% fat, choline-deficient	8-12	×	×	×	✓	✓	✓	×	N/A	NASH and moderate fibrosis after 12 weeks	(27,28)
CD-HFD	45% fat, choline-deficient	8-24	✓	×	✓	✓	✓	Mild - moderate	?	Long-acting FGF21, exericse	No change in fasting glucose; mice are hyperinsulinemic; NASH after 16 weeks; mild-moderate fibrosis after 16-24 weeks	(27,29–31)
CDAA	30% fat	Varies	×	✓	×	✓	✓	Mild - moderate	✓	rFGF-1, Ipragliflozin	Weight loss or lack of weight gain; when CDAA diet is combined with the AMLN diet, NASH and fibrosis develops more rapidly (6-9 weeks)	(32,33)

Appendix A. A review of current NASH mouse models

	Diet	Time (wks)	Obes.	Dys. Lip.	Gluc. Intol.	Steat.	NASH	Fibrosis	HCC	E.g., of drugs tested in model	Comments on mod el	Ref.
*Wks: weeks; Obes.: Obesity; Dys. Lip.: dyslipidemia; Gluc. Intol.: glucose intolerance; HCC: hepatocellular carcinoma; Ref.: References												
HFCC	30-65% fat, 1.25-2.5% cholest., 0.5% cholic acid	12	×	✓	×	✓	✓	Mild-moderate	?	Pioglitazone, liraglutide	Hepatic and serum triglycerides are unchanged; decreased serum VLDL-TG and ApoB; elevated hepatic and serum total cholest. and LDL-C; mild NASH after 12 weeks; fibrosis after 12 weeks but requires high cholest. (2%) to develop moderate fibrosis	(34,35)
Toxin +/- Diet Models												
CCL_4	*Chow* 10% fat, 70% carb., 20% protein	0.5-8	×	×	×	×	✓	Severe	✓	Sorafenib, BAR502, cilostazol, brivanib, obeticholic acid, PXS-5153A	Weight loss, dose-dependent fibrosis; HCC after >12 weeks	(9,36–41)
	HFHC combinations 20-60% fat, 1-2% cholest., +/- fructose *(e.g., FAT-NASH model)*	3-24	×	✓	×	✓	✓	Mild-moderate	✓	Elafibranor	Weight loss; elevated serum NEFAs and TGs at 1-4 weeks, but normalized at 8 weeks; mild fibrosis at 4 weeks, moderate fibrosis at 8 weeks; severe fibrosis at 12 weeks; HCC after 24 weeks	(5,37, 41)
TAA	*Chow* 10% fat, 70% carb., 20% protein	4-8	×	?	✓	×	✓	Severe	✓	Sorafenib, brivanib	Weight loss; dose-dependent fibrosis; HCC after >40 weeks	(42)
*Wks: weeks; Obes.: Obesity; Dys. Lip.: dyslipidemia; Gluc. Intol.: glucose intolerance; HCC: hepatocellular carcinoma; Ref.: References												

Appendix A. A review of current NASH mouse models

	Diet	Time (wks)	Obes.	Dys. Lip.	Gluc. Intol.	Steat.	NASH	Fibrosis	HCC	E.g., of drugs tested in model	Comments on mod el	Ref.
STAM™	*HFD* 45% fat	2-16	×	✓	✓	✓	✓	Severe	✓	Empagliflozin, linagliptin, telmisartan, cenicriviroc, ezetimibe, rosuvastatin, fenofibrate, PXS-5153A, bempedoic acid	Nenatal STZ model; early-onset diabetes; Weight loss, dose-dependent fibrosis; HCC after >16 weeks on diet	(38,42–45)
DEN	*HFD* 20-71% fat	14-25	✓	✓	✓	✓	✓	×	✓	N/A	HCC after 25 weeks; DEN models are used more for HCC therapeutic testing	(29,46–48)
	CD-HF ~60% fat, choline-deficient	12-24	✓	✓	✓	✓	✓	Mild-moderate	✓	N/A	NASH after 16 weeks; mild-moderate fibrosis after 24 weeks; HCC after 20-24 weeks; DEN models are used more for HCC therapeutic testing	(29,47)
HFCC-CDX	*HFCC* 1.25% cholest., 0.5% cholic acid with 2% cyclodextrin in drinking water	3	×	✓	✓	✓	✓	Moderate-severe	?	Elafibranor, liraglutide	Weight neutral or weight loss	(49,50)
Genetic +/- Diet Models												
ob/ob	*Chow* 10% fat, 70% carb., 20% protein	Varies	✓	✓	✓	✓	✓	×	×	MK-0626, rFGF1	Requires additional stimuli to induce moderate NASH	(32,51,52)

*Wks: weeks; Obes.: Obesity; Dys. Lip.: dyslipidemia; Gluc. Intol.: glucose intolerance; HCC: hepatocellular carcinoma; Ref.: References

Appendix A. A review of current NASH mouse models

	Diet	Time (wks)	Obes.	Dys. Lip.	Gluc. Intol.	Steat.	NASH	Fibrosis	HCC	E.g., of drugs tested in model	Comments on mod el	Ref.
ob/ob	*MCD* 21% fat, 63% carb., 16% protein	10	✓	✓	✓	✓	✓	Mild	×	LY2405319; yo jyo hen shi ko (YHK)	Weight loss; fibrosis after >8weeks	(53,54)
	FRUC 9% fat, 22% protein, 69% carb. (60% fructose)	8	✓	✓	×	✓	×	×	×	Teneligliptin, sitagliptin		(55,56)
	AMLN/GAN 40% fat (trans fat/palm oil), 22% fructose, 2% cholest.	6-12	✓	✓	✓	✓	✓	Moderate	×	AC3174, elafibranor, obeticholic acid, INT-767, liraglutide, SR9238	Fibrosis after <12 weeks; more severe NASH phenotype compared to wildtype AMLN mice; since the ban of trans fat, trans fat was replaced mainly with palm oil	(12–14,52, 57,58)
db/db	*Chow* 10% fat, 70% carb., 20% protein	Varies	✓	✓	✓	✓	×	×	×	Liraglutide, MSDC-0602K	Steatosis milder than *ob/ob* mice, more microvesicular	(51,59)
	MCD 21% fat, 63% carb., 16% protein	4-8	✓	✓	×	✓	✓	Mild	×	Exendin-4, elafibranor (GFT505)	Fibrosis induction after 7-14 weeks	(60–62)
	Chow+DEN 10% fat, 70% carb., 20% protein + DEN	14-36	✓	✓	✓	?	✓	Mild	✓	Pitavastatin, metformin	Fibrosis after 16-20 weeks	(63)
	Chow +iron. 10% fat, 70% carb., 20% protein supplemented with 2% carbonyl iron	8	×	?	✓	✓	Mild	?	?	N/A	Weight loss or absence of weight gain	(64)

*Wks: weeks; Obes.: Obesity; Dys. Lip.: dyslipidemia; Gluc. Intol.: glucose intolerance; HCC: hepatocellular carcinoma; Ref.: References

Appendix A. A review of current NASH mouse models

	Diet	Time (wks)	Obes.	Dys. Lip.	Gluc. Intol.	Steat.	NASH	Fibrosis	HCC	E.g., of drugs tested in model	Comments on mod el	Ref.
foz/foz	*HFHC* 23% fat, 45% carb., 0.2% cholest.	16-24	✓	✓	✓	✓	✓	Moderate	✓	Ezetimibe, atorvastatin, obeticholic acid	Requires HFD to progress steatosis to NASH; fibrosis after >16 weeks	(65–67)
ApoE*3-Leiden	*HFHC* Varies (1-2% cholest.)		✓	✓	✓	✓	✓	Moderate	?	Atorvastatin, CAT-2003	Fibrosis after >16 weeks of age; mice develop atherosclerosis; requires HF-HC diets to induce NASH and fibrosis	(68,69)
ApoE*3-Leiden. CETP	*HFHC* 30% fat, 1% cholest.	12-15	✓	✓	✓	✓	✓	Moderate	?	MK-0354, torcetrapib, exendin-4, Salsalate	Fibrosis after >12 weeks of age; increased atherosclerosis development compared to ApoE*3-Leiden (addition of CETP transgene creates a cholest. profile more similar to humans; requires HF-HC diets to induce NASH and fibrosis	(70–76)
LDLr$^{-/-}$	*HFHC* Varies (20-60% fat, 0.2-2% cholest.)	3-20	✓	✓	✓	✓	✓	Moderate	?	Rosiglitazone	Fibrosis after >12 weeks of age; requires HF-HC diets to induce NASH and fibrosis	(77–79)
LDLr$^{-/-}$ Leiden	*HFD* 40-45% fat	10-30	✓	✓	✓	✓	✓	Moderate-severe	?	Ac-YVAD-cmk, obeticholic acid	Steatosis after <10 weeks; NASH after 10-20 weeks; fibrosis development at 20-30 weeks; requires HF-HC diets to induce NASH and fibrosis	(80–83)
FLS	*Chow* 10% fat, 70% carb., 20% protein.	13-20	×	✓	×	✓	✓	Mild	×	Fenofibrate, ezetimibe	Inbred strain with high heterogeneity; fibrosis after >24 weeks	(84–86)
FLS-*ob/ob*	*Chow* 10% fat, 70% carb., 20% protein.	20-24	✓	✓	✓	✓	✓	Moderate-severe	✓	Sitagliptin, aliskiren, ambrisenten, irbesartan	Inbred strain with high heterogeneity; glucosuria; spontaneous NASH; fibrosis after >24 weeks	(84,87–90)

*Wks: weeks; Obes.: Obesity; Dys. Lip.: dyslipidemia; Gluc. Intol.: glucose intolerance; HCC: hepatocellular carcinoma; Ref.: References

Appendix A. A review of current NASH mouse models

	Diet	Time (wks)	Obes.	Dys. Lip.	Gluc. Intol.	Steat.	NASH	Fibrosis	HCC	E.g., of drugs tested in model	Comments on mod el	Ref.
*SREBP1*c Tg	*HF-FRUC* 60% fat + 30% fructose water	12	×	✓	✓	✓	✓	Moderate	?	Eplerenone	SREBP1c overexpression to mimic human NASH (HFD alone lowers SREBP1c expression); decreased adiposity	(91)
Agouti (KK-A^{Y})	*Chow* 10% fat, 70% carb., 20% protein.	4-8	✓	✓	✓	✓	×	×	×	Pioglitazone	Hyperphagic model; mice do not progress to NASH spontaneously	(92,93)
Agouti (KK-A^{Y})	*HF-HC-FRUC-cholic acid.* 40% fat, 20% fructose, 2% cholest., 0.5% cholic acid	4-12	✓	✓	✓	✓	×	×	×	N/A	Hyperphagic model; NASH after 4 weeks; fibrosis after 12 weeks; requires HFD to induce NASH	(94)
PTEN KO	*Chow* 10% fat, 70% carb., 20% protein.	10-78	×	×	×	✓	✓	Moderate	✓	Probiotics, Eicosapentaenoic acid (EPA)	Hepatocyte-specific PTEN KO; moderate NASH by 8 weeks; 47% livers with adenomas by 44 weeks of age; 100% livers with adenomas and 66% with HCC by 74-78 weeks of age	(95–97)
PTEN KO	*HFD* 45% fat	12	✓	✓	✓	✓	✓	Moderate	✓	N/A	Addition of HFD has no additional benefit on fibrosis or HCC development, but does progress to steatosis and hepatocellular damage	(98)
MUP-uPA Tg	*HFD* 60% fat	16-52	✓	✓	✓	✓	✓	Mild-severe	✓	N/A	Weight gain, glucose intolerance, and dyslipidemia only with a HFD; Steatosis after 4 weeks; NASH develops after 16 weeks; moderate-severe fibrosis after 24 weeks; 90% of mice develop HCC after 32-52 weeks	(99,100)

*Wks: weeks; Obes.: Obesity; Dys. Lip.: dyslipidemia; Gluc. Intol.: glucose intolerance; HCC: hepatocellular carcinoma; Ref.: References

Appendix A. A review of current NASH mouse models

	Diet	Time (wks)	Obes.	Dys. Lip.	Gluc. Intol.	Steat.	NASH	Fibrosis	HCC	E.g., of drugs tested in model	Comments on mod el	Ref.
DIAMOND	*HF-FRUC* 42% fat, 0.1% cholest. + high fructose-glucose solution in drinking water	8-52	✓	✓	✓	✓	✓	Mild-severe	✓	N/A	Zone 3 steatosis within 8 weeks; NASH within 16-24 weeks; mild fibrosis between 16-24 weeks; severe fibrosis after 52 weeks; 90% of mice develop HCC after 32-52 weeks	(101)
FRGN KO	*AMLN/GAN* 40% fat, 20% fructose, 2% cholest.	8-24	✓	✓	✓	✓	✓	Mild-severe	?	META4	Steatosis after 8 weeks on AMLN diet; NASH after 12-16 weeks; fibrosis after 12-16; bridging fibrosis after 24 weeks	(102, 103)
MS-NASH (Formerly FATZO)	*HF-FRUC* 41% fat, 43% carb., 17% protein + 5% fructose in drinking water	4-20	✓	✓	✓	✓	✓	Mild-moderate	?	MSDC-0602K, liraglutide, obeticholic acid	HFD required to induce NASH and fibrosis; NASH after 16-20 weeks; Mild fibrosis after 16 weeks; moderate fibrosis after 20 weeks	(104–106)

*Wks: weeks; Obes.: Obesity; Dys. Lip.: dyslipidemia; Gluc. Intol.: glucose intolerance; HCC: hepatocellular carcinoma; Ref.: References

Note: all models use mice on C57BL/6 backgrounds unless stated otherwise. This table includes a comprehensive summary of the most commonly used mouse models; however, additional combinations of dietary components, toxins and genetic models have been employed and might not be reflected in this summary.

HFD: high-fat diet (45% fat); TN: thermoneutrality (housed at 29°C); cholest.: cholesterol; carb.: carbohydrate; HF: high-fat (40-60% fat); HC: high cholesterol (1-2% cholesterol); FRUC: fructose; AMLN: Amylin liver NASH model; GAN: Gubra Amylin NASH diet; MCD: methionine- and choline-deficient diet; CD: choline-deficient; CD-HFD: choline-deficient + HFD-treated mice; CDAA: choline-deficient, L-amino acid-defined; HFCC: 1.25% cholesterol, 0.5% cholic acid; CCl_4: carbon tetrachloride; TAA: thioacetamide; STAM™: streptozotocin + HFD-treated mice; HFD-DEN: diethylnitrosamine + HFD-treated mice; HFCC-CDX: 1.25% cholesterol, 0.5% cholic acid with 2% cyclodextrin in drinking water; *ob/ob:* leptin-deficient mice; *db/db:* leptin-receptor-deficient mice; *foz/foz*: Alstrom syndrome 1 (mutated ALMS1 gene; hyperphagic); ApoE*3-Leiden: mutation in *Apoe* leading to hyperlipodemia and atherosclerosis (lab developed mutation in ApoE); ApoE*3-Leiden.huCETP: ApoE*3-Leiden transgene + cholesteryl ester transfer protein (CETP) transgene; $LDLr^{-/-}$-Leiden: mutation in *Ldlr* leading to hyperlipodemia (lab developed mutation); FLS: fatty liver Shionogi; *SREBP1c* Tg: sterol regulatory element-binding protein 1c transgenic mice; Agouti: KK-A^y-a mice (crossbreed of diabetic KK mice with yellow obese (A^y) mice); PTEN KO: phosphatase and tensin homolog deleted on chromosome 10 knockout mice; AOX KO: acetyl-coenzyme A oxidase-deficient mice; MUP-uPA Tg: mice expressing transiently high amounts of urokinase plasminogen activator in hepatocytes; DIAMOND: diet-induced animal model of NAFLD (isogenic BL6/129 hybrid strain fed an obesogenic HFD supplemented by high fructose and sucrose); FRGN KO: non-obese diabetic (NOD) $Fah^{-/-}$ $Rag2^{-/-}$ $IL2rg^{-/-}$; MS-NASH (FATZO): Crossbreed of C57BL/6 and AKR/J mice; NEFAs: non-esterified fatty acids; TGs: triglycerides; VLDL-C: very-low-density lipoprotein-cholesterol; ApoE: apolipoprotein A; ApoB: apoliporotein B. ✓: present; ×: not present; ? : not reported or assessed; N/A: not applicable.

Appendix A References

1. Velázquez KT, Enos RT, Bader JE, Sougiannis AT, Carson MS, Chatzistamou I, et al. Prolonged high-fat-diet feeding promotes non-alcoholic fatty liver disease and alters gut microbiota in mice. World J Hepatol. 2019 Aug 8;11(8):619.
2. Yang G, Lee HE, Lee JY. A pharmacological inhibitor of NLRP3 inflammasome prevents non-alcoholic fatty liver disease in a mouse model induced by high fat diet. Sci. Rep. 2016 Apr 14;6(1):1–11.
3. Barreyro FJ, Holod S, Finocchietto P V, Camino AM, Aquino JB, Avagnina A, et al. The pan-caspase inhibitor Emricasan (IDN-6556) decreases liver injury and fibrosis in a murine model of non-alcoholic steatohepatitis. Liver Int. 2014 Mar; 35(3):953-66.
4. Giles DA, Moreno-Fernandez ME, Stankiewicz TE, Graspeuntner S, Cappelletti M, Wu D, et al. Thermoneutral housing exacerbates nonalcoholic fatty liver disease in mice and allows for sex-independent disease modeling. Nat Med. 2017 Jun 12;23(7):829–38.
5. Kubota N, Kado S, Kano M, Masuoka N, Nagata Y, Kobayashi T, et al. A high-fat diet and multiple administration of carbon tetrachloride induces liver injury and pathological features associated with non-alcoholic steatohepatitis in mice. Clin Exp Pharmacol Physiol. 2013 Jul;40(7):422–30.
6. Yang F, Shang L, Wang S, Liu Y, Ren H, Zhu W, et al. TNFα-mediated necroptosis aggravates ischemia-reperfusion injury in the fatty liver by regulating the inflammatory response. Oxid Med Cell Longev. 2019 May 12;2301903.
7. Zheng S, Hoos L, Cook J, Tetzloff G, Davis H, van Heek M, et al. Ezetimibe improves high fat and cholesterol diet-induced non-alcoholic fatty liver disease in mice. Eur J Pharmacol. 2008 Apr 14;584(1):118–24.
8. Bruckbauer A, Banerjee J, Fu L, Li F, Cao Q, Cui X, et al. A Combination of Leucine, Metformin, and Sildenafil Treats Nonalcoholic Fatty Liver Disease and Steatohepatitis in Mice. Int J Hepatol. 2016;9185987.
9. Carino A, Cipriani S, Marchianò S, Biagioli M, Santorelli C, Donini A, et al. BAR502, a dual FXR and GPBAR1 agonist, promotes browning of white adipose tissue and reverses liver steatosis and fibrosis. Sci Rep. 2017 Feb 16;7:42801.
10. Rahman K, Liu Y, Kumar P, Smith T, Thorn NE, Farris AB, et al. C/EBP homologous protein modulates liraglutide-mediated attenuation of non-alcoholic steatohepatitis. Lab. Investig. 2016 May 30;96(8):895–908.
11. Bahirat UA, Shenoy RR, Goel RN, Nemmani KVS. APD668, a G protein-coupled receptor 119 agonist improves fat tolerance and attenuates fatty liver in high-trans fat diet induced steatohepatitis model in C57BL/6 mice. Eur J Pharmacol. 2017 Apr 15;801:35–45.
12. Honda Y, Imajo K, Kato T, Kessoku T, Ogawa Y, Tomeno W, et al. The Selective SGLT2 Inhibitor Ipragliflozin Has a Therapeutic Effect on Nonalcoholic Steatohepatitis in Mice. PLoS One. 2016 Jan 5;11(1):e0146337.
13. Trevaskis JL, Griffin PS, Wittmer C, Neuschwander-Tetri BA, Brunt EM, Dolman CS, et al. Glucagon-like peptide-1 receptor agonism improves metabolic,

biochemical, and histopathological indices of nonalcoholic steatohepatitis in mice. Am J Physiol Gastrointest Liver Physiol. 2012 Apr 15;302(8):762–72.
14. Tølbøl KS, Kristiansen MNB, Hansen HH, Veidal SS, Rigbolt KTG, Gillum MP, et al. Metabolic and hepatic effects of liraglutide, obeticholic acid and elafibranor in diet-induced obese mouse models of biopsy-confirmed nonalcoholic steatohepatitis. World J Gastroenterol. 2018 Jan 1;24(2):179.
15. Hansen HH, Ægidius HM, Oró D, Evers SS, Heebøll S, Eriksen PL, et al. Human translatability of the GAN diet-induced obese mouse model of non-alcoholic steatohepatitis. BMC Gastroenterol. 2020 Jul 6;20(1):1–12.
16. Møllerhøj MB, Veidal SS, Thrane KT, Oró D, Overgaard A, Salinas CG, et al. Hepatoprotective effects of semaglutide, lanifibranor and dietary intervention in the GAN diet-induced obese and biopsy-confirmed mouse model of NASH. Clin Transl Sci. 2022 May 1;15(5):1167–86.
17. Green CD, Weigel C, Brown RDR, Bedossa P, Dozmorov M, Sanyal AJ, et al. A new preclinical model of western diet-induced progression of non-alcoholic steatohepatitis to hepatocellular carcinoma. FASEB J. 2022 Jul 1;36(7):e22372.
18. Valdecantos MP, Pardo V, Ruiz L, Castro-Sánchez L, Lanzón B, Fernández-Millán E, et al. A novel glucagon-like peptide 1/glucagon receptor dual agonist improves steatohepatitis and liver regeneration in mice. Hepatology. 2017 Mar 1;65(3):950–68.
19. Ip E, Farrell G, Hall P, Robertson G, Leclercq I. Administration of the Potent PPARα Agonist, Wy-14,643, Reverses Nutritional Fibrosis and Steatohepatitis in Mice. Hepatology. 2004 May;39(5):1286–96.
20. Zhang S, Wang J, Liu Q, Harnish DC. Farnesoid X receptor agonist WAY-362450 attenuates liver inflammation and fibrosis in murine model of non-alcoholic steatohepatitis. J Hepatol. 2009 Aug 1;51(2):380–8.
21. Park HS, Jang JE, Ko MS, Woo SH, Kim BJ, Kim HS, et al. Statins Increase Mitochondrial and Peroxisomal Fatty Acid Oxidation in the Liver and Prevent Non-Alcoholic Steatohepatitis in Mice. Diabetes Metab J. 2016;40(5):376–85.
22. Nagasawa T, Inada Y, Nakano S, Tamura T, Takahashi T, Maruyama K, et al. Effects of bezafibrate, PPAR pan-agonist, and GW501516, PPARdelta agonist, on development of steatohepatitis in mice fed a methionine- and choline-deficient diet. Eur J Pharmacol. 2006 Apr 24;536(1–2):182–91.
23. Jung YA, Choi YK, Jung GS, Seo HY, Kim HS, Jang BK, et al. Sitagliptin attenuates methionine/choline-deficient diet-induced steatohepatitis. Diabetes Res Clin Pract. 2014;105(1):47–57.
24. Mridha AR, Wree A, Robertson AAB, Yeh MM, Johnson CD, Van Rooyen DM, et al. NLRP3 inflammasome blockade reduces liver inflammation and fibrosis in experimental NASH in mice. J Hepatol. 2017 May 1;66(5):1037.
25. Nan YM, Fu N, Wu WJ, Liang BL, Wang RQ, Zhao SX, et al. Rosiglitazone prevents nutritional fibrosis and steatohepatitis in mice. Scand J Gastroenterol. 2009 Mar;44(3):358–65.

26. Koppe SWP, Sahai A, Malladi P, Whitington PF, Green RM. Pentoxifylline attenuates steatohepatitis induced by the methionine choline deficient diet. J Hepatol. 2004 Oct;41(4):592–8.
27. Raubenheimer PJ, Nyirenda MJ, Walker BR. A Choline-Deficient Diet Exacerbates Fatty Liver but Attenuates Insulin Resistance and Glucose Intolerance in Mice Fed a High-Fat Diet. Diabetes. 2006 Jul 1;55(7):2015–20.
28. Achiwa K, Ishigami M, Ishizu Y, Kuzuya T, Honda T, Hayashi K, et al. DSS colitis promotes tumorigenesis and fibrogenesis in a choline-deficient high-fat diet-induced NASH mouse model. Biochem Biophys Res Commun. 2016 Jan 29;470(1):15–21.
29. Kishida N, Matsuda S, Itano O, Shinoda M, Kitago M, Yagi H, et al. Development of a novel mouse model of hepatocellular carcinoma with nonalcoholic steatohepatitis using a high-fat, choline-deficient diet and intraperitoneal injection of diethylnitrosamine. BMC Gastroenterol. 2016 Jun 13;16(1):1–13.
30. Guarino M, Kumar P, Felser A, Terracciano LM, Guixé-Muntet S, Humar B, et al. Exercise Attenuates the Transition from Fatty Liver to Steatohepatitis and Reduces Tumor Formation in Mice. Cancers (Basel). 2020;12:1407.
31. Bao L, Yin J, Gao W, Wang Q, Yao W, Gao X. A long-acting FGF21 alleviates hepatic steatosis and inflammation in a mouse model of non-alcoholic steatohepatitis partly through an FGF21-adiponectin-IL17A pathway. Br J Pharmacol. 2018 Aug 1;175(16):3379–93.
32. Liu W, Struik D, Nies VJM, Jurdzinski A, Harkema L, De Bruin A, et al. Effective treatment of steatosis and steatohepatitis by fibroblast growth factor 1 in mouse models of nonalcoholic fatty liver disease. Proc Natl Acad Sci USA. 2016 Feb 23;113(8):2288–93.
33. Hayashizaki-Someya Y, Kurosaki E, Takasu T, Mitori H, Yamazaki S, Koide K, et al. Ipragliflozin, an SGLT2 inhibitor, exhibits a prophylactic effect on hepatic steatosis and fibrosis induced by choline-deficient l-amino acid-defined diet in rats. Eur J Pharmacol. 2015 May 5;754:19–24.
34. Daniels SJ, Leeming DJ, Detlefsen S, Bruun MF, Hjuler ST, Henriksen K, et al. Biochemical and histological characterisation of an experimental rodent model of non-alcoholic steatohepatitis - Effects of a peroxisome proliferator-activated receptor gamma (PPAR-γ) agonist and a glucagon-like peptide-1 analogue. Biomed Pharmacother. 2019 Mar 1;111:926–33.
35. Ichimura-Shimizu M, Tsuchiyama Y, Morimoto Y, Matsumoto M, Kobayashi T, Sumida S, et al. A Novel Mouse Model of Nonalcoholic Steatohepatitis Suggests that Liver Fibrosis Initiates around Lipid-Laden Macrophages. Am J Pathol. 2022 Jan 1;192(1):31–42.
36. Nakamura I, Zakharia K, Banini BA, Mikhail DS, Kim TH, Yang JD, et al. Brivanib Attenuates Hepatic Fibrosis In Vivo and Stellate Cell Activation In Vitro by Inhibition of FGF, VEGF and PDGF Signaling. PLoS One. 2014 Apr 7;9(4):e92273.

37. Zhang DG, Zhang C, Wang JX, Wang BW, Wang H, Zhang ZH, et al. Obeticholic acid protects against carbon tetrachloride-induced acute liver injury and inflammation. Toxicol Appl Pharmacol. 2017 Jan 1;314:39–47.
38. Schilter H, Findlay AD, Perryman L, Yow TT, Moses J, Zahoor A, et al. The lysyl oxidase like 2/3 enzymatic inhibitor, PXS-5153A, reduces crosslinks and ameliorates fibrosis. J Cell Mol Med. 2019 Mar 1;23(3):1759–70.
39. Saito S, Hata K, Iwaisako K, Yanagida A, Takeiri M, Tanaka H, et al. Cilostazol attenuates hepatic stellate cell activation and protects mice against carbon tetrachloride-induced liver fibrosis. Hepatol. Res. 2014 Apr 1;44(4):460–73.
40. Deng YR, Ma H Di, Tsuneyama K, Yang W, Wang YH, Lu FT, et al. STAT3-mediated attenuation of CCl4-induced mouse liver fibrosis by the protein kinase inhibitor sorafenib. J Autoimmun. 2013 Oct 1;46:25–34.
41. Tsuchida T, Lee YA, Fujiwara N, Ybanez M, Allen B, Martins S, et al. A simple diet- and chemical-induced murine NASH model with rapid progression of steatohepatitis, fibrosis and liver cancer. J Hepatol. 2018 Aug 1;69(2):385–95.
42. Lefebvre E, Moyle G, Reshef R, Richman LP, Thompson M, Hong F, et al. Antifibrotic Effects of the Dual CCR2/CCR5 Antagonist Cenicriviroc in Animal Models of Liver and Kidney Fibrosis. PLoS One. 2016 Jun 1;11(6):e0158156.
43. Klein T, Fujii M, Sandel J, Shibazaki Y, Wakamatsu K, Mark M, et al. Linagliptin alleviates hepatic steatosis and inflammation in a mouse model of non-alcoholic steatohepatitis. Med Mol Morphol. 2014 Sep 1;47(3):137–49.
44. Orime K, Shirakawa J, Togashi Y, Tajima K, Inoue H, Nagashima Y, et al. Lipid-lowering agents inhibit hepatic steatosis in a non-alcoholic steatohepatitis-derived hepatocellular carcinoma mouse model. Eur J Pharmacol. 2016 Feb 5;772:22–32.
45. Morrow MR, Batchuluun B, Wu J, Ahmadi E, Leroux JM, Mohammadi-Shemirani P, et al. Inhibition of ATP-citrate lyase improves Non-Alcoholic Steatohepatitis (NASH), liver fibrosis, and dyslipidemia. Cell Metab. 2022 Jun 7;34(6):919-936.e8.
46. Park EJ, Lee JH, Yu GY, He G, Ali SR, Holzer RG, et al. Dietary and Genetic Obesity Promote Liver Inflammation and Tumorigenesis by Enhancing IL-6 and TNF Expression. Cell. 2010 Jan 22;140(2):197–208.
47. Vanessa Márquez-Quiroga L, Arellanes-Robledo J, Rocío Vásquez-Garzón V, Villa-Treviño S, Muriel P. Models of nonalcoholic steatohepatitis potentiated by chemical inducers leading to hepatocellular carcinoma. Biochem Pharmacol. 2022 Jan;195:114845.
48. Duan XY, Pan Q, Yan SY, Ding WJ, Fan JG, Qiao L. High-saturate-fat diet delays initiation of diethylnitrosamine-induced hepatocellular carcinoma. BMC Gastroenterol. 2014 Nov 20;14(1):1–10.
49. Briand F, Heymes C, Bonada L, Angles T, Charpentier J, Branchereau M, et al. A 3-week nonalcoholic steatohepatitis mouse model shows elafibranor benefits on hepatic inflammation and cell death. Clin Transl Sci. 2020 May 1;13(3):529.
50. Duparc T, Briand F, Trenteseaux C, Merian J, Combes G, Najib S, et al. Liraglutide improves hepatic steatosis and metabolic dysfunctions in a 3-week dietary mouse

model of nonalcoholic steatohepatitis. Am J Physiol Gastrointest Liver Physiol. 2019 Oct 1;317(4):G508–17.
51. Trak-Smayra V, Paradis V, Massart J, Nasser S, Jebara V, Fromenty B. Pathology of the liver in obese and diabetic ob/ob and db/db mice fed a standard or high-calorie diet. Int J Exp Pathol. 2011 Dec;92(6):413.
52. Kristiansen MNB, Veidal SS, Rigbolt KTG, Tølbøl KS, Roth JD, Jelsing J, et al. Obese diet-induced mouse models of nonalcoholic steatohepatitis-tracking disease by liver biopsy. World J Hepatol. 2016 Jun 8;8(16):673–84.
53. Lee JH, Kang YE, Chang JY, Park KC, Kim HW, Kim JT, et al. An engineered FGF21 variant, LY2405319, can prevent non-alcoholic steatohepatitis by enhancing hepatic mitochondrial function. Am J Transl Res. 2016;8(11):4750–63.
54. Stefano JT, De Oliveira CPMS, Corrêa-Giannella ML, De Lima VMR, De Sá SV, De Oliveira EP, et al. Nonalcoholic steatohepatitis (NASH) in ob/ob mice treated with yo jyo hen shi ko (YHK): effects on peroxisome proliferator-activated receptors (PPARs) and microsomal triglyceride transfer protein (MTP). Dig Dis Sci. 2007 Dec;52(12):3448–54.
55. Sujishi T, Fukunishi S, Ii M, Nakamura K, Yokohama K, Ohama H, et al. Sitagliptin can inhibit the development of hepatic steatosis in high-fructose diet-fed ob/ob mice. J Clin Biochem Nutr. 2015;57(3):244.
56. Nakamura K, Fukunishi S, Yokohama K, Ohama H, Tsuchimoto Y, Asai A, et al. A long-lasting dipeptidyl peptidase-4 inhibitor, teneligliptin, as a preventive drug for the development of hepatic steatosis in high-fructose diet-fed ob/ob mice. Int J Mol Med. 2017 Apr 1;39(4):969–83.
57. Griffett K, Welch RD, Flaveny CA, Kolar GR, Neuschwander-Tetri BA, Burris TP. The LXR inverse agonist SR9238 suppresses fibrosis in a model of non-alcoholic steatohepatitis. Mol Metab. 2015 Apr 1;4(4):353–7.
58. Roth JD, Feigh M, Veidal SS, Fensholdt LKD, Rigbolt KT, Hansen HH, et al. INT-767 improves histopathological features in a diet-induced ob/ob mouse model of biopsy-confirmed non-alcoholic steatohepatitis. World J Gastroenterol. 2018 Jan 1;24(2):195.
59. Song JX, An JR, Chen Q, Yang XY, Jia CL, Xu S, et al. Liraglutide attenuates hepatic iron levels and ferroptosis in db/db mice. Bioengineered. 2022 Apr;13(4):8334-8348.
60. Staels B, Rubenstrunk A, Noel B, Rigou G, Delataille P, Millatt LJ, et al. Hepatoprotective effects of the dual peroxisome proliferator-activated receptor alpha/delta agonist, GFT505, in rodent models of nonalcoholic fatty liver disease/nonalcoholic steatohepatitis. Hepatology. 2013 Dec 1;58(6):1941–52.
61. Yamamoto T, Nakade Y, Yamauchi T, Kobayashi Y, Ishii N, Ohashi T, et al. Glucagon-like peptide-1 analogue prevents nonalcoholic steatohepatitis in non-obese mice. World J Gastroenterol. 2016 Feb 28;22(8):2512–23.
62. Rinella ME, Elias MS, Smolak RR, Fu T, Borensztajn J, Green RM. Mechanisms of hepatic steatosis in mice fed a lipogenic methionine choline-deficient diet. J Lipid Res. 2008 May 1;49(5):1068.

63. Ohno T, Shimizu M, Shirakami Y, Baba A, Kochi T, Kubota M, et al. Metformin Suppresses Diethylnitrosamine-Induced Liver Tumorigenesis in Obese and Diabetic C57BL/KsJ-+Leprdb/+Leprdb Mice. PLoS One. 2015 Apr 16;10(4):e0124081.
64. Handa P, Morgan-Stevenson V, Maliken BD, Nelson JE, Washington S, Westerman M, et al. Iron overload results in hepatic oxidative stress, immune cell activation, and hepatocellular ballooning injury, leading to nonalcoholic steatohepatitis in genetically obese mice. Am J Physiol Gastrointest Liver Physiol. 2016;310(2):G117–27.
65. Haczeyni F, Poekes L, Wang H, Mridha AR, Barn V, Geoffrey Haigh W, et al. Obeticholic acid improves adipose morphometry and inflammation and reduces steatosis in dietary but not metabolic obesity in mice. Obesity. 2017 Jan 1;25(1):155–65.
66. Bell-Anderson KS, Aouad L, Williams H, Sanz FR, Phuyal J, Larter CZ, et al. Coordinated improvement in glucose tolerance, liver steatosis and obesity-associated inflammation by cannabinoid 1 receptor antagonism in fat Aussie mice. IJO. 2011 Mar 8;35(12):1539–48.
67. Ioannou GN, Van Rooyen DM, Savard C, Haigh WG, Yeh MM, Teoh NC, et al. Cholesterol-lowering drugs cause dissolution of cholesterol crystals and disperse Kupffer cell crown-like structures during resolution of NASH. J Lipid Res. 2015 Feb 1;56(2):277–85.
68. Inia JA, Van Den Hoek AM, Stokman G, Pieterman EJ, Morrison MC, Jukema WJ, et al. Atorvastatin attenuates diet-induced non-alcoholic steatohepatitis in ApoE*3-Leiden mice by reducing hepatic inflammation. Atherosclerosis. 2022 Aug 1;355:21.
69. Zimmer M, Bista P, Benson EL, Lee DY, Liu F, Picarella D, et al. CAT-2003: A novel sterol regulatory element-binding protein inhibitor that reduces steatohepatitis, plasma lipids, and atherosclerosis in apolipoprotein E*3-Leiden mice. Hepatol Commun. 2017 Jun 1;1(4):311–25.
70. Schierwagen R, Maybüchen L, Zimmer S, Hittatiya K, Bäck C, Klein S, et al. Seven weeks of Western diet in apolipoprotein-E-deficient mice induce metabolic syndrome and non-alcoholic steatohepatitis with liver fibrosis. Sci Rep. 2015 Aug 11;5:12931.
71. Schierwagen R, Maybüchen L, Hittatiya K, Klein S, Uschner FE, Braga TT, et al. Statins improve NASH via inhibition of RhoA and Ras. Am J Physiol Gastrointest Liver Physiol. 2016 Oct 1;311(4):G724–33.
72. In het Panhuis W, Kooijman S, Brouwers B, Verhoeven A, Pronk ACM, Streefland TCM, et al. Mild Exercise Does Not Prevent Atherosclerosis in APOE*3-Leiden.CETP Mice or Improve Lipoprotein Profile of Men with Obesity. Obesity. 2020 Jul 1;28(S1):S93–103.
73. Wang Y, Parlevliet ET, Geerling JJ, Van Der Tuin SJL, Zhang H, Bieghs V, et al. Exendin-4 decreases liver inflammation and atherosclerosis development simultaneously by reducing macrophage infiltration. Br J Pharmacol. 2014 Feb;171(3):723–34.

74. Liang W, Verschuren L, Mulder P, Van Der Hoorn JWA, Verheij J, Van Dam AD, et al. Salsalate attenuates diet induced non-alcoholic steatohepatitis in mice by decreasing lipogenic and inflammatory processes. Br J Pharmacol. 2015 Nov 1;172(22):5293–305.
75. De Haan W, De Vries-Van Der Weij J, Van Der Hoorn JWA, Gautier T, Van Der Hoogt CC, Westerterp M, et al. Torcetrapib does not reduce atherosclerosis beyond atorvastatin and induces more proinflammatory lesions than atorvastatin. Circulation. 2008 May 13;117(19):2515–22.
76. van den Hoek AM, Verschuren L, Caspers MPM, Worms N, Menke AL, Princen HMG. Beneficial effects of elafibranor on NASH in E3L.CETP mice and differences between mice and men. Sci Rep. 2021 Dec 1;11(1):5050.
77. Bieghs V, Van Gorp PJ, Wouters K, Hendrikx T, Gijbels MJ, van Bilsen M, et al. LDL Receptor Knock-Out Mice Are a Physiological Model Particularly Vulnerable to Study the Onset of Inflammation in Non-Alcoholic Fatty Liver Disease. PLoS One. 2012 Jan 25;7(1):e30668.
78. Gupte AA, Liu JZ, Ren Y, Minze LJ, Wiles JR, Collins AR, et al. Rosiglitazone attenuates age- and diet-associated nonalcoholic steatohepatitis in male low-density lipoprotein receptor knockout mice. Hepatology. 2010 Dec 1;52(6):2001–11.
79. Kong B, Luyendyk JP, Tawfik O, Guo GL. Farnesoid X Receptor Deficiency Induces Nonalcoholic Steatohepatitis in Low-Density Lipoprotein Receptor-Knockout Mice Fed a High-Fat Diet. JPET. 2009 Jan 1;328(1):116–22.
80. van den Hoek AM, Özsezen S, Caspers MPM, van Koppen A, Hanemaaijer R, Verschuren L. Unraveling the Transcriptional Dynamics of NASH Pathogenesis Affecting Atherosclerosis. Int J Mol Sci. 2022 Aug 1;23(15):8229.
81. van den Hoek AM, Verschuren L, Worms N, van Nieuwkoop A, de Ruiter C, Attema J, et al. A Translational Mouse Model for NASH with Advanced Fibrosis and Atherosclerosis Expressing Key Pathways of Human Pathology. Cells. 2020 Sep 1;9(9).
82. Morrison MC, Mulder P, Salic K, Verheij J, Liang W, Van Duyvenvoorde W, et al. Intervention with a caspase-1 inhibitor reduces obesity-associated hyperinsulinemia, non-alcoholic steatohepatitis and hepatic fibrosis in LDLR−/−.Leiden mice. IJO. 2016 May 28;40(9):1416–23.
83. Morrison MC, Verschuren L, Salic K, Verheij J, Menke A, Wielinga PY, et al. Obeticholic Acid Modulates Serum Metabolites and Gene Signatures Characteristic of Human NASH and Attenuates Inflammation and Fibrosis Progression in Ldlr-/-.Leiden Mice. Hepatol Commun. 2018 Dec 1;2(12):1513–32.
84. Sugihara T, Koda M, Kishina M, Kato J, Tokunaga S, Matono T, et al. Fatty liver Shionogi-ob/ob mouse: A new candidate for a non-alcoholic steatohepatitis model. Hepatol. Res. 2013 May;43(5):547–56.
85. Wang X, Sugimoto K, Fujisawa T, Shindo N, Minato S, Kamada Y, et al. Novel effect of ezetimibe to inhibit the development of non-alcoholic fatty liver disease in Fatty Liver Shionogi mouse. Hepatol. Res. 2014 Jan 1;44(1):102–13.

86. Harano Y, Yasui K, Toyama T, Nakajima T, Mitsuyoshi H, Mimani M, et al. Fenofibrate, a peroxisome proliferator-activated receptor α agonist, reduces hepatic steatosis and lipid peroxidation in fatty liver Shionogi mice with hereditary fatty liver. Liver Int. 2006 Jun 1;26(5):613–20.
87. Onoyama T, Koda M, Okamoto T, Kishina M, Matono T, Sugihara T, et al. Therapeutic effects of the dipeptidyl peptidase-IV inhibitor, sitagliptin, on non-alcoholic steatohepatitis in FLS-ob/ob male mice. Mol Med Rep. 2015 Sep 1;12(5):6895–902.
88. Kishina M, Koda M, Kato J, Tokunaga S, Matono T, Sugihara T, et al. Therapeutic effects of the direct renin inhibitor, aliskiren, on non-alcoholic steatohepatitis in fatty liver Shionogi ob/ob male mice. Hepatol. Res. 2014 Aug 1;44(8):888–96.
89. Okamoto T, Koda M, Miyoshi K, Onoyama T, Kishina M, Matono T, et al. Antifibrotic effects of ambrisentan, an endothelin-A receptor antagonist, in a non-alcoholic steatohepatitis mouse model. World J Hepatol. 2016 Aug 8;8(22):933–41.
90. Kato J, Koda M, Kishina M, Tokunaga S, Matono T, Sugihara T, et al. Therapeutic effects of angiotensin II type 1 receptor blocker, irbesartan, on non-alcoholic steatohepatitis using FLS-ob/ob male mice. Int J Mol Med. 2012 Jul 1;30(1):107–13.
91. Wada T, Miyashita Y, Sasaki M, Aruga Y, Nakamura Y, Ishii Y, et al. Eplerenone ameliorates the phenotypes of metabolic syndrome with NASH in liver-specific SREBP-1c Tg mice fed high-fat and high-fructose diet. Am J Physiol Endocrinol Metab. 2013;305:1415–25.
92. Aoyama T, Ikejima K, Kon K, Okumura K, Arai K, Watanabe S. Pioglitazone promotes survival and prevents hepatic regeneration failure after partial hepatectomy in obese and diabetic KK-Ay mice. Hepatology. 2009 May 1;49(5):1636–44.
93. Okumura K, Ikejima K, Kon K, Abe W, Yamashina S, Enomoto N, et al. Exacerbation of dietary steatohepatitis and fibrosis in obese, diabetic KK-A(y) mice. Hepatol Res. 2006 Nov;36(3):217–28.
94. Sakuma T, Nakamura M, Chiba T, Iwanaga T, Kan M, Kojima R, et al. A diet-induced murine model for non-alcoholic fatty liver disease with obesity and insulin resistance that rapidly develops steatohepatitis and fibrosis. Lab Invest. 2022 Oct 1;102(10).
95. Horie Y, Suzuki A, Kataoka E, Sasaki T, Hamada K, Sasaki J, et al. Hepatocyte-specific Pten deficiency results in steatohepatitis and hepatocellular carcinomas. J. of Clin. Investig. 2004 Jun 6;113(12):1774.
96. Arai N, Miura K, Aizawa K, Sekiya M, Nagayama M, Sakamoto H, et al. Probiotics suppress nonalcoholic steatohepatitis and carcinogenesis progression in hepatocyte-specific PTEN knockout mice. Sci. Rep. 2022 Sep 28;12(1):1–12.
97. Ishii H, Horie Y, Ohshima S, Anezaki Y, Kinoshita N, Dohmen T, et al. Eicosapentaenoic acid ameliorates steatohepatitis and hepatocellular carcinoma in hepatocyte-specific Pten-deficient mice. J Hepatol. 2009 Mar 1;50(3):562–71.

98. Shearn CT, Mercer KE, Orlicky DJ, Hennings L, Smathers-McCullough RL, Stiles BL, et al. Short Term Feeding of a High Fat Diet Exerts an Additive Effect on Hepatocellular Damage and Steatosis in Liver-Specific PTEN Knockout Mice. PLoS One. 2014 May 12;9(5):e96553.
99. Shalapour S, Lin XJ, Bastian N, Brain J, Burt AD, Aksenov AA, et al. Inflammation-induced IgA + cells dismantle anti-liver cancer immunity. Nature. 2017 Nov 8;551(7680):340-345.
100. Nakagawa H, Umemura A, Taniguchi K, Font-Burgada J, Dhar D, Ogata H, et al. ER Stress Cooperates with Hypernutrition to Trigger TNF-Dependent Spontaneous HCC Development. Cancer Cell. 2014 Sep 8;26(3):331–43.
101. Asgharpour A, Cazanave SC, Pacana T, Seneshaw M, Vincent R, Banini BA, et al. A diet-induced animal model of non-alcoholic fatty liver disease and hepatocellular cancer. J Hepatol. 2016 Sep 1;65(3):579–88.
102. Ma J, Tan X, Kwon Y, Delgado ER, Zarnegar A, DeFrances MC, et al. A Novel Humanized Model of NASH and Its Treatment With META4, A Potent Agonist of MET. Cell Mol Gastroenterol Hepatol. 2022 Jan 1;13(2):565.
103. Minniti ME, Foquet L, Gierer E, Pedrelli M, Goldman D, Copenhaver R, et al. Liver-humanized mice fed a NASH-diet are an advanced model to study cardiometabolic diseases. Atherosclerosis. 2021 Aug 1;331:e143.
104. Kamm DR, Pyles KD, Sharpe MC, Healy LN, Colca JR, McCommis KS. Novel insulin sensitizer MSDC-0602K improves insulinemia and fatty liver disease in mice, alone and in combination with liraglutide. JBC. 2021 Jan 1;296:100807.
105. Sun G, Jackson C V., Zimmerman K, Zhang LK, Finnearty CM, Sandusky GE, et al. The FATZO mouse, a next generation model of type 2 diabetes, develops NAFLD and NASH when fed a Western diet supplemented with fructose. BMC Gastroenterol. 2019 Mar 18;19(1):1–11.
106. Peterson RG, Van Jackson C, Zimmerman KM, Alsina-Fernandez J, Michael MD, Emmerson PJ, et al. Glucose dysregulation and response to common anti-diabetic agents in the FATZO/Pco mouse. PLoS One. 2017 Jun 1;12(6):e0179856.

Appendix B.

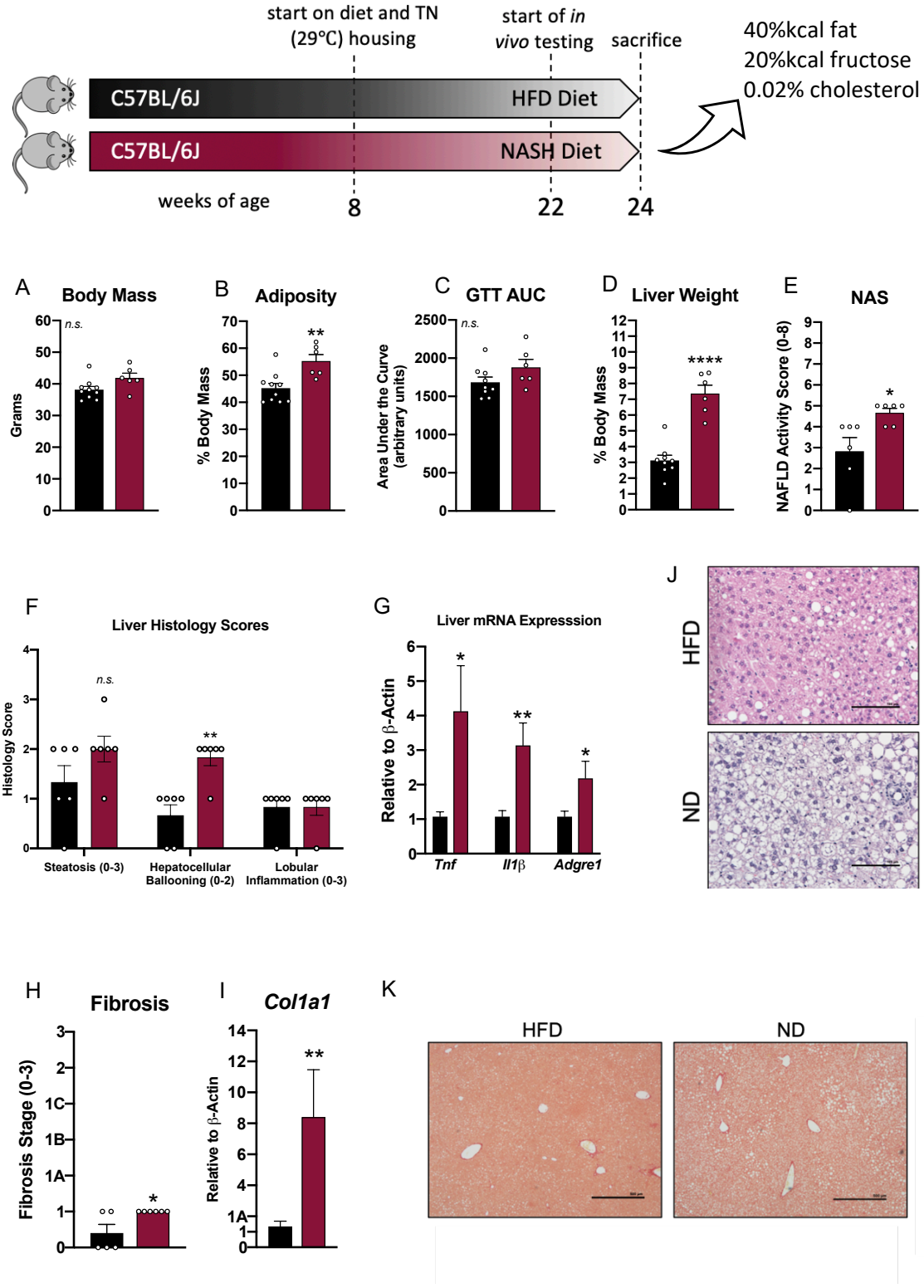
start on diet and TN (29°C) housing
start of *in vivo* testing
sacrifice
40%kcal fat
20%kcal fructose
0.02% cholesterol
C57BL/6J
HFD Diet
C57BL/6J
NASH Diet
weeks of age
8
22
24
A
Body Mass
Grams
n.s.
B
Adiposity
% Body Mass
**
C
GTT AUC
Area Under the Curve (arbitrary units)
n.s.
D
Liver Weight
% Body Mass
****
E
NAS
NAFLD Activity Score (0-8)
*
F
Liver Histology Scores
Histology Score
n.s.
**
Steatosis (0-3)
Hepatocellular Ballooning (0-2)
Lobular Inflammation (0-3)
G
Liver mRNA Expresssion
Relative to β-Actin
*
**
*
Tnf
Il1β
Adgre1
J
HFD
ND
H
Fibrosis
Fibrosis Stage (0-3)
1C
1B
1A
*
I
Col1a1
Relative to β-Actin
**
K
HFD
ND

Appendix B. The addition of fructose to a regular HFD increases adiposity, NASH, and liver fibrosis in mice housed at thermoneutrality for 16 weeks

Mice were fed a high-fat diet (HFD: 45% fat) or NASH diet (ND) and housed at thermoneutrality for 16 weeks to induce metabolic disease and NASH. **(A)** Body mass and **(B)** percent adiposity (adipose mass/body mass) at sacrifice (n=9 for HFD, n=8 for ND). **(C)** Glucose tolerance test (GTT) was performed at 15 weeks and area under the curve ($AUC_{0\text{-}120\ min}$) was calculated (n=9 for HFD, n=8 for ND). **(D)** Percent liver weights (liver mass/body mass) at sacrifice (n=9 for HFD, n=8 for ND). **(E)** NAFLD activity scores and **(F)** steatosis, ballooning, and inflammation scores obtained from liver H&E sections (n=6 for HFD, n=8 for ND). **(G)** Liver mRNA expression of *Tnf, IL1β,* and *Adgre1* (n=7 for HFD, n=5 for ND). **(H)** Fibrosis scores obtained from liver PSR and MTC sections (n=5 for HFD, n=8 for ND). **(I)** Liver mRNA expression of *Col1a1*. Representative liver histology images by **(J)** H&E staining at 20X and **(K)** PSR staining at 4X. Unpaired t-test was used to detect statistical difference; $*p < 0.05$.

Appendix C. TGF-β increases phosphorylation of ACLY in human hepatic stellate cells

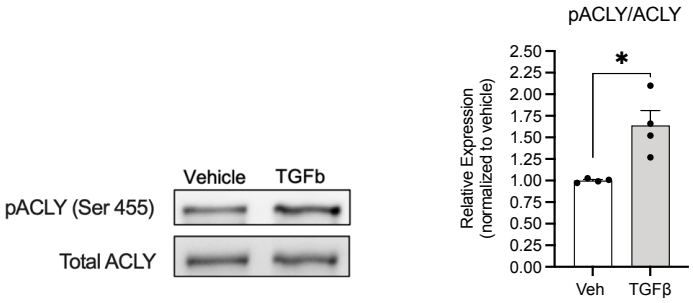

Appendix C. TGF-β increases phosphorylation of ACLY in human hepatic stellate cells

Human hepatic stellate cells were treated with vehicle or TGF-β for 30 minutes and protein levels of phosphorylated and total ACLY were measured using densitometry.